Universidad Autónoma de Madrid

Biochemistry Department

Role of the immune receptor NOD1 in vascular dysfunction and atherogenesis

Silvia González Ramos

Thesis for Doctoral Degree (Ph.D.)

Madrid, 2016

Biochemistry Department

Faculty of Medicine

Universidad Autónoma de Madrid

Role of the immune receptor NOD1 in vascular dysfunction and atherogenesis

Silvia González Ramos

Bachelor's Degree in Biotechnology

Supervisors:

Dr. Lisardo Boscá Gomar

Dra. Maria Fernández Velasco

Instituto de Investigaciones Biomédicas Alberto Sols

Silvia González Ramos holds a FPI fellowship (BES-2012-053953)
from the Spanish Ministry of Economy and Competitiveness
(*Ministerio de Economía y Competitividad*)
at the Biochemistry Department in the
Instituto de Investigaciones Biomédicas Alberto Sols
CSIC-UAM.

"I was taught that the way of progress

was neither swift nor easy"

- Marie Curie -

Acknowledgements

This Thesis work would not be completed without the support from my family, friends, and colleagues.

First of all, I would like to thank my main supervisor, **Lisardo Boscá**, for accepting me as your PhD student, for training me to gain scientific independence and for your tremendous support and trust. You have been an excellent guide on these four years' adventure.
I must also thank **Paloma Martín**, for bringing up interesting discussions and clever ideas and sharing your experience in life and science; **Antonio Castrillo**, for your warm encouragement, clear guidance and your effort to help me to improve; **Alfonso Luque**, for always putting on your best smile and help me altruistically, and **Susana Alemany** for your mildness, generosity and specially for creating an open and friendly atmosphere.

As I am writing this part, all joyful moments and memories come back, and I must thank all the colleagues and friends for these.
Marta Paz, thank you for always being reliable and supportive, and for your generous help with all your enthusiasm on all matters, big or small. If we find strength through unity, it also creates friendships when the project is related to a mission we share. This concerted effort will make it possible to take decisive steps forward. **César Rosales**, your attitude brings in so much joy in the atmosphere. The more I know you, the more I appreciate your personality. Advocating alone is tough; but there is power in numbers. Thank you for always being kind and willing to help, and special thanks for feeding us with the best Mexican food ever! **Marina Mojena**, thanks for your love and caring, and for that you feed me with *Things Valencian People Love* when the black hole into my insides is hungry. **Omar Motiño**, thank you for working for free for a shabby Ph.D. student and thank you very much for this four years' perspective, knowledge, and humour, of course.

Some colleagues and friends have left the group, but I would like to acknowledge them as well. Thank you, **Gemma Benito**, for your humble personality and for your cheerful influences when I was a new Ph.D. student. **Daniel Francés**, thank you for sharing your knowledge and intelligence, as well as your continuous support even when you left Spain.

Thank you **Luis Castro** for your high spirit, your laugh and your kindness. **Emilio Acosta**, it was short your introduction this year, but thank you for your passion, maturity and enthusiasm at work and life.

Acknowledgement for the support and the company of people in the IIB and others, is also worthy in this Thesis. In this regard, I would like to thank **Sandra Muñoz, Ane Larrañaga** and **Elvira Alonso** for unconditionally being in the good, the bad and the ugly and for always being a shoulder I can depend on. Many thanks to **Cristina Rius**, not only for her contribution to the project but for her guidance, for sharing thoughts about life and future, and for those encouraging conversations in the intravital room. Thank you **Ángela Sánchez** and **Marta Celorio**, for your always positive attitude, your support, your hospitality and sweetness. Thank you to the personnel of the Animal Facility (**Miguel, Manu, Rakel…**) and especially to **Cris**, for always willing to help me, for their closeness, cheerfulness and all the laughter and joy that made the hardest days less tough. And thank you also to all the colleagues in the rest of the IIB and in the great forgotten Biochemistry Department at the Faculty: **Bea, Belén, Cristina, Daniela, Eunice, Jose, Lourdes, LuisCar, Mireia, Raúl, Sara, Sol, Sonia**… it is a great pleasure to be your neighbour in the corridors!

Support outside the IIB was very important for me to complete this work, thus I would like to give my great thanks to these people. **Oliver Soehnlein**, great thanks for your tremendous help with my career, for your warmest encouragement with all your honest and kind advices you gave me. I am so lucky I had such an incredible mentor this year! My **Valencian boy**, I am also very grateful for your spirit of sharing. It was great pleasure to meet you and work with you again this year. Thank you **Almudena Ortega** for your contributions to the project, for running with my sodding Spanish stamp in the last minute and for always 'bringing a little bit of south' to the rainy Munich. Thank you also my dearest Italian, **Bartolo Ferraro** and Mexican **Maria Sánchez**. I still sometimes sit and remember all the good times we had, all the laughs we shared, all the bad moments we overcame together… and I am just waiting for that day we meet again. Thank you to the cutest south European women in the basement, **Giovanna Leoni** (Congrats! ☺) and **Joana**

Viola, for being kind, comforting, supportive and encouraging no matter when or where! Thank you to the best and the kindest technicians ever: **Janine Brauner**, **Patricia Lemnitzer**, and **Yvone Jansen**. And thank you to the rest of the basement (**Ariane, Carlos, Carla, Emiel, Maik, Nicole, Quinte, Renske, Remco, Sanne and Yvonne**) for receiving me arms wide open, sharing your knowledge and expertise and for being so friendly and generous.

Of course I would never forget to send my sincere gratitude to the people that accompanied me at the starting point of this scientific path. **Vicente Andrés** and **Herminia González**, thank you very much for introducing me to science with patience and tolerance, and for still being always willing to lend me a helping hand in this path. You truly set an example of outstanding professors and researchers. Thank you very much also to all my old colleagues in their labs, as well as people at **Francisco Javier Chorro**'s group, **Antonio Diez** and **Pilar Sepúlveda**'s laboratory, for the continuous encouragement, for your extraordinary intelligence and wisdom and for caring about me after all these years.

Last, but not least, I would like to thank my dearest **Mom, Dad** and **Bubu.** I cannot imagine this day has finally come. You have been my pillars of support, guidance and love since the day I was born. I hope I made you feel proud of me as much as I feel of you.
Especially I would like to thank my beloved **Alex.** You have inspired me to continue to strive to be the best version of myself every day. You have truly been the best support I could have asked for during this 4 years.
I would also like to thank my near-future sister-in-law **Ana**, as well as my far-future parents-in-law and brother-in-law **Maica**, **Vicente** and **Luis**. Thank you for your encouragement and love. You gave me strength to overcome the challenges during this work.

Thank you all for acknowledging how hard I have worked, but also know that I would not have achieved it without each and every one of you. I love and cherish you with all my heart!

Abstract / Resumen

Abstract

According to the World Health Organization, cardiovascular diseases are the first cause of death globally and atherosclerosis underpins most of the incidence. It is a chronic disease characterized by two fundamental hallmarks: lipid retention and inflammation. Even though sterile inflammation in atherosclerosis can be triggered by danger signals such as cholesterol crystals and oxidized LDLs (oxLDLs) through a set of pattern recognition receptors (PRRs), systemic or transient infection might also activate the innate immune system and affect atherosclerosis through the same set of receptors.

The main target of this Thesis, the nucleotide-binding oligomerization domain-containing protein 1 (NOD1), is an intracellular sensor from the innate immune system receptors PRRs. On the basis of the background relating NOD1 and cardiovascular diseases, we hypothesized an active role of NOD1 in regulating immune responses in the pathogenesis of atherosclerosis. Interestingly, we found *Nod1* induction in atherosclerotic mouse tissues and its genetic inactivation reduced atherosclerosis in the early onset in *ApoE*$^{-/-}$ mice.

The earliest process of atherosclerosis is perhaps the accumulation of lipids in the intima of arteries, which supposedly results from endothelial dysfunction because of insult-induced damage. Accordingly, we found that the 'protective' effect of *Nod1* deletion, was dependent on cells from a non–bone marrow origin – concretely endothelial cells (ECs). *Nod1* regulates VCAM-1 expression in ECs through the sensing of both pathogens and oxLDLs, being the latter the danger signal par excellence in human atherosclerosis now established as the first putative NOD1 endogenous ligand. This mechanistic effect was found *in vivo* to significantly reduce firm adhesion and subsequent recruitment of monocytes and neutrophils to the inflamed micro- and macro-vasculature in *ApoE*$^{-/-}$*Nod1*$^{-/-}$ mice, providing new light to the controversial contribution of PRRs in leukocyte recruitment in response to damage.

In summary, our data define a major role for non-haematopoietic *Nod1* in early leukocyte recruitment to the athero-prone vasculature, suggesting new focus on early detection of endothelial NOD1 activation as prognostic marker of the disease and therapies aimed at inhibiting endothelial NOD1 activity to curb the pandemic of cardiovascular diseases without compromising immunity.

De acuerdo con la Organización Mundial de la Salud, las enfermedades cardiovasculares son la primera causa de muerte a nivel mundial y la aterosclerosis el mayor causante. Es una enfermedad crónica caracterizada por dos marcas distintivas: la retención de lípidos y la inflamación. La aterosclerosis puede ser activada por la inflamación estéril que originan señales de daño como los cristales de colesterol o las LDLs oxidadas (oxLDLs) cuando son reconocidas por los receptores de reconocimiento de patrones (PRRs), pero también se puede activar por infección sistémica o transitoria a través de estos mismos receptores.

El objetivo principal de esta Tesis, la proteína *nucleotide-binding oligomerization domain* 1 (NOD1), es un sensor intracelular PRR del sistema inmune innato. En base a los antecedentes de NOD1 y las enfermedades cardiovasculares, nos planteamos la hipótesis del papel activo de NOD1 en la regulación de las respuestas inmunes en la patogénesis de la aterosclerosis. Curiosamente, encontramos que *Nod1* se induce en tejidos murinos ateroscleróticos y que su inactivación genética reduce la aterosclerosis desarrollada en ratones *ApoE*$^{-/-}$ en estadios tempranos.

El primer paso en el desarrollo de aterosclerosis es probablemente la acumulación de lípidos en la íntima de las arterias, como consecuencia de la disfunción endotelial que éstos inducen. De acuerdo con esto, nosotros encontramos que el efecto "protector" de la deleción de *Nod1* es dependiente de células no-hematopoyéticas – concretamente, células endoteliales (ECs). *Nod1* regula la expresión de VCAM-1 en ECs a través de la detección de patógenos y oxLDLs, siendo las últimas las señales de daño por excelencia en la aterosclerosis humana y ahora establecidas posiblemente como el primer ligando endógeno de NOD1. *In vivo* encontramos una reducción significativa en la adhesión firme y posterior reclutamiento de monocitos y neutrófilos en la micro- y macro-vasculatura inflamada de ratones *ApoE*$^{-/-}$*Nod1*$^{-/-}$, aportando nuevos conocimientos a la contribución de los PRRs en el reclutamiento de leucocitos en respuesta a daño.

En resumen, nuestros resultados definen un papel clave de *Nod1* en células no hematopoyéticas en el reclutamiento temprano de leucocitos en vasos propensos a la aterosclerosis, sugiriendo la detección temprana de NOD1 como marcador de prognosis de la enfermedad y terapias dirigidas a inhibir la actividad de NOD1 en el endotelio para frenar la pandemia de las enfermedades cardiovasculares sin comprometer la inmunidad.

Contents

Contents

Non-Standard Abbreviations And Acronyms

Non-standard abbreviations and acronyms

^{18}F-FDG	Fluorine-18-deoxyglucose
AIM	Absent-in-melanoma
ALR	AIM-like receptor
APAF-1	Apoptotic protease activating factor-1
APC	Antigen-presenting cell
APOB	Apolipoprotein B
APOE	Apolipoprotein E
BM	Bone marrow
C12-IE-DAP	Acylated derivative of iE-DAP
CAD	Coronary artery disease
CARD	Caspase-activated recruitment domain
CCL/CXCL	Chemokine ligand
CCR/CXCR	Chemokine receptor
CLR	C-type lectin receptor
CT	Computed tomography
CVD	Cardiovascular disease
DAMP	Damage-associated molecular pattern
DKO	Double-knockout
DM	Diabetes mellitus
EBD	Effector-binding domain
EC	Endothelial cell
ECAM	Endothelial cell adhesion molecule
ECGS	Endothelial cell growth supplement
ECM	Extracellular matrix
ERK	Extracellular signal–regulated kinases
ET-1	Endothelin-1
GlcNAc–MurNAc	N-acetyl glucosamine N-acetyl muramic acid
GM-TriDAP	GlcNAc-MurNAc-l-Ala-γ-d-Glu-*meso*-DAP
HBSS	Hank's balanced salt solution
HFD	High-fat diet

HUVEC	Human umbilical vein endothelial cells
ICAM-1	Intercellular adhesion molecule-1
IE-DAP	γ-D-glutamyl-*meso*-diaminopimelic acid
IKK	I kappa B kinase
IRF	Interferon regulatory factors
JNK	C-Jun N-terminal kinase
LDLr	Low-density lipoprotein receptor
LFA-1	Lymphocyte function-associated antigen-1
LOX-1	Lectin-like oxidized low-density lipoprotein receptor-1
LPC	1-acyl-sn-glycero-3-phosphocholine, lysophophatidilcholine
LRD	Ligand-recognition domain
LRR	Leucine-rich repeats
Ly6C	Lymphocyte antigen 6 complex
Ly6G	Lymphocyte antigen 6 complex locus G6D
MAMP	Microbe-associated molecular pattern
*m*DAP	*meso*-diaminopimelate acid
MDP	Muramyl dipeptide acid
MDS	Most diseased segment
MI	Myocardial infarction
MLEC	Mouse lung endothelial cell
NF- κB	Nuclear factor kappa B
NLR	Nucleotide-binding leucine-rich repeat-containing receptor
NOD	Nucleotide-binding oligomerization domain
ORO	Oil Red O
OXLDL	Oxidised low-density lipoprotein
PAMP	Pathogen-associated molecular pattern
PECAM-1	Platelet endothelial cell adhesion molecule-1
PFA	Paraformaldehyde
PGN	Peptidoglycan
PRR	Pattern-recognition receptor

Non-standard abbreviations and acronyms

PSGL-1	P-selectin glycoprotein ligand-1
QRT-PCR	Quantitative reverse transcription polymerase chain reaction
RIG-I	Retinoic acid-inducible gene-I
RIP-2/RICK	Receptor interacting protein-2
RLR	RIG-I-like receptor
ROS	Reactive oxygen species
SMA	Smooth muscle α-actin
SR	Scavenger receptor
SUV	Standardized uptake value
SUV_{max}	Maximum SUV
TBI	Total-body irradiation
TBR	Target-to-background
TEM	Transendothelial migration
TLR	Toll-like receptor
TNFR	Tumour necrosis factor receptor
VCAM-1	Vascular cell adhesion protein-1
VLA-4	Very late antigen-4
VSMC	Vascular smooth muscle cell

1. Introduction

1.1. THE IMMUNE SYSTEM

The immune system is a complex network of tissues, cells and molecules that work together to defend the body against attacks by "harmful" invaders. It can recognize and remember millions of different "enemies", and it can produce secretions and cells to match up with and wipe out each one of them. The secret to its success is an elaborate and dynamic communications network that trigger two different types of reactions: the innate and the adaptive responses, that account for how quickly and for how long it responds against pathogens, its central effector cell types and its specificity for different classes of microbes (5) (Figure 1).

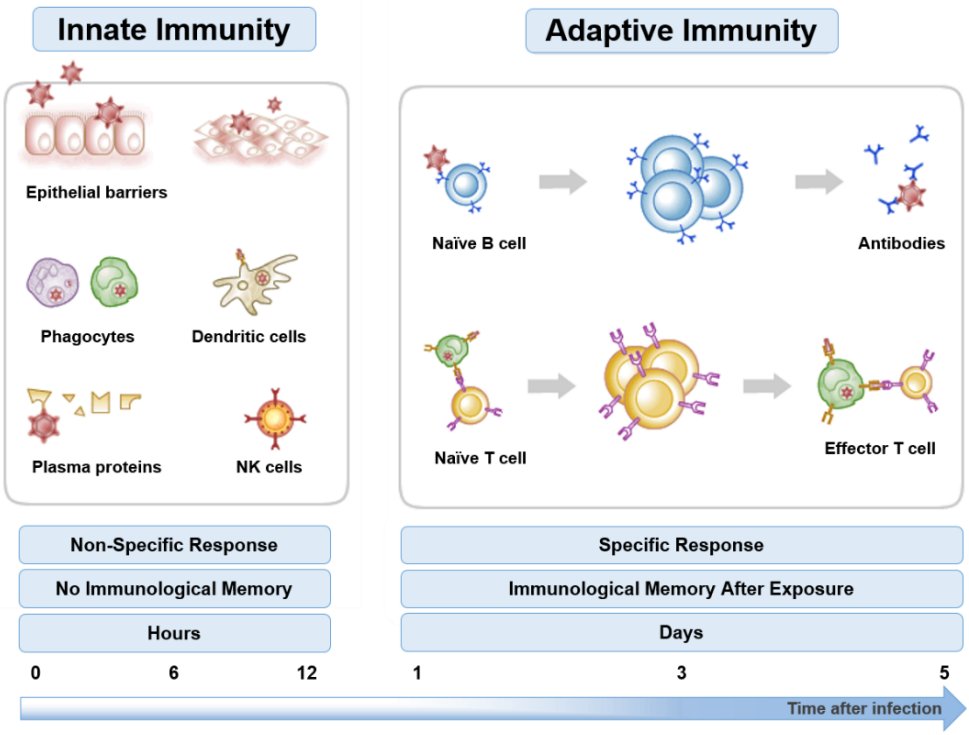

Figure 1. Main features of *the innate and adaptive immune responses.* In simple terms, physical barriers (skin, mucous) prevent pathogens such as bacteria and viruses from entering the organism. If a pathogen breaches these barriers, the innate immune system provides a non-specific response mediated by phagocytes, natural killer cells (NKs) and plasmatic proteins (interferons and the complement system). If pathogens successfully evade the innate response, vertebrates possess a second layer of protection: the adaptive immune system. Antigen-presenting cells (APCs), in the picture represented as dendritic cells - the most specialised APCs together with B-cells, will serve as linkers between the innate response and the adaptive response. This improved response is then retained after the pathogen has been eliminated, in the form of an immunological memory, and allows the adaptive immune system to mount faster and stronger attacks each time this pathogen is encountered (154, 236). The timeline along the bottom of the drawing represents the time-lapse between pathogen sensing and the maximal response.

1.1.1. Self *vs.* Non-Self: the Very Core of Immunology.

Paradoxically, "infection" is not only inevitable but a paramount feature of our physiology. Actually, reported values in the literature account for equivalent numbers in the total amount of bacteria residing in our body and the total number of human cells (257). How these "good" microbes are spared while the "bad" bacteria are attacked is still one of the biggest questions in immunology today.

Self-awareness is fundamental to life and clear proof is that, from complex animals to single-celled bacterium (155) have developed hard-wired mechanisms to recognize and defend itself from intruders.

In multicellular organisms, the innate immune system is the first line of defence and it responds to pathogens in a generic way by the recognition of few evolutionarily conserved structures on pathogens. These molecular motifs are the so-called PAMPs or 'pathogen-associated molecular patterns' (119), even though this term is a misnomer and can also be referred as 'microbe-associated molecular patterns' (MAMPs). The reason behind this long criticism is that non-pathogens also synthesize these molecules (9).

Since pattern recognition takes advantage of the long evolutionary distance that separates humans from microbes like bacteria and viruses, it is thereof a highly efficient way for our immune system to detect potential threats.

1.1.2. The Danger Theory: a Renewed Concept of Self.

Although Janeway's extended paradigm of Self *vs.* Non-Self (119) has been proven over decades as central in host defence and immunity, years of detailed examination have revealed a number of inherent problems such as why do mammalian mothers not reject their foetuses?, or, why do we fail to reject tumours, even when many clearly express new or mutated proteins?

To answer some of these questions, in 1994 P. Matzinger proposed the "Danger model" (180), which suggests that the immune system is more concerned with damage than with foreignness, and is called into action by alarm signals from injured tissues, rather than by the recognition of non-self.

Nevertheless, given clear evidence for both theories (23, 81), in 2004 both models were bring together. In the contemporary theory (258), it is proposed that many PAMPs and

endogenous alarm signals belong to an ancient subfamily of universal DAMPs (or 'damage-associated molecular patterns') that consist of exposed hydrophobic portions (*hyppos*) to which the 'pattern-recognition receptors' (PRRs) have evolved to recognize and react, suggesting that there might be a universal language of injury and repair shared by most, if not all, living organisms.

It is notable that threshold for the detection of microbes by PRRs is much lower than the detection of tissue damage and perhaps, this correlates with the magnitude of the threat to the host.

1.1.3. PRR: Primer to the Inflammatory Response.

Though nowadays it is appreciated that immune and non-immune cells express a plethora of PRRs that are comprised of proteins of various superfamilies (reviewed in (277)), convincing molecular proof that such molecules existed did not come until the functional discovery of the first human PRR in 1997, known as Toll-like receptor (TLR) 4 (187).

PRRs can recognize PAMPs and DAMPs in diverse localizations including the cell surface, intracellular vesicles, and alternatively in either the extracellular milieu, the cytoplasm or the nucleus (Figure 2). Apart from its cellular location, broadly, the PRRs can be classified attending to their function into:

- *Signalling* PRRs: mediate cellular activation and include the large families of cell membrane-bound Toll-like receptors (TLRs) and the intracellular retinoic acid-inducible gene (RIG)-I-like receptors (RLRs), the Absent-in-melanoma (AIM)-like receptor (ALRs) and most of the nucleotide-binding leucine-rich repeat-containing receptors (NLRs).
- *Endocytic* PRRs: promote the attachment, engulfment and destruction of danger signals by phagocytes, without relaying an intracellular signal. These PRRs include C-type lectin receptors (CLRs) that recognize carbohydrates, scavenger receptors (SRs) that recognize charged ligands as well as diverse non-cell-associated PRRs.

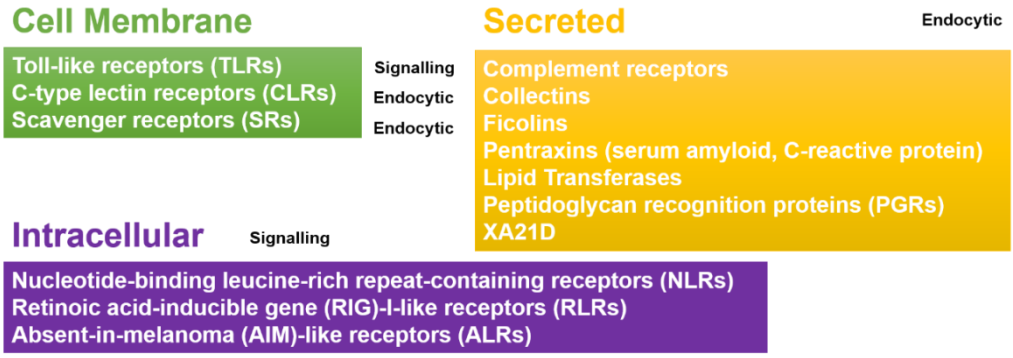

Figure 2. Classification of the PRRs. Membrane-bound receptors are Toll-like receptors (or TLRs) and Scavenger Receptors (SRs), which are considered to be the most essential PRRs involved in atherosclerosis, as well as C-type lectin Receptors (or CLRs). Intracellular receptors are the majority of the nucleotide-binding leucine-rich repeat-containing receptors (or NLRs), the retinoic acid-inducible gene-I-like receptors (or RLRs) and the recently emerged AIM-like receptors (ALRs). A number of PRRs do not remain associated with the cell that produces them even though they promote phagocytosis of the danger signal: complement receptor, collectins, ficolins, pentraxins, lipid transferases, peptidoglycan recognition proteins (PGRs).

The inflammatory response is the host's response to a perceived threat in the form of an invading pathogen or tissue damage (118) and its critical first step is the signal transduction through PRRs, that converge on common intracellular pathways, including those mediated by nuclear factor-κB (NF-κB), mitogen-activated protein kinases (MAPKs), interferon regulatory factors (IRFs) and the inflammasome signalling (130, 152, 234).

Without the inflammatory response, the host would succumb to the threat, while excessive responses will cause cell and tissue damage and death (Figure 3).

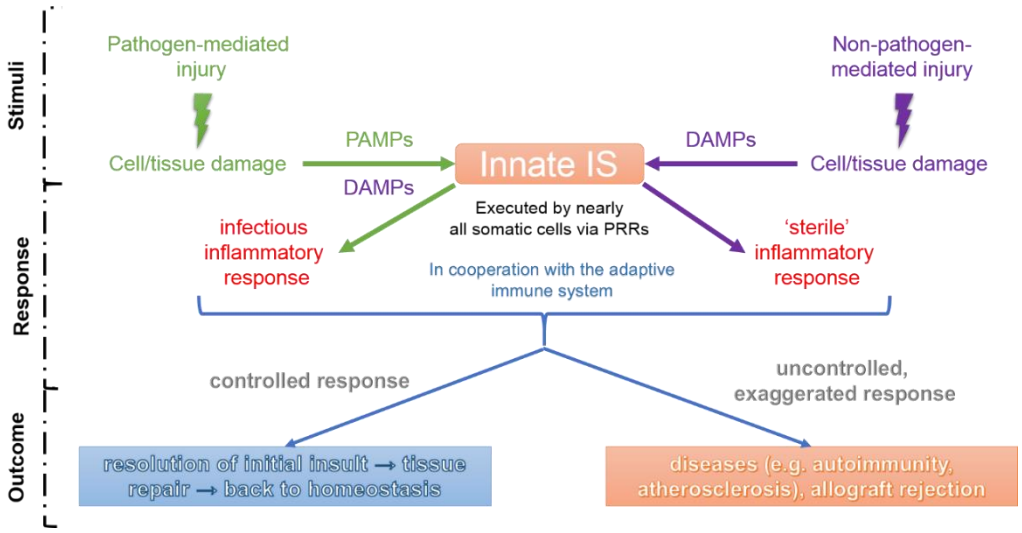

Figure 3. Principles in the PRRs-driven inflammatory response. The innate immune system is a highly sensitive organ of perception sensing any cell stress and tissue injury. The highly conserved first-line defence system as represented by most somatic cells reacts to any tissue injury with an inflammatory response aiming to eliminate the dangerous challenges and to repair the destroyed

tissue, thereby maintaining homeostasis in cooperation with the adaptive immune system. However, when uncontrolled and exaggerated, the system leads to diseases such as atherosclerosis, autoimmune disorders or other pathologies including chronic allograft rejection. Besides, tissue damaging infectious pathogens may induce DAMPs that finally trigger a vigorous anti-pathogen or infectious inflammatory response; conversely, tissue primarily damaged by non-infectious agents is prone to get contaminated with pathogens that may lead to a long-lasting excessive inflammatory response.

Not to be underappreciated is the role of non-immune cells in the host response to acute infection or injury where most PRR are widely expressed (121, 181, 246, 255). Of the non-immune cell types that participate directly in the inflammatory response, endothelial cells (ECs) are probably the best characterized. In response to activation of PRR, ECs upregulate leukocyte adhesion molecules as well as inflammatory cytokines and chemokines that direct the accumulation of leukocytes into the tissues (246, 247). Final outcome in acute inflammation by ECs is leakage of plasma and leukocytes, together with an increase in local blood flow. These features of ECs make up the signs of swelling, redness, and heat associated with inflammation.

1.1.3.1. NLRs: Versatile Cytosolic Sentinels.

As stated before, most but not all NLRs may act as PRRs. This skilful family of receptors can recognize diverse and dissimilar ligands that range from danger signals (microbial pathogens, host cells or environmental factors) to cytokines such as interferons.

Likewise, even though important roles in developmental processes have been also attributed to these receptors (150, 283, 312), the activated NLR family can be divided into four broad functional categories: transactivation of major histocompatibility complexes, autophagy, regulation of the NF-κB pathway, and inflammasome assembly.

To date, in humans, there are 22 known NLRs (284) all of which are implicated in a plethora inflammatory and autoimmune human diseases (314) arguing for an important role for these proteins in the regulation of immune responses *in vivo*.

The human NLR family is comprised of 4 subfamilies according to four recognizable N-terminal domains, being NLRA, NLRB, NLRC and NLRP, and the cytoplasmic nucleotide-binding oligomerization domain (NOD) receptors are contained within the NLRC subfamily (198).

As depicted in Figure 4, NOD-like receptors share a common domain at their NH2-terminal which is at least one caspase-activated recruitment domain (CARD) that enables protein:protein interactions, and is essential for the recruitment of downstream adaptor proteins through haemophilic and heterophilic protein interactions. Besides, a canonical organization with two more defined domains is characteristic of these receptors: a central NOD domain (also known as NACHT domain), that facilitates homodimerization of the receptor and a COOH-terminal leucine-rich repeats (LRR) that functions to detect the NOD ligand (115).

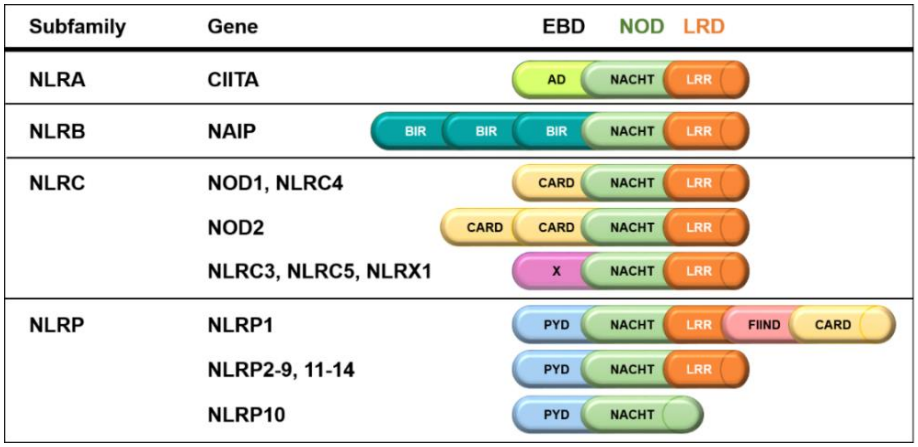

Figure 4. Classification and protein structure of human NLR family. Most NLR proteins are composed of variable amino-terminal effector-binding domains (EBDs), a centrally located nucleotide-binding oligomerization domain (NOD) and a carboxy-terminal ligand-recognition domain (LRD). The putative EBDs of NOLRC3, NLRC5 and NLRX1 (represented by X) do not have marked homology with any known protein. The number of leucine-rich repeats (LRRs) varies between NOD proteins. AD, acidic transactivation domain; BIR, baculovirus inhibitor of apoptosis repeat; X, unidentified; PYD, pyrin domain, FIIND, function to find domain.

The NOD domain consists of seven distinct conserved motifs, including the ATP/GTPase specific loop, the Mg^{2+}-binding site, and five more specific motifs (143). It was first found in apoptotic protease activating factor-1 (APAF-1) and its nematode homologue CED-4, which are two essential regulators of developmental and p53-dependent programmed cell death (54, 114). Subsequently, two NOD-containing molecules, NOD1 (CARD4) and NOD2 (CARD15), were identified through database searches for APAF-1/CED-4 homologues and since then, the NOD-protein family has greatly expanded.

NOD1 and NOD2: Gene Expression, Mapping and Protein Structure.

By genomic sequence analysis, Inohara et al. (112) determined that the *NOD1* gene maps to 7p15-p14 and contains 7 coding and 7 non-coding exons. Likewise, by analysis of BAC

clones, Ogura et al. determined that the *NOD2* gene maps to 16q12 and contains 12 coding exons (214), even though later on, an alternative first exon about 3.5 kb upstream of the canonical first exon of the *NOD2* gene was identified (135).

After post-transcriptional processing, two different isoforms have been described for NOD1, being the canonical sequence composed by 953 aa (112); and three different isoforms for NOD2, being the canonical isoform of 1,040 aa (214). As depicted in Figure 4, both canonical isoforms for NOD1 and NOD2 contain a LRR and NOD domain, but differ in containing one or two copies of the CARD domain respectively.

Moreover, although both NOD1 and NOD2 are located within the cytosol of host cells, there are differences in the cellular expression of both receptors. NOD1 is ubiquitously expressed by most cell types (67, 77, 230), however, it is predominantly expressed by epithelial cells and in the intestinal tract. In contrast, NOD2 is predominantly restricted to cells of myeloid origin, including T cells (232), neutrophils (42), macrophages (214) and dendritic cells, with low level expression by epithelial cells of primary or cell line origin (98, 106, 112).

NOD1 and NOD2: Activation and Response.

Initially, NOD1 and NOD2 were proposed to be intracellular sensors of bacterial lipopolysaccharide (LPS) (91, 116, 213). However, subsequent studies using purified bacterial cell preparations identified that NODs detect bacterial peptidoglycan (PGN) fragments contained within the cell wall of Gram negative and Gram positive bacteria.

Specifically, NOD1 detects a conserved region of PGN (γ-D-glutamyl-*meso*-diaminopimelic acid, iE-DAP) common to almost all Gram negative and some Gram positive bacteria such as *Bacillus subtilis* and *Listeria monocytogenes* (32, 89), meanwhile NOD2 detects a PGN component (muramyl dipeptide, MDP) contained within both Gram positive and Gram negative bacteria (90, 117), and therefore is considered to be a pan sensor of bacteria (Figure 5A).

Upon detection of bacterial ligand via their LRR domains, NOD1 and NOD2 homodimerise via their central NOD domains and subsequently interact at their CARD domains (104, 113, 139) with their essential adaptor molecule: the receptor interacting protein-2 (RIP-2 or RICK), a serine/threonine kinase that through the assembly to large

multi-protein complexes (including the IkB kinase (IKK) complex) lately activates the nuclear factor kappa B (NF-κB) signalling pathway (214) that enhance transcription of pro-inflammatory cytokines such as TNF-α and CXCL8 (89, 98, 290) (Figure 5B-C).

In addition to NOD-induced NF-κB activation and involving similar components such as RIP-2, NOD1 and NOD2 activate the mitogen-activated protein kinase (MAPK)-signalling pathway (p38, JNKs, and ERKs) resulting in subsequent secretion of pro-inflammatory cytokines (91)(113) although the mechanism involved awaits further investigation. Similarly, NOD1 can also promote activation of caspase-1 with subsequent IL-1β secretion (305), induction of apoptosis dependent of caspase-8 (48) and both NOD1 and NOD2, can stimulate a type I interferon response by IRF (interferon regulatory factors) activation (242, 292).

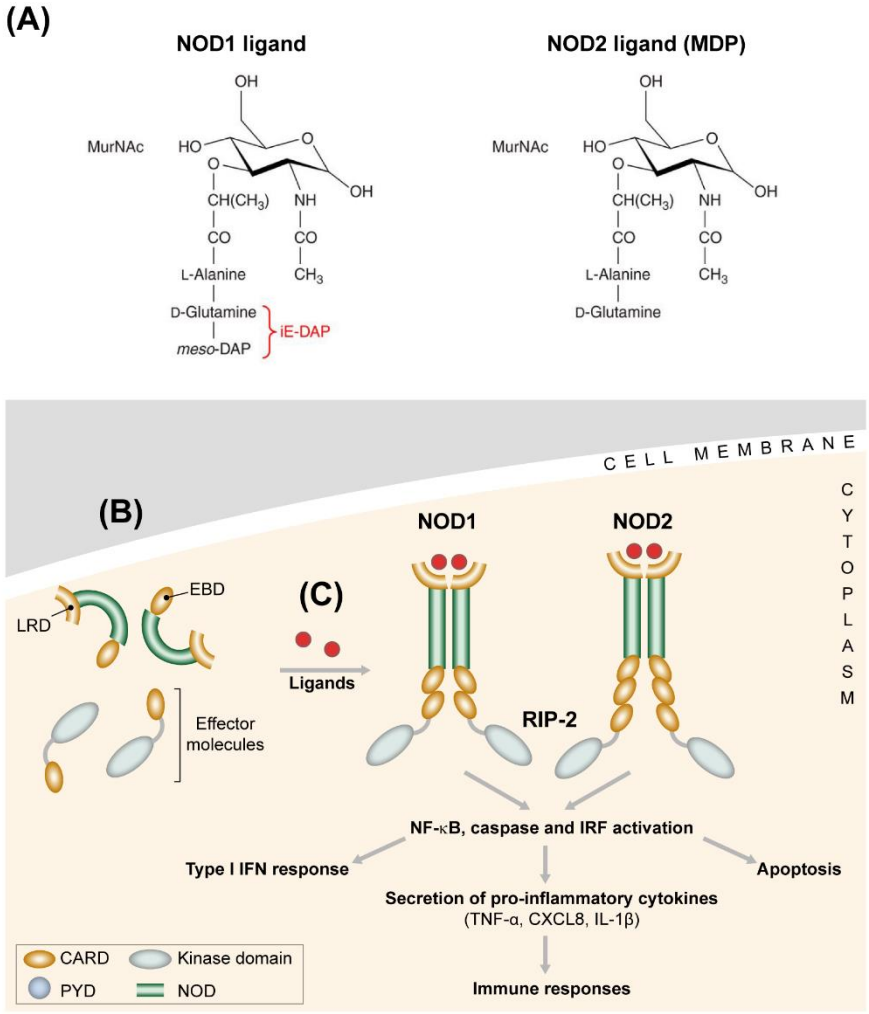

Figure 5. PGN drives NOD1 and NOD2 activation. (A) The structure identified by both NOD1 and NOD2 share a core containing N-acetyl glucosamine N-acetyl muramic acid (GlcNAc–MurNAc). In NOD1, this structure is linked to a tripeptide of which the terminal amino acid is

meso-diaminopimelate (*meso*-DAP). The minimal PGN component detected by NOD1 is γ-D-glutamyl-*meso*-diaminopimelic acid (iE-DAP). In contrast, in NOD2 ligand, the core is linked to muramyl dipeptide (MDP). **(B)** NOD ligands are recognized through the LRD of NOD proteins, which induces self-oligomerization and the recruitment of downstream effector molecules through the EBD. Oligomerization is mediated through the centrally located NOD, which induces proximity and activation of effector molecules, resulting in signalling. **(C)** Signalling through NOD1 and NOD2 is mediated through the kinase RIP-2, K63-polyubiquitinated within its kinase domain (14, 147) that assembles to large multi-protein complexes including the IKK complex (1, 104, 112, 113, 214, 303) that ultimately results in the dissociation of NF-κB p50 and the phosphorylation of the p65 complex. Phosphorylated p65 then translocates into the nucleus where it enables the transcription of pro-inflammatory cytokines. Recently, a role for NOD1 in apoptosis has been implicated (48) as well as the innate immune response mediated by type I interferon (IFN).

However, the current understanding of NLRs in innate immunity does not end here. As described at the beginning of 1.1.3.1, these versatile intracellular receptors have also crucial functions in autophagy, a bulk cytoplasmic degradation system for maintaining cellular homeostasis. Interestingly and becoming increasingly recognized, activated NOD1 and NOD2 are able to induce autophagy in a RIP-2 independent manner (47, 287).

Thus, having expressly regard to NOD1 and NOD2 receptors, the simple recognition of their danger signals, can trigger a wide variety of outcomes including pro-inflammatory, apoptotic and autophagy responses.

NOD1 and NOD2 in Cardiovascular Diseases.

While it is true that NLRs actively communicate with a myriad of cell death regulators so as to defend us against pathogens, they also have other functions independently of microbes. Therefore, it is not surprising that genome-wide association studies have shown a significant association between polymorphisms in NLR genes and numerous and disparate diseases including allergic rhinitis, multiple sclerosis, inflammatory bowel disease, asthma, Alzheimer's disease, cancer, multi-bacillary leprosy, vitiligo, early-onset menopause, and bone density loss in elderly women (51, 314).

Traditionally, these PRRs have always been known for their advantageous position at sites with high host-microbiome interactions like the gut and this is the reason why most studies regarding NOD1 and NOD2 have been focused on the study of intestinal inflammation (16, 35, 140, 290). Actually, NOD2 polymorphisms represent the greatest risk for Crohn's disease (110, 213), a type of inflammatory bowel disease targeted against a yet incompletely

defined subset of commensal gut microbiota that occurs on the background of a genetic predisposition under the influence of environmental factors (55).

However, in the past few years an increasing interest in studying the NLRs in cardiovascular diseases (CVDs) has emerged.

These proteins have been defined as key factors implied in the inflammation caused by the high fat diet (HFD) and insulin resistance. In fact, mice lacking NOD1 and NOD2 receptors are protected against insulin resistance, lipid accumulation and inflammation in adipose tissue and liver challenged by HFD (251, 278). In this regard, our group has proved the role of NOD1 in the myocardium of diabetic patients (228), one of the main risk factors to atherosclerosis development and subsequent myocardial infarction (MI).

It is on studying the role of both receptors in acute MI that has also been placed great effort lately, and nowadays it can be ascertained that both receptors contribute to the cardiac dysfunction after heart attack (170, 302).

With respect to the target disease of the present research, to date, fully contradictory concluding results showing the impact of NOD2 in the development of atherosclerosis have been published (122, 306). Contrarily, in the early 2014, Kanno *et al.* reported the implication of the NOD1 immune receptor in the development of atherosclerosis (125) with the statement that NOD1 activation in non–bone marrow-derived cells accelerates the development of atherosclerosis in apolipoprotein E knockout ($ApoE^{-/-}$) mice.

1.2. ATHEROSCLEROSIS

1.2.1. The Epidemic of the XXIst Century: Atherosclerosis.

Being an uncommon disease in the early years of the 20th century, when infectious diseases such as pneumonia and tuberculosis were the most common causes of death (221), a marked increase in death attributed to CVDs arose by mid-century and has reached its top nowadays. Actually, according to World Health Organization and 2014 estimates, of the approximately 47.5 million people who die per year worldwide, 14.5 million (30%) do so as a consequence of CVDs - being coronary atherosclerosis, the major cause of death (Figure 6).

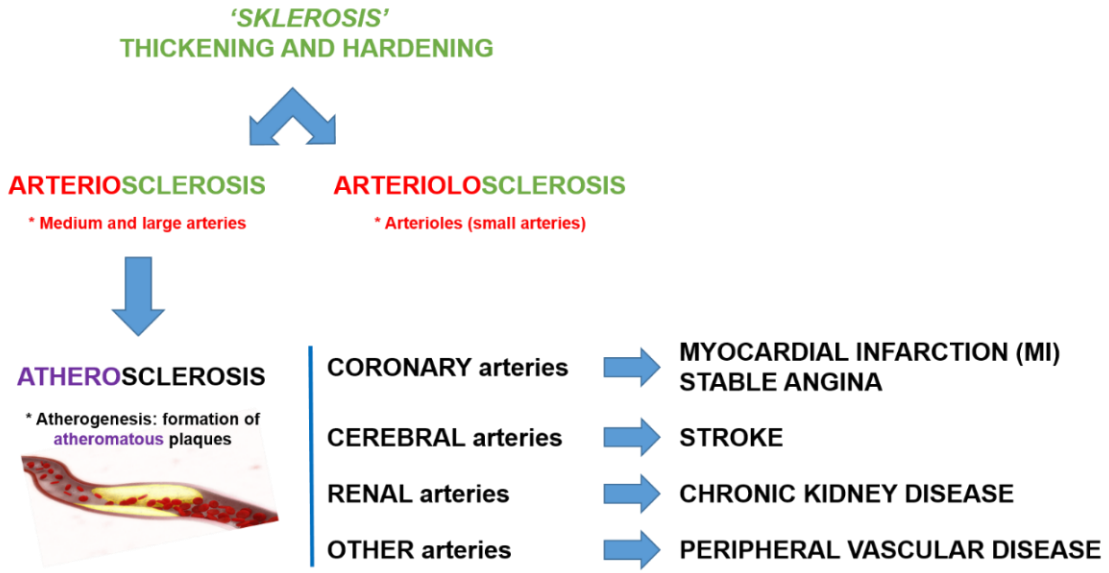

Figure 6. Atherosclerosis, the major cause of death in contemporary history. Atherosclerosis is a type of arteriosclerosis, from the Greek *sklerosis* that means any thickening and hardening of medium- and large-sized arteries and though similar, must be distinguished from arteriolosclerosis, which refers to the same process but in arterioles (small arteries). Therefore, atherosclerosis is a type of *sklerosis* specifically due to the *athere* (Greek term for atheroma), or accumulation of lipid. When the disease affects the coronary arteries, it is called coronary artery disease (CAD) and is the root cause of angina and myocardial infarction (MI). Other CVDs with atherosclerosis as the underlying cause, include stroke, chronic kidney disease and peripheral vascular disease.

Atherosclerosis is a multifactorial disease and the impact on CAD of traditional risk factors such as age, sex, elevated systolic blood pressure, smoking, family history of premature MI, diabetes mellitus (DM), high levels of low-density lipoprotein (LDL) cholesterol, low levels of high-density lipoprotein (HDL) cholesterol, as well as hypertriglyceridemia, has long been demonstrated beyond any doubt (7, 8, 209). However, more recent analyses show as promising novel risk factors hyperhomocysteinemia (21, 75) and high levels of C-reactive protein (301).

Perhaps, the autopsy-based study that better unifies the vast majority of these risks factors is the 'Pathological Determination of Atherosclerosis in Youth' study that evaluates the effect of most of these risk factors in different vascular beds. Here, they show the regional selectivity in atherosclerotic responses to risk factors (269).

Thus, atherosclerosis is a complex disease that affects very specific sites of the vascular tree. These high-susceptibility sites are thought to be conditioned by hemodynamic parameters, being particularly associated with regions of low shear stress, oscillatory flow, or turbulent

flow that are found in areas of branching or high vessel curvature (194, 308). Because of the obvious difficulties in studying pathogenic mechanisms in individual human subjects, the characterization of these prone-sites has been done in experimental animal models of atherosclerosis (Figure 7), even though there must be some regional dissimilarities, such as in the aortic sinus, being the starting point of atherosclerosis in mouse models but not characteristically involved in human atherosclerosis (10) where conversely, carotid sinus develop earlier lesions.

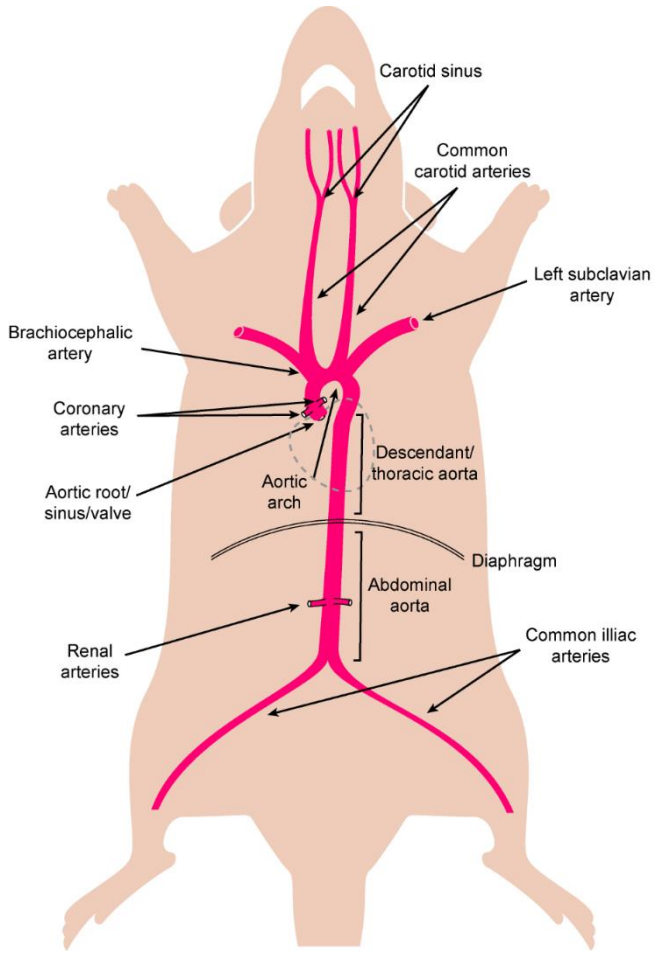

Figure 7. Diagram of the major arterial vasculature illustrating high-susceptibility sites for atherosclerosis. In both *LDL receptor*–and *ApoE*-deficient mice, lesions develop first in the aortic sinus, the innominate artery (brachiocephalic) and other branches of the aorta, as well as the pulmonary and carotid arteries. In advanced stages of atherosclerosis, lesions are detected in the descending thoracic, lower abdominal, proximal coronary, common iliac and femoral arteries (207).

Notwithstanding, the health, economic, and social burden of CVDs is tremendous, yet it is a largely preventable and treatable disease in which we are missing the target. Literally, if known and available measures and guidelines were appropriately used, CVDs consequences would decrease by up to 80% (99).

1.2.2. Atherosclerosis is an Inflammatory Disease After All.

Always seen solely as a lipid deposition disorder within a passive arterial wall, the presence of leukocytes within atherosclerotic arteries was reported in the early 1980s (86). Initially, investigators thought that only macrophages were predominantly present within atherosclerotic vessels. However, several studies reported the presence of most known leukocytes in both mouse and human aortas (79, 102), representing the disease as a series of highly specific cellular and molecular responses that can best be described, in aggregate, as an inflammatory disease (239) (Figure 8).

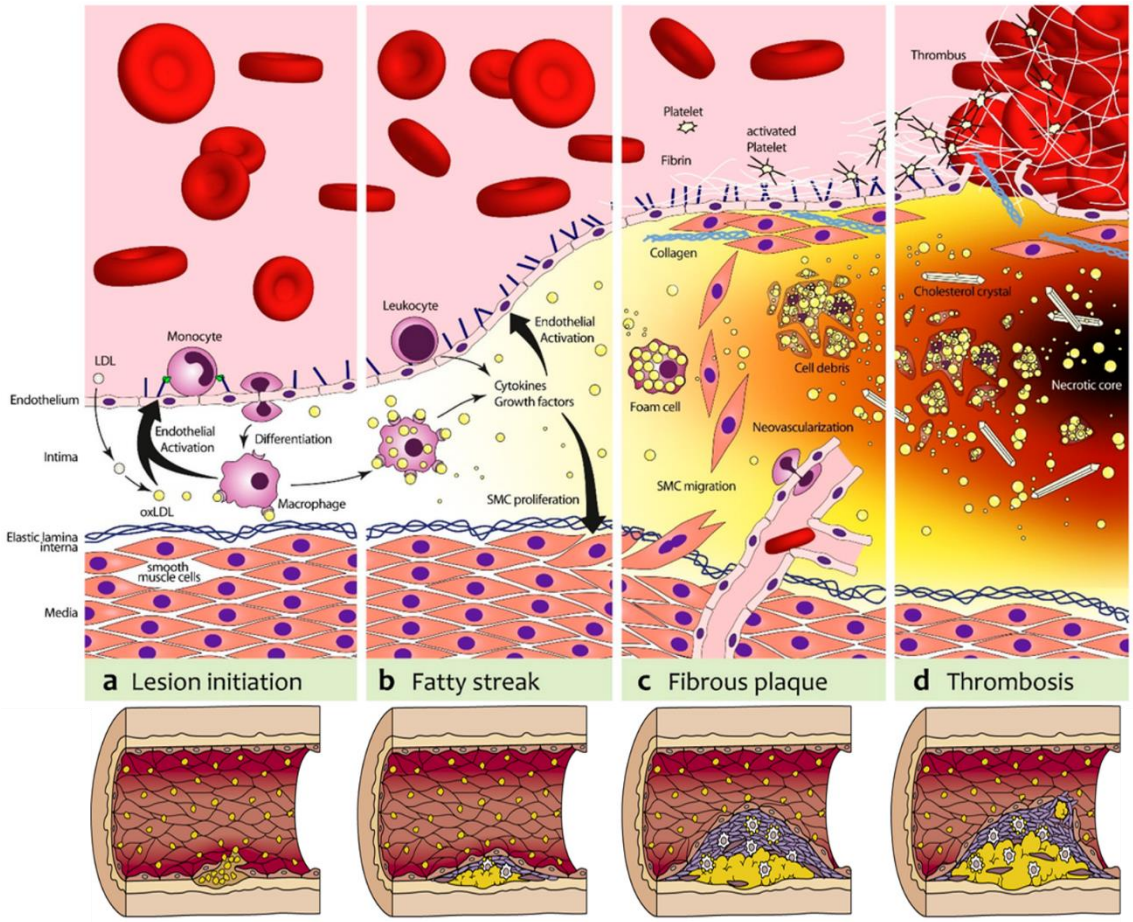

Figure 8. Pathogenesis of atherosclerosis. (a) Lesion initiation. In the first stage, LDL is deposited in the sub-endothelial space and undergoes oxidative modification, resulting in oxidised (ox)-LDL. OxLDL activates ECs to express endothelial cell adhesion molecules (49) as well as chemokines, that permits interaction among circulating leukocytes and ECs and subsequent transmigration into the intima, where monocytes differentiate into macrophages. **(b) Fatty-streak formation.** Macrophages harvest residual oxLDL via their SRs and switch into foam cells, further activating the endothelium to favour the recruitment of more inflammatory cells. **(c) Fibrous plaque formation.** The increasing plaque volume promotes neovascularization and induces smooth muscle cells to proliferate and form a fibrous layer that stabilizes the nascent lesion. With deposition of fibrin and activated platelets on the dysfunctional endothelium, a pro-thrombotic milieu is formed. **(d) Thrombosis.** Foam cells can undergo apoptosis and release cell-debris and lipids, which will result in the formation of a necrotic core. In advanced disease stages, destabilization of

the plaque by proteases secreted from foam cells, lead to the rupture of this fibrous cap and may expose the necrotic core contents; therefore, platelets and fibrin form a blood clot (thrombus) that results in a partial or total ischemic arterial obstruction (165, 240). Adapted from (267).

Interestingly, although neutrophils have classically received limited attention as cells with a major pathogenetic role in atherosclerosis, if we look at the several clinical and basic studies in recent years, we can find a direct correlation between neutrophils and CVD such as atherosclerosis (36, 70, 148, 210, 241, 256, 259). Specifically, upon endothelial transmigration from either bloodstream or plaque-formed *neo*-vessels (68, 188), neutrophils are able to perpetuate the oxidative stress through the release of oxidative enzymes present in their characteristic granules (29, 58, 291) as well as driving monocytes to the atherosclerotic plaques given the chemotactic activity of these granule proteins (58, 175). Furthermore, the recently spotlighted neutrophil extracellular traps (NETs), trigger activation of newly recruited neutrophils by fostering a type I IFN proinflammatory response (59, 138). And not only this, but the role of neutrophils can be also expanded to vulnerable plaques, since there is evidence that neutrophil-derived proteases could participate in degrading the fibrous cap that leads to plaque disruption and atherothrombosis progression (28, 120).

Thus, at the present time, though we are still in a phase of characterization of the different players involved in the atherosclerotic process, appreciation of the inflammatory character of atherosclerosis has spawned new avenues in basic, translational, and clinical research.

1.2.3. Pathogenesis of Lesion Initiation: Theories of Atherosclerosis.

From the very start, theories concerning the pathogenesis of atherosclerosis have been proposed to explain the initiation and growth of atherosclerotic plaques. The two major mechanisms postulated to explain the underlying cause, not mutually exclusive and linked to each other are:

- The *response-to-retention* hypothesis that submits Apolipoprotein B (APOB)-containing LDL retention as the inciting event for atherosclerosis, or, in other words: 'decreasing blood cholesterol, significantly reduces coronary heart disease' (2, 294). However, evidence does not support it, and shows proof of mechanisms independent of blood cholesterol levels (96, 280).

- The *response-to-injury* theory, which is the most accepted by the scientific community, stating that the initial event is injury to the endothelium (239). The generated endothelial dysfunction is sufficient to initiate atherogenesis through increased endothelial permeability to atherogenic lipoproteins (mainly LDL) and activation of endothelial cell adhesion molecules (ECAMs) to promote infiltration of leukocytes into the subendothelial space.

In this sense, although the best-investigated danger signal in human atherosclerosis is the accumulation of oxidised low-density lipoprotein (oxLDL)(92), the atherosclerotic lesion contains a mixture of PRR ligands also implicated in orchestrating either simultaneously or consecutively, the inflammatory response in the vessel wall (315) (Figure 9) and the discovery of the PRRs had a significant role in furthering the understanding and the treatment of atherosclerosis (69, 196).

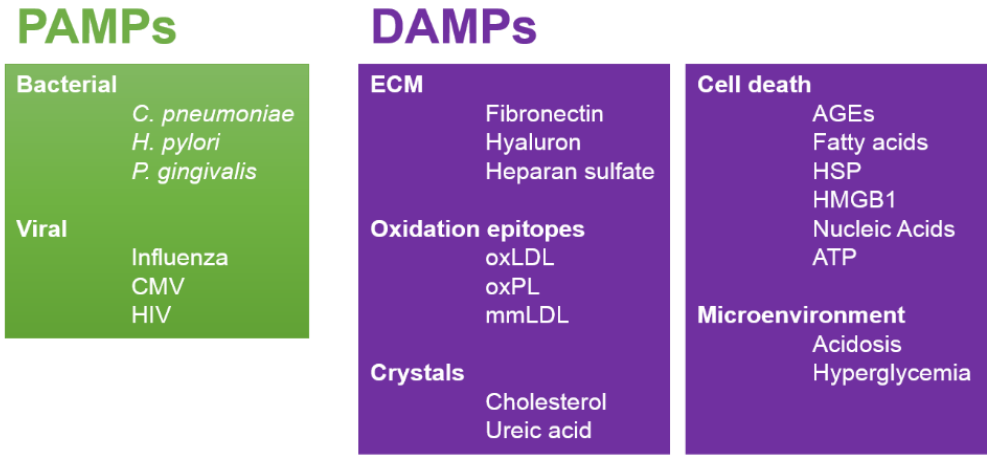

Figure 9. Overview of danger signals in atherosclerosis. Both pathogen-associated molecular patterns (PAMPs) from bacteria and viruses, as well as endogenous damage-associated molecular patterns (DAMPs) have been linked to cardiovascular disease. AGEs indicates advanced glycation end-products; ATP, adenosine triphosphate; CMV, cytomegalovirus; HIV, human immunodeficiency virus; HMGB1, high-mobility group box 1; HSP, heat shock proteins; mmLDL, minimally modified LDL; and oxPL, oxidized phospholipids.

Yet, what definitely is accepted is the idea that atherosclerosis constitutes a state of high levels of oxidative stress and this phenomenon is associated with lipid and protein oxidation in the vascular wall (208, 289). Whether oxidative stress is cause or consequence of the atherogenic process, it is not clear. In this sense, it has been proposed that inflammation could be considered as a primary process and oxidative stress as a secondary event of atherosclerosis (268).

1.2.3.1. Endothelial Dysfunction: The Early Predictor of Atherosclerosis.

The endothelium is a continuous layer of cells that separates blood from the vessel wall. Under homeostatic conditions, the endothelium maintains normal vascular tone and blood fluidity and there is little or no expression of pro-inflammatory factors (94). The arterial endothelium responds to increases in flow and changes in shear forces in the blood via the potent vasodilator nitric oxide (NO), thus leading to vasodilatation (24, 56, 254). The functional hallmark of endothelial dysfunction is characterized by a reduction in the bioavailability of vasodilators, in particular NO, whereas endothelium-derived vasoconstrictors such as endothelin-1 (ET-1) are increased (20, 304).

Many of the classical and 'newer' risk factors associated with atherosclerosis have been linked to endothelial dysfunction either alone, or in combination. The exact nature of the link is unknown, but may also involve reactive oxygen species (ROS).

Actually, it has been postulated that in early stages of the atherosclerotic process on the one hand, oxLDLs may activate NF-κB, increasing the transcription of genes encoding pro-atherosclerotic factors such as angiotensin converting enzyme, ECAMs and enzymes that further promote oxidative stress (27, 166, 203), and, on the other hand, accumulation of extracellular matrix (ECM) components (especially proteoglycans) in the sub-endothelial space may cause the retention of such particles (25). In the long run, ROS- and oxLDL-derived processes result in failure of producing sufficient amounts of NO (203, 216) and a reduction on its physical bioavailability (286, 307) (Figure 10).

Another causative parameter to take into account are the haemodynamic forces such as shear stress, which have been recognized as important modulators of endothelial function (93) by "priming the soil" in which lesions develop. Actually, atherosclerotic-prone areas have decreased secretion of NO, meaning that NO production is also modulated by flow shear.

In this context, Caro *et al.* in 1969 (30) and others thereafter (149, 194, 308), pointed to the important correlation between atherosclerotic susceptibility and shear stress, by means of plaque deposition in areas with increased particle residence time. Accordingly, when oscillatory shear stress, ECs express higher levels of NF-κB and concomitant VCAM-1, ICAM-1 and E-selectin, triggering a more sensitive response to fatty streak formation.

Contrarily, areas with laminar flow, are relatively resistant to atherosclerosis and have a more restricted expression of NF-κB and ECAMs (34, 100, 193).

Furthermore, Sims (260) has studied the elastic lamina in the human coronary artery, where lipids and macrophages accumulate in fragmented regions of it; meanwhile in the internal mammary artery, the internal elastic lamina is closely applied to the endothelium without notable discontinuities and therefore the artery is atherosclerosis-resistant. These results are in accordance with the evidence of increased permeability in atherosclerotic-prone areas even before lesion development (11, 185). Whether these findings are attributable to hemodynamic differences alone or to variations in the inherent properties of these vessels is not yet clear.

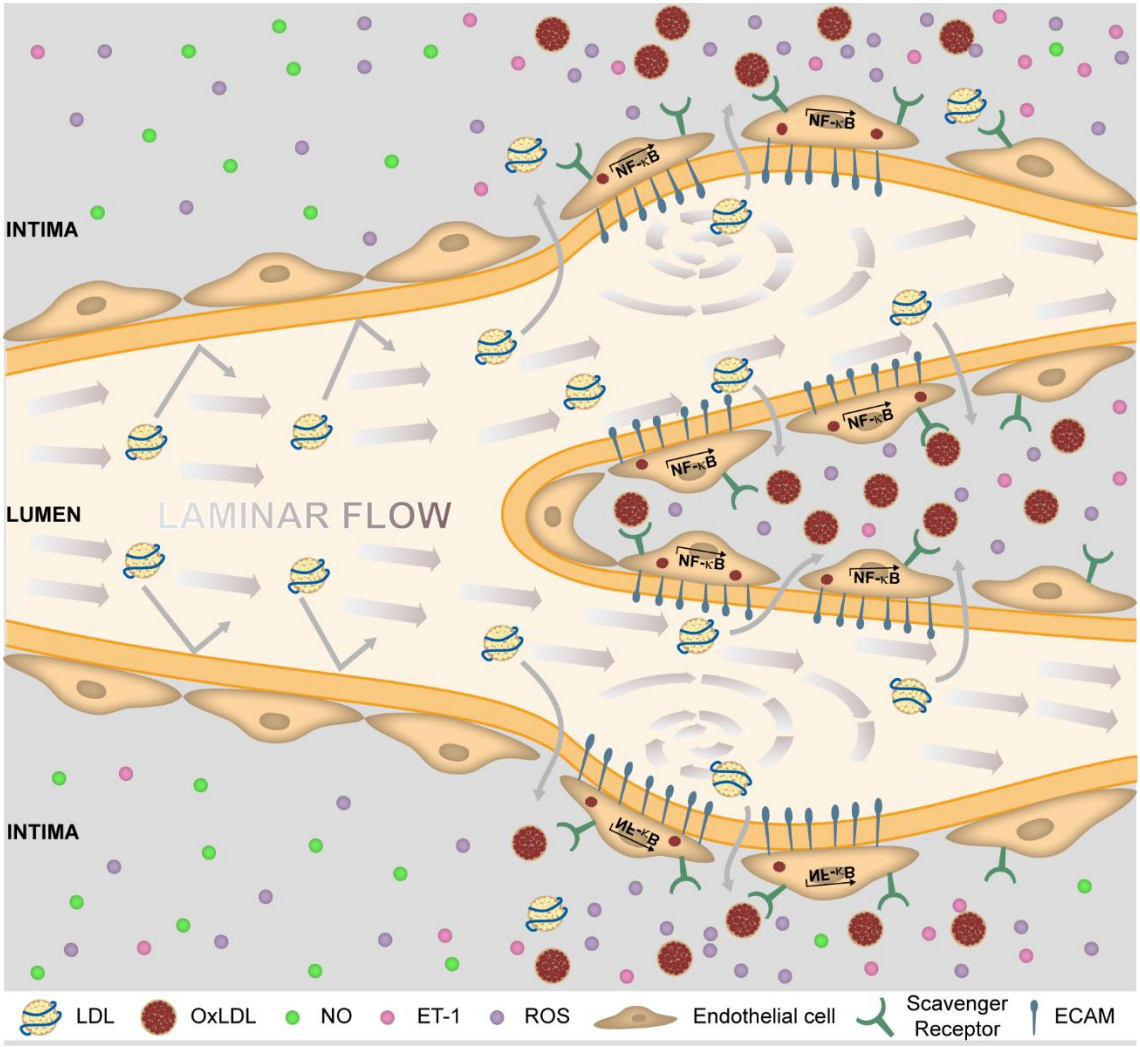

Figure 10. Role of oxLDL and shear stress in endothelial dysfunction. The tractive force of fluid flow (shear stress), is sensed by the endothelium that induce the release of vasoactive factors (i.e. nitic oxygen, NO) and the expression of genes affecting vascular function and structure. The response to physiological laminar flow and disturbed flow (such as that observed at bends, branches,

and bifurcations) is quite different and the response activated by disturbed flow predisposes to atherogenesis. Increased EC permeability has been simplified to EC intercellular spaces formation.

It is clear thereof that balance between pro-oxidant and antioxidant elements may determine the likelihood of developing atherosclerosis at a particular vascular site and that this balance is influenced by shear stress magnitude and oscillation (46, 103, 264). Other balances among adhesion molecules, chemoattractant molecules, cytokines, growth factors, and survival factors all potentially play a role in either promoting or inhibiting the process of atherosclerosis at any given vascular site.

1.2.3.2. Mobilization of Innate Immunity to the Site of Inflammation.

The discussion so far has mainly focused on the links between cholesterol accumulation and inflammatory responses in atherosclerotic plaques; however, another important connection occurs at the level of the bone marrow.

Blood monocyte and neutrophil numbers are strongly associated with atherosclerotic cardiovascular disease in human populations (43), and studies in animal models indicate a causal relationship (233, 273), which suggests that the excessive production of inflammatory cells in the bone marrow and spleen under hypercholesteraemic conditions and further release of this excess of leukocytes to the circulation, is important in the atherogenic process (60, 65, 204, 229, 274).

Leukocyte recruitment into sites of inflammation is a tightly regulated process where adhesion molecules and chemokines play crucial roles. The nature of the inflammatory stimulus will determine whether lymphocytes, monocytes, neutrophils, or eosinophils predominate and accordingly, high receptivity to distinct combinations of molecular signals will be under demand in the different leukocyte classes and lymphocyte subpopulations so as to trigger the appropriate selective response.

Although further expanded in the past decade, the original model of leukocyte adhesion into vascular tissues proposed three critical steps: selectin-mediated rolling, chemokine-triggered activation and integrin-dependent arrest (26, 265) (Figure 11).

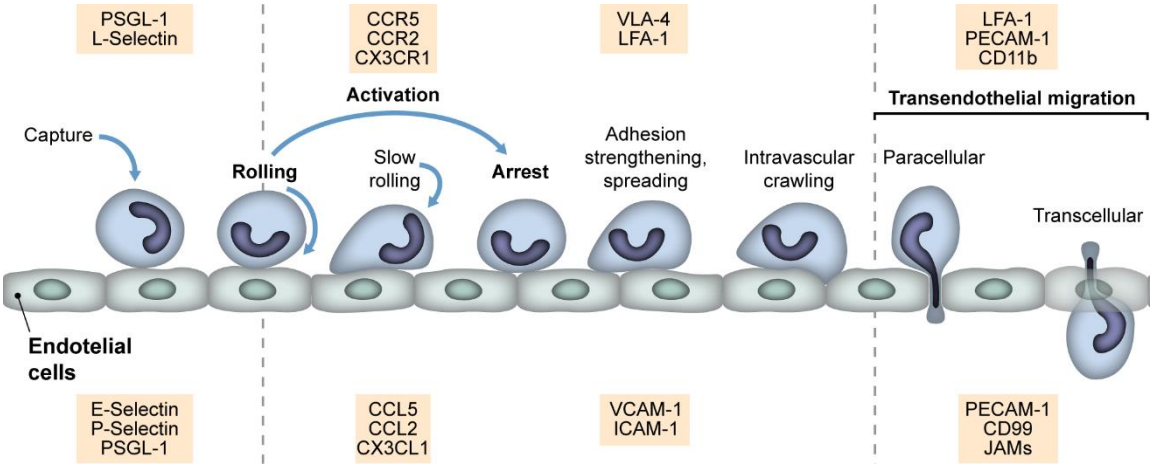

Figure 11. The leukocyte adhesion cascade. The original three steps are shown in bold: rolling, which is mediated by selectins, activation, which is mediated by chemokines, and arrest, which is mediated by integrins. Progress has been made in defining additional steps: capture (or tethering), slow rolling, adhesion strengthening and spreading, intravascular crawling, and paracellular and transcellular transmigration. Key molecules involved in each step are indicated in boxes: upper panels are molecules leukocyte-related and panels in the lower part refer to ECs. Adapted from (79).

Initial Selectin-Dependent Rolling.

Rolling greatly slows the transit of leukocytes and lymphocytes through inflamed vessels by getting new bonds formed before the old ones are broken (300), allowing time for the immune cells to sample the local environment or the EC surface for getting activated. It is mediated by endothelial P-selectin, E-selectin and leukocyte L-selectin (126) that interact with P-selectin glycoprotein ligand 1 (PSGL-1) (184) and other glycosylated ligands on leukocytes or ECs correspondingly. This interaction requires, in most of the cases, shear stress to support the adhesion (74, 158).

Chemokine-Dependent Leukocyte Activation and Arrest.

Cytokines are a diverse group of low-molecular weight proteins with over 100 identified so far, clustered into several classes such as the interleukins (IL), chemokines, colony-stimulating factors, tumor necrosis factors (TNF), interferons (IFN) and transforming growth factors (4, 137, 186). Many cytokines are expressed in atherosclerotic plaques and all cells involved in the disease are capable of producing cytokines and responding to them (186).

Chemokines are a large family of structurally related, chemoattractant cytokines that are divided into four subgroups on the basis of the position of the amino terminal cysteine residues (CC, CXC, CX3C, XC) (141, 293, 310). The roles of chemokines in

atherosclerosis, particularly in the recruitment of monocytes and neutrophils, has been reviewed extensively (164, 195, 263, 297) and hence is only briefly addressed here.

Classical chemokines are produced in the dysfunctional endothelium or seeded onto it by cells interacting with the endothelium like platelets. The capture and rolling phase for $Lys6C^+$ monocytes and $Ly6G^+$ neutrophils importantly involves immobilization of CCL5, CCL2 and CX3CL1 on proteoglycans (45) and P- and E-selectins on ECs (30, 40, 43, 101, 115, 150). Classical chemokines are the most powerful physiological activators of integrin-mediated adhesion.

Integrins most relevant to leukocyte arrest belong to the β_1-integrin and β_2-integrin subfamilies that mediate firm leukocyte adhesion. In this regard, monocytes and T-cells preferably (13, 33, 111, 261), roll dependent of endothelial vascular cell-adhesion molecule 1 (VCAM-1) by engaging their cell-surface ligand very late antigen 4 (VLA-4; also known as $\alpha_4\beta_1$-integrin)(13) meanwhile neutrophils use the intercellular adhesion molecule 1 (ICAM-1) to transiently bind to its ligand lymphocyte function-associated antigen 1 (LFA-1; also known as $\alpha_L\beta_2$-integrin) (37, 244).

Transendothelial Cell Migration.

The last step, transmigration across endothelium (164, 265), was not included in the classical adhesion cascade although first described 200 years ago (64) and occurs with minimal disruption of the complex structure of vessel walls.

As summarized in the figure, two major models for leukocyte transendothelial migration (TEM) have been proposed. One involves a traditional paracellular pathway which has been on the main focus (199), where leukocytes migrate across the endothelial monolayer at cell-cell junctions involving ECAMs such as platelet endothelial cell adhesion molecule-1 (PECAM-1) and CD99. The other route of migration is the transcellular pathway that involves TEM of leukocytes at non-junctional locations, or "through" the endothelial cell (73) and it seems that pseudopods extensions mediated by LFA-1– ICAM-1 interactions facilitate leukocyte diapedesis into endothelial cells (ECs).

2. Objectives

To implement this Thesis, the following objectives were undertaken:

- **To obtain the phenotypic and physiological characterization of *ApoE$^{-/-}$Nod1$^{-/-}$ versus ApoE$^{-/-}$* mice at different time points in the context of atherosclerosis development.** Determination of aortic plaque lesion in terms of area, lipid deposition, glucose uptake and composition as well as blood profiling of inflammatory and lipidic parameters.

- **To identify the cellular mechanisms involved in the development of atherosclerosis in *ApoE$^{-/-}$Nod1$^{-/-}$* mice.** Establishment of the cellular origin and the molecular mechanism by which these cells exert the observed effects in NOD1-associated atherosclerosis.

- **To find out endogenous ligands that may contribute to the ligand-specific effects in the NOD1-driven atherosclerosis.**

3. Experimental Procedures

3.1. ANIMAL ETHICS

Animal studies were in accordance with the guidelines of the EU Directive 2010/63/EU and Recommendation 2007/526/EC regarding care of experimental animals, enforced in Spanish law under Real Decreto 53/2013, and approved by the Institutional Ethics Committee.

3.2. MOUSE MODELS AND DIETS

Wild type (*Wt*) mice are relatively atherosclerosis resistant probably due to the fact that all but 20% total cholesterol in plasma of these mice is HDL cholesterol.

On this behalf, murine atherosclerotic models were developed owing to a non-HDL mediated hypercholesterolemia by the genetic ablation of *ApoE* and the LDL receptor (*LDLr*) (87). The advantage of the *ApoE*$^{-/-}$ model is that foam cell lesions firstly appear in the aortic root at 8 to 10 weeks of age and complex vascular lesions can be found beyond 20 weeks of age in animals fed with normal low-fat rodent chow (207). This phenomenon is accelerated by the hyperlipidaemia caused when they are fed with a high fat diet (HFD).

In the current project, C57BL/6 (*Wt*) and *ApoE*$^{-/-}$ mice (226, 313) were obtained from Charles Rivers (JAX mice stock #000664 and 002052, respectively). Briefly, the full-knockout *ApoE* gene is generated by homologous recombination with a neomycin resistance cassette that replaces part of the exon III and part of the intron III of the *ApoE* gene (Figure 12A).

The conventional knockout mouse carrying the constitutive deletion of the gene under study, the homozygous *Nod1*$^{-/-}$ mice (mixed C57BL/6 and 129/C57BL/6 background), had been previously described (32) and were kindly gifted from Dr. Gabriel Núñez (University of Michigan Health System, UMHS, Michigan, USA). These mice were generated by homologous recombination using a targeting construct designed to replace the first and the second coding exons of *Nod1* gene with a neomycin resistance cassette (Figure 12B).

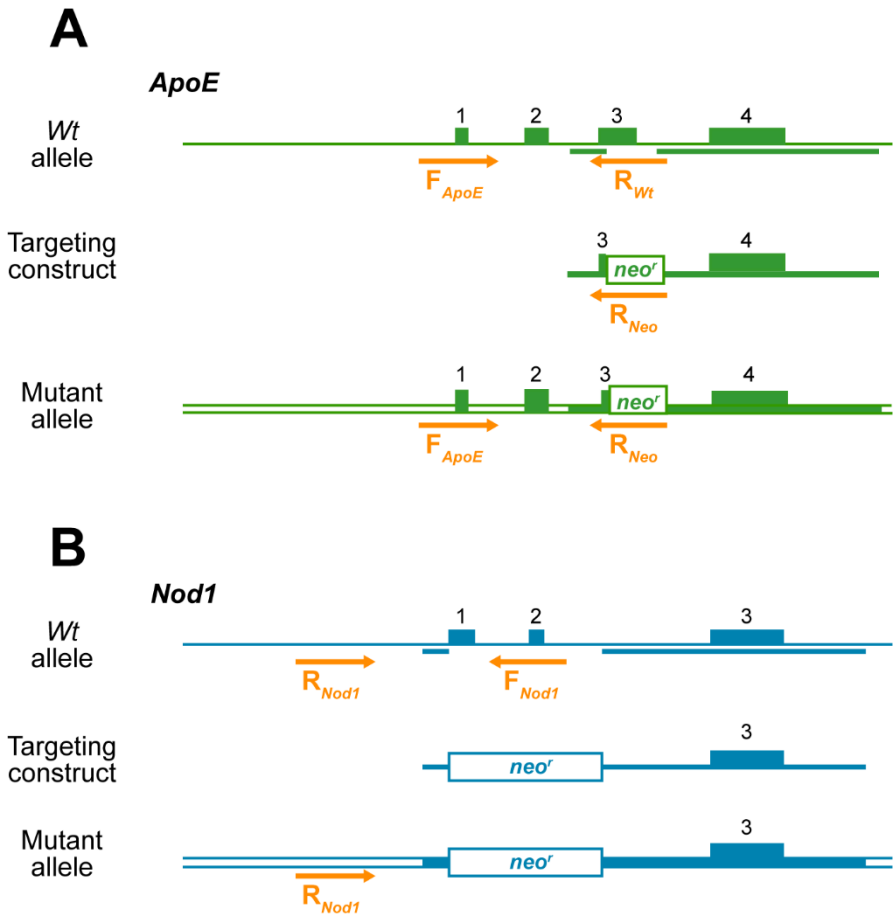

Figure 12. *Nod1* and *ApoE* knockout constructions. Schematic representation of the targeted *ApoE* **(A)** and *Nod1* **(B)** alleles, the gene-targeting construct and the resulting targeted allele. In *ApoE* knkockout gene, the targeting vector was designed to replace part of the exon III and part of the intron III of the *ApoE* gene with a neomycin-resistant (*neo*^{r}) cassette, meanwhile in *Nod1*$^{-/-}$, the *neo*^{r} cassette replaces exons I and II of the wild type *Nod1* mouse gene. Roughly, in the approximate depicted gene positions, arrows represent primers used for genotyping (see Table 1).

Double-knockout *ApoE*$^{-/-}$*Nod1*$^{-/-}$ mice were generated by crossing *ApoE*$^{-/-}$ mice with *Nod1*$^{-/-}$ mice. Heterozygous mice were intercrossed to generate homozygous *ApoE*$^{-/-}$ bearing combinations of *Nod1*$^{+/+}$ and *Nod1*$^{-/-}$ mice at the expected mendelian ratio. All mice were genotyped by polymerase chain reaction (PCR) from ear samples with the primers in Table 1 using standard procedures. The absence of NOD1 expression in cells from *ApoE*$^{-/-}$*Nod1*$^{-/-}$ mice was confirmed by reverse transcriptase-polymerase chain reaction (RT-PCR) analysis (data not shown).

Table 1. Mice Genotyping Primers.

Strain name	Sequence 5' -> 3'	Primer type
***ApoE*$^{-/-}$**	5'-GCCTAGCCGAGGGAGAGCCG-3'	Common (F_{ApoE})
	5'-TGTGACTTGGGAGCTCTGCAGC-3'	Wild type reverse (R_{Wt})
	5'-GCCGCCCCGACTGCATCT-3'	Mutant reverse (R_{Neo})
***Nod1*$^{-/-}$**	5'-GCTTGGCTCCTTTGTCATTG-3'	Wild type forward (F_{Nod1})
	5'-ACTGCTGCTTGGCTTTATTCTC-3'	Wild type reverse (R_{Nod1})

Genomic DNA from *ApoE*$^{-/-}$*Nod1*$^{-/-}$ mice amplified a single band of 245 bp, corresponding to mutant *ApoE* gene, meanwhile from *ApoE*$^{+/+}$*Nod1*$^{+/+}$ mice, two bands of 155 bp and 374 bp were respectively detected for *ApoE* and *Nod1* wild-type alleles. Primer abbreviations refer to those on Figure 12.

All experiments compared *ApoE*$^{-/-}$ mice to *ApoE*$^{-/-}$*Nod1*$^{-/-}$ littermates. In order to accelerate the development of atherosclerotic lesions, at 12 weeks of age, males were placed on HFD (10.7% total fat, 0.75% cholesterol; S8492-E010, Sniff) for 3 or 6 weeks.

3.3. HISTOLOGICAL ANALYSIS AND IMMUNOSTAINING

As previously explained, in *ApoE*$^{-/-}$ mice lesions develop at different rates at each of the atherosclerosis prone sites, being the starting point the aortic valve. Therefore, it is imperative to perform plaque analysis in this region, classically by histological analysis.

To this aim, after mouse cardiac perfusion with PBS supplemented with 5mM of EDTA, mouse hearts were harvested and fixed in 4% paraformaldehyde (PFA) for 24 h at 4ºC, incubated 24h in PBS supplemented with 30% sucrose, embedded in OCT and cryopreserved at -70ºC.

Cryocut cross-sections (5-µm) of aortic roots were evaluated for conventional haematoxylin-eosin (H&E) staining or were processed for immunofluorescence. To avoid specific biases due to potential differences in lesion shape, instead of focusing on a single predetermined region as conventional protocols state (313), cross sections of the entire lesion were analysed and averaged.

For immunostaining, cryo-section samples and endothelial cells were stained with antibodies specific for mouse (Table 2) followed by secondary staining using standard procedures. Secondary antibodies for immunofluorescence were Alexa Fluor 647-conjugated anti-rabbit (Invitrogen), Alexa Fluor 594-conjugated anti-rat (Invitrogen),

FITC-conjugated anti-rat (Sigma-Aldrich), FITC-conjugated anti-goat (Sigma-Aldrich) and Cy3-conjugated anti-Armenian hamster (Jackson ImmunoResearch Laboratories). Nuclei were counter-stained by 4',6-Diamidino-2-phenylindol (DAPI, Life Technologies). Immunofluorescence stainings of cryo-sections were mounted in Prolong Gold Antifade mounting medium (Life Technologies).

Primary control panel was performed with an appropriate isotype control IgG in the same concentration as the primary antibody, to determine the effect of the IgG on non-specific background staining. The secondary control incubations were performed in the absence of primary antibody so as to fix signal threshold for fluorochrome background staining.

Table 2. Primary Antibodies for Immunostaining.

Antibody	Clone	Manufacturer	Catalog number
CD31	MEC 13.3	BD Biosciences	550274
CD54	3E2	BD Biosciences	553250
CD68	Rabbit polyclonal	Abcam	ab125212
Ly6G	1A8	BD Biosciences	551459
SMA	1A4	Sigma	F3777
VCAM-1	112734	R&D Systems	MAB6432

A DM4000 microscope with a 10x/0.40 or a 25x/0.95 water immersion objective (Leica Microsystems) and a Leica DFC 365FX camera were used to capture images. Images were analysed using ImageJ (National Institutes of Health, USA) and were processed for presentation with Leica Qwin Imaging software. Immunofluorescence images for *in vitro* experiments -either on primary endothelial cells or VCAM-1 coated surfaces- were taken using a DMi8 for Live Cell Imaging inverted microscope (Leica Microsystems) and further analysed and processed for presentation with Leica Application Suite X software.

3.4. ATHEROSCLEROTIC LESION ANALYSIS

As the disease progresses, lesions develop gradually downstream throughout the aorta, with uniform ”fatty streaks” that can be nicely stained with fat-soluble dyes such as Oil Red O

($C_{26}H_{24}N_4O$), that stains neutral fats like cholesterol esters and triglycerides. By using this approach, a detailed *en face* morphologic examination of the aortic plaque can be done.

To obtain the aortas for the analysis, firstly, hearts from euthanized mice were perfused through the left ventricle with PBS containing 5mM of EDTA. After fixing in PFA overnight at 4°C, the aortas were thoroughly cleaned to remove all adventitial fat and connective tissue. Aortas were whole-mount stained with 0.2% Oil Red O (Sigma) in 80% methanol, opened longitudinally and pinned to black wax to expose the entire luminal surface.

Images were acquired using a Leica MZ6 SZX10 stereomicroscope (Leica Microsystems, Germany) coupled to a Leica DFC300 digital colour camera (Leica Microsystems, Germany). The planimetric area of atherosclerotic plaques was measured in pixels using ImageJ.

3.5. BONE MARROW TRANSPLANTATION

Many methods can be used to ablate the recipient's immune system. The easiest and most commonly used in experimental models is total-body irradiation (TBI), which is performed by placing the mice in special containers within specifically designed γ-irradiators. The irradiation destroys the recipient's bone marrow containing the precursors of the immune cells. Subsequently, the recipient's bone marrow is reconstituted by either the control or the target bone marrow from the donor animals (63).

Bone marrow (BM) transplantation was performed as previously described (167) (Figure 13). Briefly, 8 weeks-old male *ApoE*$^{-/-}$ and *ApoE*$^{-/-}$*Nod1*$^{-/-}$ mice were irradiated (two same-day doses of 4.5 Gy) and transplanted by intravenous injection through the orbital vein under general anaesthesia of the animal (inhalant isoflurane, Abbott Laboratories). Bone marrow-derived cells (10^7) were obtained from tibias and femurs of euthanized donors *ApoE*$^{-/-}$ or *ApoE*$^{-/-}$*Nod1*$^{-/-}$ mice (refer to 3.9.2.) giving four groups (Table 3).

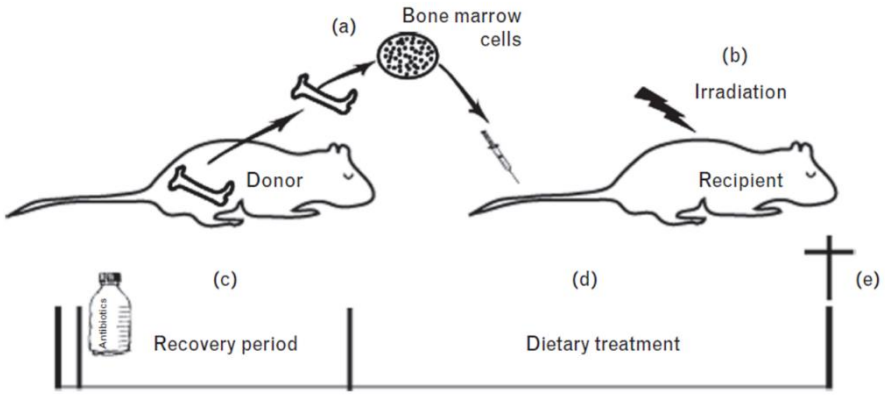

Figure 13. Schematic representation of bone marrow (BM) transplantation experiments. (a) BM cells are collected from tibias and femurs of the donor mouse. (b) The recipient mouse receives these cells after being subjected to a depletion of its own BM cells by irradiation. (c) Before and after the BM transplantation, the mice are treated with antibiotics. They receive a regular chow diet and have a recovery period of 4-6 weeks in which the BM cells from the donor mice repopulate the hematopoietic system of the recipient mouse. (d) After the recovery period, the mice are subjected to high-fat dietary treatment. (e) Harvesting for further studies. Adapted from (6).

Table 3. Bone Marrow Transplantation Groups.

Donor mice	**Recipient mice**	**Transplanted mice**
ApoE$^{-/-}$	*ApoE$^{-/-}$*	*ApoE$^{-/-}$ BM -> ApoE$^{-/-}$* ***(KO > KO)*** **[Control]**
ApoE$^{-/-}$	*ApoE$^{-/-}$Nod1$^{-/-}$*	*ApoE$^{-/-}$ BM -> ApoE$^{-/-}$Nod1$^{-/-}$* ***(KO > DKO)*** **[Experimental]**
ApoE$^{-/-}$Nod1$^{-/-}$	*ApoE$^{-/-}$Nod1$^{-/-}$*	*ApoE$^{-/-}$Nod1$^{-/-}$ BM -> ApoE$^{-/-}$Nod1$^{-/-}$* ***(DKO > DKO)*** **[Control]**
ApoE$^{-/-}$Nod1$^{-/-}$	*ApoE$^{-/-}$*	*ApoE$^{-/-}$Nod1$^{-/-}$ BM -> ApoE$^{-/-}$* ***(DKO > KO)*** **[Experimental]**

After 6 weeks on chow diet, transplanted mice were placed on HFD for 3 weeks. Successful engraftment was confirmed by PCR (data not shown).

3.6. ^{18}F-FDG PET/CT IMAGING

Positron emission tomography (PET) imaging of atherosclerosis using fluorine-18-deoxyglucose (^{18}F-FDG) allows *in vivo* visualization of vascular inflammation and related pathogenic processes, providing a reproducible and quantifiable measure of plaque activity. Normally, PET is combined with an X-ray computed tomography (CT) scanner, which depicts anatomic imaging, allowing the metabolic activity distribution obtained by PET to be precisely aligned into a physical structure. The ^{18}F-FDG, chemically 2-deoxy-2-(^{18}F)fluoro-D-glucose, is the radiopharmaceutical analogue of glucose used in this study.

^{18}F-FDG PET/CT images were acquired by using combined modality PET/CT as previously described (78). Briefly, ^{18}F-FDG (37 MBq/kg; 0.2 mL) was administered intraperitoneally in overnight starved animals to permit blood clearance of glucose and increase signal-to-noise ratio at the expense of sensitivity.

PET/CT imaging was performed in animals under general anaesthesia (inhaled isoflurane) in an INVEON microCT-microSPECT-microPET (Siemens) system for small animals in the SIME service at the Institute of Biomedical Research Alberto Sols (Madrid, Spain).

Dr. Ahmed A. Tawakol and his group in Massachusetts General Hospital (Boston, USA) conducted the data processing and analysis of the ^{18}F-FDG uptake. The parameter for the relative measure of FDG uptake was the standardized uptake value (SUV). According to Kinahan *et al.* (134), in order to decrease variability in SUV measurements, the target-to-background (TBR) ratio was calculated as a quotient between the maximum SUV (SUV_{max}) of 5 regions of interest in the descending aorta corrected by mean SUV in the reference tissue, in our case the paraspinus muscle on the axial view.

3.7. PLASMA LIPOPROTEIN AND INFLAMMATORY MEDIATORS ANALYSIS

The lipid fraction of blood plasma has a profound effect on the development of cardiovascular diseases such as atherosclerosis (182) as well as the inflammatory mediators, which have been shown to enhance the expression of adhesion molecules (282).

To outline the inflammatory profile in blood plasma from our animal models, whole blood was extracted *post-mortem* by cardiac puncture, placed on K3 EDTA treated tubes (Sarstedt) to prevent clotting, and plasma was obtained by centrifugation at 6000 rpm during 10 min at 4ºC. The plasma was then aliquoted and stored at -80ºC for subsequent analysis.

Plasma concentrations of total cholesterol, free cholesterol, LDL-cholesterol, HDL-cholesterol and triglycerides were measured enzymatically using Kinetic colorimetric kits (Spinreact) according to manufacturer's instructions in the Comparative Medicine Unit at the Spanish National Centre for Cardiovascular Research (CNIC, Madrid, Spain).

Mouse inflammatory mediators were detected in plasma using the Milliplex™ Map Mouse Cytokine/Chemokine Magnetic Bead Panel (Millipore) in a Luminex™ 100 IS system

(Luminex) as per manufacturer's specifications in the Flow Cytometry Facility at the National Centre for Biotechnology (Madrid, Spain). The antibody bead kit included: interleukin (IL)-1β, IL-6, monocyte chemoattractant protein-1 (MCP-1/CCL2), chemokine ligand 5 (CCL5/RANTES) and tumor necrosis factor-α (TNF-α).

Data were collected using xMAX Technology (Luminex) software and were analysed using xPONENT 3.1. (Millipore) software. Concentrations of cytokines (pg/mL) were calculated using a standard curve that defined a range or level of quantification. All samples were measured once and three technical replicate were run per sample.

3.8. QUANTITATIVE PCR ANALYSIS

Minimal alterations in the homeostatic levels of messenger RNA (mRNA) and the encoded proteins, result in alterations in essential cellular functions that can lead to disease (298). Therefore, gene expression profiling by quantitative reverse transcription polymerase chain reaction (qRT-PCR) is a pivotal tool in molecular diagnosis and its sensitivity makes it invaluable when it comes to scarce sample sources, like the affected mouse arteries.

To obtain the mouse aortic arches, hearts from euthanized mice were perfused through the left ventricle with PBS RNAse-free (Ambion). After harvesting the aorta, aortic arches were separated and stored in RNAlater (Thermo Fischer Sci.).

Total RNA was isolated by homogenization in QUIAZOL® by a TissueLyser LT and eluted using MinElute columns (Qiagen). RNA integrity was assessed by RNA Nano Chip (Agilent Technologies).

250 ng of RNA were retro-transcribed by using High-Capacity cDNA Reverse Transcription Kit (Applied Bioscience) and real-time qRT-PCR was conducted using a Taqman Gene Expression Assay specific for mouse *Nod1* (1308180; Applied Biosystems).

Calculations were made from measurement of technical triplicates of each sample. The relative amount of mRNA was calculated with the comparative $2^{-\Delta\Delta C_t}$ method using mouse *18S* and *36b4* as control endogenous transcripts.

3.9. CELL PROCEDURES

3.9.1. Mouse Lung Endothelial Cells Isolation and Culture.

Endothelial cells provide a useful research model in many areas of vascular biology. Since its first isolation (179), human umbilical vein endothelial cells (HUVECs) have shown to be convenient, easy to obtain and culture, and thus are the most widely studied ECs. However, not only due to physiology, but also to the need of investigating the cell-specific roles of targeted molecules like in our project, the isolation of ECs from knockout mice has been a must since it provides a useful tool for analysis of protein function *ex vivo*.

Several approaches to isolate and culture vascular ECs of different origin have been reported to date (53, 71, 124, 190), but consistent isolation and culture of pure ECs is still a major technical problem in many laboratories caused by, not only the inherent difficulties associated to long-term primary cell culture, but also by those associated to the time-consuming isolation of pure populations of ECs.

One of the greatest sources of endothelial cells is the pulmonary endothelium, a continuous endothelial monolayer on the luminal surface of the lung vasculature. Therefore, to boost the yield of the primary endothelial cell isolation, we isolated mouse lung endothelial cells (MLECs) from *ApoE*$^{-/-}$*Nod1*$^{-/-}$ and *ApoE*$^{-/-}$ lungs by positive selection using mouse anti-CD102 antibody (3C4 (mIC2/4) clone; cat. No. 553326; BD Biosciences) bound to magnetic beads (Dynabeads®, Invitrogen) as described previously (172).

Subconfluent primary cell cultures underwent then a second round of positive selection using mouse anti-CD31 antibody (MEC 13.3 clone; cat. No. 550274; BD Biosciences). The endothelial cell culture purity was further assessed by flow cytometry (FACSCanto II; Becton Dickinson) for endothelial cell surface markers (VCAM-1 – 112734 clone, R&D- and CD54 -3E2 clone, BD Biosciences-) using standard procedures. This procedure resulted in a ≥99% pure population of endothelial cells.

MLECs were grown on 0.1% gelatine (Sigma) in low-glucose DMEM-F12 (Sigma) supplemented with 20% FBS, endothelial cell growth supplement (ECGS, 50 μg/mL, Sigma) and antibiotics (100 units/mL penicillin and 100 μg/mL streptomycin).

For adhesion-associated studies in endothelial cells, MLECs were treated with 50 μg/mL oxidized LDL (Lipids and Lipoproteins Unit at *Ramon y Cajal* Institute for Sanitary

Research, Madrid, Spain), 10 ng/mL mouse TNF-α (PeproTech) or 1 μg/mL C12-iE-DAP (Invivogen) for 24 hours.

3.9.2. Isolation of Mouse whole Bone Marrow Cells.

Bones not only serve as mechanical support, protection, mobility and mineral storage but also as centre of blood production, in a process known as haematopoiesis. Haematopoiesis takes place in the hematopoietic (red) bone marrow (146) and all cellular blood components, that include erythrocytes, monocytes, myelocytes and lymphocytes, are derived from haematopoietic stem cells (15).

Although monocytes and neutrophils can be easily isolated in large numbers from human blood, this method is suboptimal in mice due to the limited volume of mouse blood that precludes isolation of sufficient cells for functional studies or adoptive transfer experiments. Thus, the bone marrow is a convenient reservoir for harvesting large numbers of either unstimulated or activated leukocytes.

Consequently, whole bone marrow-derived cells from euthanized 8-12 weeks old male mice were used from either *ApoE*$^{-/-}$*Nod1*$^{-/-}$ and *ApoE*$^{-/-}$ mouse genotypes to assess leukocyte- and/or endothelial-dependent adhesion as properly indicated.

Cells were freshly isolated using a modified version from previous reports (271). Briefly, mouse tibias and femurs were flushed with Hank's Balanced Salt Solution (HBSS, Gibco) supplemented with 10 mM Hepes and BSA 0.5% (pH 7.4), with a 27-gauge needle until blanching of bones.

After filtering the cell suspension with a 70 μm cell strainer (Falcon) and further centrifuged at 300g for 5 min at 4ºC; erythrocytes were lysed for 1 min on ice with lysis buffer (150 mM NH_4Cl, 10 mM $KHCO_3$, 0.1 mM EDTA). After this step, hypotonic buffer was carefully removed by washing to avoid bone marrow cell death.

3.9.3. Flow Cytometry of White Blood Cells derived from Peripheral Blood.

Analysis of cell surface phenotype using specific antibodies and flow cytometry is widely accepted as a means to identify and distinguish *ex vivo* cell subsets. Under this premise, we examined the gross of two leukocyte subpopulations of interest, neutrophils and monocytes, in peripheral blood.

To obtain the circulating leukocyte populations in the blood, *ApoE*$^{-/-}$*Nod1*$^{-/-}$ and *ApoE*$^{-/-}$ mice were euthanized and blood was collected in K3 EDTA Tubes (Sarstedt) by cardiac puncture. After mouse bleeding, hearts were perfused (PBS containing 5mM of EDTA).

All single cell suspensions were centrifuged for 5 min at 300g, subjected to red-blood-cell lysis as in 3.9.2. and cell pellets were stained with different antibody cocktails for flow cytometry analysis. Cell populations were discriminated by Table 4 antibody cocktails against mouse and DAPI (Life Technologies) was used to identify dead cells. For cell counting, absolute counting beads were used (CountBright^{TM}, Invitrogen).

Flow cytometry was conducted in a FACSCanto II (Beckton Dickinson). Leukocyte subsets were defined using FlowJo software: neutrophils (CD45^{+}CD115^{-}Ly6G^{+}), inflammatory monocytes (CD45^{+}CD115^{+}CD11b^{+}Ly6C^{+}) and patrolling monocytes (CD45^{+}CD115^{+}CD11b^{+}Ly6C^{-}).

Table 4. Flow Cytometry Conjugated Antibodies.

Antigen	Clone	Fluorophore	Manufacturer
CD11b	M1/70	PeCy7	eBioscience
CD45	30-F11	APCCy7	eBioscience
CD115	AFS98	PE	eBioscience
Ly6C	HK1.4	FITC	Biolegend
Ly6G	RB6-8C5	PerCpCy5.5	Biolegend

This protocol was also used for the corrections in cell adhesion assays by the total amount of neutrophils and monocytes on each mouse after isolation of bone marrow resident cells as described in 3.9.2.

3.10. CELL ADHESION ASSAYS

The following cell adhesion assays are versatile tools for assessing and quantifying cell to cell interactions of endothelial cells with leukocytes under a variety of conditions.

3.10.1. Recombinant VCAM-1.

The soluble mouse VCAM-1 used on *in vitro* adhesion studies is a recombinant form of VCAM-1 produced in a mouse myeloma cell line (R&D systems).

For the flow adhesion assay, 10µg/mL VCAM-1 were used to uniformly coat the flow chamber (µ-Slide $VI^{0.1}$ Uncoated, Ibidi). For the static adhesion assay, 1µg/mL VCAM-1 was used to coat a 96-well flat bottom cell culture plate (Corning).

In both cases, the coating was performed overnight at 4ºC. Unbound sites on the surfaces were then blocked with bovine serum albumin (BSA) 2% for 1 hour at room temperature. Control adherence was measured in wells coated with PBS alone and blocked with BSA 2%.

3.10.2. Adhesion Assays under Static Conditions.

For leukocyte VCAM-1 dependent adhesion assays, *ApoE*$^{-/-}$*Nod1*$^{-/-}$ and *ApoE*$^{-/-}$ bone marrow-derived cells were labelled for Ly6C (Alexa Fluor 488, HK1.4 clone; eBioscience) and Ly6G (PE, 1A8 clone; Biolegend) surface markers and suspended in flow adhesion buffer (complete HBSS supplemented with 1 mM $MgCl_2$, 1 mM $CaCl_2$; pH 7.4).

$2x10^6$ cells/mL were then added to the VCAM-1 pre-coated 96-well plate in triplicate and incubated for 30 min at 37ºC. Afterwards, the cell suspension was removed, the wells were carefully washed and adhered cells were fixed with PFA.

The adhesion of monocytes and neutrophils was quantified as adherent cells per field of view and corrected by the relative amount of isolated neutrophils and macrophages per mice, determined by flow cytometry (refer to 3.9.3.).

For *Nod1*-dependent endothelial adhesion, bone marrow-derived cells from *ApoE*$^{-/-}$ mice were labelled with the same antibodies for Ly6C classical monocytes and Ly6G neutrophils and suspended in the same HBSS buffer to activate ECAMs.

$2x10^6$ leukocytes/mL were added per triplicate to the *ApoE*$^{-/-}$*Nod1*$^{-/-}$ and *ApoE*$^{-/-}$ pre-treated MLECs monolayers and co-cultured for 30 min at 37ºC. After 30 min, the cell suspension was removed, the wells were carefully washed to remove non-adhered leukocytes and adhered cells were fixed with PFA.

The adhesion of monocytes and neutrophils was quantified as adherent leukocytes per field of view in five randomly-selected fields and corrected by the relative amount of neutrophils and macrophages adhered on each experimental control group.

3.10.3. Adhesion Assays under Flow Conditions.

Experimental use of a flow chamber can create an *in vitro* environment with fluid shear stress similar to that observed in the blood vessel environment *in vivo*. The highly controlled environment of the flow chamber allows assessment of leukocyte binding to purified adhesion ligands such as VCAM-1 to facilitate the study of specific receptor-ligand interactions.

Hence, isolated *ApoE*$^{-/-}$*Nod1*$^{-/-}$ and *ApoE*$^{-/-}$ bone marrow cells were labelled for Ly6C (Alexa Fluor 488) and Ly6G (PE) surface epitopes and suspended in flow adhesion buffer. The leukocyte cell suspension concentration was 2x10^6 cells/mL and was kept in dark at 37^{0}C in a water bath until use.

Perfusion was done with a standard infuse/withdraw syringe pump (PHD Ultra, Harvard Apparatus) in a parallel wall flow chamber, VCAM-1 pre-coated. Laminar flow was set up at a shear rate of 1.5 dynes/cm^2, and kept running for 5 min following leukocytes entrance in the flow channel.

Monitoring and recording on video for offline analysis, was performed on a DMi8 for Live Cell Imaging (Leica Microsystems) inverted microscope with Leica Application Suite X software. Eventually, cell suspension was removed from the reservoir, the channel perfused for 3 min with PFA and further washed to remove non-adhered leukocytes.

The adhesion of monocytes and neutrophils to the VCAM-1-coated surface was quantified by counting the number of arrested cells per field of view in each well and corrected by the relative amount of neutrophils and macrophages on each mouse, assessed on the perfused solution by flow cytometry as described in 3.9.3.

3.11. INTRAVITAL MICROSCOPY

Intravital imaging is an invaluable tool that enables *in vivo* visualization of dynamic processes in a variety of contexts at subcellular and sub-second resolutions by using high-speed multichannel epifluorescence and two-photon laser scanning microscopy platforms.

This method enables the visualization of inflammatory phenomena (by using fluorescent probes to track various subsets of inflammatory cells and subcellular structures) within the lumen of not only large blood vessels (such as the carotid artery), but also *vasa vasorum* microvessels like in the cremaster muscle, at high spatial and temporal resolutions in up to four dimensions (183).

Leukocyte-endothelial interactions along the carotid artery and the cremaster microcirculation were analysed in *ApoE*$^{-/-}$*Nod1*$^{-/-}$ and *ApoE*$^{-/-}$ mice that received high-fat diet for 3 weeks.

3.11.1. *In vivo* Imaging of the External Carotid Artery.

The carotid arteries are two large blood vessels that supply oxygenated blood to the large, front part of the brain. Like the arteries that supply blood to the heart -the coronary arteries-, the carotid arteries can also develop atherosclerosis. This hardening of the arteries decreases in the long run the blood flow to the brain and increases the risk of stroke (295).

The common carotid artery runs in the carotid sheath with the internal jugular vein and the vagus nerve. The jugular vein, as it is large, central and relatively superficial, it is often used to place central venous catheters, allowing easy intravenous administration.

In this real-time experimental analysis, the blood flow in carotid arteries from alive animals was recorded under general anaesthesia of the mice (ketamine/xylazine combination at 100 mg/kg mice and 10 mg/kg mice, respectively).

Next, mice were placed in supine position, and the right jugular vein was cannulated with a catheter (PE10, Becton Dickinson) for antibody injection. Antibodies (at 0.5 μg) against Ly6G (PE), Ly6C (AF488), and CD11b (M1/70 clone, 650NC, eBioscience) were administered to label myeloid cell subsets. Antibodies were allowed to circulate for 10 min.

The left external carotid artery, which is one of the two terminal branches of the common carotid artery, was surgically exposed as previously described (263). The exposed tissue was superfused with bicarbonate-buffered saline solution at 37^{0}C.

Intravital microscopy was performed using a BX51 microscope (Olympus) equipped with a 9100-02 EMCCD camera (Hamamatsu Photonics) and a 10x saline immersion objective. For image acquisition and analysis Olympus Cell R software was used.

Rolling flux was determined as the number of cells passing a reference line perpendicular to blood flow within 30 seconds. Monocytes and neutrophils were considered adherent when no rolling was observed for at least 30 seconds.

These experiments were performed in collaboration with Dr. Oliver Soehnlein (*Institut für Prophylaxe und Epidemiologie der Kreislaufkrankheiten* at Ludwig-Maximilians University, IPEK-LMU, Munich, Germany).

3.11.2. *In vivo* Imaging of Microvasculature in the Cremaster Muscle

The cremaster muscle is derived from the internal oblique and transverse abdominus muscles as the testes descend through the inguinal canal (97). It serves to support (the Greek word *cremaster* means suspender) and maintain temperature of the testes. As described below, the cremaster muscle was prepared as a thin flat sheet for outstanding optical resolution.

Primarily, mice were anaesthetised as for the carotid intravital microscopy, and the cremaster surgical exposure was performed as previously described (237). Briefly, the cremaster muscle was first dissected free of surrounding tissues. Once exteriorised, it was placed onto an optical clear viewing pedestal, cut longitudinally with a high temperature surgical cautery (Lifeline Medical) and held extended at the corners of the exposed tissue using surgical suture. To maintain the correct temperature and physiological conditions, the cremaster muscle was perfused continuously with 37^{0}C pre-warmed Tyrode's buffer (139 mM NaCl, 3mM KCl, 17 mM $NaHCO_3$, 12 mM Glucose, 3 mM $CaCl_2$ and 1 mM $MgCl_2$).

10 min prior to start recording the videos, antibodies (at 1 μg) against CD115 (AFS98 clone, APC, Biolegend) and Ly6G (PE) were injected intravenously to label leukocyte subsets. The cremasteric microcirculation was then observed using a DM6000-FS fixed stage fluorescence microscope with an Apo 40x NA 1.0 water-immersion objective equipped with a DFC350-FX camera (Leica Microsystems). Leica LASAF software was employed for acquisition and image processing.

Five randomly-selected arterioles and venules were analysed per mouse, and leukocyte rolling and adhesion were measured as described for the carotid in 150-µm vessel segments for 5 min.

These experiments were implemented in collaboration with Dr. Vicente Andrés (Spanish National Centre for Cardiovascular Research, CNIC, Madrid, Spain).

3.12. STATISTICAL ANALYSIS

All values are expressed as means ± SEM. Statistical calculations were performed using GraphPad Prism 6 (GraphPad Software Inc.). After calculating for normality by D'Agostino-Pearson omnibus test, either a non-parametric test (Mann-Whitney U-test, Kruskal-Wallis test), or a normality test (unpaired Student's t test with Welch's correction, Regular two-way ANOVA with Dunn-Šidák correction) was used as appropriate. Statistical significance was deemed at p values <0.05. Removal of outliers was assessed by ROUT method. Statistical tests and p values are specified for each panel in the respective figure legends. n indicated in the figure legends refers to the number of individual animals for *in vivo* and *ex vivo* assays.

4. Results

4.1. NOD1 IS PRO-ATHEROGENIC AND ITS DELETION PREVENTS EARLY ATHEROSCLEROSIS DEVELOPMENT IN *ApoE*$^{-/-}$ MICE.

4.1.1. *Nod1* is Upregulated in Mouse Atherosclerotic Lesions.

The starting point to decipher whether NOD1 is involved in the physiopathology of atherosclerosis was to assess the expression of *Nod1* at different time points in the process of the lesion development. To that aim, we compared transverse aortic arches from atherosclerotic (*ApoE*$^{-/-}$) mice with non-atherosclerotic (*Wt*) mice fed HFD for 3 and 6 weeks.

Real time qRT-PCR analysis revealed markedly higher *Nod1* gene expression in atherosclerotic vessels than in non-atherosclerotic arteries (Figure 14), meaning that considerable alterations in the homeostatic levels of *Nod1* mRNA and likely their encoded protein, may lead to the development of atherosclerosis. This difference was strongly pronounced (up to 30-fold increase) in advanced inflammatory stages (6 weeks on HFD).

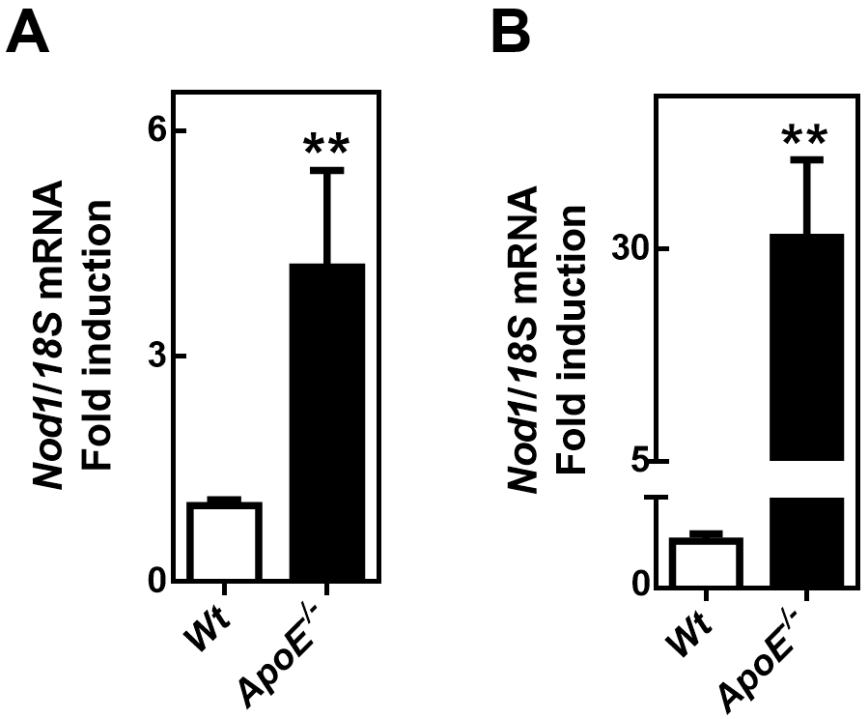

Figure 14. *Nod1* is induced in atherosclerotic mouse arteries. QRT-PCR analysis of *Nod1* mRNA expression in the aortic arch of C57BL/6 (*Wt*) and *ApoE*$^{-/-}$ mice fed with HFD for 3 **(A)** and 6 **(B)** weeks. mRNA amounts were normalized to m*18S* expression (mean ± SEM; n=6 and 10, respectively). Mann-Whitney U-test, $^{**}p < 0.01$.

Due to lack of specificity in commercial monoclonal antibodies against mouse NOD1, differences in *Nod1* mRNA expression are not accompanied by correspondingly differences in protein expression in this work.

4.1.2. *Nod1* Inactivation Reduces Aortic Lesion Burden.

To investigate the contribution of *Nod1* in atherosclerosis we took advantage of the non-invasive ^{18}F-FDG PET/CT imaging technology in our facilities and we applied it to determine the inflammatory extent in aortas from *ApoE*$^{-/-}$ *versus ApoE*$^{-/-}$*Nod1*$^{-/-}$ mice.

The course of an atherosclerotic plaque is largely determined by the activity of macrophages and by using this morpho-functional technique, the vascular ^{18}F-FDG signal mainly indicates increased macrophage activity; *i.e.* inflammation within atherosclerotic plaques correlates with metabolically active pro-inflammatory macrophages accumulating and demanding increased glucose turnover (279).

^{18}F-FDG gamma counts evaluation highlighted a significant decrease in the arterial FDG uptake in *ApoE*$^{-/-}$*Nod1*$^{-/-}$ mice compared to *ApoE*$^{-/-}$ (Figure 15), meaning that *Nod1* deletion evokes a hypometabolic state in the cellular infiltrate of the atherosclerotic tissue. Given this lethargic metabolic rate, atherosclerotic plaques in *ApoE*$^{-/-}$*Nod1*$^{-/-}$ mice might be less vulnerable (281).

Although a defined tendency to increase, no statistical significance intragroup was found concerning the number of weeks on HFD, meaning that vascular inflammation is still low to find out marked differences likely due to the fact that the analysis is performed in the thoracic aorta where lesions at these stages are still naïve.

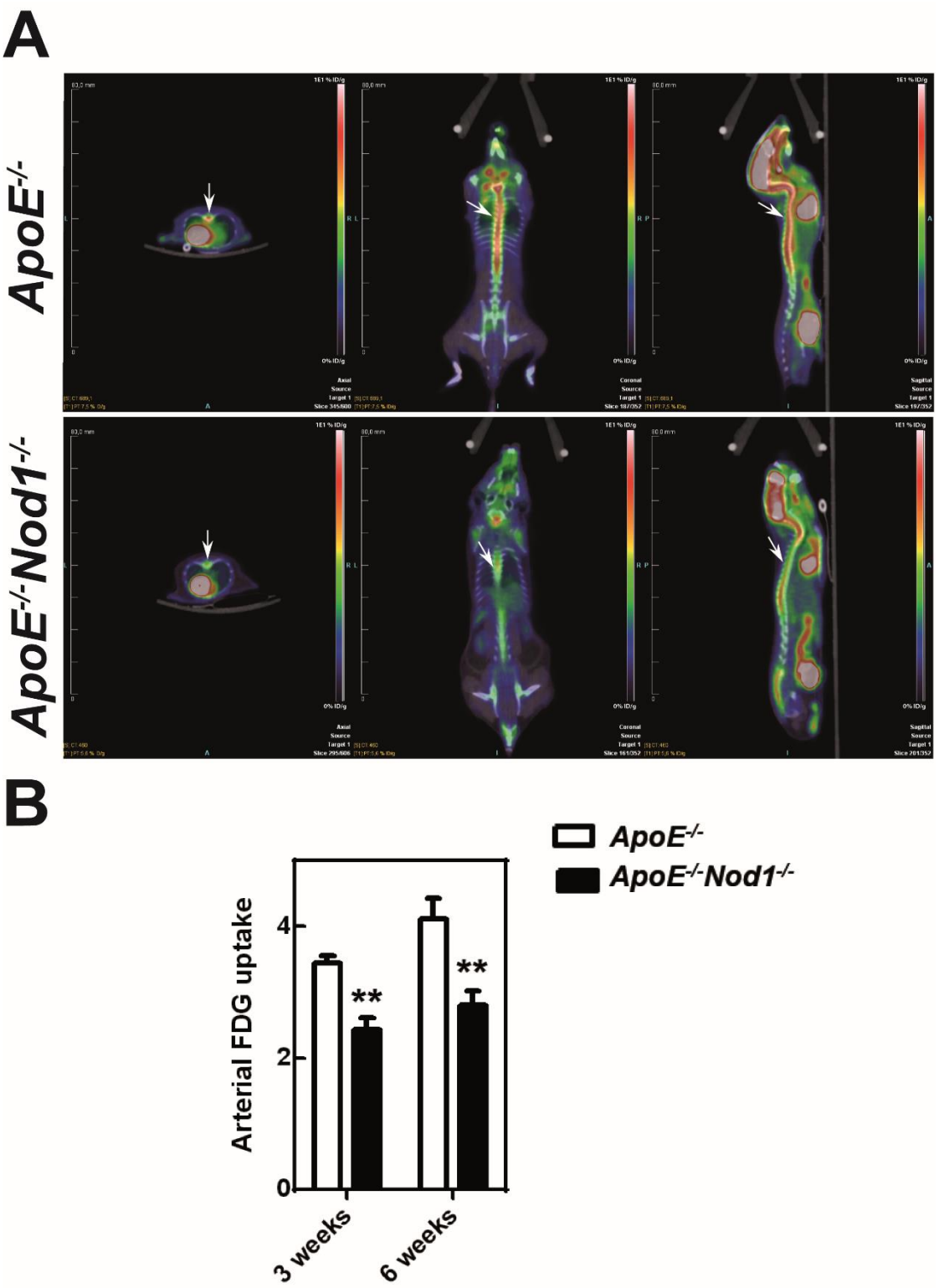

Figure 15. ***Nod1*** **deficiency decreases macrophage activity in aortic lesions. (A)** Representative fused PET-CT images of *ApoE*$^{-/-}$ and *ApoE*$^{-/-}$*Nod1*$^{-/-}$ mice after 6 weeks on HFD. Left, axial section; middle and right, planar and transverse views, respectively. White arrows indicate aortic ^{18}F-FDG uptake (the higher uptake, the reddish). **(B)** Target-to-background (TBR) ratio of arterial ^{18}F-FDG uptake in *ApoE*$^{-/-}$ and *ApoE*$^{-/-}$*Nod1*$^{-/-}$ mice fed a HFD for 3 (n=5; n=8, respectively) and 6 weeks (n=11; n=14, respectively). Results are expressed in means ± SEM. Mann-Whitney U-test (3 weeks) and Student's t-test (6 weeks). $^{**}p < 0.01$.

Nonetheless, low metabolic activity in the inflamed aorta may not be the echo of less plaque artery buildup. Actually, it is the growth of the cholesterol plaques what slowly narrows the vessel lumen and blocks the blood flow deriving in more complex cardiovascular complications linked to atherosclerosis.

To further confirm the hypothesis of the active role of NOD1 in the gross of atherosclerosis, we performed aorta *en face* analysis of Oil Red O (ORO) staining. Atherosclerotic plaques revealed that aortic lesion size in *ApoE*$^{-/-}$*Nod1*$^{-/-}$ mice was significantly smaller than in *ApoE*$^{-/-}$ mice (Figure 16B). Lipids were seen as subendothelial streaks of grape-like clusters of red granules perpendicular to the blood flow, with a heaviest lipid staining in the aortic arch and gradually decreased distally as judged by microscopic examination (Figure 16A).

In order to test the exclusive value of *Nod1* in atherosclerosis and discard any collateral impact from the dietary treatment, we included correspondingly standard diet groups as control groups for 3 and 6 weeks on HFD. Accordingly, both genotype groups presented a significant progressive increase in time of ORO positive staining despite the diet, further confirming the critical role for *Nod1* in atherosclerosis development.

Not only this, but also the percentage of reduction in lesion size was calculated in *ApoE*$^{-/-}$ *Nod1*$^{-/-}$ aortas with respect to the corresponding time point in *ApoE*$^{-/-}$ mice. The impressive ≈75% reduction at 3 weeks on standard diet was significantly decreased as time passed to up to *ca.* 38% at 6 weeks on HFD, meaning that the positive effect of *Nod1* in atherosclerosis is lessened as the disease progresses (Figure 16C).

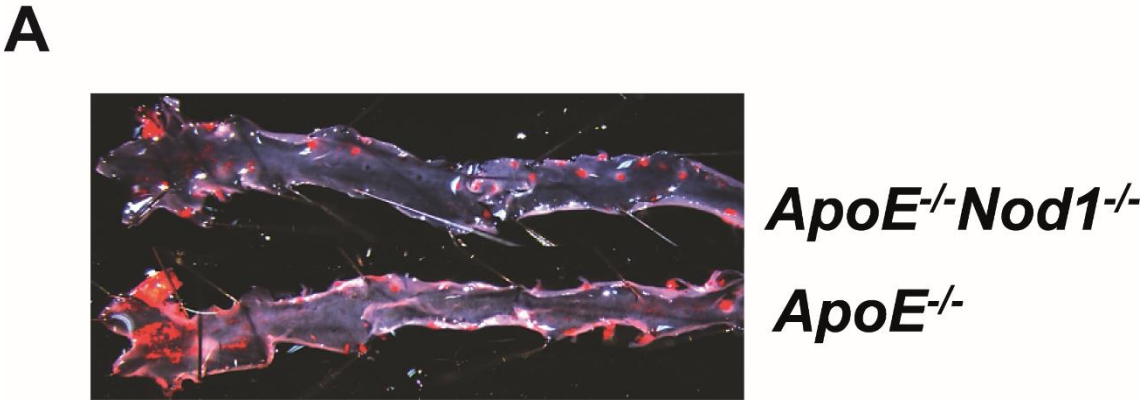

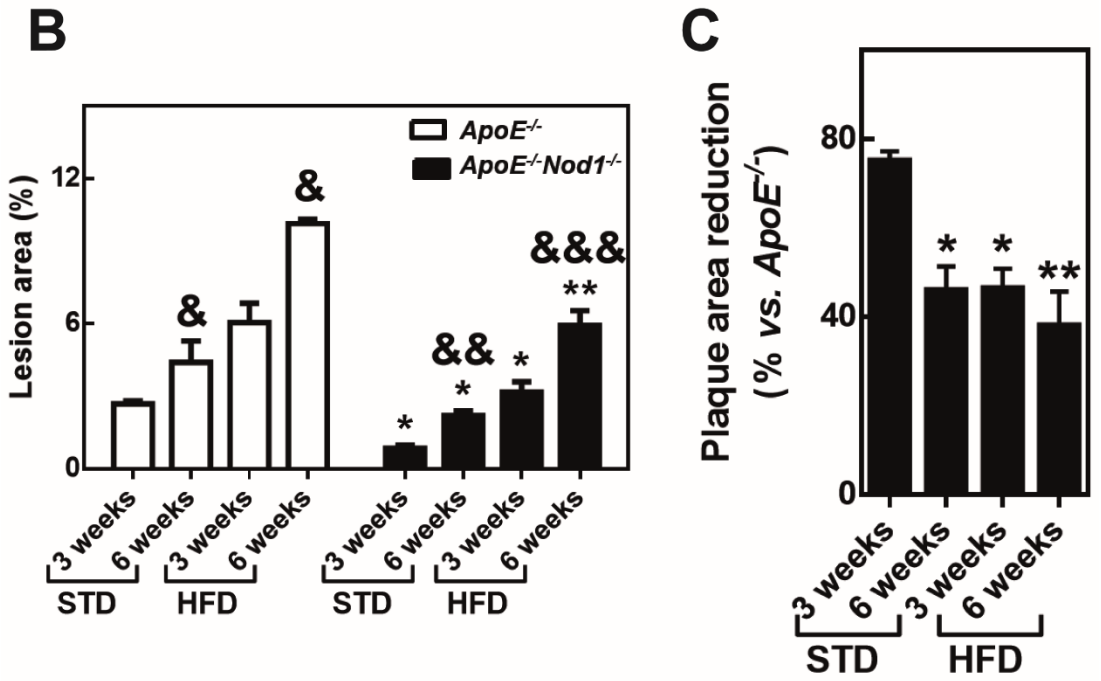

Figure 16. ***Nod1*** **deficiency decreases aortic lesion size. (A)** Representative *en face* Oil red O staining of aortas from *ApoE*$^{-/-}$ and *ApoE*$^{-/-}$*Nod1*$^{-/-}$ mice fed with a HFD for 6 weeks. **(B)** Quantification of lesion area (mean ± SEM) in aortas from *ApoE*$^{-/-}$ (n =5) and *ApoE*$^{-/-}$*Nod1*$^{-/-}$ (n=7) fed with either standard diet (STD) or HFD for 3 and 6 weeks. Mann-Whitney U-test. $^{*}p < 0.05$; $^{**}p < 0.01$ *vs. ApoE*$^{-/-}$; $^{\&}p < 0.05$; $^{\&\&}p < 0.01$; $^{\&\&\&}p < 0.001$ *vs.* 3 weeks. **(C)** Quantification of the percentage in plaque area reduction in the same cohort of *ApoE*$^{-/-}$*Nod1*$^{-/-}$ aortas *vs. ApoE*$^{-/-}$ (mean ± SEM). Kruskal-Wallis test. $^{*}p < 0.05$; $^{**}p < 0.01$ *vs.* 3 weeks on STD.

4.1.3. *Nod1* Plays a Role in Early Stages of Atherosclerosis.

In most, if not all atherosclerosis-prone mouse models, lesion development can be first detected at the aortic sinus. Thus, to further confirm whether NOD1 plays a pivotal role in early stages of atherosclerosis we also compared the lesion area in more advanced atherosclerotic lesions found in the aortic valve.

Under this statement, H&E staining of cross-sections revealed a significantly smaller lesion area at 3 weeks on HFD in *ApoE*$^{-/-}$*Nod1*$^{-/-}$ mice compared to *ApoE*$^{-/-}$ mice, but this decline is almost equalized in advanced stages (6 weeks on HFD) (Figure 17B). At first sight, what we could clearly appreciate are intermediate (at 3 weeks on HFD) and advanced (at 6 weeks on HFD) plaques containing lipidic cores composed either by foam cells or/and cholesterol clefts, respectively (Figure 17A).

These results, together with those from the ORO staining (Figure 16C), point towards the fact that *Nod1* has a crucial role in early stages of the disease. Likely, considering that

atherosclerosis is a complex disease, the accumulation over time of all additive factors may soften the preventive effect of NOD1 in plaque formation.

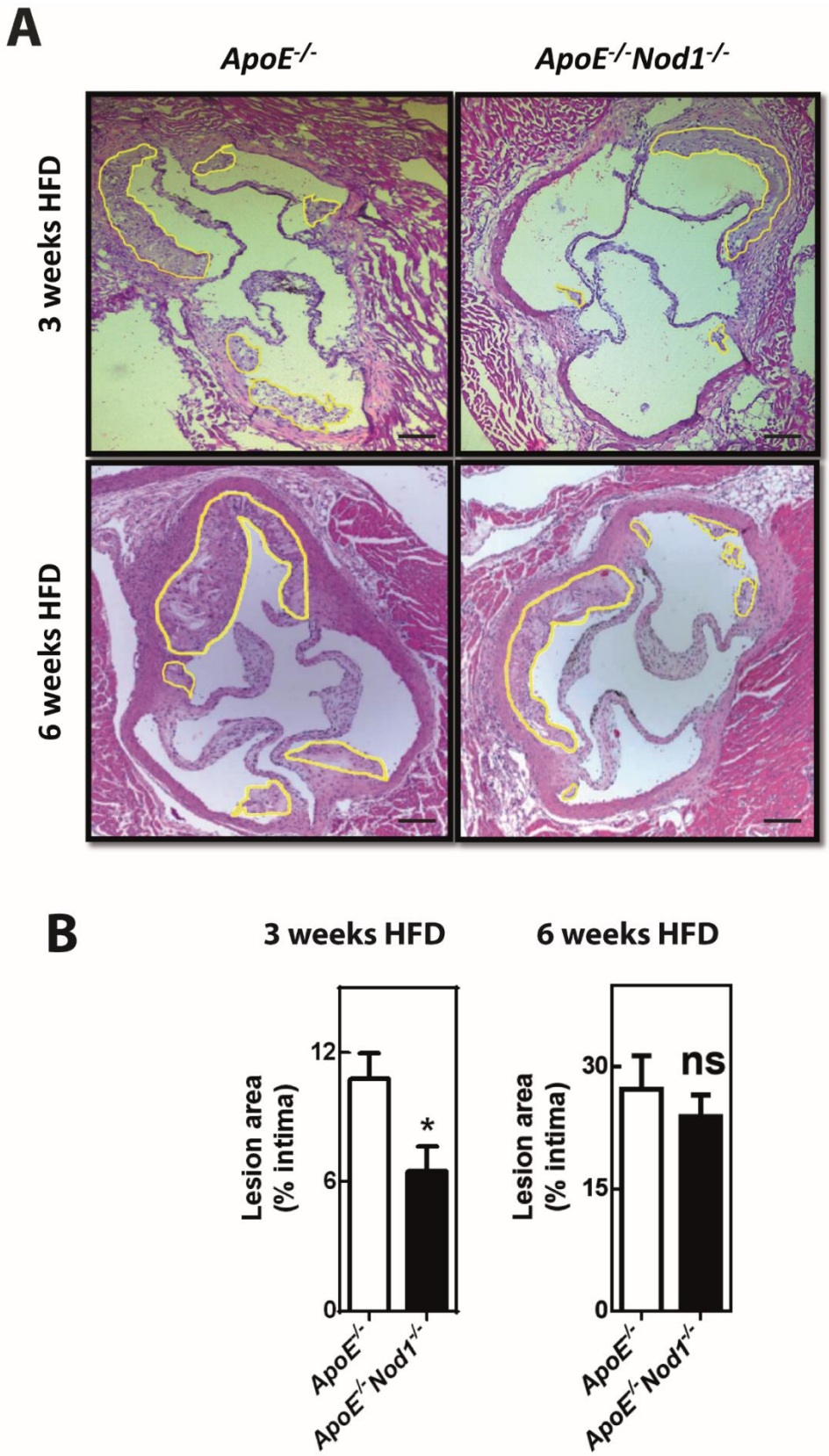

Figure 17. ***Nod1*** **deficiency decreases plaque size in early stages of atherosclerosis. (A)** Representative H&E staining of the aortic sinus in *ApoE*$^{-/-}$*Nod1*$^{-/-}$ and *ApoE*$^{-/-}$ mice on HFD for 3

and 6 weeks. The yellow line outlines the lesion area. Scale bar, 200 μm. **(B)** Quantification of lesion area (mean ± SEM) in the semilunar valve cusps in *ApoE*$^{-/-}$*Nod1*$^{-/-}$ (n=8) mice compared to *ApoE*$^{-/-}$ (n=8) mice fed with HFD for 3 (left panel) and 6 (right panel) weeks. Mann-Whitney U-test. *$p < 0.05$.

Thus, we hereinafter decided to study the role of *Nod1* in early atherosclerosis by using *ApoE*$^{-/-}$ and *ApoE*$^{-/-}$*Nod1*$^{-/-}$mice subjected to treatment with HFD for 3 weeks. We decided to discard the time point with higher rates of improvement (3 weeks on standard diet) because lesions at that time point in *ApoE*$^{-/-}$*Nod1*$^{-/-}$mice were very subtle, what complicated the study.

4.2. *Nod1* DOES NOT AFFECT METABOLITE PROFILING IN *ApoE*$^{-/-}$ BLOOD PLASMA.

4.2.1. *Nod1* Gene Ablation does not Affect HFD-Induced Body Weight nor Lipid Profile.

The APOE plays a central role in lipoprotein metabolism and it is required for the efficient clearance by the liver of both diet-derived chylomicrons and liver-derived VLDL remnants (174). Consequently, *ApoE*$^{-/-}$ mice are not only a practical model of atherosclerosis, but also of hyperlipidaemia, an essential prerequisite in these mice for the development of atherosclerotic lesions. Although extremely rare, but similar to that on *ApoE*$^{-/-}$ mice, humans lacking APOE are reported to have elevated remnant cholesterol in plasma (249).

In addition to its primary site of synthesis in the liver, APOE is also synthesized in peripheral tissues, including adipose tissue (61) what makes *ApoE*$^{-/-}$ mice protected to obesity even when fed cholesterol-rich diets (82).

Under these premises, we aimed at testing whether NOD1 was relevant in the gross of lipoprotein metabolism and found that *ApoE*$^{-/-}$ and *ApoE*$^{-/-}$*Nod1*$^{-/-}$ mice show similar body weight increases after 3 weeks on HFD (Figure 18A), and no significant inter-group differences in plasma concentrations of triglyceride, total and free cholesterol, HDL cholesterol and LDL cholesterol (Figure 18B).

A

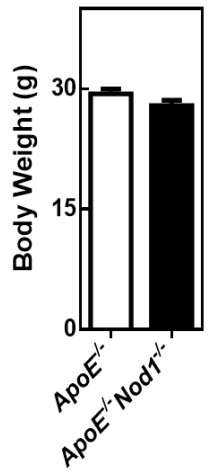

B

mg/dL	*ApoE*$^{-/-}$	*ApoE*$^{-/-}$*Nod1*$^{-/-}$
TGA	34,33 ± 3,74	27,86 ± 4,19
LDL	195,25 ± 21,59	268,20 ± 26,76
HDL	62,07 ± 5,07	99,13 ± 18,22
Total Cholesterol	309,11 ± 36,72	396,98 ± 44,67
Free Cholesterol	204,49 ± 18,83	256,72 ± 23,80

Figure 18. HFD-induced body weight and lipid profile changes are not mediated by *Nod1*. **(A)** Body weight gain of *ApoE*$^{-/-}$ (*Nod1*$^{+/+}$; n=16) and *ApoE*$^{-/-}$ *Nod1*$^{-/-}$ (*Nod1*$^{-/-}$; n=20) mice after 3 weeks on HFD. **(B)** Plasma concentration of triglyceride (TGA), free cholesterol, total cholesterol, HDL and LDL in the same mice after 3 weeks on HFD (means ± SEM). Student's t-test.

Thus, so far our data discard any susceptibility to obesity due to *Nod1* but a real connection to one of its associated complications: atherosclerosis.

4.2.2. *Nod1* Does Not Regulate Pro-Atherogenic Cytokine Secretion.

NOD1 has a consistent role in host responses against bacterial infection (76) and these responses are usually associated with multiple disturbances in intermediary metabolism including hypertriglyceridemia. This raise in serum triglycerides is primarily due to the accumulation of very low density lipoprotein (VLDL) (80) and it is mediated by three cytokines: IL-1, IL-6 and TNF-α (72). Consistent with our previous results, no differences were found in plasmas from our animal groups for none of these three cytokines (Figure 19), further confirming that under an APOE-deficient background, NOD1 does not seem to have any pivotal role on lipid metabolism.

However, in the context of atherosclerosis, chemotactic cytokines (chemokines) and their receptors coordinate communication between peripheral blood cells and the arterial wall, triggering an essential step in the onset and further development of atherosclerosis. Therefore, we measured the plasmatic concentration of CCL5, the major chemoattractant responsible for recruiting monocytes, T cells and neutrophils to the atherosclerotic plaque, as well as CCL2 chemokine, another key player in monocyte recruitment.

Consistent with the previous results given TNF-α, IL-6 and IL-1β also participate in early stages of atherosclerosis (109, 136, 217, 252), and contrary to what Kanno *et al.* postulated (125) for CCL5, no differences in plasma secretion for CCL2 and CCL5 chemokines were found in plasma from *ApoE*$^{-/-}$*Nod1*$^{-/-}$ mice compared to *ApoE*$^{-/-}$ mice when challenged for 3 weeks with HFD.

Given the results, and independently of NOD1, a chronic inflammatory status inherent to the *ApoE*$^{-/-}$ background together with the high-fat dietary treatment will be expected to be found in the blood stream and within the atherosclerotic plaques of both mouse genotypes.

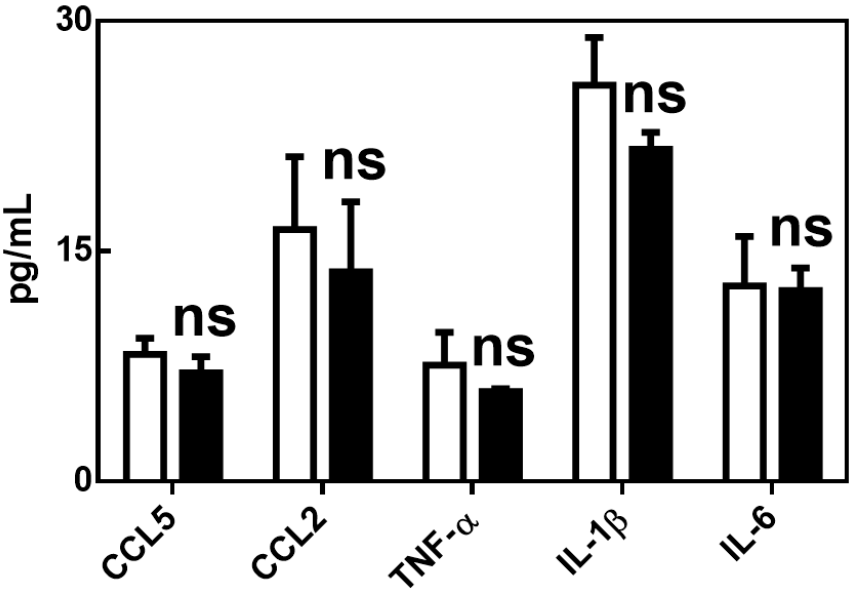

Figure 19. *Nod1* deficiency does not affect plasma cytokines in *ApoE*$^{-/-}$ mice fed with HFD. Plasma was collected in *ApoE*$^{-/-}$ (n=6) and *ApoE*$^{-/-}$ *Nod1*$^{-/-}$ (n=6) mice after 3 weeks on HFD. Plasma concentration of CCL5, IL-1β, IL-6, CCL2 and TNF-α was assessed by multiplex bead-based assay. Data points of cytokine concentrations above detection level were considered and represented (means ± SEM). Mann-Whitney U-test.

4.3. *Nod1* DELETION IMPEDES LEUKOCYTE PLAQUE INFILTRATION.

4.3.1. Atherosclerotic Plaque in Aortic Valves of ApoE$^{-/-}$ *Nod1*$^{-/-}$ Mice has Less Macrophage Content Compared to ApoE$^{-/-}$ mice.

A central feature of inflammatory diseases such as atherosclerosis is the migration of leukocytes from the circulation, across the endothelium to the sub-endothelial space where they become activated by the retained oxLDL.

In order to find out how the immune receptor NOD1 arbitrates between the high inflammatory *milieu* and the decreased atheroma buildup, we further characterized the lesions in the aortic valve of *ApoE*$^{-/-}$*Nod1*$^{-/-}$ mice after 3 weeks on HFD (Figure 20).

Macrophages boost lesion development at the early stage of the disease and drives to the dangerous prospect of lesion rupture and thrombosis in advanced stages (123). Quantification of monocyte/macrophage content in *ApoE*$^{-/-}$*Nod1*$^{-/-}$ atherosclerotic plaques showed a significant reduction in the CD68^{+} lesion area compared to the *ApoE*$^{-/-}$ control group that correlates with the lesser ^{18}F-FDG uptake in 4.1.2. as well as the lesser extent of the disease progression.

Given these results and considering that in the *ApoE*$^{-/-}$ mouse model, hyperlipidaemia induces neutrophilia and the degree of neutrophilia is positively correlated with the extent of early atherosclerotic lesion formation (60), we performed Ly6G staining in the same aortic lesions. However, few or no- neutrophils were found in the analysed lesions (data not shown), probably due to their short life span (270).

Furthermore, in the centre of an atheroma, foam cells and extracellular lipid droplets form a core region, which is surrounded by a cap of smooth muscle cells and a collagen rich matrix (101) that further enlarges and restructures the lesion. As cycles of mononuclear cell accumulation take place, VSMCs migrate from the media to the intima, proliferate, and produce ECM converting the fatty streak into mature fibrofatty atheroma. In our case, no significant differences were found in the smooth muscle α-actin (SMA) positive area in *ApoE*$^{-/-}$*Nod1*$^{-/-}$ mice when compared to their counterparts, probably because at 3 weeks on HFD, our *ApoE*$^{-/-}$ model has still early intermediate lesions composed mainly by foamy lipidic cores.

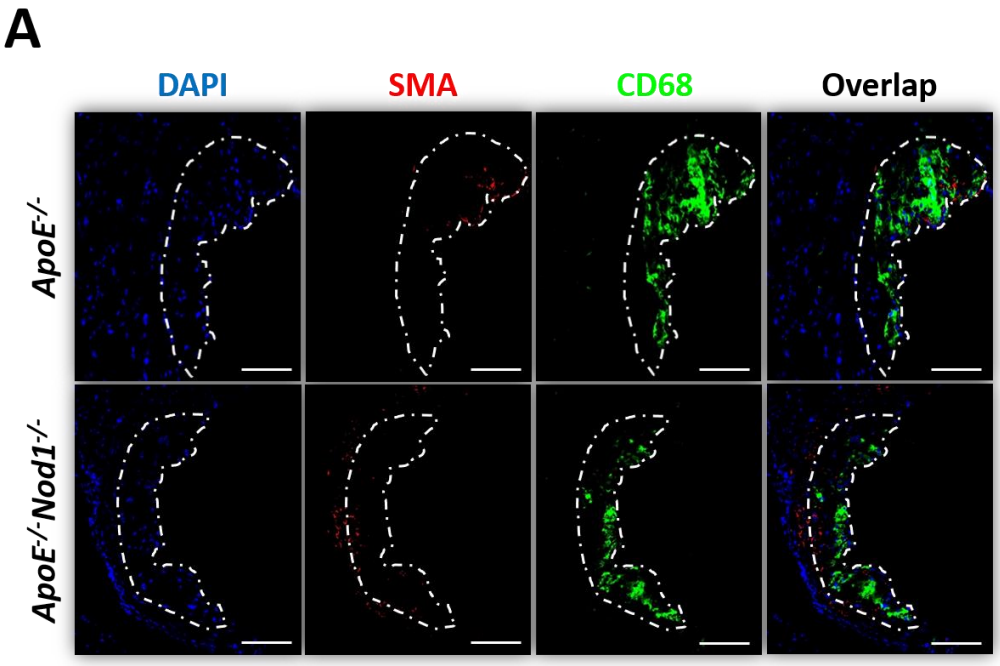

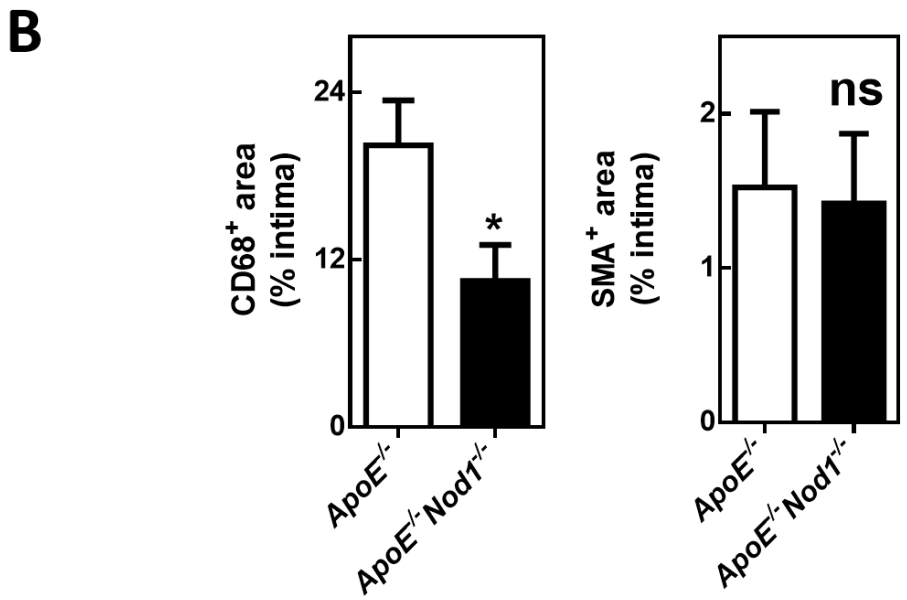

Figure 20. Characterization of *ApoE*$^{-/-}$*Nod1*$^{-/-}$ lesions in the aortic valve. (A) Representative immunofluorescence images of anti-CD68 and anti-SMA. The dotted lines delimit the lesion area. Scale bar, 100μm. **(B)** Quantification of neointimal monocyte/macrophage and VSMC content in lesions on the aortic sinus of ApoE$^{-/-}$ (n=8) and ApoE$^{-/-}$Nod1$^{-/-}$ (n=8) mice fed with HFD for 3 weeks. Graphs represent mean ± SEM. Mann-Whitney U test, $^{*}p < 0.05$.

Considering the results obtained, we wanted to ensure whether the lesser extent in the infiltration of CD68^{+} cells was not due to a decreased number of blood leukocyte subsets in *ApoE*$^{-/-}$*Nod1*$^{-/-}$ mice. In mice, classical Ly6C^{high} cells dominate hyperlipidemia-induced monocytosis, and upon plaque infiltration, they differentiate into macrophages, whereas entry of patrolling Ly6C^{low} monocytes occurs less frequently (272, 276).

Under HFD conditions, blood cell counts for Ly6C^{high} and Ly6C^{low} monocyte subsets were indistinguishable between *ApoE*$^{-/-}$ and *ApoE*$^{-/-}$*Nod1*$^{-/-}$ mice. Similarly, no statistically significant differences were found in the total number of neutrophils in the blood of these mice (Figure 21).

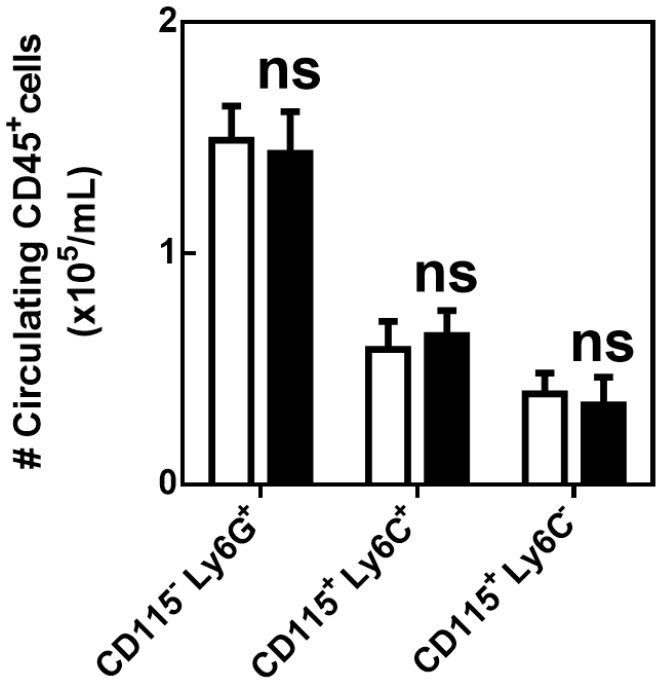

Figure 21. *Nod1* does not mediate HFD-induced blood cell counts changes in *ApoE*$^{-/-}$ mice. Flow cytometry analysis of neutrophils and monocyte subsets in blood cells from *ApoE*$^{-/-}$ (n=7) and *ApoE*$^{-/-}$*Nod1*$^{-/-}$ (n=8) mice after 3 weeks on HFD. Classical and non-classical monocytes were detected based on the expression of Ly6C in CD115^{+} CD11b^{+} cells meanwhile neutrophils were detected based on their CD115^{-} CD11b^{+} Ly6G^{+} expression. Graphs represent mean ± SEM. Student's t-test.

These results together with those obtained for the cytokine profile in 4.2.2. made us evade the focus of this study on the mobilization of leukocytes from the BM and the spleen to the blood (65, 204, 274). Instead, we aimed attention to the cellular mechanisms that account for the lesser infiltration of monocytes and likely neutrophils to the early atheroma and prevents the onset of the disease thereof.

4.3.2. Lack of *Nod1* Impedes Rolling and Adhesion of Inflammatory Neutrophils and Monocytes to the Carotid Bifurcation.

It is the sequential recruitment of circulating platelets, neutrophils and macrophages to the wall vessel (275) that leads to the resulting transmigrated leukocytes in 4.3.1. In this early stage of atherogenesis, it is the endothelial dysfunction what plays a crucial role.

Over the last decades it has become evident that the endothelium is not an inert, single-cell lining covering the internal surface of blood vessels, but in fact plays a crucial role in regulating vascular tone and structure. Importantly, a healthy endothelium maintains a

balance of profibrinolytic and prothrombotic activity (165) that prevents platelet and leukocyte adhesion to the vascular surface. When endothelial dysfunction occurs, the endothelium alteration into a pro-inflammatory phenotype evokes the attachment and the subsequent migration of leukocytes (157).

One of the best methods to visualize in real time and *in vivo* the blood cells interacting with the endothelium within the vessels is the intravital microscopy. Accordingly, by using this methodology, we assessed the rolling and the adhesion of leukocytes to the carotid artery of *ApoE*$^{-/-}$ and *ApoE*$^{-/-}$ *Nod1*$^{-/-}$ mice after 3 weeks on HFD.

We recorded in time the rolling and the adhesion of Ly6G^{+} neutrophils and Ly6C^{+} classical monocytes to the carotid bifurcation in these mice, as well as CD11b^{+} activated-leukocytes. Cluster of differentiation molecule 11B (CD11b), also known as Integrin alpha M (ITGAM), is considered a pan-myeloid marker and it is stored in granules that can be rapidly (within minutes) mobilized to the cell surface of leukocytes following its activation (200). Functionally, CD11b regulates intraluminal crawling of leukocytes to nearby endothelial borders in preparation for extravasation (224, 250).

In *ApoE*$^{-/-}$ *Nod1*$^{-/-}$ mice, we found reduced adhesion of both Ly6C- and Ly6G-labeled leukocytes (Figure 22B). Injection of antibody against CD11b revealed that most of these adherent cells were inflammatory myeloid cells. Their adhesion was found to be significantly diminished in *ApoE*$^{-/-}$ *Nod1*$^{-/-}$ mice compared to *ApoE*$^{-/-}$ littermates. The same tendency was found in the number of rolling leukocytes in the carotid artery (Figure 22A), meaning that *Nod1* seems to play a major role in the leukocyte adhesion cascade to the inflamed artery in atherosclerotic mice.

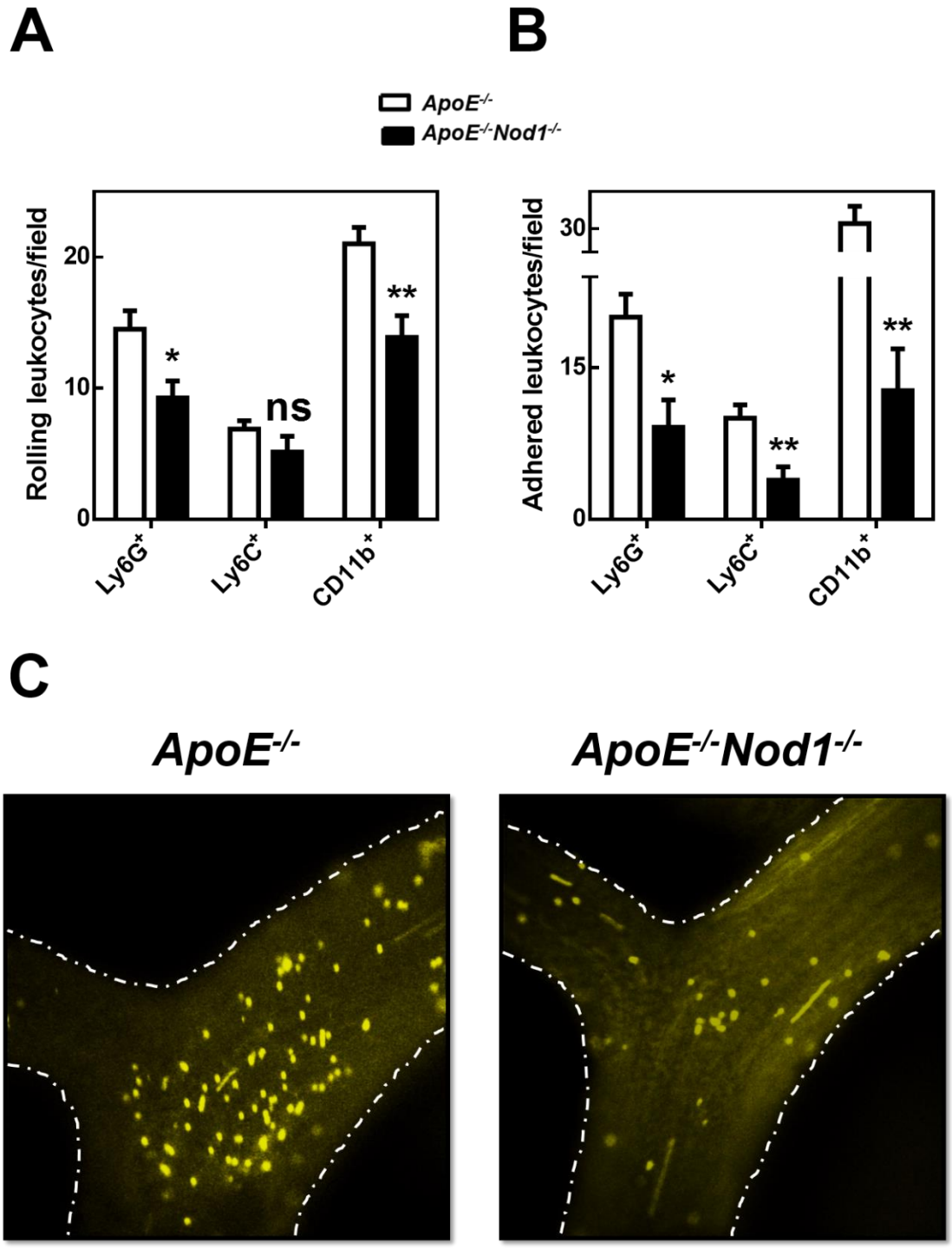

Figure 22. *ApoE*$^{-/-}$*Nod1*$^{-/-}$ monocytes and neutrophils have impaired adhesion and rolling to the carotid artery. Intravital microscopy analysis of monocyte and neutrophil adhesion to the endothelium in the carotid bifurcation from *ApoE*$^{-/-}$ (n=8) and *ApoE*$^{-/-}$*Nod1*$^{-/-}$ (n=8) mice to quantify leukocyte-arteriole wall interactions 3 weeks after HFD. Neutrophils were stained with an anti-Ly6G antibody, classical monocytes with an anti-Ly6C antibody and activated leukocytes with and anti-CD11b antibody (coloured in yellow in **(C)**). **(A)** Quantification of rolling flux for neutrophils, classical monocytes and inflammatory leukocytes and **(B)** the number of these cells adhered to the endothelium. Bars indicate mean ± SEM. Student's t-test, $^{*}p < 0.05$; $^{**}p<0.01$.

In order to extend our observations to other tissues, we also studied by intravital microscopy the behaviour of neutrophils and monocytes in recruitment in the cremaster muscles of mice fed HFD, a microcirculation-based inflammatory model. Consistent with our previous results, rolling and adhesion of these leukocyte subsets to the endothelium were significantly reduced in *ApoE*$^{-/-}$*Nod1*$^{-/-}$ mice when compared to *ApoE*$^{-/-}$ mice in cremasteric post-capillary venules (Figure S1).

This harmony in the leukocyte recruitment pattern to the macro- and microcirculation of *ApoE*$^{-/-}$ mice independently of the tissue, highlights the substantial importance of the genetic ablation of *Nod1* on impairing the peripheral blood leukocyte recruitment to the blood vessels.

4.3.3. Atherosclerotic Plaque in Aortic Valve of *ApoE*$^{-/-}$ *Nod1*$^{-/-}$ Mice has Less VCAM-1 Expression, but Not ICAM-1 Nor PECAM-1, Compared to *ApoE*$^{-/-}$ mice.

In atherosclerosis, the recruitment of specialized leukocytes across the vascular endothelial barrier is mediated by the expression of specific ECAMs. Distinct adhesion molecules appear to regulate different stages of leukocyte immigration at inflammatory sites in a multistep process (85), but those of classical importance are VCAM-1/CD106C, ICAM-1/CD54 and PECAM-1/CD31. Meanwhile VCAM-1 and ICAM-1 mediate flowing cells to firmly adhere to the vessel wall, PECAM-1 is required for leukocyte transendothelial migration (19, 201).

Immunohistochemical staining of the aortic valve in our mouse models, revealed that the adhesion molecule VCAM-1, but not ICAM-1 nor PECAM-1, was expressed to a lesser extent in the endothelium of *ApoE*$^{-/-}$*Nod1*$^{-/-}$ lesions compared to those on *ApoE*$^{-/-}$ mice (Figure 23), both fed HFD for 3 weeks.

Remarkably, less VCAM-1 expression correlates with the less observed leukocyte homing. Taken together, our data suggest that NOD1 signalling in the endothelium promotes myeloid leukocyte recruitment by sustaining the expression of VCAM-1.

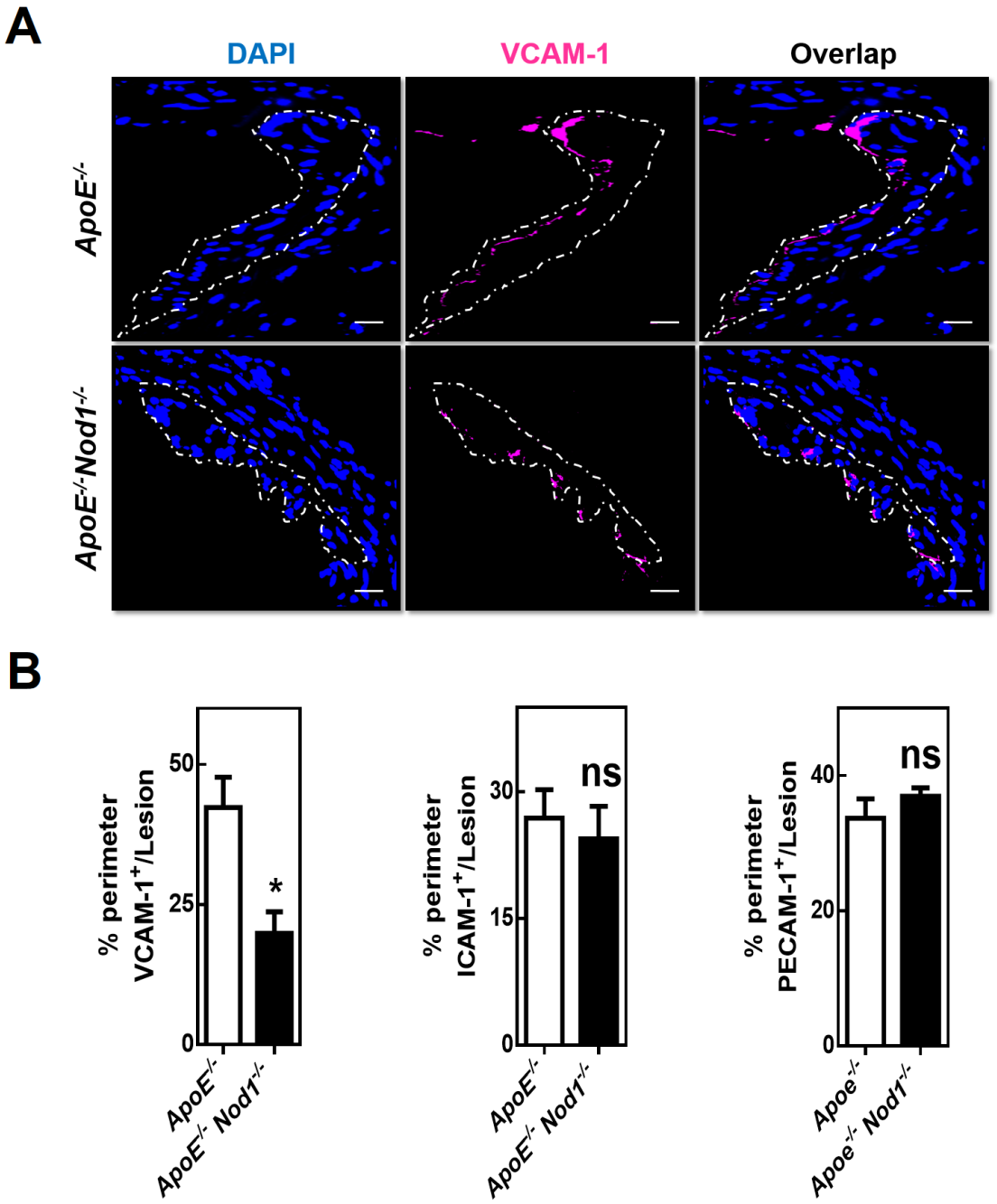

Figure 23. *Nod1* regulates VCAM-1 expression in aortic roots lesions. (A) Representative immunofluorescence images of VCAM-1$^+$ staining and **(B)** quantification of VCAM-1$^+$, ICAM-1$^+$ and PECAM-1$^+$ perimeter in lesions from the aortic sinus of *ApoE*$^{-/-}$ (n=6) and *ApoE*$^{-/-}$*Nod1*$^{-/-}$ mice (n=6) fed HFD for 3 weeks. Graphs represent mean ± SEM. Mann-Whitney U test. The dotted line outlines the lesion area. Scale bar, 100µm.

4.4. NOD1 CONTRIBUTION TO ATHEROSCLEROSIS IS DUE TO NON-HAEMATOPOIETIC CELLS.

Integrin-mediated adhesion of circulating leukocytes to endothelium during inflammation involves multiple adhesion molecules on both leukocytes and endothelium. Leukocytes can circulate as non-adherent cells in the blood stream and, upon activation, they can adhere to

the vascular ECs and migrate into the target tissues via the intercellular junctions between these cells.

So as to differentiate the possible additive contribution of circulating blood cells from that of ECs in the evolution of the atherosclerotic plaque in mice fed 3 weeks HFD, we performed BM transplantation in our *ApoE*$^{-/-}$ and *ApoE*$^{-/-}$*Nod1*$^{-/-}$ mice.

As expected, according to Kanno *et al.* (125), e*n face* analysis of ORO aorta staining revealed markedly larger lesions in *ApoE*$^{-/-}$ mice with *ApoE*$^{-/-}$ BM cells than those of *ApoE*$^{-/-}$ *Nod1*$^{-/-}$ mice transplanted with *ApoE*$^{-/-}$*Nod1*$^{-/-}$ BM (Figure 24). Similarly, in chimeric *ApoE*$^{-/-}$ mice with *ApoE*$^{-/-}$*Nod1*$^{-/-}$ BM cells, the atherosclerotic lesions were significantly larger than those of *ApoE*$^{-/-}$*Nod1*$^{-/-}$ mice transplanted with either *ApoE*$^{-/-}$ or *ApoE*$^{-/-}$*Nod1*$^{-/-}$ BM, meaning that NOD1 expression in BM-derived cells is not critical in the course of atherosclerosis development. Conversely, chimeric *ApoE*$^{-/-}$ *Nod1*$^{-/-}$ mice with *ApoE*$^{-/-}$ BM cells had pretty smaller atherosclerotic lesions than did *ApoE*$^{-/-}$ mice transplanted with either *ApoE*$^{-/-}$ or *ApoE*$^{-/-}$ *Nod1*$^{-/-}$ BM.

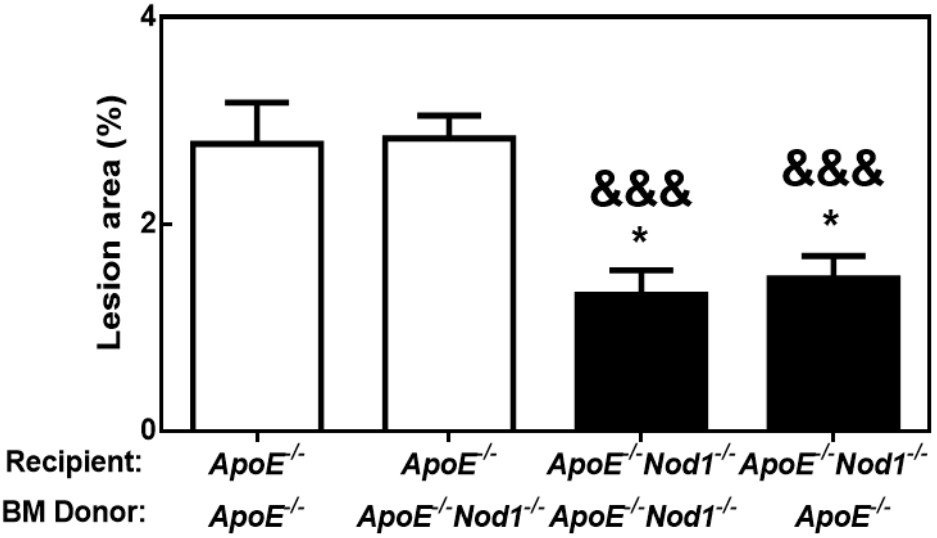

Figure 24. Retardation of atherosclerosis depends on *Nod1* deficiency in non-haematopoietic cells. Quantification of the atherosclerotic lesion areas (mean ± SEM) in aortas from *Apoe*$^{-/-}$ (n=14) and *Apoe*$^{-/-}$ *Nod1*$^{-/-}$ (n=8) mice that underwent BM reconstitution with *Apoe*$^{-/-}$ or *Apoe*$^{-/-}$*Nod1*$^{-/-}$ donors as indicated. All mice groups were fed 3 weeks HFD. Student's t-test, $^{*}p < 0.05$ (*vs. Apoe*$^{-/-}$ control); $^{\&\&\&}p < 0.001$ (*vs. Apoe*$^{-/-}$*Nod1*$^{-/-}$ BM -> *Apoe*$^{-/-}$).

These results point to non–BM-derived cells as key players in a declined development of atherosclerosis in mice lacking expression of *Nod1*.

4.4.1. Deficiency of *Nod1* in Monocytes and Neutrophils does Not Affect VCAM-1 Dependent Adhesion.

The effect of BM transplantation on plaque formation has been suggested (108, 253, 288). Accordingly, we further studied *in vitro* the role of *Nod1* expressly in BM-derived monocytes and neutrophils to rigorously confirm the former statement.

Among the adhesion receptors on immune cells, the integrins $\alpha_4\beta_1$ (VLA-4) and $\alpha_L\beta_2$ (LFA-1) play a major role in the tight adhesion of leukocytes to endothelium. Their main ligands on endothelium are VCAM-1 and ICAM-1, respectively (66, 176).

It had been long thought that VCAM-1 was specific for monocytes. Thus, most studies of neutrophil adhesion had been focusing on its adhesion to ICAM-1 (18). However, in the last decade, the neutrophil adhesion to activated endothelium through the interaction with VCAM-1, came to light (171).

Thus, having confirmed that deficient VCAM-1 expression in ECs likely impairs the monocyte and neutrophil migration to the intima in *ApoE*$^{-/-}$ *Nod1*$^{-/-}$ mice, we aimed to decipher if there was any other dysfunctionality due to the *Nod1* deficiency in both leukocyte subsets in terms of cell arrest to VCAM-1.

For that purpose, we took advantage of laminar flow chamber assays and investigated *in vitro* under flow conditions the role for VCAM-1 in *Nod1*$^{-/-}$ leukocyte adhesion. The activated endothelial monolayer, which *in vivo* will initiate leukocyte recruitment, was mimicked by pre-coating the flow chamber surface with VCAM-1, the ECAM that in our model is the key feature.

Accordingly, leukocytes were perfused over VCAM-1 coated surfaces in a parallel plate flow chamber for 5 min at a shear stress of 1.5 dyne/cm^2 and the number of leukocytes arrested was subsequently assessed. As expected, recombinant VCAM-1 increased the arrest of BM-derived leukocytes as compared with BSA, whereas the number of shear-resistant classical monocytes and neutrophils showed no statistical difference between both *ApoE*$^{-/-}$ and *ApoE*$^{-/-}$ *Nod1*$^{-/-}$ mouse genotypes (Figure 25B). Similar concluding results were obtained when the adhesion of *Nod1*$^{-/-}$ monocytes and neutrophils to plates coated with VCAM-1 was tested under static conditions (Figure S2).

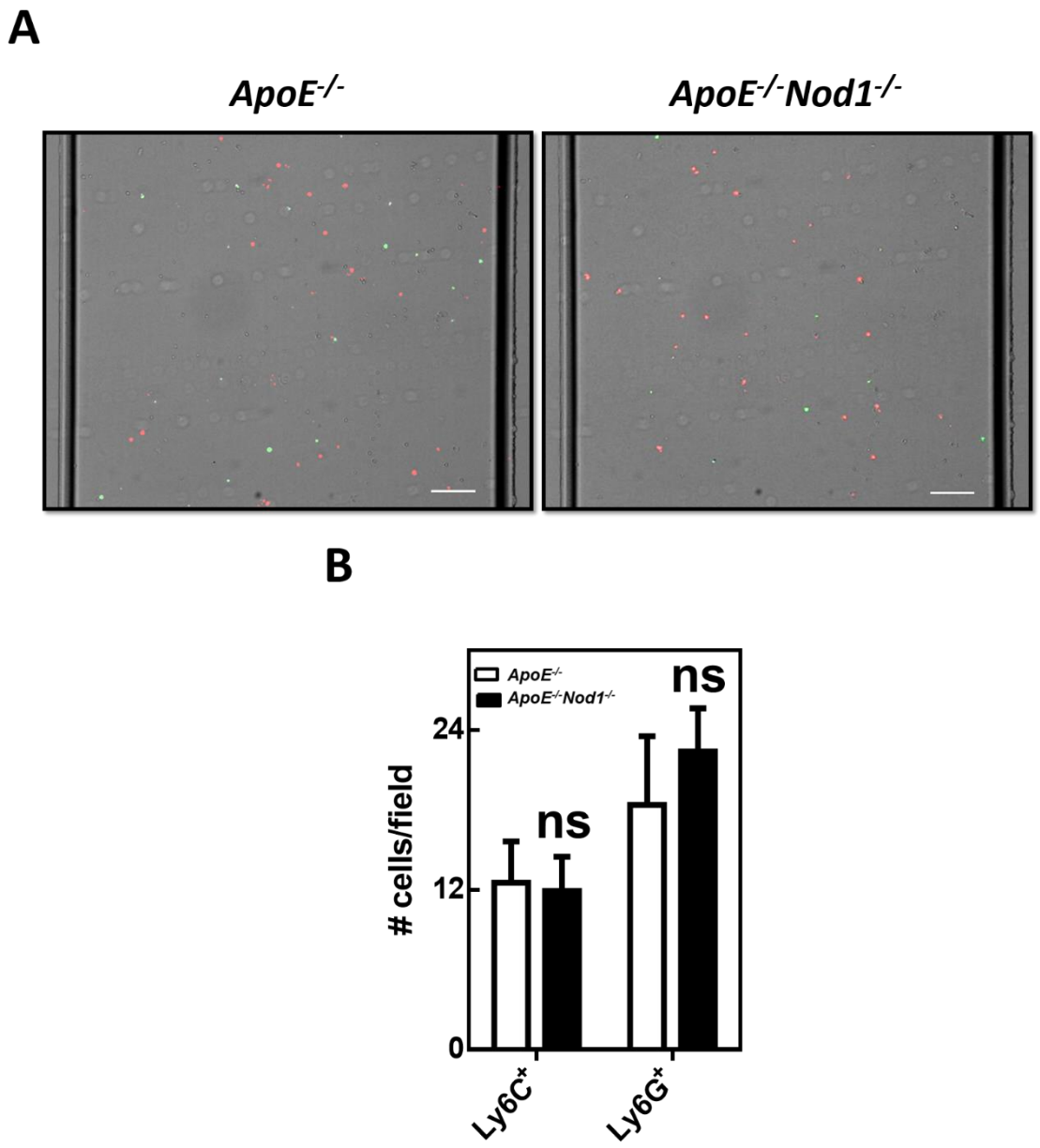

Figure 25. Deficiency of *Nod1* in monocytes and neutrophils does not affect VCAM-1-dependent shear-stress adhesion. (A) BM-derived monocytes and neutrophils from *ApoE*$^{-/-}$ (n=7) and *ApoE*$^{-/-}$ *Nod1*$^{-/-}$ (n=7) mice were isolated and immunolabelled for Ly6C (coloured in green) and Ly6G (coloured in red). VCAM-1 pre-coated ibidi® chambers were used to perfuse for 5 minutes the immunolabelled leukocytes under shear-stress conditions. Scale bar, 200 µm. **(B)** Quantification of Ly6C$^+$ cells and Ly6G$^+$ cells per field is represented (mean ± SEM; Student's t-test). Data was corrected by the corresponding relative number of monocytes or neutrophils perfused per individual mouse.

The results obtained in BM transplantation, together with those obtained *in vitro* on adhesion assays to VCAM-1 coated surfaces, advocate the vascular endothelium to play a key role in our model for the arrest of monocytes and neutrophils to the atherosclerotic plaque. Indeed, it can be ascertained that the NOD1-evoked response upon inactivation

that improves the atherosclerosis prognosis, is primarily due to a defect on the endothelial VCAM-1 expression with no major active support from leukocytes.

4.5. VCAM-1 REDUCED EXPRESSION REGULATED BY *Nod1* IMPEDES LEUKOCYTE ADHESION IN MLECs.

4.5.1. NOD1 Controls VCAM-1 Expression in MLECs and oxLDL is a Potential NOD1 Endogenous Ligand.

Having discarded the counterreceptors for ECAMs expressed on immune cells, we focused all our efforts towards the endothelial phenotype associated with NOD1 that contributes to the VCAM-1 surface expression and subsequent leukocyte arrest to the *ApoE*$^{-/-}$ vasculature.

In inflammatory diseases, VCAM-1 expression is induced by cytokines produced in the tissue, high levels of ROS, oxLDL, 25-hydroxycholesterol, turbulent shear stress, hyperglycaemia, and microbial stimulation of EC TLRs (107, 131, 178, 206, 225, 235).

Herein, we designed a straightforward approach by immunofluorescence staining towards VCAM-1 surface expression where different danger signals in atherosclerosis were tested. However, data of those stimuli that generated statistical differences in VCAM-1 expression concerning presence or absence of *Nod1* will be presented.

The stimuli most commonly accepted by the scientific community so as to induce VCAM-1 expression in vascular ECs is TNF-α (178), which we therein set up as positive control group for a VCAM-1 induced response. Not surprisingly, both *ApoE*$^{-/-}$ and *ApoE*$^{-/-}$ *Nod1*$^{-/-}$ MLECs responded as expected when challenged with this cytokine compared to the non-treated control group (Figure 26), meaning that our cells comprise a good system to further investigate the role of *Nod1* regarding VCAM-1-induced surface expression.

Further conceivably furnish inflammatory stimuli that accentuate atherogenesis might be infectious agents, and herein the axis of the innate immune receptors NODs plays a major role.

Expressly, epidemiological data suggest that the risk of developing atherosclerosis is correlated with chronic infections by various pathogens, including bacteria such as *Chlamydia pneumoniae*, *Helicobacter pylori*, and *Porphyromonas gingivalis* which have been widely linked to the receptor NOD1 (133, 169, 285, 315).

In order to decipher the effect of NOD1 non-sterile activation on the VCAM-1 expression, we took advantage of the synthetic C12-iE-DAP (acetylated γ-D-Glu-mDAP), a dipeptide present in PGN of Gram-negative bacteria and some Gram-positive bacteria which is recognized by and activates NOD1.

The VCAM-1 expression observed in cells treated with TNF-α, is maintained when *Nod1*$^{+/+}$ ECs are activated for NOD1 (iE-DAP). However, this effect is avoided in *Nod1*$^{-/-}$ ECs (Figure 26), what corroborates that iE-DAP is a specific agonist for NOD1. Up to this point, it seems confirmed that NOD1 plays a role in the expression of VCAM-1 in the endothelial monolayer as we have previously observed in the aortic valves of atherosclerotic *ApoE*$^{-/-}$ *Nod1*$^{-/-}$ mice.

Even though the evidence for pathogens as danger signals and inducers of atherosclerosis is profound and consistently increasing, several questions remain to be answered. That is the reason why our appreciation of the real need to discover endogenous antigens to the orphan NOD1 receptor has increased dramatically, aimed to define novel targets for inflammatory diseases therapeutics.

As mentioned before, early features in the pathogenesis of atherosclerosis include accumulation of lipids in the sub-endothelial space that renders the dysfunction of vascular ECs. The best-investigated lipidic product in human atherosclerosis is oxLDL, and it is known that it controls the expression of ECAMs involved in early atherosclerosis, promoting leukocyte recruitment into the vessel wall (131).

On this basis, we tested the response of *ApoE*$^{-/-}$ *Nod1*$^{-/-}$ ECs to oxLDL. As expected, *ApoE*$^{-/-}$ ECs showed increased VCAM-1 expression when primed with oxLDL. However, the expression of VCAM-1 in *ApoE*$^{-/-}$ *Nod1*$^{-/-}$ ECs treated with oxLDL was significantly reduced to levels comparable to the experimental control group (Figure 26). Therefore, here we unveil that the pro-atherogenic oxLDLs may potentially work as NOD1 endogenous ligands that mediate the response through the control of VCAM-1 expression.

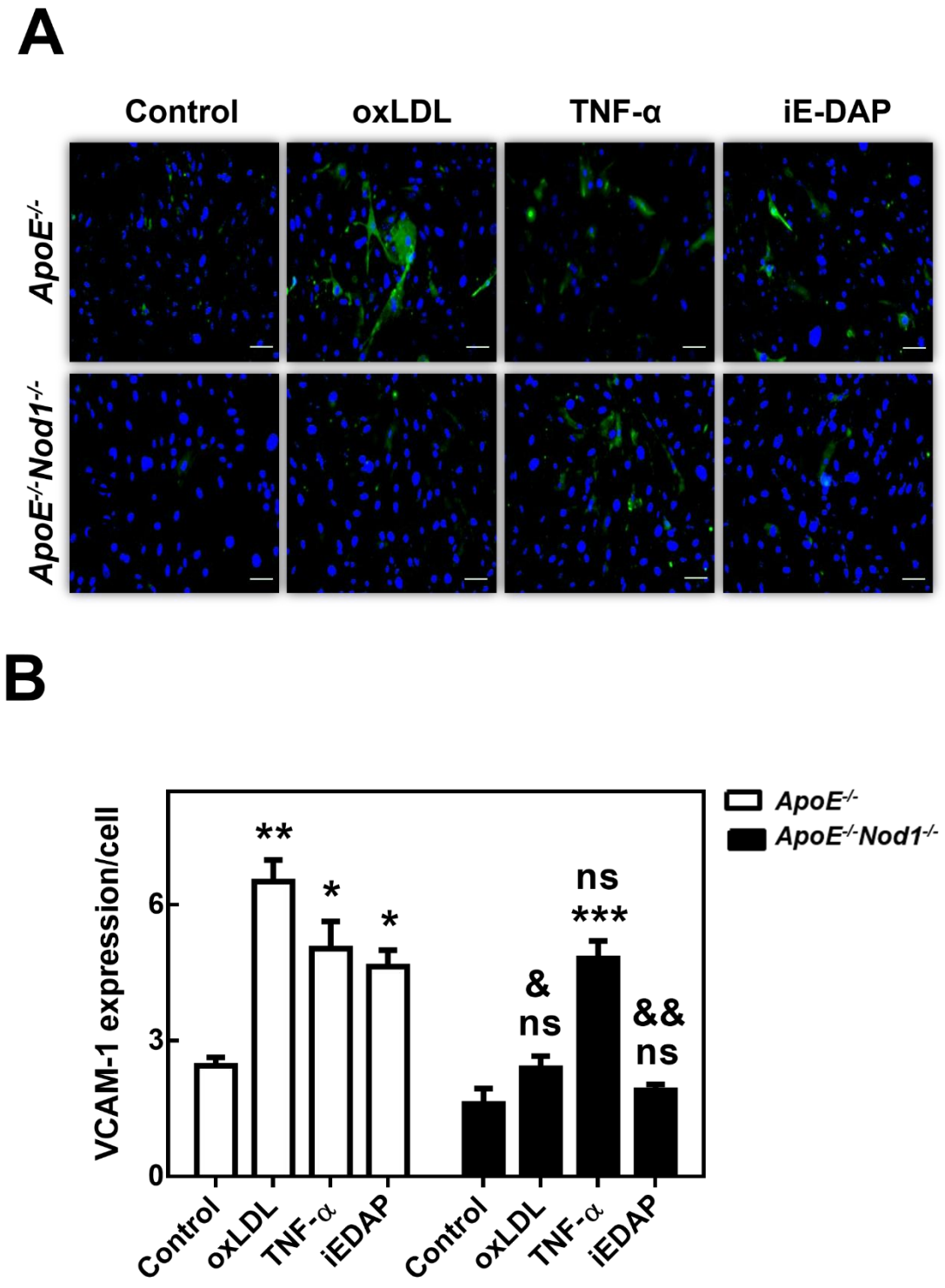

Figure 26. *Nod1* regulates VCAM-1 expression in response to oxLDL and PGN in *ApoE*$^{-/-}$ ECs. Immortalized primary ECs from *ApoE*$^{-/-}$ (n=6) or *ApoE*$^{-/-}$ *Nod1*$^{-/-}$ (n=8) mice were exposed to 50 µg/mL oxLDL, 10 ng/mL TNF-α or 1 µg/mL (C12-)iE-DAP for 24 hours and then immunostained for VCAM-1. **(A)** Representative images and **(B)** quantification of VCAM-1-FITC fluorescence intensity (green) relative to DAPI intensity (blue) are shown in cells stained out of three independent experiments (mean ± SEM). Kruskal-Wallis test, ($^{*}p<0.05$; $^{**}p<0.01$; $^{***}p<0.001$ *vs.* genotype control group) and Mann-Whitney U-test ($^{\&}p<0.05$; $^{\&\&}p<0.01$ *vs.* same condition in *ApoE*$^{-/-}$). Scale bar, 100 µm.

4.5.2. Upon NOD1 activation, Adhesion of BM-Derived Monocyte and Neutrophil to Primary MLECs is Enhanced.

Since enhanced adhesion molecule expression is associated with increased leukocyte adhesion to the endothelium, we analysed if under static conditions and with the same stimuli as in 4.5.1., the decreased VCAM-1 expression observed in *Nod1*$^{-/-}$ MLECs also resulted in reduced classical monocyte and neutrophil adhesion. To this intent, *ApoE*$^{-/-}$ and *ApoE*$^{-/-}$*Nod1*$^{-/-}$ MLECs were left either resting or treated with oxLDL, TNF-α or iE-DAP for 24 hours prior to co-culture with monocytes and neutrophils derived from *ApoE*$^{-/-}$ whole BM.

As expected, when both *ApoE*$^{-/-}$ and *ApoE*$^{-/-}$*Nod1*$^{-/-}$ MLECs were pre-activated with TNF-α, the classical monocyte adhesion together with that of neutrophils was significantly increased compared to the control groups (Figure 27B). Likewise, *ApoE*$^{-/-}$ ECs showed a significantly increased adhesion of both types of leukocytes when pre-treated with either oxLDL -the novel putative NOD1 ligand, and its already-known ligand iE-DAP, suggesting that NOD1 activation is part of the mechanisms contributing to leukocyte recruitment to the endothelial monolayer.

Accordingly, adherence of classical monocytes and neutrophils was not affected in the presence of oxLDL nor iE-DAP in *ApoE*$^{-/-}$*Nod1*$^{-/-}$ MLECs, further confirming that NOD1 may respond to the signalling mediated by modified lipids as well as it does for peptidoglycans.

We hence confirm that NOD1 is highly important in the complex amalgam of regulatory signals that mediate the interaction of leukocytes with vascular ECs in the inflammatory response characteristic of early atherosclerosis. Altogether, we have witnessed strong correlation in ECs between this innate immune receptor and its ability to express VCAM-1 in response to an important regulator of atherogenesis (oxLDL). Our findings therefore strongly support the notion that naturally occurring oxidant signals may sensitize the vasculature to inflammatory signals through modulation of endothelial molecule gene expression.

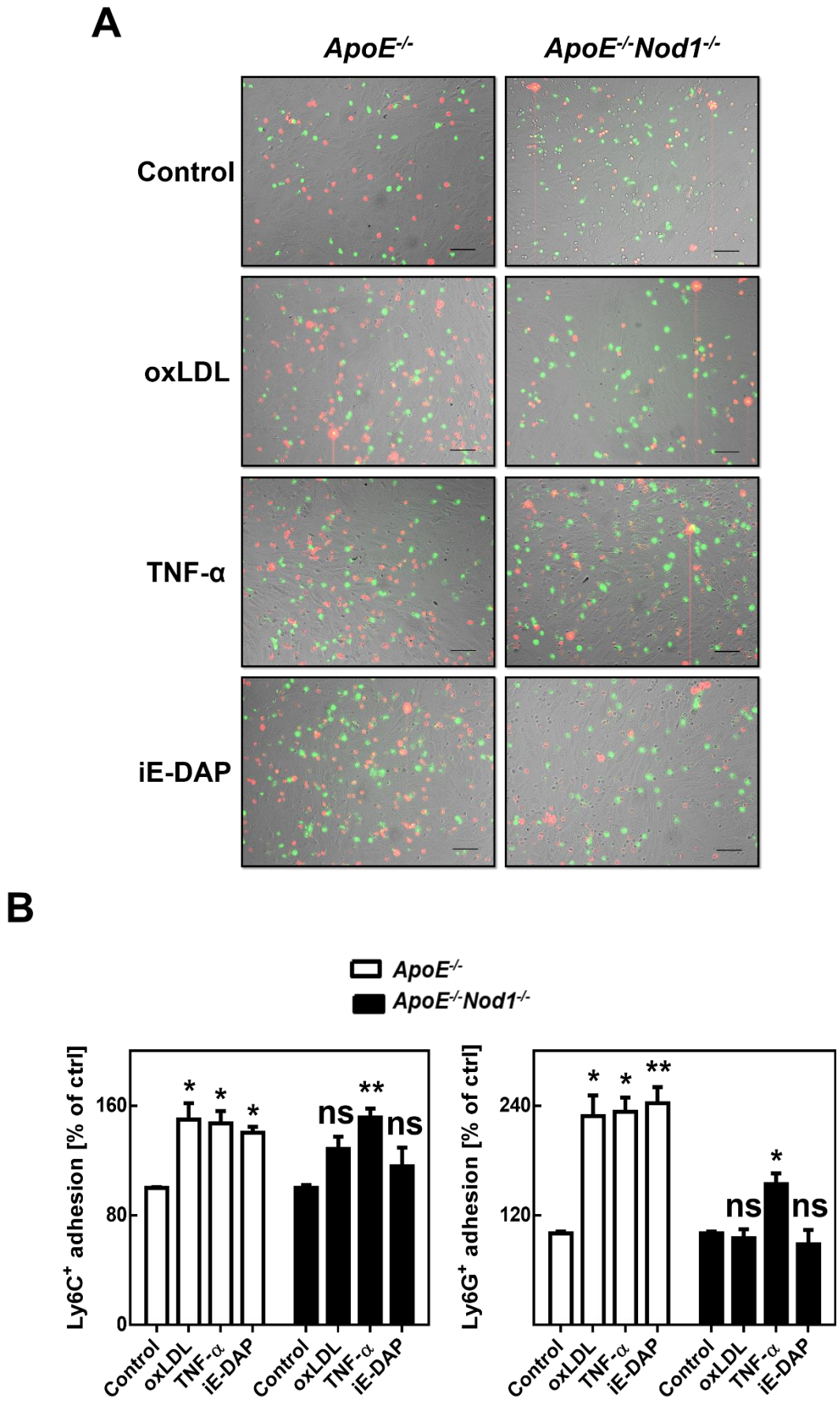

Figure 27. *Nod1* regulates monocyte and neutrophil static adhesion in response to oxLDL and PGN in *ApoE*$^{-/-}$ ECs. Immortalized primary ECs from *ApoE*$^{-/-}$ (n=6) or *ApoE*$^{-/-}$ *Nod1*$^{-/-}$ (n=8) mice

were exposed to 50 μg/mL oxLDL, 10 ng/mL TNF-α or 1 μg/mL (C12-)iE-DAP for 24 hours. Prior to the co-culture, BM-derived monocytes and neutrophils from *ApoE*$^{-/-}$ mice (n=3) were isolated and immunolabelled for Ly6C and Ly6G. **(A)** MLEC monolayers in 96-well plates were co-cultured for 30 minutes with the immunolabelled leukocytes under static conditions. **(B)** Quantification of adhered Ly6C^{+} cells and Ly6G^{+} cells per field of view is represented (mean ± SEM). Kruskal-Wallis test, (*p<0.05; **p<0.01; ***p<0.001 vs. genotype control group). Data was corrected by the corresponding relative number of monocytes or neutrophils adhered to each experimental control group.

5. Discussion

Atherosclerosis is a complex disease involving lipid accumulation and the central participation of ECs, VSMCs, neutrophils and monocyte-derived macrophages.

Our results demonstrate that *Nod1* expression is induced in mouse atherosclerosis and strongly suggest that *Nod1* promotes its outcome at early stages of the disease. In addition, we have identified several mechanisms underlying NOD1-dependent atherosclerosis development. In particular, we have shown that *Nod1* mediates monocyte and neutrophil infiltration into atheromatous lesions through the regulation of *Vcam1* expression in the endothelial monolayer lining blood vessels. Not only this, but here we show for the first time, a potential endogenous agonist for NOD1, the oxLDL particles, atherosclerotic causative danger signals par excellence that regulate the expression of *Vcam1* in ECs and subsequent monocyte and neutrophil firm arrest.

5.1. NOD1 DEFICIENCY PREVENTS ATHEROSCLEROSIS IN EARLY STAGES OF THE DISEASE

Previously, only limited studies have shown *in vivo* the effect of NOD1 in the cardiovascular field (228, 251, 302). Consistent with a previous study (125), here we found that genetic ablation of *Nod1* prevents the early onset of atherosclerosis in *ApoE*$^{-/-}$ mice, independently of cholesterol and triglyceride levels, immune cell counts and pro-inflammatory cytokine profile in blood, providing evidence of a solid relationship between NOD1 and atherosclerosis.

An impressive ≈75% reduction in aortic plaque formation in 15-week-old *ApoE*$^{-/-}$ mice indicates that the contribution of NOD1 to atherogenesis in early stages of the disease is as strong as those of TLR2 and TLR4 suggested by previous studies (105, 189, 202). Nevertheless, the positive impact of *Nod1* deletion in atherosclerosis development in terms of both lesion area and content of extracellular lipids, is weakened as the disease progresses, represented by the still exciting 50 and 40% plaque reduction in the aortas of 12-week-old *ApoE*$^{-/-}$ mice fed HFD for 3 and 6 weeks respectively, and the indistinguishable necrotic lesions in the aortic sinus of the latter *ApoE*$^{-/-}$ and *ApoE*$^{-/-}$*Nod1*$^{-/-}$ mice group.

Given activation of NOD1 in ECs has been found to induce profound increases in the release of the vasodilator NO that controls vascular smooth muscle tone (10, 34), it is likely that decreased production of NO in the *ApoE*$^{-/-}$*Nod1*$^{-/-}$ mouse model, exacerbates

proliferation of VSMCs and subsequent aggravation of the disease (12). That is the reason why our results do not exclude an antagonistic role for NOD1 in VSMCs in later stages of atherogenesis. The eventual production of tissue-specific *Nod1*-targeted mice will help to solve this question.

In any case and taking into account that atherosclerosis is a complex disease, it must be ascertained that the accumulation over time of all additive factors may also soften the preventive effect of NOD1 in plaque formation.

5.2. NOD1 EXERTS ITS ROLE IN PREVENTIVE ATHEROSCLEROSIS THROUGH NON-HAEMATOPOIETIC CELLS

In addition to immune cells, stromal cells of the cardiovascular system sense pathogens and danger signals directly, clearly contributing to the development of atherosclerosis. By transplantation experiments and *in vitro* leukocyte adhesion assays, we certainly proved that the *Nod1* major effector cells in our model of decelerated atherogenesis were non-haematopoietic cells. This is consistent with the observation that in non-haematopoietic cells NOD1 plays a key role not only in the activation of human endothelial cells (84, 211), but also in the complex scenario of vascular inflammation in *C. pneumoniae* sensing (219), a chronic or recurrent infection reported to have a close relationship to the development of atherosclerosis (173).

Alternatively, Levin et al. (163) showed that increased lipid intake in *RIP-2*$^{-/-}$ macrophages resulted in increased atherosclerotic lesions in *ApoB*$^{-/-}$ *LDLr*$^{-/-}$ mice transplanted with *RIP-2*$^{-/-}$ bone marrow. By bone-marrow transplantation experiments, *Nod1* showed no significant difference in plaque formation in our study, and myeloid-specific depletion of *Nod2*, but not *Rip-2*, has shown a significant reduction in the lipid-rich necrotic area in *LDLr*$^{-/-}$ mice (122) but also promoted atherosclerosis due to an accumulation of monocytes/macrophages in the intima of *ApoE*$^{-/-}$ mice (306).

Given a possible cross-talk between NOD2, TLRs and IL-1 receptors in non-T cells through the recruitment of RIP-2 and subsequent activation of the MAPK-signalling pathway (245), it is likely that *Rip-2*$^{-/-}$ macrophages exert their pro-atherogenic effects mainly through the alteration of lipid metabolism upon TLR and/or IL-1 receptors priming rather than classical activation of NOD-mediated NF-κB signalling pathway.

However, further studies on the precise mechanism that exerts the preventive effect of NOD1 and NOD2 in atherosclerosis will bring light to this issue.

5.3. NOD1 PREVENTS ATHEROSCLEROSIS THROUGH THE MODULATION OF VCAM-1 AND CONCOMITANT LEUKOCYTE PLAQUE INFILTRATION

Along these lines, it has been reported that chronic or repeated infection is a strong risk factor for the development and aggravation of atherosclerosis (38, 132, 173, 243) and several studies have shown bacterial PGNs or DNA fragments existing in atherosclerotic plaques (144, 156, 222). Furthermore, the metagenomic analysis of gut microbiome in patients with symptomatic atherosclerotic plaques and healthy controls has proved that patient metagenomes are enriched in genes encoding PGN biosynthesis (129).

Although no clear contribution of PRRs has been described in leukocyte recruitment in response to damage, few studies have pointed towards its potential importance in ECAM expression. In this regard, the TLR signal has been showed as one of the pathways that mediate VCAM-1 expression in response to PGNs in human ECs (162, 212, 311). In turn, with concern to NLRs, it was just recently reported that VCAM-1 and ICAM-1 expression is induced in periodontal fibroblasts in response to *Porphyromonas gingivalis* through NOD1/2-dependent NF-κB signalling pathway (168, 169). Therefore, up to now, little was known whether NODs regulate ECAM expression in ECs.

So far, to the best of our knowledge, this is the first evidence that NOD1 directly contributes to the expression of VCAM-1, but not ICAM-1 nor PECAM-1 *in vitro* and *in vivo*. Besides, provided these results and our real-time *in vivo* observations, it is highly likely that NOD1 participates not in the leukocyte trafficking across the vessel wall, but on the tethering and subsequent rolling of monocytes and neutrophils along it.

Although VCAM-1 and ICAM-1 are members of the same Ig superfamily, VCAM-1 is unique in that its expression is largely restricted to lesions and lesion-predisposed regions, whereas ICAM-1 expression extends into uninvolved aorta and lesion-protected regions (178). This difference in expression patterns relies on the fact that VCAM-1 plays a major role in the initiation of the disease process, explaining thereof the phenotype observed in our model.

Thus, atherosclerosis develops at sites of disturbed flow where emigrating leukocytes have to withstand a shear force many fold higher than in the microcirculation (39). As a consequence, differences in surface display of proteins and glycocalyx composition between both endothelia are accompanied (3, 220). However, in our hands, intravital microscopy in the cremaster microcirculation and carotid bifurcation in *ApoE*$^{-/-}$ mice, yield consistent results pointing to a novel and imperative role of NOD1 in rolling and firm leukocyte adhesion to the inflamed endothelia. Accordingly, the far-reaching significance of the herein identified process, may also extend to other arterial pathologies such as peripheral vascular disease, aneurysm formation or arteritis (40, 95, 161).

Since PGNs from microbiota were recently detected in systemically circulating blood and found to modulate the innate immune system through NOD1 (41), taking all together, systemically circulating PGN fragments from endogenous microbiota may activate vascular endothelial cells through NOD1 to increase VCAM-1 synthesis, promoting accumulation of inflammatory cells in the atherosclerotic-prone sites and eventually accelerating the atherosclerotic formation in vessels.

Although it is still controversial whether *Nod1* deficiency contributes to the alteration of the composition of the gut microbiota (22, 205, 238), further investigation is thereof needed on deciphering the role of the microflora in the acceleration of atherosclerosis through NOD1 activation by influence on nutrient processing and metabolism (142).

5.4. OXIDIZED LDL IS A PUTATIVE NOD1 ENDOGENOUS LIGAND

Several studies involving endogenous ligands towards other PRRs such as TLR2, TLR4, and NLRP3 have been found to be linked to atherosclerosis (62, 128, 215, 218, 262). To date, endogenous NOD1/2 ligands are still unknown, however here we also describe for the first time the putative role of oxLDL as an endogenous NOD1 ligand that likely contributes to the development of atherosclerosis through the modulation of the VCAM-1 expression in ECs.

OxLDL is the best-investigated oxidized product in human atherosclerosis and to date, multiple PRRs belonging mainly to the SRs family have been identified to recognize oxLDL. In short, its recognition depends on specific components of the particle with

modifications of the protein being critical for SR-A1/2 and LOX-1 receptors and modifications of the lipids being critical for CD36 and TLR receptors (192).

In particular, over the past 20 years, abundant evidence has accumulated about the direct pro-inflammatory and pro-atherogenic effects of LPC (lysophophatidylcholine or lysolecithin), a dramatically increased phospholipid component of native LDL upon oxidation. Multiple roles in altering the functions and properties of ECs, monocytes/macrophages, T-lymphocytes, and VSMCs have been associated to LPC (151, 223, 231, 266, 296).

Noteworthy, LPC outstands for being the bioactive component of oxLDL capable of selectively induce VCAM-1 and ICAM-1 expression through NF-κB (17) not only in arterial ECs (153), but also in the microvasculature (248), and modulates leukocyte recruitment to the vascular endothelia thereof. Apart from this, LPC has been shown to massively decrease endothelial NO bioavailability, contributing to vascular dysfunction (145, 299, 309).

Given the molecular pattern that LPC drives in endothelial dysfunction, together with the reported increase in LPC concentration in atherosclerotic arterial lesions of animals fed an atherosclerotic diet (227), could be that the minimal oxLDL epitope that can exert a pro-inflammatory and pro-atherogenic response through NOD1 is LPC. Whether it is LPC the oxLDL-derived bioactive component that exactly triggers the modulation of *Vcam1* expression through NOD1 in ECs remains to be determined.

Likewise, the precise molecular mechanism involved in VCAM-1 regulation by NOD1 signalling upon oxLDL challenge, remains yet to be identified.

NF-κB is a master regulator of inflammatory responses, both in the initial stages of atheroma formation and in the resolution phases (88, 127, 159) through a signalling mechanism in the endothelium (83).

Classical Nod1 signalling pathway activates the NF-κB complex (214) meanwhile activation of *Vcam-1* gene expression is regulated mainly by NF-κB (178). Thus, it is likely that Nod1 activation by oxidized LDLs may trigger the translocation of NF-κB to the nucleus and hence promote the transcription of *Vcam-1*.

However, it has been described that activation of both NOD1 and NF-κB in ECs promotes TNF-α production (84, 98), reported as a classical transcriptional activator of the *Vcam-1* promoter in endothelial cells (178). Even though in HFD conditions, plasmatic levels of pro-inflammatory TNF-α in *ApoE*$^{-/-}$*Nod1*$^{-/-}$ mice did not show any significant difference with respect to *ApoE*$^{-/-}$ mice, we do not exclude that this cytokine may be involved in the signalling dependent of NOD1, due to its short half-life (191). Moreover, feed-forward signalling between TNF receptor (TNFR)/NOD1 and NF-κB may constitute a "priming" mechanism that ensures rapid propagation of the inflammatory response from locally athero-susceptible regions to the rest of the endothelium.

Thus, whether *Vcam-1* upregulation in response to oxLDL is an independent or a synergic mechanism mediated by the production of TNF-α in a NOD1-dependent manner and/or just NOD1 signalling will demand careful consideration (Figure 28).

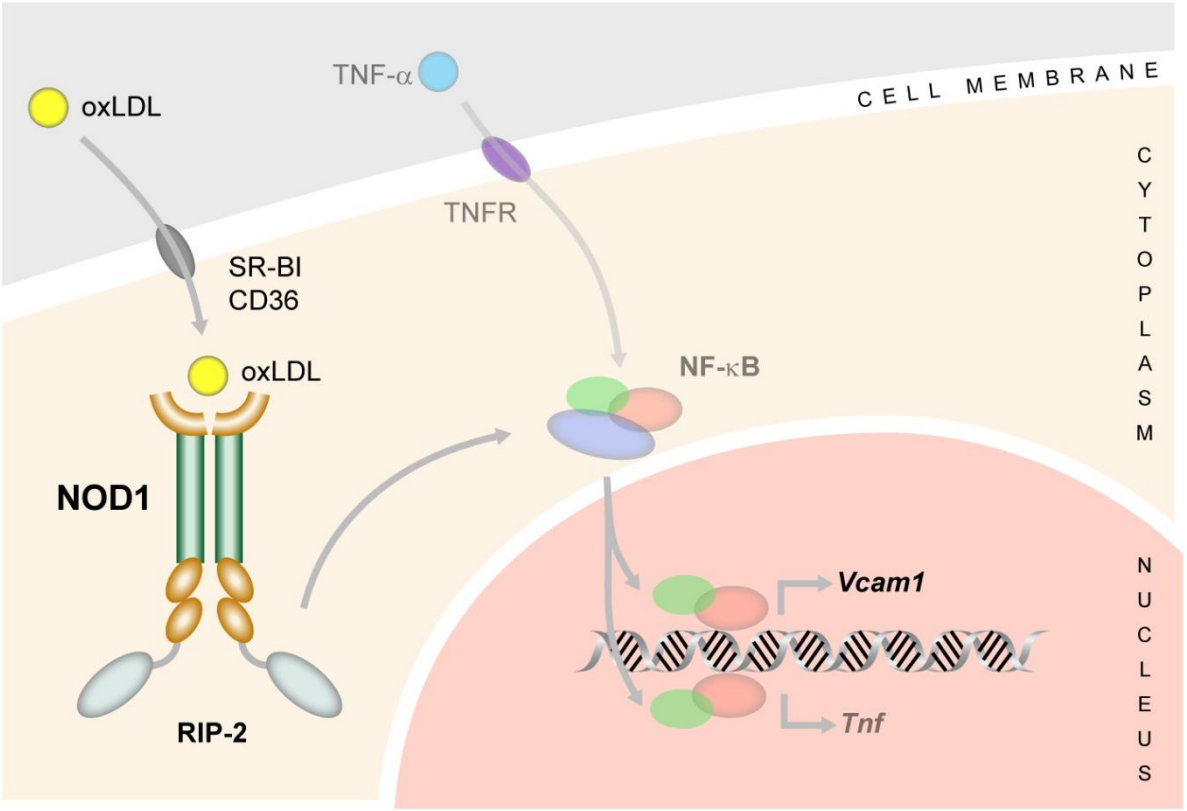

Figure 28. Schematic diagram illustrating the putative NOD1 receptor-binding specificity to oxLDL in ECs and the NF-κB signalling pathway.

5.5. NOD1 AS ATHEROSCLEROSIS DETECTION MARKER AND PHARMACOLOGICAL TARGET

Here we demonstrate that endothelial cell-restricted *Nod1* inactivation leads to a downregulation of the adhesion molecule VCAM-1 and likely other inflammatory mediators in the vessel wall, thereby preventing the recruitment of monocytes and neutrophils into developing plaques, resulting in delayed progression of atherosclerosis in *ApoE*$^{-/-}$ mice (Figure 29).

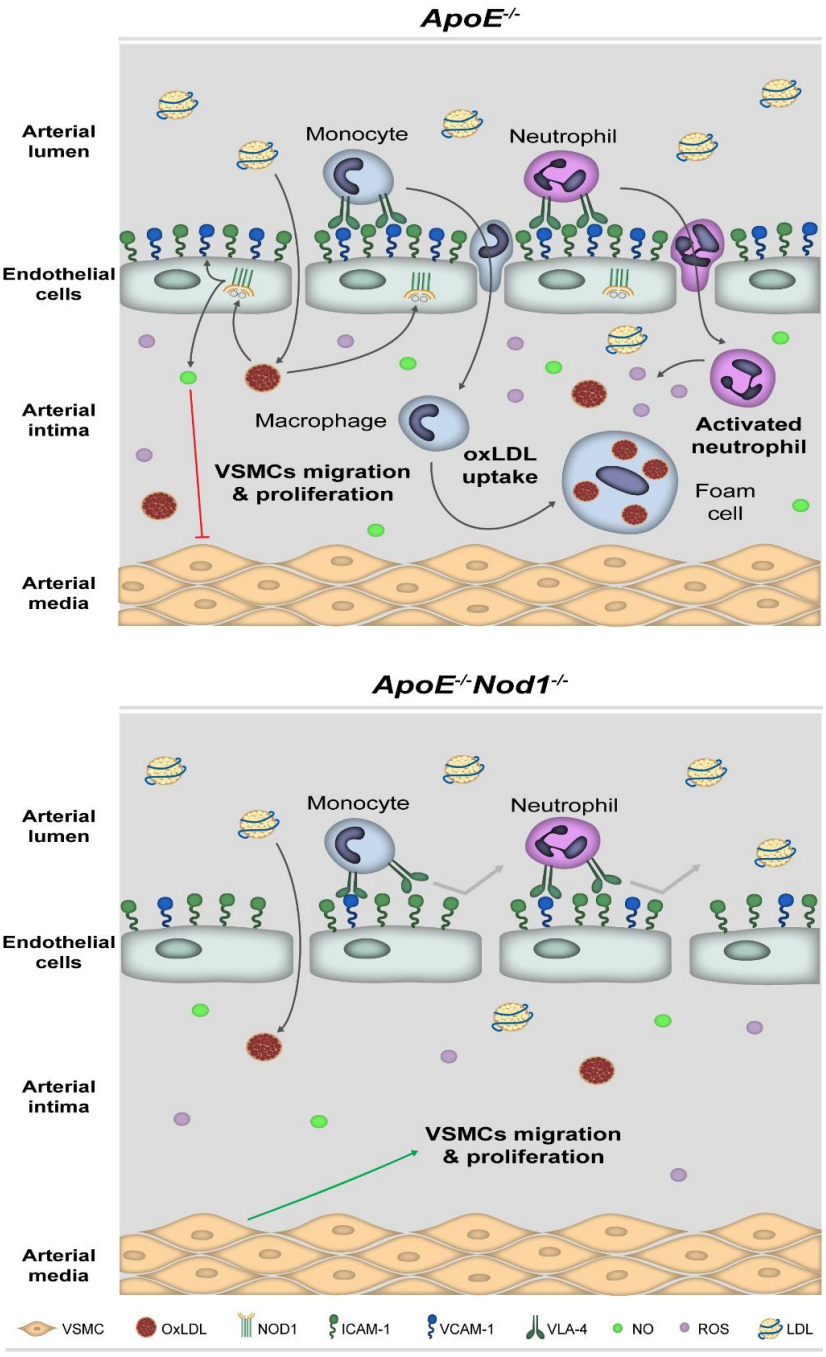

Figure 29. Proposed cellular mechanism for NOD1 in early stages of atherosclerosis.

Early detection of endothelial NOD1 activation may have prognostic value in atherosclerosis, given that endothelial activation and subsequent dysfunction contributes to atherosclerosis severity and progression (20, 50, 52, 177). Moreover, it is important to highlight that dysfunction of the arterial endothelium is important not only at the inception of the atherosclerotic lesion, but at every stage in the life of the plaque, including in particular the events surrounding plaque rupture. This is the reason why we do not exclude further studies aimed to identify the feasibility of endothelial NOD1 as a target in clinical treatments for plaque stability.

Understanding arterial myeloid cell recruitment to ultimately tailor strategies to boycott arterial leukocyte recruitment has provided trendy appeal in the last years, with some of them already patented for the treatment of seizures and epilepsy (please refer to EP2029164A2, US20130230539A1 and WO2007146188A2).

If it holds true that regulation of VCAM-1 by NOD1 inhibition in endothelial cells is mediated by the transcription factor NF-κB, endothelial NF-kB would be thereof reinforced as a potentially important drug target in atherosclerosis (83). Though there is considerable interest in the therapeutic inhibition of NF-κB, several recent reports suggest that inhibition of NF-κB after the initial inflammatory insult, and during the resolution phase, may in certain conditions prolong rather than inhibit inflammation, thereby delaying tissue repair (160).

In this context, NOD1 constitutes a potential early therapeutic target for the blockade of atherosclerosis and development of CAD, but also for other diseases where the endothelium plays a key role such as the pathogenesis of sepsis and its sequelae, since NOD1 outstands as determinant in arterial leukocyte recruitment in ECs but not in circulating monocytes and neutrophils. Future development of strategies aimed at local or arterial endothelial-specific neutralization of NOD1 (e.g. nanodelivery, arterial sonoporation) may open new therapeutic approaches for the prevention and treatment of this disease either alone or in combination with standard treatments, with great social and economic benefits regarding the commitment to curb the pandemic of cardiovascular diseases without compromising immunity.

6. Conclusions / Conclusiones

This Thesis illustrates the distinct roles of NOD1 on the complex pathogenesis of atherosclerosis. Specific conclusions include the following:

1. *Nod1* is pro-atherogenic and its deletion prevents early atherosclerosis development in *Apoe*$^{-/-}$ mice regardless of cholesterol and triglyceride levels, immune cell counts and pro-inflammatory cytokine profile in blood. It is likely that exacerbated proliferation of vascular smooth muscle cells in the *ApoE*$^{-/-}$*Nod1*$^{-/-}$ mouse model aggravates the atheromatous plaque in later stages of the disease.

2. The *Nod1* major effector cells in our model of decelerated atherogenesis are non-haematopoietic cells elucidated both by bone-marrow transplant experiments and integrin-mediated cell adhesion assays in *Nod1*$^{-/-}$ monocytes and neutrophils.

3. Early atherosclerotic plaque in the aortic sinus of *Apoe*$^{-/-}$ *Nod1*$^{-/-}$ mice has less CD68^{+} cell infiltration and VCAM-1 expression compared to *ApoE*$^{-/-}$ mice, but equal expression of ICAM-1 and PECAM-1, meaning that NOD1 does not participate in leukocyte trafficking across the vessel wall, but on the tethering and subsequent rolling along it.

4. Monocytes and neutrophils have impaired rolling and adhesion to *Apoe*$^{-/-}$*Nod1*$^{-/-}$ endothelia from the carotid artery and the cremaster microvasculature in the inflammatory context of atherosclerosis.

5. Oxidized LDL is a potential endogenous ligand for NOD1 that regulates VCAM-1 expression in endothelial cells and concomitant leukocyte adherence to the monolayer.

Esta Tesis ilustra las distintas funciones de NOD1 en la compleja patogénesis de la aterosclerosis. Las conclusiones específicas incluyen:

1. *Nod1* es pro-aterogénico y su deleción previene el desarrollo temprano de aterosclerosis en ratones *Apoe*$^{-/-}$ con independencia de los niveles de colesterol y triglicéridos, del recuento leucocitario y del perfil de citoquinas pro-inflamatorias en sangre. Es probable que en el modelo murino *ApoE*$^{-/-}$*Nod1*$^{-/-}$, una proliferación excesiva de células de músculo liso vascular agrave la placa ateromatosa en estadios más tardíos de la enfermedad.

2. Las células efectoras *Nod1* en nuestro modelo de aterogénesis ralentizada son de origen no hematopoyético elucidado tanto por experimentos de trasplante de médula ósea como en ensayos de adhesión celular mediados por integrinas en monocitos y neutrófilos *Nod1*$^{-/-}$.

3. La placa de ateroma en el seno aórtico de ratones *Apoe*$^{-/-}$ *Nod1*$^{-/-}$ en estadios tempranos presenta en comparación con los ratones *Apoe*$^{-/-}$ una menor infiltración de células CD68^{+} y un reducción en la expresión de VCAM-1; sin embargo la expresión de ICAM-1 y PECAM-1 es idéntica, por lo que NOD1 no participa en la transmigración leucocitaria a través de la pared del vaso, sino en el rodamiento y su consiguiente inmovilización a ésta.

4. Los monocitos y neutrófilos tienen alterados dentro del contexto inflamatorio de la aterosclerosis el rodamiento y la adhesión al endotelio *Apoe*$^{-/-}$*Nod1*$^{-/-}$ tanto de la arteria carótida como en la microvasculatura cremastérica.

5. Las LDLs oxidadas son un potencial ligando endógeno de NOD1 que regula la expresión de VCAM-1 en células endoteliales y la posterior adhesión leucocitaria.

7. References

1. Abbott DW, Wilkins A, Asara JM, Cantley LC. 2004. The crohn's disease protein, nod2, requires rip2 in order to induce ubiquitinylation of a novel site on nemo. *Curr. Biol.* 14(24):2217–27
2. Ahrens EJ. 1976. The management of hyperlipidemia: whether, rather than how. *Ann Intern Med.* 85(1):87–93
3. Aird WC. 2007. Phenotypic heterogeneity of the endothelium: ii. representative vascular beds. *Circ. Res.* 100(2):174–90
4. Ait-Oufella H, Taleb S, Mallat Z, Tedgui A. 2011. Recent advances on the role of cytokines in atherosclerosis. *Arterioscler. Thromb. Vasc. Biol.* 31(5):969–79
5. Alberts B, Johnson A, Lewis J, Raff M, Roberts K, Walter P. 2002. Pathogens, infection, and innate immunity. In *Molecular Biology of the Cell.* New York: Garland Science. 4th Ed. ed.
6. Aparicio-Vergara M, Shiri-Sverdlov R, Koonen DPY, Hofker MH. 2012. Bone marrow transplantation as an established approach for understanding the role of macrophages in atherosclerosis and the metabolic syndrome. *Curr. Opin. Lipidol.* 23(2):111–21
7. Assmann G, Cullen P, Schulte H. 2002. Simple scoring scheme for calculating the risk of acute coronary events based on the 10-year follow-up of the prospective cardiovascular munster (procam) study. *Circulation.* 105(3):310–15
8. Assmann G, Schulte H, von Eckardstein A. 1996. Hypertriglyceridemia and elevated lipoprotei (a) are risk factors for major coronary events in middle-aged men. *Am. J. Cardiol.* 77(14):1179–84
9. Ausubel FM. 2005. Are innate immune signaling pathways in plants and animals conserved? *Nat. Immunol.* 6(10):973–79
10. Bassiouny HS, Zarins CK, Lee DC, Skelly CL, Fortunato JE, Glagov S. 2002. Diurnal heart rate reactivity: a predictor of severity of experimental coronary and carotid atherosclerosis. *J Cardiovasc Risk.* 9(6):331–38
11. Bell F, Day A, Gent M, Schwarts C. 1975. Differing patterns of cholesterol accumulation and 3-h-cholesterol influx in areas of the cholesterol-fed pig aorta identified by evans blue dye. *Exp. Mol. Pathol.* 22(3):336–75

12. Bennett MR, Sinha S, Owens GK. 2016. Vascular smooth muscle cells in atherosclerosis. *Circ. Res.* 118(4):692–702

13. Berlin C, Bargatze RF, Campbell JJ, von Andrian UH, Szabo MC, et al. 1995. A4 integrins mediate lymphocyte attachment and rolling under physiologic flow. *Cell.* 80(3):413–22

14. Bertrand MJM, Doiron K, Labbé K, Korneluk RG, Barker PA, Saleh M. 2009. Cellular inhibitors of apoptosis ciap1 and ciap2 are required for innate immunity signaling by the pattern recognition receptors nod1 and nod2. *Immunity.* 30(6):789–801

15. Birbrair A, Frenette PS. 2016. Niche heterogeneity in the bone marrow. *Ann. N. Y. Acad. Sci.* 1370(1):82–96

16. Biswas A, Liu Y-J, Hao L, Mizoguchi A, Salzman NH, et al. 2010. Induction and rescue of nod2-dependent th1-driven granulomatous inflammation of the ileum. *Proc. Natl. Acad. Sci. U. S. A.* 107(33):14739–44

17. Bochkov VN, Leitinger N. 2003. Anti-inflammatory properties of lipid oxidation products. *J. Mol. Med.* 81(10):613–26

18. Bochner BS, Luscinskas FW, Gimbrone MAJ, Newman W, Sterbinsky S, et al. 1991. Adhesion of human basophils, eosinophils, and neutrophils to interleukin-1-activated human vascular endothelial cells: contribution of endothelial cell adhesion molecules. *J Exp Med.* 173(6):1553–57

19. Bogen S, Pak J, Garifallou M, Deng X, Muller WA. 1994. Monoclonal antibody to murine pecam-1 (cd31) blocks acute inflammation in vivo. *J. Exp. Med.* 179(3):1059–64

20. Bonetti PO, Lerman LO, Lerman A. 2003. Endothelial dysfunction: a marker of atherosclerotic risk. *Arterioscler. Thromb. Vasc. Biol.* 23(2):168–75

21. Bostom AG, Silbershatz H, Rosenberg IH, Selhub J, D'Agostino RB, et al. 1999. Nonfasting plasma total homocysteine levels and all-cause and cardiovascular disease mortality in elderly framingham men and women. *Arch Intern Med.* 159(10):1077–80

22. Bouskra D, Brézillon C, Bérard M, Werts C, Varona R, et al. 2008. Lymphoid tissue

genesis induced by commensals through nod1 regulates intestinal homeostasis. *Nature*. 456(7221):507–10

23. Brightbill HD, Libraty DH, Krutzik SR, Yang R-B, Belisle JT, et al. 1999. Host defense mechanisms triggered by microbial lipoproteins through toll-like receptors. *Science (80-.).* 285(5428):732–36
24. Brouet A, Sonveaux P, Dessy C, Balligand JL, Feron O. 2001. Hsp90 ensures the transition from the early ca2+-dependent to the late phosphorylation-dependent activation of the endothelial nitric-oxide synthase in vascular endothelial growth factor-exposed endothelial cells. *J. Biol. Chem.* 276(35):32663–69
25. Bryan MT, Duckles H, Feng S, Hsiao ST, Kim HR, et al. 2014. Mechanoresponsive networks controlling vascular inflammation. *Arterioscler. Thromb. Vasc. Biol.* 34(10):2199–2205
26. Butcher EC. 1991. Leukocyte-endothelial cell recognition: three (or more) steps to specificity and diversity. *Cell.* 67(6):1033–36
27. Cai H, Harrison DG. 2000. Endothelial dysfunction in cardiovascular diseases: the role of oxidant stress. *Circ. Res.* 87(10):840–44
28. Carbone F, Mach F, Montecucco F. 2015. Update on the role of neutrophils in atherosclerotic plaque vulnerability. *Curr Drug Targets.* 16(4):321–33
29. Carbone F, Nencioni A, Mach F, Vuilleumier N, Montecucco F. 2013. Pathophysiological role of neutrophils in acute myocardial infarction. *Thromb. Haemost.* 110(3):501–14
30. Caro C, Fitz-Gerald J, Schroter R. 1969. Arterial wall shear and distribution of early atheroma in man. *Nature.* 223(5211):1159–60
31. Cartwright N, Murch O, McMaster SK, Paul-Clark MJ, Van Heel DA, et al. 2007. Selective nod1 agonists cause shock and organ injury/dysfunction in vivo. *Am. J. Respir. Crit. Care Med.* 175(6):595–603
32. Chamaillard M, Hashimoto M, Horie Y, Masumoto J, Qiu S, et al. 2003. An essential role for nod1 in host recognition of bacterial peptidoglycan containing diaminopimelic acid. *Nat. Immunol.* 4(7):702–7
33. Chan JR, Hyduk SJ, Cybulsky MI. 2001. Chemoattractants induce a rapid and

transient upregulation of monocyte alpha4 integrin affinity for vascular cell adhesion molecule 1 which mediates arrest: an early step in the process of emigration. *J. Exp. Med.* 193(10):1149–58

34. Chappell DC, Varner SE, Nerem RM, Medford RM, Alexander RW. 1998. Oscillatory shear stress stimulates adhesion molecule expression in cultured human endothelium. *Circ. Res.* 82(5):532–39
35. Chen GY, Núñez G. 2009. Gut immunity: a nod to the commensals. *Curr. Biol.* 19(4):171–74
36. Chen J, Chen M, Li S, Guo Y, Zhu C, et al. 2014. Usefulness of the neutrophil-to-lymphocyte ratio in predicting the severity of coronary artery disease: a gensini score assessment. *J. Atheroscler. Thromb.* 21(12):1271–82
37. Chesnutt BC, Smith DF, Raffler N a, Smith ML, White EJ, Ley K. 2006. Induction of lfa-1-dependent neutrophil rolling on icam-1 by engagement of e-selectin. *Microcirculation.* 13(2):99–109
38. Chiu B, Viira E, Tucker W, Fong I. 1997. Chlamydia pneumoniae, cytomegalovirus, and herpes simplex virus in atherosclerosis of the carotid artery. *Circulation.* 96(7):2144–48
39. Chiu J, Chien S. 2011. Effects of disturbed flow on vascular endothelium: pathophysiological basis and clinical perspectives. *Physiol rev.* 91(1):1–106
40. Cid MC, Cebrián M, Font C, Coll-Vinent B, Hernández-Rodríguez J, et al. 2000. Cell adhesion molecules in the development of inflammatory infiltrates in giant cell arteritis: inflammation-induced angiogenesis as the preferential site of leukocyte-endothelial cell interactions. *Arthritis Rheum.* 43(1):184–94
41. Clarke T, Davis K, Lysenko E, Zhou A, Yu Y, Weiser J. 2010. Recognition of peptidoglycan from the microbiota by nod1 enhances systemic innate immunity. *Nat. Med.* 16(2):228–31
42. Clarke TB, Davis KM, Lysenko ES, Zhou AY, Yu Y, Weiser JN. 2010. Recognition of peptidoglycan from the microbiota by nod1 enhances systemic innate immunity. *Nat. Med.* 16(2):228–31
43. Coller BS. 2005. Leukocytosis and ischemic vascular disease morbidity and mortality:

is it time to intervene? *Arterioscler. Thromb. Vasc. Biol.* 25(4):658–70

44. Collins RG, Velji R, Guevara N V, Hicks MJ, Chan L, Beaudet AL. 2000. P-selectin or intercellular adhesion molecule (icam)-1 deficiency substantially protects against atherosclerosis in apolipoprotein e-deficient mice. *J. Exp. Med.* 19(1):189–94
45. Combadière C, Potteaux S, Rodero M, Simon T, Pezard A, et al. 2008. Combined inhibition of ccl2, cx3cr1, and ccr5 abrogates ly6chi and ly6clo monocytosis and almost abolishes atherosclerosis in hypercholesterolemic mice. *Circulation.* 117(13):1649–57
46. Cooke JP. 2003. Flow , no, and atherogenesis. *Proc. Natl. Acad. Sci.* 100:768–70
47. Cooney R, Baker J, Brain O, Danis B, Pichulik T, et al. 2010. Nod2 stimulation induces autophagy in dendritic cells influencing bacterial handling and antigen presentation. *Nat. Med.* 16(1):90–97
48. da Silva Correia J, Miranda Y, Leonard N, Hsu J, Ulevitch RJ. 2007. Regulation of nod1-mediated signaling pathways. *Cell Death Differ.* 14(4):830–39
49. Davies MJ, Gordon JL, Gearing AJH, Pigott R, Woolf N, et al. 1993. The expression of the adhesion molecules icam-1, vcam-1, pecam, and e-selectin in human atherosclerosis. *J. Pathol.* 171(3):223–29
50. Davignon J, Ganz P. 2004. Role of endothelial dysfunction in atherosclerosis. *Circulation.* 109(Suppl III):27–32
51. Davis BK, Wen H, Ting JP. 2011. The inflammasome nlrs in immunity, inflammation, and associated diseases. *Annu Rev Immunol.* 29:707–35
52. Deanfield JE, Halcox JP, Rabelink TJ. 2007. Endothelial function and dysfunction: testing and clinical relevance. *Circulation.* 115(10):1285–95
53. Demeule M, Labelle M, Re A, Berthelet F, Béliveau R. 2001. Isolation of endothelial cells from brain , lung , and kidney : expression of the multidrug resistance p-glycoprotein isoforms. *Biochem. Biophys. Res. Commun.* 281(3):827–34
54. Derry WB, Putzke AP, Rothman JH. 2001. Caenorhabditis elegans p53: role in apoptosis, meiosis, and stress resistance. *Science (80-.).* 294(5542):591–95
55. Dessein R, Chamaillard M, Danese S. 2008. Innate immunity in crohn's disease. *J. Clin. Gastroenterol.* 42:144–47

56. Dimmeler S, Fleming I, Fisslthaler B, Hermann C, Busse R, Zeiher a M. 1999. Activation of nitric oxide synthase in endothelial cells by akt-dependent phosphorylation. *Nature.* 399(6736):601–5

57. Dong ZM, Chapman SM, Brown AA, Frenette PS, Hynes RO, Wagner DD. 1998. The combined role of p- and e-selectins in atherosclerosis. *J. Clin. Invest.* 102(1):145–52

58. Döring Y, Drechsler M, Soehnlein O, Weber C. 2015. Neutrophils in atherosclerosis: from mice to man. *Arterioscler. Thromb. Vasc. Biol.* 35(2):288–95

59. Döring Y, Manthey HD, Drechsler M, Lievens D, Megens RTA, et al. 2012. Auto-antigenic protein-dna complexes stimulate plasmacytoid dendritic cells to promote atherosclerosis. *Circulation.* 125(13):1673–83

60. Drechsler M, Megens RTA, Van Zandvoort M, Weber C, Soehnlein O. 2010. Hyperlipidemia-triggered neutrophilia promotes early atherosclerosis. *Circulation.* 122(18):1837–45

61. Driscoll DM, Getz GS. 1984. Extrahepatic synthesis of apolipoprotein e. *J. Lipid Res.* 25(12):1368–79

62. Duewell P, Kono H, Rayner KJ, Sirois CM, Bauernfeind FG, et al. 2010. Nlrp3 inflammasomes are required for atherogenesis and activated by cholesterol crystals. *Nature.* 464(7293):1357–61

63. Duran-struuck R, Dysko RC. 2009. Principles of bone marrow transplantation (bmt): providing optimal veterinary and husbandry care to irradiated mice in bmt studies. *J. Am. Assoc. Lab. Anim. Sci.* 48(1):11–22

64. Dutrochet H. 1824. *Recherches anatomiques et physiologiques sur la structure intime des animaux et des vêgetaux, et dur leur motilité.* Paris. 1-233 pp. Bailliere ed.

65. Dutta P, Courties G, Wei Y, Leuschner F, Gorbatov R, et al. 2012. Myocardial infarction accelerates atherosclerosis. *Nature.* 487(7407):325–29

66. Elices MJ, Osborn L, Takada Y, Crouse C, Luhowskyj S, et al. 1990. Vcam-1 on activated endothelium interacts with the leukocyte integrin vla-4 at a site distinct from the vla-4/fibronectin binding site. *Cell.* 60(4):577–84

67. Enoksson M, Ejendal KFK, McAlpine S, Nilsson G, Lunderius-Andersson C. 2011.

Human cord blood-derived mast cells are activated by the nod1 agonist m-tridap to release pro-inflammatory cytokines and chemokines. *J. Innate Immun.* 3(2):142–49

68. Eriksson EE. 2011. Intravital microscopy on atherosclerosis in apolipoprotein e-deficient mice establishes microvessels as major entry pathways for leukocytes to advanced lesions. *Circulation.* 124(19):2129–38
69. Falck-Hansen M, Kassiteridi C, Monaco C. 2013. Toll-like receptors in atherosclerosis. *Int. J. Mol. Sci.* 14(7):14008–23
70. Farah R, Schurtz-Swirski R, Dorlechter F. 2010. Primed polymorphonuclear leukocytes constitute a possible link between inflammation and oxidative stress in hyperlipidemic patients: effect of statins. *Minerva Cardioangiol.* 58(2):175–81
71. Fehrenbach M, Cao G, Williams J., Finklestein J, Delisser H. 2009. Isolation of murine lung endothelial cells. *Am J Physiol Lung Cell Mol Physiol.* 296(6):L1096-103
72. Feingold K, Soued M, Adi S, Staprans I, Neese R, et al. 1991. Effect of interleukin-1 on lipid metabolism in the rat: similarities to and differences from tumor necrosis factor. *Arterioscler. Thromb. Vasc. Biol.* 11:495–500
73. Feng D, Nagy JA, Pyne K, Dvorak HF, Dvorak AM. 1998. Neutrophils emigrate from venules by a transendothelial cell pathway in response to fmlp. *J. Exp. Med.* 187(6):903–15
74. Finger EB, Puri KD, Alon R, Lawrence MB, von Andrian UH, Springer TA. 1996. Adhesion through l-selectin requires a threshold hydrodynamic shear. *Nature.* 379(6562):266–69
75. Folsom AR, Javier N, McGovern PG, Tsai MY, Malinow MR, et al. 1998. Prospective study of coronary heart disease incidence in relation to fasting total homocysteine, related genetic polymorphisms, and b vitamins: the atherosclerosis risk in communities (aric) study. *Circulation.* 98(3):204–10
76. Franchi L, Warner N, Viani K, Nuñez G. 2009. Function of nod-like receptors in microbial recognition and host defense. *Immunol. Rev.* 227(1):106–28
77. Fritz JH, Girardin SE, Fitting C, Werts C, Mengin-Lecreulx D, et al. 2005. Synergistic stimulation of human monocytes and dendritic cells by toll-like receptor 4 and nod1- and nod2-activating agonists. *Eur. J. Immunol.* 35(8):2459–70

78. Fueger BJ, Czernin J, Hildebrandt I, Tran C, Halpern BS, et al. 2006. Impact of animal handling on the results of 18 f-fdg pet studies in mice. *J. Nucl. Med.* 47(6):999–1007

79. Galkina E, Ley K. 2007. Leukocyte influx in atherosclerosis. *Curr. Drug Targets.* 8(12):1239–48

80. Gallin J, Kaye D, WM O. 1969. Serum lipids in infection. *N. Engl. J. Med.* 281(20):1081–86

81. Gallucci S, Lolkema M, Matzinger P. 1999. Natural adjuvants: endogenous activators of dendritic cells. *Nat. Med.* 5(11):1249–55

82. Gao J, Katagiri H, Ishigaki Y, Yamada T, Ogihara T, et al. 2007. Involvement of apolipoprotein e in excess fat accumulation and insulin resistance. *Diabetes.* 56(1):24–33

83. Gareus R, Kotsaki E, Xanthoulea S, van der Made I, Gijbels MJJ, et al. 2008. Endothelial cell-specific nf-κb inhibition protects mice from atherosclerosis. *Cell Metab.* 8(5):372–83

84. Gatheral T, Reed DM, Moreno L, Gough PJ, Votta BJ, et al. 2012. A key role for the endothelium in nod1 mediated vascular inflammation: comparison to tlr4 responses. *PLoS One.* 7(8):1–13

85. Gerhardt T, Ley K. 2015. Monocyte trafficking across the vessel wall. *Cardiovasc. Res.* 107(3):321–30

86. Gerrity RG, Naito HK, Richardson M, Schwartz CJ. 1979. Dietary induced atherogenesis in swine. morphology of the intima in prelesion stages. *Am. J. Pathol.* 95(3):775–92

87. Getz GS, Reardon CA. 2012. Animal models of atherosclerosis. *Arterioscler. Thromb. Vasc. Biol.* 32(5):1104–15

88. Ghosh S, Hayden MS. 2008. New regulators of nf-kappab in inflammation. *Nat. Rev. Immunol.* 8(11):837–48

89. Girardin SE, Boneca IG, Carneiro LAM, Antignac A, Jéhanno M, et al. 2003. Nod1 detects a unique muropeptide from gram-negative bacterial peptidoglycan. *Science (80-.).* 300(5625):1584–87

90. Girardin SE, Boneca IG, Viala J, Chamaillard M, Labigne A, et al. 2003. Nod2 is a general sensor of peptidoglycan through muramyl dipeptide (mdp) detection. *J. Biol. Chem.* 278(11):8869–72

91. Girardin SE, Tournebize R, Mavris M, Page a L, Li X, et al. 2001. Card4/nod1 mediates nf-kappab and jnk activation by invasive shigella flexneri. *EMBO Rep.* 2(8):736–42

92. Glass CK, Witztum JL. 2001. Atherosclerosis : the road ahead. *Cell.* 104(4):503–16

93. Gokce N, Keaney JF, Hunter LM, Watkins MT, Menzoian JO, Vita JA. 2002. Risk stratification for postoperative cardiovascular events via noninvasive assessment of endothelial function: a prospective study. *Circulation.* 105(13):1567–72

94. Gonzalez MA, Selwyn AP. 2003. Endothelial function, inflammation, and prognosis in cardiovascular disease. *Am. J. Med.* 115(Suppl. 8A):99S–106S

95. Gopal K, Kumar K, Nandini R, Jahan P, Kumar MJM. 2010. High fat diet containing cholesterol induce aortic aneurysm through recruitment and proliferation of circulating agranulocytes in apoe knock out mice model. *J. Thromb. Thrombolysis.* 30(2):154–63

96. Gotto AJ. 1984. Directions of atherosclerosis research in the 1980s and 1990s. *Circulation.* 70(5 Pt 2):III88-94

97. Grant RT. 1966. The effects of denervation on skeletal muscle blood vessels (rat cremaster). *J. Anat.* 100(2):305–16

98. Gutierrez O, Pipaon C, Inohara N, Fontalba A, Ogura Y, et al. 2002. Induction of nod2 in myelomonocytic and intestinal epithelial cells via nuclear factor-kb activation. *J. Biol. Chem.* 277(44):41701–5

99. Hackam DG, Spence JD. 2007. Combining multiple approaches for the secondary prevention of vascular events after stroke: a quantitative modeling study. *Stroke.* 38(6):1881–85

100. Hajra L, Evans AI, Chen M, Hyduk SJ, Collins T, Cybulsky MI. 2000. The nf-kappa b signal transduction pathway in aortic endothelial cells is primed for activation in regions predisposed to atherosclerotic lesion formation. *Proc. Natl. Acad. Sci. U. S. A.* 97(16):9052–57

101. Hansson GK. 2005. Inflammation, atherosclerosis and coronary artery disease. *N. Engl. J. Med.* 352:1685–95

102. Hansson GK, Libby P. 2006. The immune response in atherosclerosis: a double-edged sword. *Nat. Rev. Immunol.* 6(7):508–19

103. Harrison D, Griendling K, Landmesser U, Hornig B, Drexler H. 2003. Role of oxidative stress in atherosclerosis. *Am. J. Cardiol.* 91(3A):7A–11A

104. Hasegawa M, Fujimoto Y, Lucas PC, Nakano H, Fukase K, et al. 2008. A critical role of rick/rip2 polyubiquitination in nod-induced nf-kappab activation. *EMBO J.* 27(2):373–83

105. Higashimori M, Tatro JB, Moore KJ, Mendelsohn ME, Jonas B, Beasley D. 2011. Role of toll-like receptor 4 in intimal foam cell accumulation in apolipoprotein e-deficient mice. *Arterioscler. Thromb. Vasc. Biol.* 31(1):50–57

106. Hisamatsu T, Suzuki M, Reinecker H-C, Nadeau WJ, McCormick BA, Podolsky DK. 2003. Card15/nod2 functions as an antibacterial factor in human intestinal epithelial cells. *Gastroenterology.* 124(4):993–1000

107. Hortelano S, López-Fontal R, Través PG, Villa N, Grashoff C, et al. 2010. Ilk mediates lps-induced vascular adhesion receptor expression and subsequent leucocyte trans-endothelial migration. *Cardiovasc. Res.* 86(2):283–92

108. Hoving S, Heeneman S, Gijbels MJJ, te Poele JAM, Russell NS, et al. 2008. Single-dose and fractionated irradiation promote initiation and progression of atherosclerosis and induce an inflammatory plaque phenotype in apoe-/- mice. *Int. J. Radiat. Oncol. Biol. Phys.* 71(3):848–57

109. Huber SA, Sakkinen P, Conze D, Hardin N, Tracy R. 1999. Interleukin-6 exacerbates early atherosclerosis in mice. *Arterioscler. Thromb. Vasc. Biol.* 19(10):2364–67

110. Hugot JP, Chamaillard M, Zouali H, Lesage S, Cézard JP, et al. 2001. Association of nod2 leucine-rich repeat variants with susceptibility to crohn's disease. *Nature.* 411(6837):599–603

111. Huo Y, Hafezi-Moghadam A, Ley K. 2000. Role of vascular cell adhesion molecule-1 and fibronectin connecting segment-1 in monocyte rolling and adhesion on early atherosclerotic lesions. *Circ. Res.* 87(2):153–59

112. Inohara N, Koseki T, del Peso L, Hu Y, Yee C, et al. 1999. Nod1, an apaf-1-like activator of caspase-9 and nuclear factor-κb. *J. Biol. Chem.* 274(21):14560–67

113. Inohara N, Koseki T, Lin J, Peso L, Lucas PC, et al. 2000. An induced proximity model for nf-κb activation in the nod1/rick and rip signaling pathways. *J Biol Chem.* 275(36):27823–31

114. Inohara N, Nuñez G. 2001. The nod: a signaling module that regulates apoptosis and host defense against pathogens. *Oncogene.* 20(44):6473–81

115. Inohara N, Nuñez G. 2003. Nods: intracellular proteins involved in inflammation and apoptosis. *Nat. Rev. Immunol.* 3(5):371–82

116. Inohara N, Ogura Y, Chen FF, Muto A, Nuñez G. 2001. Human nod1 confers responsiveness to bacterial lipopolysaccharides. *J. Biol. Chem.* 276(4):2551–54

117. Inohara N, Ogura Y, Fontalba A, Gutierrez O, Pons F, et al. 2003. Host recognition of bacterial muramyl dipeptide mediated through nod2. implications for crohn's disease. *J. Biol. Chem.* 278(8):5509–12

118. Iwasaki A, Medzhitov R. 2010. Regulation of adaptive immunity by the innate immune system. *Science (80-.).* 327(5963):291–95

119. Janeway CAJ, Medzhitov R. 2002. Innate immune recognition. *Annu. Rev. Immunol.* 20:197–216

120. Jickling GC, Liu D, Ander BP, Stamova B, Zhan X, Sharp FR. 2015. Targeting neutrophils in ischemic stroke: translational insights from experimental studies. *J. Cereb. blood flow Metab.* 35(6):888–901

121. Jilling T, Simon D yan, Lu J, Meng FJ, Li D, et al. 2006. The roles of bacteria and tlr4 in rat murine models of necrotizing enterocolitis. *J Immunol.* 177(5):3273–82

122. Johansson ME, Zhang XY, Edfeldt K, Lundberg AM, Levin MC, et al. 2014. Innate immune receptor nod2 promotes vascular inflammation and formation of lipid-rich necrotic cores in hypercholesterolemic mice. *Eur. J. Immunol.* 44(10):3081–92

123. Jones CB, Jones CB, Sane DC, Sane DC, Herrington DM, Herrington DM. 2003. Matrix metalloproteinases: a review of their structure and role in acute coronary syndrome. *Cardiovasc. Res.* 59(4):812–23

124. Kajimoto K, Hossen MN, Hida K, Ohga N, Akita H, et al. 2010. Isolation and

culture of microvascular endothelial cells from murine inguinal and epididymal adipose tissues. *J. Immunol. Methods.* 357(1–2):43–50

125. Kanno S, Nishio H, Tanaka T, Motomura Y, Murata K, et al. 2014. Activation of an innate immune receptor, nod1, accelerates atherogenesis in apoe-/- mice. *J. Immunol.* 194(2):773–80
126. Kansas G. 1996. Selectins and their ligands: current concepts and controversies. *Blood.* 88(9):3259–87
127. Kanters E, Gijbels MJJ, Made I Van Der, Vergouwe MN, Heeringa P, et al. 2004. Hematopoietic nf-kb1 deficiency results in small atherosclerotic lesions with an inflammatory phenotype. *Blood.* 103(3):934–41
128. Kanwar R, Kanwar J, Wang D, Ormrod D, Krissansen G. 2001. Temporal expression of heat shock proteins 60 and 70 at lesion-prone sites during atherogenesis in apoe-deficient mice. *Arterioscler. Thromb. Vasc. Biol.* 21(12):1991–97
129. Karlsson FH, Fak F, Nookaew I, Tremaroli V, Fagerberg B, et al. 2012. Symptomatic atherosclerosis is associated with an altered gut metagenome. *Nat Commun.* 3:1245
130. Kawai T, Akira S. 2007. Tlr signaling. *Semin. Immunol.* 19(1):24–32
131. Khan B V, Parthasarathy SS, Alexander RW, Medford RM. 1993. Modified low density lipoprotein and its constituents augment cytokine-activated vascular cell adhesion molecule-1 gene expression in human vascular endothelial cells. *J.Clin.Invest.* 95(3):1262–70
132. Kiechl S, Egger G, Mayr M, Wiedermann CJ, Bonora E, et al. 2001. Chronic infections and the risk of carotid atherosclerosis: prospective results from a large population study. *Circulation.* 103(8):1064–71
133. Kim BJ, Kim JY, Hwang ES, Kim JG. 2015. Nucleotide binding oligomerization domain 1 is an essential signal transducer in human epithelial cells infected with helicobacter pylori that induces the transepithelial migration of neutrophils. *Gut Liver.* 9(3):358–69
134. Kinahan PE, Fletcher JW. 2010. Positron emission tomography-computed tomography standardized uptake values in clinical practice and assessing response to therapy the use of standardized uptake. *Semin Ultrasound CT MR.* 31(6):496–505

135. King K, Bagnall R, Fisher SA, Sheikh F, Cuthbert A, et al. 2007. Identification, evolution, and association study of a novel promoter and first exon of the human nod2 (card15) gene. *Genomics.* 90(4):493–501

136. Kirii H, Niwa T, Yamada Y, Wada H, Saito K, et al. 2003. Lack of interleukin-1b decreases the severity of atherosclerosis in apoe-deficient mice. *Arterioscler. Thromb. Vasc. Biol.* 23(4):656–60

137. Kleemann R, Zadelaar S, Kooistra T. 2008. Cytokines and atherosclerosis: a comprehensive review of studies in mice. *Cardiovasc. Res.* 79(3):360–76

138. Knight JS, Luo W, O'Dell AA, Yalavarthi S, Zhao W, et al. 2014. Peptidylarginine deiminase inhibition reduces vascular damage and modulates innate immune responses in murine models of atherosclerosis. *Circ. Res.* 114(6):947–56

139. Kobayashi K, Inohara N, Hernandez LD, Galan JE, Nunez G, et al. 2002. Rick/rip2/cardiak mediates signalling for receptors of the innate and adaptive immune systems. *Nature.* 416(6877):194–99

140. Kobayashi KS, Chamaillard M, Ogura Y, Henegariu O, Inohara N, et al. 2005. Immunity in the intestinal tract nod2-dependent regulation of innate and adaptive immunity in the intestinal tract. *Science (80-.).* 307:731–34

141. Koenen RR, Weber C. 2010. Therapeutic targeting of chemokine interactions in atherosclerosis. *Nat. Rev. Drug Discov.* 9(2):141–53

142. Koeth R a, Wang Z, Levison BS, Buffa J a, Org E, et al. 2013. Intestinal microbiota metabolism of l-carnitine, a nutrient in red meat, promotes atherosclerosis. *Nat. Med.* 19(5):576–85

143. Koonin E V., Aravind L. 2000. The nacht family - a new group of predicted ntpases implicated in apoptosis and mhc transcription activation. *Trends Biochem. Sci.* 25(5):223–24

144. Koren O, Spor A, Felin J, Fåk F, Stombaugh J, et al. 2011. Human oral, gut, and plaque microbiota in patients with atherosclerosis. *Proc. Natl. Acad. Sci. U. S. A.* 108(Supplement_1):4592–98

145. Kozina A, Opresnik S, Wong MSK, Hallström S, Graier WF, et al. 2014. Oleoyl-lysophosphatidylcholine limits endothelial nitric oxide bioavailability by induction of

reactive oxygen species. *PLoS One*. 9(11):1–20

146. Kricun M. 1985. Red-yellow marrow conversion: its effect on the location of some solitary bone lesions. *Skelet. Radiol.* 14(1):10–19
147. Krieg A, Correa RG, Garrison JB, Le Negrate G, Welsh K, et al. 2009. Xiap mediates nod signaling via interaction with rip2. *Proc. Natl. Acad. Sci. U. S. A.* 106(34):14524–29
148. Kristal B, Shurtz-Swirski R, Chezar J, Manaster J, Levy R, et al. 1998. Participation of peripheral polymorphonuclear leukocytes in the oxidative stress and inflammation in patients with essential hypertension. *Am. J. Hypertens.* 11(8 Pt 1):921–28
149. Ku DN, Giddens DP, Zarins CK, Glagov S. 1985. Pulsatile flow and atherosclerosis in the human carotid bifurcation: positive correlation between plaque location and low and oscillating shear stress. *Arterioscler. Thromb. Vasc. Biol.* 5:293–302
150. Kufer T a, Sansonetti PJ. 2011. Nlr functions beyond pathogen recognition. *Nat. Immunol.* 12(2):121–28
151. Kugiyama K, Kerns SA, Morrisett JD, Roberts R, Henry PD. 1990. Impairment of endothelium-dependent arterial relaxation by lysolecithin in modified low-density lipoproteins. *Nature*. 344(6262):160–2.
152. Kumar H, Kawai T, Akira S. 2011. Pathogen recognition by the innate immune system. *Int. Rev. Immunol.* 30(1):16–34
153. Kume N, Cybulsky MI, Gimbrone MA. 1992. Lysophosphatidylcholine, a component of atherogenic lipoproteins, induces mononuclear leukocyte adhesion molecules in cultured human and rabbit arterial endothelial cells. *J. Clin. Invest.* 90(3):1138–44
154. Kurosaki T, Kometani K, Ise W. 2015. Memory b cells. *Nat. Rev. Immunol.* 15(3):149–59
155. Labrie SJ, Samson JE, Moineau S. 2010. Bacteriophage resistance mechanisms. *Nat. Rev. Microbiol.* 8(5):317–27
156. Laman JD, Schoneveld AH, Moll FL, Van Meurs M, Pasterkamp G. 2002. Significance of peptidoglycan, a proinflammatory bacterial antigen in atherosclerotic arteries and its association with vulnerable plaques. *Am. J. Cardiol.* 90(2):119–23

157. Landmesser U, Burkhard H, Drexler H. 2004. Endothelial function: a critical determinant in atherosclerosis? *Circulation.* 109(21_suppl_1):II-27-II-33

158. Lawrence M, Kansas G, Kukel E, Ley K. 1997. Threshold levels of fluid shear promote leukocyte adhesion through selectins (cd62l, p, e). *J Cell Biol.* 136(3):717–27

159. Lawrence T. 2009. The nuclear factor nf-kappab pathway in inflammation. *Cold Spring Harb. Perspect. Biol.* 1(6):1–10

160. Lawrence T, Gilroy DW, Colville-Nash PR, Willoughby DA. 2001. Possible new role for nf-kappab in the resolution of inflammation. *Nat. Med.* 7(12):1291–97

161. Lee ES, Van Spyk E, Chun K, Pitts RL, Wu MH, Yuan SY. 2012. Monocytic adhesion molecule expression and monocyte-endothelial cell dysfunction are increased in patients with peripheral vascular disease versus patients with abdominal aortic aneurysms. *J Surg Res.* 177(2):373–81

162. Lee I-T, Lin C-C, Hsu C-K, Wu M-Y, Cho R-L, Yang C-M. 2014. Resveratrol inhibits staphylococcus aureus-induced tlr2/myd88/nf-κb-dependent vcam-1 expression in human lung epithelial cells. *Clin. Sci.* 127(6):375–90

163. Levin MC, Jirholt P, Wramstedt A, Johansson ME, Lundberg AM, et al. 2011. Rip2 deficiency leads to increased atherosclerosis despite decreased inflammation. *Circ. Res.* 109(11):1210–18

164. Ley K, Laudanna C, Cybulsky MI, Nourshargh S. 2007. Getting to the site of inflammation: the leukocyte adhesion cascade updated. *Nat. Rev. Immunol.* 7(9):678–89

165. Libby P. 2002. Inflammation in atherosclerosis. *Nature.* 420(6917):868–74

166. Libby P, Ridker PM, Maseri A. 2002. Inflammation and atherosclerosis. *Circulation.* 105(9):1135–43

167. Lichtenstein L, Serhan N, Espinosa-delgado S, Annema W, Tietge UJF, et al. 2015. Increased atherosclerosis in p2y 13 / apolipoprotein e double-knockout mice : contribution of p2y 13 to reverse cholesterol transport. *Cardiovasc. Res.* 106(2):314–23

168. Liu J, Duan J, Wang Y, Ouyang X. 2014. Intracellular adhesion molecule-1 is regulated by porphyromonas gingivalis through nucleotide binding oligomerization

domain-containing proteins 1 and 2 molecules in periodontal fibroblasts. *J. Periodontol.* 85(2):358–68

169. Liu J, Wang Y, Ouyang X. 2014. Beyond toll-like receptors: porphyromonas gingivalis induces il-6, il-8, and vcam-1 expression through nod-mediated nf-kb and erk signaling pathways in periodontal fibroblasts. *Inflammation.* 37(2):522–33
170. Liu Y, Yang H, Liu L-X, Yan W, Guo H-J, et al. 2016. Nod2 contributes to myocardial ischemia/reperfusion injury by regulating cardiomyocyte apoptosis and inflammation. *Life Sci.* 149:10–17
171. Lomakina EB, Waugh RE. 2009. Adhesion between human neutrophils and immobilized endothelial ligand vascular cell adhesion molecule 1: divalent ion effects. *Biophys. J.* 96(1):276–84
172. Luque A, Carpizo DR, Iruela-arispe ML. 2003. Adamts1 / meth1 inhibits endothelial cell proliferation by direct binding and sequestration of vegf 165. *J. Biol. Chem.* 278(26):23656–65
173. Maass M, Bartels C, Engel PM, Mamat U, Sievers HH. 1998. Endovascular presence of viable chlamydia pneumoniae is a common phenomenon in coronary artery disease. *J. Am. Coll. Cardiol.* 31(4):827–32
174. Mahley RW. 1988. Apolipoprotein e: cholesterol transport protein with expanding role in cell biology. *Science (80-.).* 240(4852):622–30
175. Mantovani A, Cassatella M a, Costantini C, Jaillon S. 2011. Neutrophils in the activation and regulation of innate and adaptive immunity. *Nat. Rev. Immunol.* 11(8):519–31
176. Marlin SD, Springer TA. 1987. Purified intercellular adhesion molecule-1 (icam-1) is a ligand for lymphocyte function-associated antigen 1 (lfa-1). *Cell.* 51(5):813–19
177. Martin B-J, Anderson TJ. 2009. Risk prediction in cardiovascular disease: the prognostic significance of endothelial dysfunction. *Can. J. Cardiol.* 25 Suppl A(June):15A–20A
178. Marui N, Offermann MK, Swerlick R, Kunsch C, Rosen CA, et al. 1993. Vascular cell adhesion molecule-1 (vcam-1) gene transcription and expression are regulated through an antioxidant-sensitive mechanism in human vascular endothelial cells. *J.*

Clin. Invest. 92(4):1866–74

179. Maruyama Y. 1963. The human endothelial cell in tissue culture. *Z Zellforsch Mikrosk Anat.* 60:69–79
180. Matzinger P. 1994. Tolerance, danger, and the extended family. *Annu. Rev. Immunol.* 12:991–1045
181. Mayer AK, Muehmer M, Mages J, Gueinzius K, Hess C, et al. 2007. Differential recognition of tlr-dependent microbial ligands in human bronchial epithelial cells. *J. Immunol.* 178(5):3134–42
182. Mayr M, Chung YL, Mayr U, Yin X, Ly L, et al. 2005. Proteomic and metabolomic analyses of atherosclerotic vessels from apolipoprotein e-deficient mice reveal alterations in inflammation, oxidative stress, and energy metabolism. *Arterioscler. Thromb. Vasc. Biol.* 25(10):2135–42
183. Mcardle S, Mikulski Z, Ley K. 2016. Live cell imaging to understand monocyte , macrophage , and dendritic cell function in atherosclerosis. *J. Biol. Med.* 213(7):1117–31
184. McEver RP, Cummings RD. 1997. Role of psgl-1 binding to selectins in leukocyte recruitment. *J. Clin. Invest.* 100(3):485–91
185. McGill HJ, Geer J, Holman R. 1957. Sites of vascular vulnerability in dogs demonstrated by evans blue. *AMA Arch Pathol.* 64(3):3033–11
186. McLaren JE, Michael DR, Ashlin TG, Ramji DP. 2011. Cytokines, macrophage lipid metabolism and foam cells: implications for cardiovascular disease therapy. *Prog. Lipid Res.* 50(4):331–47
187. Medzhitov R, Preston-Hurlburt P, Janeway CA Jr. 1997. A human homologue of the drosophila toll protein signals activation of adaptive immunity. *Nature.* 388(6640):394–97
188. Michel J-B, Delbosc S, Ho-Tin-Noé B, Leseche G, Nicoletti A, et al. 2012. From intraplaque haemorrhages to plaque vulnerability: biological consequences of intraplaque haemorrhages. *J. Cardiovasc. Med.* 13(10):628–34
189. Michelsen KS, Wong MH, Shah PK, Zhang W, Yano J, et al. 2004. Lack of toll-like receptor 4 or myeloid differentiation factor 88 reduces atherosclerosis and alters

plaque phenotype in mice deficient in apolipoprotein e. *Proc. Natl. Acad. Sci.* 101(29):10679–84

190. Miebach S, Grau S, Hummel V, Rieckmann P, Tonn JC, Goldbrunner RH. 2006. Isolation and culture of microvascular endothelial cells from gliomas of different who grades. *J. Neurooncol.* 76(1):39–48
191. Mijatovic T, Houzet L, Defrance P, Droogmans L, Huez G, Kruys V. 2000. Tumor necrosis factor-α mrna remains unstable and hypoadenylated upon stimulation of macrophages by lipopolysaccharides. *Eur. J. Biochem.* 267(19):6004–11
192. Miller YI, Choi SH, Wiesner P, Fang L, Harkewicz R, et al. 2011. Oxidation-specific epitopes are danger-associated molecular patterns recognized by pattern recognition receptors of innate immunity. *Circ. Res.* 108(2):235–48
193. Mohan S, Mohan N, Sprague EA. 1997. Differential activation of nf-kappa b in human aortic endothelial cells conditioned to specific flow environments. *Am. J. Physiol.* 273(2 Pt 1):C572-8
194. Moore JE, Ku DN, Zarins CK, Glagov S. 1992. Pulsatile flow visualization in the abdominal aorta under differing physiologic conditions: implications for increased susceptibility to atherosclerosis. *J. Biomech. Eng.* 114(3):391–97
195. Moore K, Sheedy F, Fisher E. 2013. Macrophages in atherosclerosis: a dynamic balance. *Nat. Rev. Immunol.* 13(10):709–21
196. Moore KJ, Freeman MW. 2006. Scavenger receptors in atherosclerosis: beyond lipid uptake. *Arterioscler. Thromb. Vasc. Biol.* 26(8):1702–11
197. Moreno L, McMaster S, Gatheral T, Bailey L, Harrington L, et al. 2010. Nucleotide oligomerization domain 1 is a dominant pathway for nos2 induction in vascular smooth muscle cells: comparison with toll-like receptor 4 responses in macrophages. *Br. J. Pharmacol.* 160(8):1997–2007
198. Motta V, Soares F, Sun T, Philpott DJ. 2015. Nod-like receptors: versatile cytosolic sentinels. *Physiol. Rev.* 95(1):149–78
199. Muller WA. 2003. Leukocyte-endothelial-cell interactions in leukocyte transmigration and the inflammatory response. *Trends Immunol.* 24(6):326–33
200. Muller WA. 2013. Getting leucocytes to the sites of inflammation. *Vet. Pathol.*

50(1):7–22

201. Muller WA, Weigl SA, Deng X, Phillips DM. 1993. Pecam-1 is required for transendothelial migration of leukocytes. *J. Exp. Med.* 178(2):449–60
202. Mullick AE, Tobias PS, Curtiss LK. 2005. Modulation of atherosclerosis in mice by toll-like receptor 2. *J. Clin. Invest.* 115(11):3149–56
203. Murohara T, Kugiyama K, Ohgushi M, Sugiyama S, Ohta Y, Yasue H. 1994. Lpc in oxidized ldl elicits vasocontraction and inhibits endothelium- dependent relaxation. *Am. J. Physiol.* 267(6 Pt 2):H2441-9
204. Murphy AJ, Dragoljevic D, Tall AR. 2014. Cholesterol efflux pathways regulate myelopoiesis: a potential link to altered macrophage function in atherosclerosis. *Front. Immunol.* 5(490):1–6
205. Nabhani Z Al, Lepage P, Mauny P, Montcuquet N, Roy M, et al. 2016. Nod2 deficiency leads to a specific and transmissible mucosa-associated microbial dysbiosis which is independent of the mucosal barrier defect. *J Chrons Colitis*
206. Naito Y, Shimozawa M, Kuroda M, Nakabe N, Manabe H, et al. 2005. Tocotrienols reduce 25-hydroxycholesterol-induced monocyte-endothelial cell interaction by inhibiting the surface expression of adhesion molecules. *Atherosclerosis.* 180(1):19–25
207. Nakashima Y, Plump AS, Raines EW, Breslow JL, Ross R. 1994. Apoe-deficient mice develop lesions of all phases of atherosclerosis throughout the arterial tree. *Arterioscler. Thromb. Vasc. Biol.* 14(1):133–40
208. Napoli C, D'Armiento FP, Corso G, Ambrosio G, Palumbo G, et al. 1997. Occurrence of the same peroxidative compounds in low density lipoprotein and in atherosclerotic lesions from a homozygous familial hypercholesterolemic patient: a case report. *Int. J. Cardiol.* 62(1):77–85
209. National Cholesterol Education Program (NCEP) Expert Panel on Detection, Evaluation and T of HBC in A (Adult TPI. 2002. Third report of the national cholesterol education program (ncep) expert panel on detection, evaluation, and treatment of high blood cholesterol in adults (adult treatment panel iii) final report. *Circulation.* 106(25):3143–3421
210. Nijhuis J, Rensen SS, Slaats Y, van Dielen FMH, Buurman W a, Greve JWM. 2009.

Neutrophil activation in morbid obesity, chronic activation of acute inflammation. *Obesity*. 17(11):2014–18

211. Nishio H, Kanno S, Onoyama S, Ikeda K, Tanaka T, et al. 2011. Nod1 ligands induce site-specific vascular inflammation. *Arterioscler. Thromb. Vasc. Biol.* 31(5):1093–99
212. Ogawa H, Rafiee P, Heidemann J, Fisher PJ, Johnson N a., et al. 2003. Mechanisms of endotoxin tolerance in human intestinal microvascular endothelial cells. *J. Immunol.* 170(12):5956–64
213. Ogura Y, Bonen DK, Inohara N, Nicolae DL, Chen FF, et al. 2001. A frameshift mutation in nod2 associated with susceptibility to crohn's disease. *Nature*. 411(6837):603–6
214. Ogura Y, Inohara N, Benito A, Chen FF, Yamaoka S, Núñez G. 2001. Nod2, a nod1/apaf-1 family member that is restricted to monocytes and activates nf-kb. *J. Biol. Chem.* 276(7):4812–18
215. Ohashi K, Burkart V, Flohe S, Kolb H. 2000. Cutting edge: heat shock protein 60 is a putative endogenous ligand of the toll-like receptor-4 complex. *J ImmunolThe J. Immunol.* 164(2):558–61
216. Ohgushi M, Kugiyama K, Fukunaga K, Murohara T, Sugiyama S, et al. 1993. Protein kinase c inhibitors prevent impairment of endothelium-dependent relaxation by oxidatively modified ldl. *Arterioscler. Thromb. Vasc. Biol.* 13(10):1525–32
217. Ohta H, Wada H, Niwa T, Kirii H, Iwamoto N, et al. 2005. Disruption of tumor necrosis factor-a gene diminishes the development of atherosclerosis in apoe-deficient mice. *Atherosclerosis*. 180(1):11–17
218. Okamura Y, Watari M, Jerud ES, Young DW, Ishizaka ST, et al. 2001. The extra domain a of fibronectin activates toll-like receptor 4. *J. Biol. Chem.* 276(13):10229–33
219. Opitz B, Förster S, Hocke AC, Maass M, Schmeck B, et al. 2005. Nod1-mediated endothelial cell activation by chlamydophila pneumoniae. *Circ. Res.* 96(3):319–26
220. Ortega-Gómez A, Salvermoser M, Rossaint J, Pick R, Brauner J, et al. 2016. Cathepsin g controls arterial but not venular myeloid cell recruitment. *Circulation*
221. Osler W. 1901. *Principles and Practice of Medicine*. New York: D. Appleton and

Company. 108 pp. 4th Ed. ed.

222. Ott SJ, El Mokhtari NE, Musfeldt M, Hellmig S, Freitag S, et al. 2006. Detection of diverse bacterial signatures in atherosclerotic lesions of patients with coronary heart disease. *Circulation.* 113(7):929–37

223. Parthasarathy S, Quinn MT, Schwenke DC, Carew TE, Steinberg D. 1989. Oxidative modification of beta-very low density lipoprotein. potential role in monocyte recruitment and foam cell formation. *Arteriosclerosis.* 9(3):398–405

224. Phillipson M, Heit B, Colarusso P, Liu L, Ballantyne CM, Kubes P. 2006. Intraluminal crawling of neutrophils to emigration sites: a molecularly distinct process from adhesion in the recruitment cascade. *J. Exp. Med.* 203(12):2569–75

225. Piga R, Naito Y, Kokura S, Handa O, Yoshikawa T. 2007. Short-term high glucose exposure induces monocyte-endothelial cells adhesion and transmigration by increasing vcam-1 and mcp-1 expression in human aortic endothelial cells. *Atherosclerosis.* 193(2):328–34

226. Plump AS, Smith JD, Hayek T, Aalto-Set??l?? K, Walsh A, et al. 1992. Severe hypercholesterolemia and atherosclerosis in apolipoprotein e-deficient mice created by homologous recombination in es cells. *Cell.* 71(2):343–53

227. Portman OW, Alexander M. 1969. Lysophosphatidylcholine concentration and metabolism in aortic intima plus inner media: effect of nutritionally induced atherosclerosis. *J Lipid Res.* 10:158–65

228. Prieto P, Vallejo-Cremades MT, Benito G, González-Peramato P, Francés D, et al. 2014. Nod1 receptor is up-regulated in diabetic human and murine myocardium. *Clin. Sci.* 127(12):665–77

229. Puga I, Cols M, Barra C, He B, Cassis L, et al. 2011. B-helper neutrophils stimulate immunoglobulin diversification and production in the marginal zone of the spleen. *Nat. Immunol.* 13(2):170–80

230. Qiu F, Maniar A, Diaz MQ, Chapoval AI, Medvedev AE. 2011. Activation of cytokine-producing and antitumor activities of natural killer cells and macrophages by engagement of toll-like and nod-like receptors. *Innate Immun.* 17(4):375–87

231. Quinn MT, Parthasarathy S, Steinberg D. 1988. Lysophosphatidylcholine: a

chemotactic factor for human monocytes and its potential role in atherogenesis. *Proc. Natl. Acad. Sci. U. S. A.* 85(8):2805–9

232. Rahman MK, Midtling EH, Svingen P a, Xiong Y, Bell MP, et al. 2010. The pathogen recognition receptor nod2 regulates human foxp3+ t cell survival. *J. Immunol.* 184(12):7247–56
233. Randolph GJ. 2014. Mechanisms that regulate macrophage burden in atherosclerosis. *Circ. Res.* 114(11):1757–71
234. Rathinam VA, Vanaja SK, Fitzgerald KA. 2012. Regulation of inflammasome signaling. *Nat. Immunol.* 13(4):332–33
235. Reinhardt PH, Kubes P. 1998. Differential leukocyte recruitment from whole blood via endothelial adhesion molecules under shear conditions. *Blood.* 92(12):4691–99
236. Restifo NP, Gattinoni L. 2013. Lineage relationship of effector and memory t cells. *Curr. Opin. Immunol.* 25(5):556–63
237. Rius C, Sanz MJ. 2015. Intravital microscopy in the cremaster muscle microcirculation for endothelial dysfunction studies. *Methods Mol. Biol.* 1339:357–66
238. Robertson SJ, Zhou JY, Geddes K, Rubino SJ, Cho JH, et al. 2013. Nod1 and nod2 signaling does not alter the composition of intestinal bacterial communities at homeostasis. *Gut Microbes.* 4(3):222–31
239. Ross R. 1993. The pathogenesis of atherosclerosis: a perspective for the 1990s. *Nature.* 362(6423):801–9
240. Ross R. 1999. Atherosclerosis-an inflammatory disease. *N. Engl. J. Med.* 340(2):115–26
241. Rudolph TK, Rudolph V, Baldus S. 2008. Contribution of myeloperoxidase to smoking-dependent vascular inflammation. *Proc. Am. Thorac. Soc.* 5(8):820–23
242. Sabbah A, Chang TH, Harnack R, Frohlich V, Tominaga K, et al. 2009. Activation of innate immune antiviral responses by nod2. *Nat. Immunol.* 10(10):1073–81
243. Saikku P, Leinonen M, Tenkanen L, Linnanmäki E, Ekman M, et al. 1992. Chronic chlamydia pneumoniae infection as a risk factor for coronary heart disease in the helsinki heart study. *Ann Intern Med1.* 116(4):273–78

244. Salas A, Shimaoka M, Kogan AN, Harwood C, Von Andrian UH, Springer TA. 2004. Rolling adhesion through an extended conformation of integrin alb2 and relation to a i and b i-like domain interaction. *Immunity.* 20(4):393–406

245. Salek-Ardakani S, Croft M. 2009. T cells need nod too? *Nat. Immunol.* 10(12):1231–33

246. Sawa Y, Tsuruga E, Iwasawa K, Ishikawa H, Yoshida S. 2008. Leukocyte adhesion molecule and chemokine production through lipoteichoic acid recognition by toll-like receptor 2 in cultured human lymphatic endothelium. *Cell Tissue Res.* 333(2):237–52

247. Sawa Y, Ueki T, Hata M, Iwasawa K, Tsuruga E, et al. 2008. Lps-induced il-6, il-8, vcam-1, and icam-1 expression in human lymphatic endothelium. *J. Histochem. Cytochem.* 56(2):97–109

248. Scalia R, Murohara T, Campbell B, Kaji A, Lefer A. 1997. Lysophosphatidylcholine stimulates leukocyte rolling and adherence in rat mesenteric microvasculature. *Am J Physiol.* 272(6 Pt 2):H2584-90

249. Schaefer EJ, Gregg RE, Ghiselli G, Forte TM, Ordovas JM, et al. 1986. Familial apolipoprotein e deficiency. *J. Clin. Invest.* 78(5):1206–19

250. Schenkel AR, Mamdouh Z, Muller WA. 2004. Locomotion of monocytes on endothelium is a critical step during extravasation. *Nat. Immunol.* 5(4):393–400

251. Schertzer JD, Tamrakar AK, Magalhaes JG, Pereira S, Bilan PJ, et al. 2011. Nod1 activators link innate immunity to insulin resistance. *Diabetes.* 60(9):2206–15

252. Schieffer B, Selle T, Hilfiker A, Hilfiker-Kleiner D, Grote K, et al. 2004. Impact of interleukin-6 on plaque development and morphology in experimental atherosclerosis. *Circulation.* 110(22):3493–3500

253. Schiller NK, Kubo N, Boisvert W a, Curtiss LK. 2001. Effect of gamma-irradiation and bone marrow transplantation on atherosclerosis in ldl receptor-deficient mice. *Arterioscler. Thromb. Vasc. Biol.* 21(10):1674–80

254. Scotland RS, Morales-Ruiz M, Chen Y, Yu J, Rudic RD, et al. 2002. Functional reconstitution of endothelial nitric oxide synthase reveals the importance of serine 1179 in endothelium-dependent vasomotion. *Circ. Res.* 90(8):904–10

255. Seki E, Brenner DA. 2008. Toll-like receptors and adaptor molecules in liver disease: update. *Hepatology.* 48(1):322–35

256. Sela S. 2005. Primed peripheral polymorphonuclear leukocyte: a culprit underlying chronic low-grade inflammation and systemic oxidative stress in chronic kidney disease. *J. Am. Soc. Nephrol.* 16(8):2431–38

257. Sender R, Fuchs S, Milo R. 2016. Revised estimates for the number of human and bacteria cells in the body. *Plos Biol.* 14(8):e1002533

258. Seong S-Y, Matzinger P. 2004. Hydrophobicity: an ancient damage-associated molecular pattern that initiates innate immune responses. *Nat. Rev. Immunol.* 4(6):469–78

259. Shurtz-Swirski R, Sela S, Herskovits a T, Shasha SM, Shapiro G, et al. 2001. Involvement of peripheral polymorphonuclear leukocytes in oxidative stress and inflammation in type 2 diabetic patients. *Diabetes Care.* 24(1):104–10

260. Sims F. 1985. Discontinuities in the internal elastic lamina: a comparison of coronary and internal mammary arteries. *Artery.* 13(3):127–43

261. Singbartl K, Thatte J, Smith ML, Wethmar K, Day K, Ley K. 2001. A cd2-green fluorescence protein-transgenic mouse reveals very late antigen-4-dependent cd8 + lymphocyte rolling in inflamed venules. *J. Immunol.* 166(24):7520–7526

262. Smiley ST, King JA, Hancock WW. 2001. Fibrinogen stimulates macrophage chemokine secretion through toll-like receptor 4. *J. Immunol.* 167(5):2887–94

263. Soehnlein O, Drechsler M, Do Y, Lievens D, Hartwig H, et al. 2013. Distinct functions of chemokine receptor axes in the atherogenic mobilization and recruitment of classical monocytes. *EMBO Mol Med.* 5(3):471–81

264. Sorescu D, Weiss D, Lassègue B, Clempus RE, Szöcs K, et al. 2002. Superoxide production and expression of nox family proteins in human atherosclerosis. *Circulation.* 105(12):1429–35

265. Springer TA. 1994. Traffic signals for lymphocyte recirculation and leukocyte emigration: the multistep paradigm. *Cell.* 76(2):301–14

266. Steinberg D, Parthasarathy S, Carew TETE, Khoo JCJC, Witztum JLJL. 1989. Beyond cholesterol. modifications of low-density lipoprotein that increase its

atherogenicity. *N. Engl. J. Med.* 320(14):915–24

267. Steinl DC, Kaufmann BA. 2015. Ultrasound imaging for risk assessment in atherosclerosis. *Int. J. Mol. Sci.* 16(5):9749–69
268. Stocker R, Keaney JF. 2004. Role of oxidative modifications in atherosclerosis. *Physiol Rev.* 84(4):1381–1478
269. Strong JP, McGill HC, McMahan CA, Herderick EE, Tracy RE, et al. 2000. Effects of coronary heart disease risk factors on atherosclerosis of selected regions of the aorta and right coronary artery. *Arterioscler. Thromb. Vasc. Biol.* 20(3):836–45
270. Summers C, Rankin SM, Condliffe AM, Singh N, Peters AM, Chilvers ER. 2010. Neutrophil kinetics in health and disease. *Trends Immunol.* 31(8):318–24
271. Swamydas M, Lionakis MS. 2013. Isolation , purification and labeling of mouse bone marrow neutrophils for functional studies and adoptive transfer experiments. *J. Vis. Exp.*, pp. 1–7
272. Swirski FK, Libby P, Aikawa E, Alcaide P, Luscinskas FW, et al. 2007. Ly-6chi monocytes dominate hypercholesterolemia-associated monocytosis and give rise to macrophages in atheromata. *J Clin Invest.* 117(1):195–205
273. Swirski FK, Nahrendorf M. 2013. Leukocyte behavior in atherosclerosis, myocardial infarction, and heart failure. *Science (80-.).* 339(6116):161–66
274. Swirski FK, Nahrendorf M, Etzrodt M, Wildgruber M, Panizzi P, et al. 2009. Identification of splenic reservoir monocytes and their deployment to inflammatory sites. *Science (80-.).* 325(5940):612–16
275. Swirski FK, Robbins CS. 2013. Neutrophils usher monocytes into sites of inflammation. *Circ. Res.* 112(5):744–45
276. Tacke F, Alvarez D, Kaplan TJ, Jakubzick C, Spanbroek R, et al. 2007. Monocyte subsets differentially employ ccr2, ccr5, and cx3cr1 to accumulate within atherosclerotic plaques. *J Clin Invest.* 117(1):185–94
277. Takeuchi O, Akira S. 2010. Pattern recognition receptors and inflammation. *Cell.* 140(6):805–20
278. Tamrakar AK, Schertzer JD, Chiu TT, Foley KP, Bilan PJ, et al. 2010. Nod2 activation induces muscle cell-autonomous innate immune responses and insulin

resistance. *Endocrinology.* 151(12):5624–37

279. Tarkin JM, Joshi FR, Rudd JHF. 2014. Pet imaging of inflammation in atherosclerosis. *Nat. Rev.* 11:443–57
280. Taubes G. 2001. Nutrition. the soft science of dietary fat. *Science (80-.).* 30(5513):2536–45
281. Tawakol A, Migrino RQ, Bashian GG, Bedri S, Vermylen D, et al. 2006. In vivo 18f-fluorodeoxyglucose positron emission tomography imaging provides a noninvasive measure of carotid plaque inflammation in patients. *J. Am. Coll. Cardiol.* 48(9):1818–24
282. Tedgui A, Mallat Z. 2006. Cytokines in atherosclerosis : pathogenic and regulatory pathways. *Physiol Rev.* 86(2):515–81
283. Tian X, Pascal G, Monget P. 2009. Evolution and functional divergence of nlrp genes in mammalian reproductive systems. *BMC Evol. Biol.* 9:202
284. Ting JPY, Lovering RC, Alnemri ES, Bertin J, Boss JM, et al. 2008. The nlr gene family: a standard nomenclature. *Immunity.* 28(3):285–87
285. Tiszlavicz Z, Somogyvári F, Kocsis ÁK, Szolnoki Z, Sztriha LK, et al. 2009. Relevance of the genetic polymorphism of nod1 in chlamydia pneumoniae seropositive stroke patients. *Eur. J. Neurol.* 16(11):1224–29
286. Tomasian D, Keaney JF, Vita JA. 2000. Antioxidants and the bioactivity of endothelium-derived nitric oxide. *Cardiovasc. Res.* 47(3):426–35
287. Travassos L, Carneiro L, Ramjeet M, Hussey S, Kim Y, et al. 2010. Nod1 and nod2 direct autophagy by recruiting atg16l1 to the plasma membrane at the site of bacterial entry: commentary. *Nat. Immunol.* 11(1):55–64
288. Tribble DL, Barcellos-Hoff MH, Chu BM, Gong EL. 1999. Ionizing radiation accelerates aortic lesion formation in fat-fed mice via sod-inhibitable processes. *Arterioscler. Thromb. Vasc. Biol.* 19(6):1387–92
289. Uppal N, Uppal V, Uppal P. 2014. Progression of coronary artery disease (cad) from stable angina (sa) towards myocardial infarction (mi): role of oxidative stress. *J. Clin. diagnostic Res.* 8(2):40–43
290. Viala J, Chaput C, Boneca IG, Cardona A, Girardin SE, et al. 2004. Nod1 responds

to peptidoglycan delivered by the helicobacter pylori cag pathogenicity island. *Nat. Immunol.* 5(11):1166–74

291. Viola J, Soehnlein O. 2015. Atherosclerosis - a matter of unresolved inflammation. *Semin. Immunol.* 27(3):184–93
292. Watanabe T, Asano N, Fichtner-feigl S, Gorelick PL, Tsuji Y, et al. 2010. Nod1 contributes to mouse host defense against helicobacter pylori via induction of type i ifn and activation of the isgf3 signaling pathway. *J. Cl.* 120(5):1645–62
293. Weber C, Noels H. 2011. Atherosclerosis: current pathogenesis and therapeutic options. *Nat. Med.* 17(11):1410–22
294. Williams K, Tabas I. 1998. The response-to-retention hypothesis of atherogenesis reinforced. *Curr. Opin. Lipidology1*. 9(5):471–74
295. Winter MBJ, Sayre GP, Millikan CH, Barker NW. 1958. Relationship of degree of atherosclerosis of internal carotid system in the brain of women to age and coronary atherosclerosis. *Circulation.* 18(1):7–18
296. Witztum JL, Steinberg D. 1991. Role of oxidized low density lipoprotein in atherogenesis. *J. Clin. Invest.* 88(6):1785–92
297. Woollard KJ, Geissmann F. 2010. Monocytes in atherosclerosis: subsets and functions. *Nat. Rev. Cardiol.* 7(2):77–86
298. Wu SC, Zhang Y. 2010. Active dna demethylation: many roads lead to rome. *Nat. Rev. Mol. Cell Biol.* 11(9):607–20
299. Xing F, Liu J, Mo Y, Liu Z, Qin Q, et al. 2009. Lysophosphatidylcholine up-regulates human endothelial nitric oxide synthase gene transactivity by c-jun n-terminal kinase signalling pathway. *J Cell Mol Med.* 13(6):1136–48
300. Yago T, Zarnitsyna VI, Klopocki AG, McEver RP, Zhu C. 2007. Transport governs flow-enhanced cell tethering through l-selectin at threshold shear. *Biophys. J.* 92(1):330–42
301. Yamashita H, Shimada K, Seki E, Mokuno H, Daida H. 2003. Concentrations of interleukins, interferon, and c-reactive protein in stable and unstable angina pectoris. *Am. J. Cardiol.* 91(2):133–36
302. Yang H, Li N, Song LN, Wang L, Tian C, et al. 2015. Activation of nod1 by dap

contributes to myocardial ischemia/reperfusion injury via multiple signaling pathways. *Apoptosis.* 20(4):512–22

303. Yang Y, Yin C, Pandey A, Abbott D, Sassetti C, Kelliher MA. 2007. Nod2 pathway activation by mdp or mycobacterium tuberculosis infection involves the stable polyubiquitination of rip2. *J. Biol. Chem.* 282(50):36223–29
304. Yang ZH, Richard V, von Segesser L, Bauer E, Stulz P, et al. 1990. Threshold concentrations of endothelin-1 potentiate contractions to norepinephrine and serotonin in human arteries. a new mechanism of vasospasm? *Circulation.* 82(1):188–95
305. Yoo NJ, Park WS, Kim SY, Reed JC, Son SG, et al. 2002. Nod1, a card protein, enhances pro-interleukin-1b processing through the interaction with pro-caspase-1. *Biochem. Biophys. Res. Commun.* 299(4):652–58
306. Yuan H, Zelkha S, Burkatovskaya M, Gupte R, Leeman SE, Amar S. 2014. Pivotal role of nod2 in inflammatory processes affecting atherosclerosis and periodontal bone loss. *Proc. Natl. Acad. Sci.* 110(52):E5059-68
307. Yura T, Fukunaga M, Khan R, Nassar GN, Badr KF, Montero A. 1999. Free-radical-generated f2-isoprostane stimulates cell proliferation and endothelin-1 expression on endothelial cells. *Kidney Int.* 56(2):471–78
308. Zarins CK, Giddens DP, Bharadvaj BK, Sottiurai VS, Mabon RF, Gladov S. 1983. Carotid bifurcation atherosclerosis: quantative correlation of plaque localization with flow velocity profiles and wall shear stress. *Circ. Res.* 53(4):502–14
309. Zembowicz A, Tang JL, Wu KK. 1995. Transcriptional induction of endothelial nitric oxide synthase type iii by lysophosphatidylcholine. *J. Biol. Chem.* 270(28):17006–10
310. Zernecke A, Weber C. 2014. Chemokines in atherosclerosis: proceedings resumed. *Arterioscler. Thromb. Vasc. Biol.* 34(4):742–50
311. Zeuke S, Ulmer AJ, Kusumoto S, Katus HA, Heine H. 2002. T lr4-mediated inflammatory activation of human coronary artery endothelial cells by lps. *Cardiovasc. Res.* 56(1):126–34
312. Zhang P, Dixon M, Zucchelli M, Hambiliki F, Levkov L, et al. 2008. Expression

analysis of the nlrp gene family suggests a role in human preimplantation development. *PLoS One*. 3(7):1–8

313. Zhang SH, Reddick RL, Piedrahita JA, Maeda N. 1992. Spontaneous hypercholesterolemia and arterial lesions in mice lacking apolipoprotein e. *Science (80-.).* 258(5081):468–71
314. Zhong Y, Kinio A, Saleh M. 2013. Functions of nod-like receptors in human diseases. *Front. Immunol.* 4(333):1–18
315. Zimmer S, Grebe A, Latz E. 2015. Danger signaling in atherosclerosis. *Circ. Res.* 116(2):323–40

8. Supporting Information

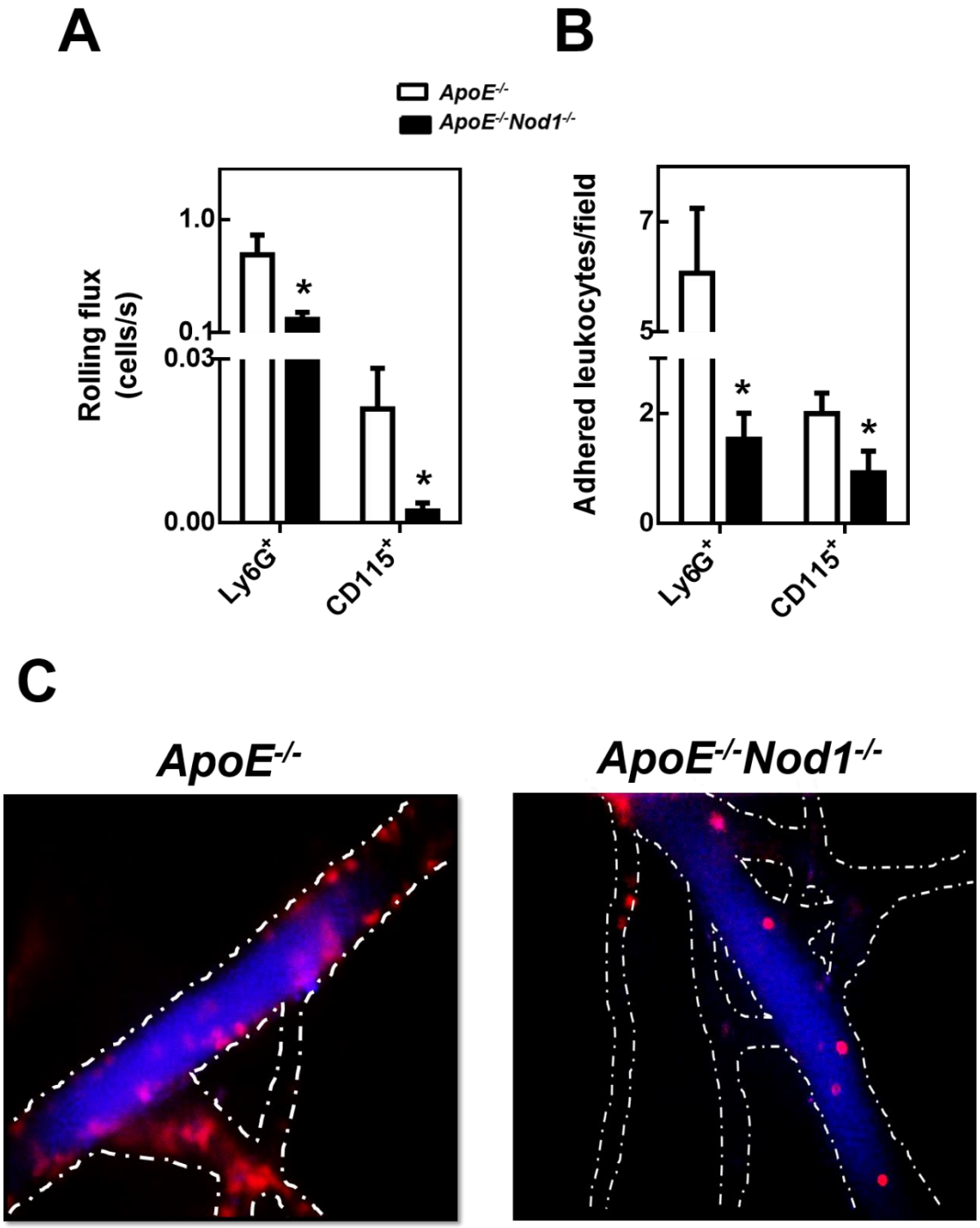

Figure S1. *ApoE*$^{-/-}$*Nod1*$^{-/-}$ monocytes and neutrophils have impaired adhesion and rolling in cremasteric microcirculation. Intravital microscopy of cremaster muscle from *ApoE*$^{-/-}$ (n=8) and *ApoE*$^{-/-}$*Nod1*$^{-/-}$ (n=7) mice to quantify leukocyte-endothelial wall interactions 3 weeks after HFD. Quantification of rolling flux for monocytes and neutrophils is represented in **(A)**, and the number of these cells adhered to the endothelium is represented in **(B)**. **(C)** Neutrophils were stained with an anti-Ly6G antibody (coloured in red) and monocytes were stained with an anti-Ly6C antibody (coloured in blue). Bars indicate mean ± SEM. Mann-Whitney U-test, $^{*}p < 0.05$.

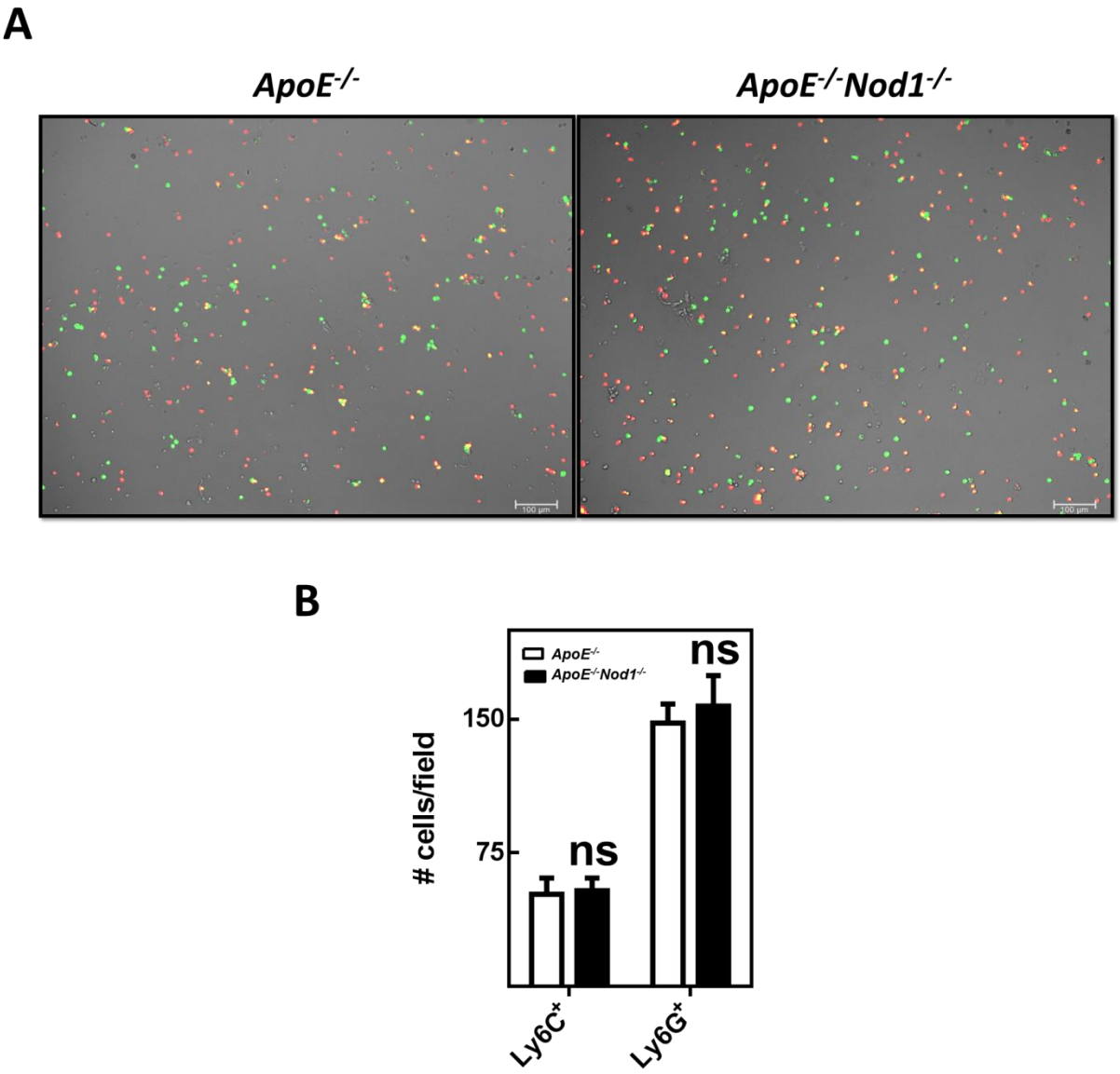

Figure S2. Deficiency of *Nod1* in monocytes and neutrophils does not affect VCAM-1-dependent static adhesion. (A) BM-derived monocytes and neutrophils from *ApoE*$^{-/-}$ (n=7) or *ApoE*$^{-/-}$ *Nod1*$^{-/-}$ (n=7) mice were isolated and immunolabelled for Ly6C (coloured in green) and Ly6G (coloured in red). VCAM-1 pre-coated 96-well plates were used to incubate for 30 minutes these isolated monocytes and neutrophils under static conditions. Scale bar, 100µm. **(B)** Quantification of Ly6C$^+$ cells and Ly6G$^+$ cells per field is represented (mean ± SEM; Student's t-test). Data was corrected by the corresponding relative number of monocytes or neutrophils perfused per individual mouse.

List of Scientific Papers

This Thesis manuscript for journal publication is in preparation.
Besides, several scientific papers have been published during the almost completed students' four-year period of Ph.D. training:

- Val-Blasco A, Piedras MJ GM*, Ruiz-Hurtado G*, Suarez N*, **González-Ramos S***, Prieto P, Gómez-Hurtado N, Delgado C, Pereira L, Benito G, Zaragoza C, Domenech N, Crespo-Leiro M, Vasquez-Echeverri D , Nuñez G, López-Collazo E, Boscá L., Fernández-Velasco M. Pivotal role of NOD1 in heart failure progression via regulation of Ca^{2+} handling. J Am Coll Cardiol. 2016. Under Revision.

- Val-Blasco A*, Prieto P*, **González-Ramos S***, Benito G*, Vallejo-Cremades MT, Pacheco I, González-Peramato P, Agra N, Terrón V, Delagado C, Martín-Sanz P, Boscá L, Fernández-Velasco M. NOD1 activation in cardiac fibroblasts induces myocardial fibrosis in a murine model of type 2 diabetes. Biochemical Journal. 2016. Revised Manuscript Submitted.

- Singh P*, **González-Ramos S***, Mojena M, Eduardo Rosales-Mendoza C, Emami H, Swanson J, Morss A, Fayad ZA, Rudd JH, Gelfand J, Paz-Garcia M, Martin-Sanz P, Bosca L, Tawakol A. GM-CSF Enhances Macrophage Glycolytic Activity in vitro and Improves Detection of Inflammation in vivo. J Nucl Med. 2016 Apr 14.

- Boscá L, **González-Ramos S**, Prieto P, Fernández-Velasco M, Mojena M, Martín-Sanz P, Alemany S. Metabolic signatures linked to macrophage polarization: from glucose metabolism to oxidative phosphorylation. Biochem Soc Trans. 2015 Aug;43(4):740-4.

- Delgado C*, Ruiz-Hurtado G*, Gómez-Hurtado N*, **González-Ramos S***, Rueda A, Benito G, Prieto P, Zaragoza C, Delicado EG, Pérez-Sen R, Miras-Portugal MT, Núñez G, Boscá L, Fernández-Velasco M. NOD1, a new player in cardiac function and calcium handling. Cardiovasc Res. 2015 Mar 30.

- Prieto P, Vallejo-Cremades MT, Benito G, González-Peramato P, Francés D, Agra N, Terrón V, **González-Ramos S**, Delgado C, Ruiz-Gayo M, Pacheco I, Velasco-Martín JP, Regadera J, Martín-Sanz P, López-Collazo E, Boscá L, Fernández-Velasco M. NOD1 receptor is up-regulated in diabetic human and murine myocardium. Clin Sci (Lond). 2014 Dec;127(12):665-77.

- Fernández-Velasco M, **González-Ramos S**, Boscá L. Involvement of monocytes/macrophages as key factors in the development and progression of cardiovascular diseases. Biochem J. 2014 Mar 1;458(2):187-93.

- **González-Ramos S.**, Carrasquero LM, Delicado EG, Miras-Portugal MT, Fernández-Velasco M, Boscá L. Determination of the Intracellular Calcium Concentration in Peritoneal Macrophages Using Microfluorimetry. Bio-protocol.org. 2013 Dec 05; 3(23): http://www.bio-protocol.org/e988.

* These authors contributed equally.

GM-CSF Enhances Macrophage Glycolytic Activity In Vitro and Improves Detection of Inflammation In Vivo

Parmanand Singh*[1], Silvia González-Ramos*[2], Marina Mojena[2], César Eduardo Rosales-Mendoza[2,3], Hamed Emami[4], Jeffrey Swanson[4], Alex Morss[4], Zahi A. Fayad[5], James H.F. Rudd[6], Jeffrey Gelfand[7], Marta Paz-García[2], Paloma Martín-Sanz[2,8], Lisardo Boscá†[2,8], and Ahmed Tawakol†[4]

[1]Cardiology Division, New York Presbyterian Hospital, Weill Cornell Medical College, New York, New York; [2]Instituto de Investigaciones Biomédicas "Alberto Sols," CSIC-UAM, Madrid, Spain; [3]Departamento de Bioquímica y Medicina Molecular, Universidad Autónoma de Nuevo León, Monterrey, Nuevo León, México; [4]Cardiac MR PET CT Program, Cardiology Division, Massachusetts General Hospital and Harvard Medical School, Boston, Massachusetts; [5]Translational and Molecular Imaging Institute, Icahn School of Medicine at Mount Sinai, New York, New York; [6]Division of Cardiovascular Medicine, University of Cambridge, Cambridge, United Kingdom; [7]Division of Infectious Diseases, Department of Medicine, Massachusetts General Hospital and Harvard Medical School, Boston, Massachusetts; and [8]Centro de Investigación Biomédica en Red de Enfermedades Hepáticas y Digestivas, Instituto de Salud Carlos III, Madrid, Spain

^{18}F-FDG accumulates in glycolytically active tissues and is known to concentrate in tissues that are rich in activated macrophages. In this study, we tested the hypotheses that human granulocyte-macrophage colony-stimulating factor (GM-CSF), a clinically used cytokine, increases macrophage glycolysis and deoxyglucose uptake in vitro and acutely enhances ^{18}F-FDG uptake within inflamed tissues such as atherosclerotic plaques in vivo. **Methods:** In vitro experiments were conducted on human macrophages whereby inflammatory activation and uptake of radiolabeled 2-deoxyglucose was assessed before and after GM-CSF exposure. In vivo studies were performed on mice and New Zealand White rabbits to assess the effect of GM-CSF on ^{18}F-FDG uptake in normal versus inflamed arteries, using PET. **Results:** Incubation of human macrophages with GM-CSF resulted in increased glycolysis and increased 2-deoxyglucose uptake ($P < 0.05$). This effect was attenuated by neutralizing antibodies against tumor necrosis factor–α or after silencing or inhibition of 6-phosphofructo-2-kinase. In vivo, in mice and in rabbits, intravenous GM-CSF administration resulted in a 70% and 73% increase ($P < 0.01$ for both), respectively, in arterial ^{18}F-FDG uptake in atherosclerotic animals but not in nonatherosclerotic controls. Histopathologic analysis demonstrated a significant correlation between in vivo ^{18}F-FDG uptake and macrophage staining ($R = 0.75$, $P < 0.01$). **Conclusion:** GM-CSF substantially augments glycolytic flux in vitro (via a mechanism dependent on ubiquitous type 6-phosphofructo-2-kinase and tumor necrosis factor–α) and increases ^{18}F-FDG uptake within inflamed atheroma in vivo. These findings demonstrate that GM-CSF can be used to enhance detection of inflammation. Further studies should explore the role of GM-CSF stimulation to enhance the detection of inflammatory foci in other disease states.

Key Words: ^{18}F-FDG-PET; glycolysis; GM-CSF; inflammation; macrophage

J Nucl Med 2016; 57:1428–1435
DOI: 10.2967/jnumed.115.167387

PET, in combination with ^{18}F-FDG, has been shown to be useful for the identification of inflamed tissues. Over the past few years, ^{18}F-FDG PET/CT imaging has been put into increasing clinical use to evaluate syndromes such as fever of unknown origin, cardiac sarcoidosis (*1,2*), prosthetic valve endocarditis (*3*), and infection of implanted devices (*4*). More recently, the use of ^{18}F-FDG PET/CT as a research tool to characterize atherosclerotic cardiovascular disease has been increasing. However, more widespread use of ^{18}F-FDG PET imaging of inflammatory foci has been limited, in part because of the relatively modest signal (*5*). Approaches to enhance ^{18}F-FDG localization to inflamed tissues could improve the clinical utility of ^{18}F-FDG PET imaging of inflammatory diseases.

Perhaps the most common chronic inflammatory disorder, atherosclerotic cardiovascular disease, remains the leading cause of mortality in the United States (*6*). Inflammation plays a pivotal role in atherogenesis, plaque progression, and thrombotic complications (*7*). In particular, the pathogenesis of atherosclerosis involves a myriad of immune mediators, with a well-accepted role for macrophages (*8*). A substantial body of cellular physiology literature has established that activated macrophages show upregulated glycolysis and hence avidly accumulate ^{18}F-FDG (*5,9*). Key enzymatic mediators of macrophage activity include the glucose transporters, the upper part of glycolysis, and specifically the expression of the ubiquitous form of 6-phosphofructo-2-kinase (PFKFB3), which has been noted to be upregulated in stimulated macrophages (compared with the constitutively expressed liver type-6-phosphofructo-2-kinase [PFKFB1] isoenzyme, which is associated with lower rates of glycolysis) (*9*). Advances in ^{18}F-FDG PET imaging have led to its use for the quantification of vascular wall inflammatory activity. ^{18}F-FDG uptake has been shown to

Received Sep. 24, 2015; revision accepted Mar. 7, 2016.
For correspondence or reprints contact: Lisardo Boscá, Instituto de Investigaciones Biomédicas "Alberto Sols" (CSIC-UAM), Arturo Duperier 4, 28029 Madrid, Spain.
E-mail: lbosca@iib.uam.es
*Contributed equally to this work.
†Contributed equally to this work.
Published online Apr. 14, 2016.

strongly correlate with arterial wall macrophage infiltration (*10*), systemic proinflammatory biomarkers (*11*), inflammatory cell gene expression (*12*), and increased risk for subsequent atherothrombotic events (*13,14*).

Granulocyte-macrophage colony-stimulating factor (GM-CSF) is a Food and Drug Administration–approved medication used to stimulate the production of white blood cells and thus prevent neutropenia after chemotherapy. It affects a wide range of immune cells, including macrophages, neutrophils, and dendritic cells (*15–18*). The drug is well tolerated, even among individuals with atherosclerosis or those with recent atherothrombotic events (*19,20*). Accordingly, we sought to evaluate whether GM-CSF could be used as an adjunctive agent to enhance the detection of inflamed foci. Specifically, we performed both in vitro and in vivo experiments to better understand the effect of GM-CSF on macrophage glycolytic flux and on ^{18}F-FDG uptake, which is dependent on glucose flux. In these studies, we tested the hypotheses that GM-CSF augments glycolytic flux in macrophages in vitro and enhances ^{18}F-FDG accumulation within inflammatory foci in vivo, thereby enhancing imaging sensitivity.

MATERIALS AND METHODS

Cellular Experiments

Chemicals. Reagents and antibodies were from Sigma-Aldrich, Roche, Invitrogen, R&D Systems, Santa Cruz Biotech, or Merck-Millipore. [U-^{14}C]-2-deoxyglucose (9,250 kBq [250 μCi]/mmol) was from New England Nuclear/Perkin Elmer. Serum and media were from BioWhittaker. Murine and human GM-CSFs were from PeproTech or Gentaur.

Preparation of Human Monocytes/Macrophages. PBMCs were isolated from the blood of healthy donors by centrifugation on Ficoll-Hypaque Plus (GE Biotech) following the manufacturer's protocol, and the CD14-enriched fraction was collected after binding to MACS-hCD14-magnetic beads (Miltenyi Biotec). Cells were differentiated with human CSF-1 (20 ng/mL, PeproTech) for 5 d in RPMI1640 supplemented with antibiotics and 10% fetal calf serum. After this period, the cells were kept for 48 h in medium lacking CSF-1 and treated with the indicated stimuli. The purity of all cultures was verified by CD14$^+$ staining; on average, more than 95% of the cells were highly positive for this surface marker.

Tumor Necrosis Factor–α (TNF-α) Neutralization. The cells were maintained in culture and, 1 h before GM-CSF challenge, were treated with a 20 ng/mL concentration of anti-TNF-α neutralizing antibody (R&D Systems) as previously described (*9*), using a mouse IgG as control.

PFKFB3 Silencing in Macrophages. The cells were transfected overnight with lipofectamine and a mixture of 3 different Silencer Select predesigned silencer RNAs from Ambion/Invivogen, following the instructions of the supplier. Controls with scrambled (negative) RNAs were used to ensure the specificity of the silencing.

Measurement of Radiolabeled Deoxyglucose Accumulation. To evaluate 2-deoxyglucose uptake, the cells (6-cm dishes) were washed with warm Dulbecco modified Eagle medium lacking glucose and incubated with this medium containing 0.3 mM glucose and 92.5 kBq (2.5 μCi) of [U-^{14}C]-2-deoxyglucose for 60–90 s, following a previous protocol (*21*). The reaction was stopped by rapid aspiration of the medium and addition of 1 mL of ice-cold Dulbecco modified Eagle medium containing 10 mM glucose and 0.1 mM phloretin. The cell layer was washed twice with ice-cold phosphate-buffered saline, and the cells were resuspended in 1 mL of 0.1 M NaOH in 0.1% sodium dodecyl sulfate. A linear incorporation of radioactivity was observed for at least 2 min by scintillation counting.

Preparation of Macrophage Extracts. The cell cultures were washed twice with ice-cold phosphate-buffered saline and homogenized in 0.2 mL of buffer containing 10 mM Tris-HCl, pH 7.5; 1 mM $MgCl_2$; 1 mM ethylene glycol tetraacetic acid; 10% glycerol; 0.5% CHAPS buffer (3-[(3-cholamidopropyl)dimethylammonio]-1-propanesulfonate); 1 mM β-mercaptoethanol; and 0.1 mM phenylmethylsulfonyl fluoride and a protease inhibitor cocktail (Sigma). The extracts were stirred in a vortex mixer for 30 min at 4°C and centrifuged for 15 min at 13,000*g*. The supernatants were stored at −20°C. Protein levels were determined using the Bio-Rad detergent-compatible protein reagent. All steps were performed at 4°C.

Western Blot Analysis. Samples of cell extracts containing equal amounts of protein (30 μg per lane) were boiled in 250 mM Tris-HCl, pH 6.8; 2% sodium dodecyl sulfate; 10% glycerol; and 2% β-mercaptoethanol and size-separated in 10%–15% sodium dodecyl sulfate polyacrylamide gel electrophoresis. The gels were blotted onto a polyvinylidene fluoride membrane (GE Healthcare) and processed as recommended by the supplier of the antibodies against the following human antigens: signal transducer and activator of transcription 5 (STAT5), P-STAT5, hexokinase-1, hexokinase-2, PFK-1, PFKFB1, PFKFB3, glyceraldehyde 3-phosphate dehydrogenase, and β-actin. The blots were developed by ECL protocol (GE Healthcare), and different exposition times were performed for each blot with a charge-coupled device camera in a luminescent image analyzer (Molecular Imager; BioRad) to ensure the linearity of the band intensities.

Measurement of TNF-α, Lactate, and Fructose-2,6-Bisphosphate (Fru-2,6-P_2). TNF-α was measured in the cell culture medium using an ELISA kit (PeproTech). Lactate accumulation was also measured in the culture medium as previously described (*9,22*). The intracellular concentration of Fru-2,6-P_2 was determined in cell extracts treated with 0.1 mL of NaOH (50 mM at 80°C) and heated at 80°C for 10 min. The metabolite was measured after the activation of the pyrophosphate-dependent 6-phosphofructo-1-kinase activity following a previous protocol (*9,22*).

Real-Time Quantitative Polymerase Chain Reaction. 3-mo-old *Apoe*$^{-/-}$ mice were fed for 2 wk with a high-fat diet and intraperitoneally administered 37.5 μg/kg of GM-CSF on day 12. On day 14, they were sacrificed and the whole aorta was cleaned to remove the adventitial fat and connective tissue in the magnifying glass, always working over a sheet of ice. The aortas were transferred to RNAlater RNA stabilization reagent (QIAGEN) and then to dry ice. Aorta total RNA was isolated by homogenization in QIAzol (QIAGEN) by a Tissue Lyser LT (QIAGEN) and eluted in a volume of 15 μL using MinElute columns (QIAGEN). RNA integrity was assessed by RNA 6000 Nano Kit (Agilent). A 250-ng quantity of RNA was retrotranscribed using a high-capacity complementary DNA reverse transcription kit (Life Technologies). Real-time polymerase chain reaction was conducted with SYBR Green (Life Technologies) in a fast real-time polymerase chain reaction system (Life Technologies). The real-time polymerase chain reaction assay was performed with 5 ng of complementary DNA per well, and the thermocycling conditions were 95°C for 10 min and 40 cycles of 95°C for 15 s followed by 60°C for 1 min. Calculations were made from measurement of triplicates of each sample. The relative amount of messenger RNA (mRNA) was calculated with the comparative $2^{-\Delta\Delta Ct}$ method. Gene expression was normalized to *36b4*. Primer sequences are available on request.

Statistical Analysis. The data shown are the mean ± SD of 3–5 experiments. Statistical significance was estimated with the Student *t* test for unpaired observations or ANOVA followed by the Bonferroni test when appropriate. Differences with values of P less than 0.05 were considered statistically significant.

Animal Model Studies

Mouse Model. Animal care and experimental procedures were performed according to directive 2010/63/EU of the European Parliament, and the studies were approved by the Institutional Committee on Bioethics (authorization 28079-37A to the Instituto de Investigaciones Biomédicas).

PFKFB3 In Vivo Silencing. A mixture of at least 3 different Silencer Select predesigned silencer RNAs for PFKFB3 was obtained from different sources (Ambion/InvivoGen, OriGene, or Sigma-Aldrich). The transfection mixture was prepared using Invivofectamine 2.0 (InvivoGen) and was administered intraperitoneally at 5 mg/kg per dose, following the instructions of the supplier. Administration of the corresponding scrambled (negative) RNAs was used to ensure the specificity of the silencing.

Atherogenesis in ApoE-Deficient Mice and ^{18}F-FDG PET Image Analysis. Thirty male ApoE-deficient mice 3–4 mo old were fed a high-fat/high-cholesterol diet for 3 wk, and after anesthesia with isoflurane, ^{18}F-FDG (37 MBq/kg; 0.2 mL) was administered intraperitoneally and the ^{18}F emission was analyzed in a small-animal CT/SPECT/PET system (Inveon; Siemens). The images were analyzed and quantified as previously described (*9*). Briefly, the first axial slice, representing the descending aorta (the first PET/CT slice clear of the aortic arch), and 5 consecutive slices at intervals of 3 mm were averaged to obtain the SUV_{max}. Measured background SUVs from the paraspinal muscles were used to obtain a corrected TBR. When PFKFB3 was silenced, the silencer RNAs were administered at days 3, 7, 10, and 12 after high-fat/high-cholesterol administration. A mixture of scrambled RNAs was used as control and administered at the same periods. GM-CSF (37.5 μg/kg) was intravenously administered on day 12. The animals were processed on day 14 for images and biochemical analyses.

Rabbit Model. Nine male New Zealand White rabbits (Charles River Breeding Laboratories) were included in the study. Seven of the rabbits were initiated on a 0.3% cholesterol, 4.7% peanut oil hyperlipidemic diet for 6 mo to precipitate the development of atherosclerosis. One week after beginning the high-cholesterol diet, the animals were briefly anesthetized using ketamine and xylazine, and aortoiliofemoral denudation was performed by balloon catheter injury using a modified Baumgartner technique (*23*). Additionally, 2 control rabbits of similar size and identical origin were maintained on standard rabbit chow for 6 mo. No catheterization or other invasive procedure was performed on the control animals.

Rabbit PET/CT Imaging Protocol. After 6 mo of the prescribed diet, 8 atherosclerotic animals and 2 healthy controls underwent ^{18}F-FDG PET imaging. The animals were injected with a 37 MBq/kg dose of ^{18}F-FDG, and PET images were obtained on a microPET P4 (Concorde MicroSystems) or similar system 3 h after ^{18}F-FDG administration to allow for maximum tracer uptake. The choice of time interval after ^{18}F-FDG injection was based on our previous work in animals (*10*). Images were obtained over 20 min and reconstructed using a filtered backprojection algorithm. The microPET P4 scanner is an animal PET tomograph with 32 planes over a 7.8-cm axial extent, 19-cm transaxial field of view, and 22-cm animal port. Within 6 d of PET imaging, multidetector CT imaging was performed for anatomic coregistration.

GM-CSF Administration to Rabbits. After baseline imaging, 6 animals (4 atherosclerotic animals and 2 healthy controls) were injected with 100 μg of sargramostim (yeast-derived recombinant human GM-CSF; Berlex) daily for a total of 3 d. Four atherosclerotic animals received saline injections at identical time points. One hour after the final injection on day 3, a 37 MBq/kg dose of ^{18}F-FDG was administered, and PET imaging was performed 3 h afterward. The biodistribution methods and results are provided in the supplemental data, available at http://jnm.snmjournals.org (Supplemental Fig. 1).

^{18}F-FDG PET Image Analysis in Rabbits. The PET images were analyzed with masking of treatment allocation and temporal sequence. First, localization of aortic ^{18}F-FDG uptake was aided by coregistering the PET images with the multidetector CT images. The temporally masked baseline and follow-up PET image pairs were registered to their common multidetector CT images using a workstation that allows multimodal standard image fusion (REVEAL-MVS; Mirada Solutions) (*24*). Thereafter, ^{18}F-FDG uptake could be compared for several stacked aortic segments over time. Aortic ^{18}F-FDG uptake was quantified by drawing a circular region of interest around the aorta in the axial view, in 4-mm increments (yielding a stack of 4-mm-thick aortic slices composing the imaged aorta). For each region of interest, the maximal SUV was recorded. The SUV is the decay-corrected tissue concentration of ^{18}F-FDG (in kBq/mL) divided by the injected dose per body weight. Background ^{18}F-FDG uptake was measured in the paraspinal muscles as an average of ten 20-mm^2 region-of-interest samples. SUV_{max} was then background-corrected to derive a target-to-background ratio (TBR) for each aortic slice.

Histologic Analysis in Rabbits. After final imaging assessments, 3 atherosclerotic animals were sacrificed using an overdose of sodium pentobarbital. The aortas were excised, placed in 10% buffered formalin, and decalcified according to the standard protocol. The aortic samples were sectioned transversely at 5-mm intervals and stained with rabbit macrophage-specific monoclonal antibody RAM11 (Dako Corp.). RAM11 staining was calculated as a percentage of the stained area over the total cross-sectional area of the transversely sectioned aortic wall. Multiple segments from each rabbit abdominal aorta were obtained and compared against the corresponding PET axial slices. The averaged RAM11 staining for each 5-mm aortic segment was also obtained and compared with the mean TBR for the same segments. The association between anatomic histologic segments and corresponding PET images was based on distances from the renal arteries measured ex vivo compared with the coregistered multidetector CT images. Control animals were not sacrificed for histologic analysis because previous work has demonstrated that there is no inflammation (percentage rabbit antimacrophage antibodies [%RAM11 staining]) within the aortic wall of control rabbits (*24*).

Statistical Analysis. Data were analyzed using SPSS, version 22 (IBM). Continuous parameters are reported as mean ± SEM. Statistical analysis comparing the change in the TBR across atherosclerotic segments (before and after treatment with GM-CSF or saline) was performed using the Wilcoxon signed-rank test. The Spearman method was used to assess the correlation between atherosclerotic tissue uptake of ^{18}F-FDG after GM-CSF (measured by PET, as TBR) and the subsequent histopathologic assessment of inflammation in those same sections (%RAM11 staining). A P value of less than 0.05 was considered statistically significant.

RESULTS

GM-CSF Augments Glycolytic Flux via Upregulation of PFKFB3

In human macrophages, incubation with GM-CSF resulted in rapid phosphorylation of STAT5 in Y694 (Fig. 1A) and metabolic reprograming of macrophages (including modest increases in hexokinase-1 and hexokinase-2; Fig. 1B). Moreover, there was a substantial increase in PFKFB3, which was negligibly expressed before GM-CSF (Figs. 1B and 1C). The PFKFB3 isoform has a much higher net kinase activity than the constitutively expressed PFKFB1 isoenzyme. Thus, upregulation of PFKFB3 would be expected to produce substantially higher glycolytic flux. The specificity of this association was demonstrated using silencing RNA for PFKFB3, which resulted in attenuated induction of PFKFB3 (Fig. 1D), but not by the scrambled RNA sequence. Additionally, the selective PFKFB3 inhibitor 3-(3-pyridinyl)-1-(4-pyridinyl)-2-propen-1-one (3PO) did not alter the induction of this gene by GM-CSF (Fig. 1D).

In line with the increased expression of glycolytic enzymes, GM-CSF resulted in a substantial increase in glycolytic flux (measured as Fru-2-6-P_2 concentration, a potent activator of glycolysis; Fig. 2A). This augmented glycolytic flux was attenuated

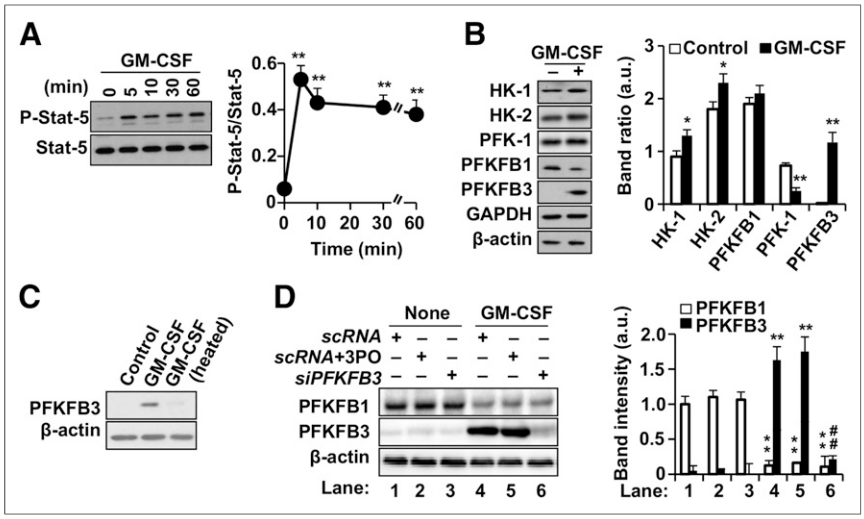

FIGURE 1. GM-CSF augments 2-deoxyglucose uptake and glycolytic flux in human macrophages via PFKFB3. (A and B) Human monocytes were differentiated to macrophages. Cells were exposed to human GM-CSF (10 ng/mL) for the specified time duration, and phosphorylation of STAT5 in Y694 (A) and levels of glycolytic enzymes (B) were determined. Addition of GM-CSF induced significant expression of hexokinase-1, hexokinase-2, and mainly PFKFB3. (C) Cells exposed to native GM-CSF demonstrated increased PFKFB3 expression compared with incubation with heat-inactivated GM-CSF (10 min at 80°C). (D) GM-CSF–mediated increase in PFKFB3 expression (right) was decreased with addition of silencer to PFKFB3 but not by selective PFKFB3 inhibiter 3PO, demonstrating specificity of silencer. Cells were treated with mixture of siPFKFB3 for silencing PFKFB3 18 h before challenge with GM-CSF. Results show mean ± SD. $^{*}P < 0.05$ vs. same condition in control (absence of GM-CSF or 0 h). $^{**}P < 0.01$ vs. same condition in control (absence of GM-CSF or 0 h). $^{\#\#}P < 0.01$ for *scRNA* vs. *siPFKFB3* with or without 3PO. a.u. = arbitrary units; GAPDH = glyceraldehyde 3-phosphate dehydrogenase; HK = hexokinase; scRNA = scrambled RNA.

after inhibition of PFKFB3 by 3PO. In concert with the rise in Fru-2-6-P_2 concentration, GM-CSF also increased lactate accumulation in the medium (Fig. 2B).

Additionally, GM-CSF resulted in a selective (not achieved by heat-denatured GM-CSF) and modest increase in proinflammatory activation of the macrophages (as evidenced by macrophage TNF-α production; Fig. 2C). Furthermore, antagonism of TNF-α (using a neutralizing anti-TNF-α antibody) attenuated the glycolytic flux (measured as Fru-2-6-P_2 concentration) after GM-CSF (Fig. 2D).

GM-CSF Augments Deoxyglucose Accumulation Within Cultured Macrophages

Incubation of macrophages with GM-CSF upregulated the incorporation of [U-^{14}C]-2-deoxyglucose in a manner that paralleled its impact on glycolytic flux (Figs. 2E and 2F). A time-dependent increase in 2-deoxyglucose uptake was observed after GM-CSF challenge (Fig. 2E). The rate of 2-deoxyglucose uptake was significantly greater than in control cells, was increased as early as 2–4 h after GM-CSF exposure, and persisted, at a more pronounced rate of increase, at later time points ($P < 0.01$). Also, in parallel with the impact of GM-CSF on glycolysis, blocking of TNF-α or inhibition (3PO) or silencing (*siPFKFB3*) of PFKFB3 resulted in reduced 2-deoxyglucose uptake (Figs. 2E and 2F).

GM-CSF Increases Atherosclerotic ^{18}F-FDG Uptake In Vivo Without Altering Lesion Area

The in vivo impact of GM-CSF on chronic atherosclerotic inflammation was investigated in 2 animal models (mouse and rabbit). In *Apoe*$^{-/-}$ mice fed for 2 wk on a high-fat diet, administration of GM-CSF (on day 12 of the diet) significantly enhanced the aortic ^{18}F-FDG uptake (TBR measured at 48 h after administration was increased by 70% relative to animals treated with vehicle; $P < 0.01$), whereas aortic ^{18}F-FDG uptake did not increase in animals given both GM-CSF and silencer mRNA for *PFKFB3* (Fig. 3A). When the lesion area was evaluated after oil red staining, the single-dose administration of GM-CSF did not influence the lipid accumulation (Fig. 3B). Moreover, the increased TBR was the result of a significant increase in target (arterial) activity, whereas the background activity did not significantly change with GM-CSF (Fig. 3C).

Further, to assess the impact of GM-CSF on potential infiltration of circulating monocytes into the aortic wall, the whole aorta from treated animals was analyzed using real-time quantitative polymerase chain reaction. As Figure 3D shows, the macrophage-specific gene, *Lxrα,* did not increase after GM-CSF administration when compared with specific endothelial and smooth muscle cell markers (i.e., *F8, Sm22a, Myh11,* and *Col1a1*). Together, these results suggest a minimal contribution of GM-CSF, if any, to enhance the recruitment of monocytes to the lesion area, in agreement with previous data (*9*).

In atherosclerotic rabbits, GM-CSF administration was associated with an approximately 73% increase in ^{18}F-FDG uptake (5.87 ± 0.14 vs. 10.09 ± 0.40 before vs. after GM-CSF, arterial TBR ± SEM, $P < 0.01$; Figs. 4A and 4B). Atherosclerotic animals injected with saline showed no statistically significant change in TBR (4.17 ± 0.32 vs. 4.08 ± 0.20, $P < 0.01$) over the same time period. Further, in healthy rabbits without atherosclerotic inflammation, GM-CSF administration was associated with a decrease in the arterial signal (2.26 ± 0.07 vs. 1.47 ± 0.17, $P < 0.01$). In contrast, blood ^{18}F-FDG activity did not differ between rabbits given GMCSF and those given saline (supplemental data). Collectively, these data demonstrate that administration of GM-CSF augments ^{18}F-FDG uptake within the arterial wall in atherosclerotic but not in normal rabbits.

Atherosclerotic ^{18}F-FDG Uptake After GM-CSF Correlates with Macrophage Density

Next, we tested the hypothesis that arterial ^{18}F-FDG uptake after GM-CSF correlates with histologic macrophage density. To do so, we compared ^{18}F-FDG uptake in atherosclerotic rabbits with macrophage-specific %RAM11 staining in histologic segments of aortas from sacrificed animals. We observed that ^{18}F-FDG uptake significantly correlated with %RAM11 staining ($R = 0.76$, $P = 0.002$; Fig. 5).

DISCUSSION

Here, we have shown that GM-CSF augments the glycolytic flux in vitro (via a mechanism that depends on PFKFB3) and

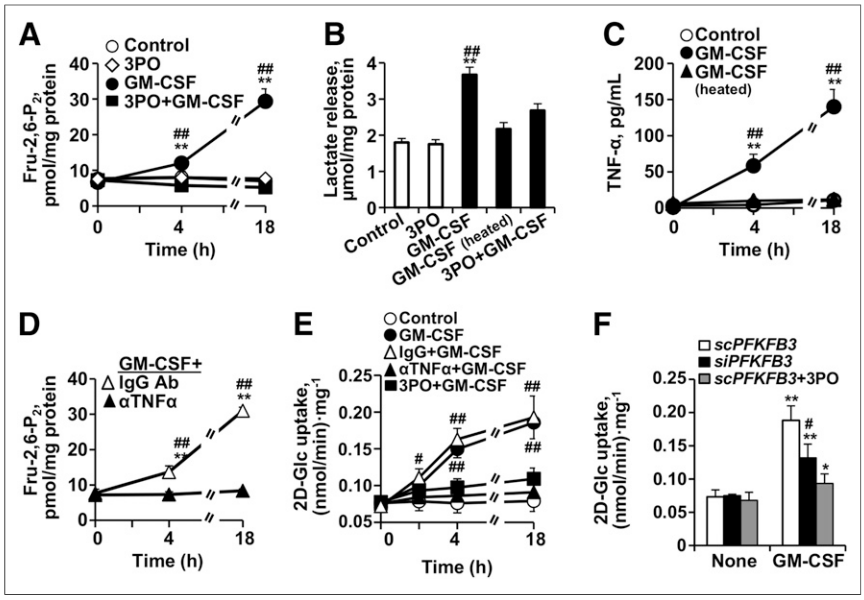

FIGURE 2. PFKFB3 mediates increase in 2-deoxyglucose uptake in human macrophages treated with GM-CSF. (A) Intracellular levels of Fru-2,6-P_2 were determined at the indicated times with and without GM-CSF and in absence or presence of PFKFB3 inhibitor 3PO (5 μM). GM-CSF augments Fru-2,6-P_2 levels, which are attenuated in presence of 3PO, demonstrating critical role of expression of PFKFB3 after GM-CSF treatment. (B) Lactate accumulation in culture medium was determined at 18 h with and without native or heat-inactivated GM-CSF and in absence or presence of 3PO (5 μM). Lactate levels (by-product of glycolysis) increase with GM-CSF exposure and are dampened by 3PO. (C) TNF-α levels were determined in culture medium after challenge with native or heat-inactivated GM-CSF. (D) Intracellular levels of Fru-2,6-P_2 were determined at the indicated times with GM-CSF and in presence of neutralizing anti-TNF-α antibody. GM-CSF augments Fru-2,6-P_2 levels, which are attenuated in presence of neutralizing anti-TNF-α antibody. (E) 2-deoxyglucose uptake was determined at the indicated times with and without GM-CSF and in absence or presence of neutralizing anti-TNF-α antibody (20 ng/mL) or PFKFB3 inhibitor 3PO (5 μM). 2-deoxyglucose significantly increases with addition of GM-CSF. This effect was diminished with neutralizing anti-TNF-α antibody and with 3PO. (F) To analyze contribution of PFKFB3 to enhancement of glycolytic flux elicited by GM-CSF, macrophages were transfected for 18 h with specific siRNA to silence PFKFB3 or with corresponding inactive RNA control (scRNA) and in absence or presence of 3PO, followed by activation for 18 h with GM-CSF. 2-deoxyglucose uptake was significantly decreased after silencing PFKFB3 compared with corresponding control (scRNA) or inhibition with 3PO. Data are mean ± SD. $^{*}P < 0.05$ vs. same condition in control (absence of GM-CSF or 0 h). $^{**}P < 0.01$ vs. same condition in control (absence of GM-CSF or 0 h). $^{\#}P < 0.05$ for GM-CSF vs. heated GM-CSF, with 3PO plus GM-CSF. $^{\#\#}P < 0.01$ for GM-CSF vs. heated GM-CSF, with 3PO plus GM-CSF. IgG vs. anti-TNF-α antibody or *scRNA* vs. *siPFKFB3* with or without 3PO. scRNA = scrambled RNA; siRNA = silencer RNA.

acutely increases ^{18}F-FDG uptake within inflamed tissues in vivo (in 2 animal atherosclerotic models). These data suggest that GM-CSF, when administered as an adjunctive imaging agent, improves the sensitivity for detecting inflammatory foci. Further investigations to evaluate the clinical impact of GM-CSF in ^{18}F-FDG PET imaging are warranted.

GM-CSF is an endogenously circulating cytokine that is present at basal levels in serum. Recombinant human GM-CSF, a widely available and clinically used immunomodulatory agent, was first approved by the Food and Drug Administration in 1991 for the acceleration of myeloid recovery after autologous bone marrow transplantation. Since that time, the use of GM-CSF has expanded. GM-CSF acts to mobilize peripheral-blood progenitor cells, resulting in shorter durations of neutropenia in patients receiving induction chemotherapy for hematologic malignancies (*25*). Further, it is widely appreciated that GM-CSF increases the hematopoietic ^{18}F-FDG signal and that the heightened signal may persist for weeks after the last dose (*16,26–31*). The findings of this study provide further understanding of the mechanisms underlying this observation.

Here, we show that GM-CSF acutely increases the expression of PFKFB3, resulting in increased glycolytic flux compared with the constitutively expressed PFKFB1, since PFKFB3 has a much higher net kinase activity, therefore increasing the intracellular levels of Fru-2,6-P_2 and accelerating the upper part of glycolysis. Further, we found that the upregulation of PFKFB3 was necessary for the increased glycolytic flux seen with GM-CSF in both in vitro (human macrophages) and in vivo models (mice): blocking PFKFB3 (with silencer RNA specific for PFKB3 or inhibiting its activity using 3PO) resulted in levels of glycolysis that were only slightly above baseline levels. Additionally, we observed that antagonism of TNF-α (using an antibody against TNF-α) resulted in an attenuation of glycolytic flux after GM-CSF. This finding is consistent with the prior observation that PFKFB3 activation results in augmented TNF-α production and that the TNF-α in turn leads to increased PFKB3 (via a mechanism that relies on HIF-1α (*9*).

Moreover, we found that GM-CSF provided a roughly 3-fold increase in glycolytic flux and a similar increase in macrophage 2-deoxyglucose uptake in vitro. Similarly, in the *Apoe*$^{-/-}$ mice and in the rabbit models of atherosclerosis, we observed an approximately 70%–73% increase in ^{18}F-FDG uptake. Such increased ^{18}F-FDG uptake might provide improved detection of infectious foci.

The studies examining the effects of chronic GM-CSF administration on atherosclerosis have provided inconsistent findings (*32*). In one study, hyperlipidemic *LDLR*−/− mice with a GM-CSF deficiency exhibited a 20%–50% decrease in aortic lesion size, depending on the location of the lesions and the sex of the animals. In another, *Apoe*−/− mice treated with GM-CSF chronically manifested an increased atherosclerotic-lesion area. However, in another study, *Apoe*−/− mice with a genetic deletion of GM-CSF demonstrated an increased atherosclerotic-lesion size (without changes in plasma cholesterol). It follows then, that both proatherogenic and antiatherogenic properties have been attributed to GM-CSF. Accordingly, the consequences of long-term GM-CSF administration have yet to be determined. However, clinical experience with short-term GM-CSF administration suggests no increased risk of cardiovascular complications (*33*).

Clinical Implications

The concept of transiently "stimulating" macrophages with GM-CSF to improve the signal-to-noise ratio of inflammatory foci is analogous to the use of exercise stress testing to enhance the detection of myocardial ischemia. With electrocardiographic exercise treadmill

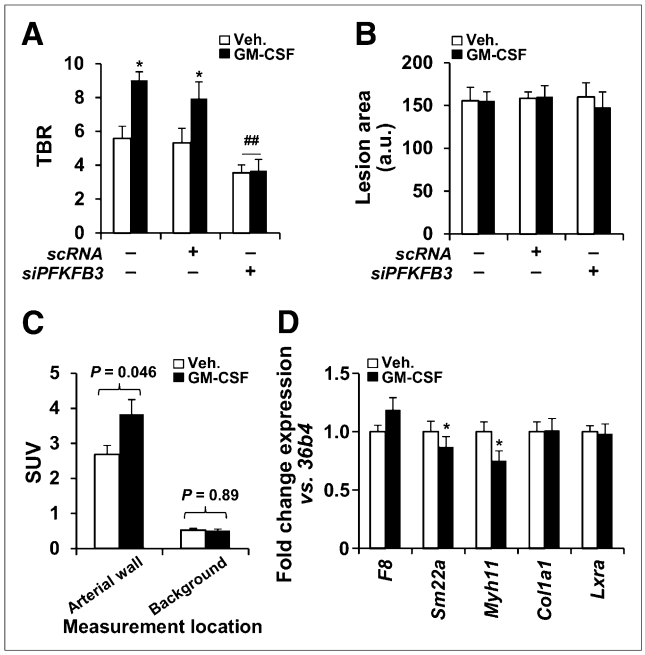

FIGURE 3. In vivo augmentation of ^{18}F-FDG uptake after GM-CSF administration in mice. (A) ^{18}F-FDG uptake in atherosclerotic mice (n = 30). Animals received *siPFKFB3* (n = 10) or *scRNA* (n = 8) at days 3, 7, 10, and 12 after high-fat/high-cholesterol administration. GM-CSF (37.5 μg/kg; n = 15) or saline (n = 15) was intravenously administered on day 12, and ^{18}F-FDG and PET analysis was performed on day 14. (B) Aortas were stained with oil red and images evaluated with Image J. (C) Average target and background SUVs from A were compared (n = 15 animals for each group). Target SUVs were higher with than without GMCSF (3.38 ± 0.46 vs. 2.70 ± 0.26; P = 0.046). Background SUVs were unchanged with vs. without GMCSF (0.54 ± 0.10 vs. 0.55 ± 0.10; P = 0.53). (D) In parallel experiment, aortas from untreated (n = 4) or GM-CSF–treated animals (n = 4) as described in A were isolated and RNA extracted for analysis of the indicated genes representative of endothelial cells (*F8*), smooth muscle cells (*Sm22a, Myh11, Col1a1*), and macrophages (*Lxra*). Data are mean ± SD. $^{*}P < 0.05$ vs. same condition in absence of GM-CSF. $^{\#\#}P < 0.01$ vs. same condition with *scRNA*. a.u. = arbitrary units; *scRNA* = scrambled RNA.

testing, the detection of occlusive coronary lesions (those that cause myocardial ischemia) is limited under resting conditions. However, when exercise is used to temporarily induce myocardial ischemia (leading to diagnostic changes on the electrocardiogram), a substantial boost in test sensitivity is yielded. At the same time, the induction of transient ischemia during exercise has been shown to be remarkably safe. Analogously, we propose further examination of the use of GM-CSF to transiently and safely provoke an inflammatory signal. This transient provocation may substantially improve the detection of inflammatory lesions, such as atherosclerotic or infectious foci.

Importantly, GM-CSF has a relatively safe track record, even when used for extended periods. The in vivo data presented within this study and from others provide some explanation of why GM-CSF has a relatively modest proinflammatory profile compared with some other cytokines. We previously reported that lipopolysaccharide induces a 50- and 15-fold greater increase in TNF-α mRNA and protein production, respectively, compared with GM-CSF (*9*). In that experiment as well, GM-CSF resulted in a 6-fold increase in Arg-1 mRNA, a prototypical marker of M2 polarization. In fact, the increase in Arg-1 mRNA exceeded the increase in TNF-α mRNA, supporting the notion that GM-CSF provides a balanced increase in M1 as well as M2 polarization, yielding an intermediate polarization profile.

Moreover, the safety of GM-CSF has already been established in patients who have a preponderance of atherosclerotic risk factors, as well as in critically ill patients (*33*). In fact, GM-CSF may have benefits in chronic atherosclerosis (potentially related to augmentation of progenitor cell release) and is being examined as a therapy for chronic peripheral arterial disease (ClinicalTrials.gov identifier NCT01408901) (*34,35*).

^{18}F-FDG PET imaging has already become a critical tool in the localization of infections in the setting of fever of unknown origin (*36,37*). Our findings offer justification to further explore the use of GM-CSF as an adjunctive agent for ^{18}F-FDG PET imaging of inflammation, in both acute and chronic inflammatory diseases (such as atherosclerosis and infections). In such cases, GM-CSF would be expected to transiently increase the ^{18}F-FDG signal within inflammatory cells and thus enhance the sensitivity, and possibly the specificity, of PET/CT imaging for detecting an inflammatory lesion.

Use of GM-CSF as an Adjunctive Imaging Agent in Other Settings

GM-CSF might also aid in the characterization of malignancies. ^{18}F-FDG PET/CT imaging has proven to be an invaluable tool in the workup of oncologic processes (*38*). The biologic basis of ^{18}F-FDG accumulation in malignant tumors results in part from the relatively high glycolytic rates found within malignant cells. However, tumor-associated macrophages also constitute an important fraction of oncologic tissues and provide an additional locus of intratumor ^{18}F-FDG accumulation (*10*). Occasionally, one cannot

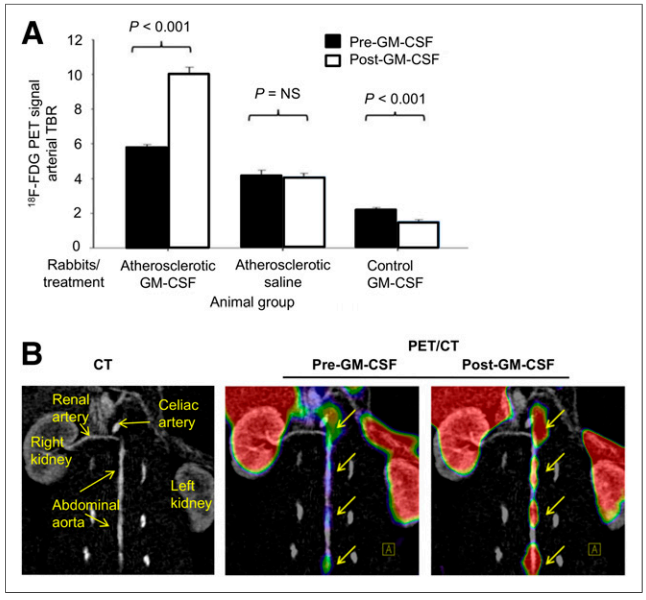

FIGURE 4. In vivo augmentation of ^{18}F-FDG uptake after GM-CSF administration in rabbits. (A) ^{18}F-FDG uptake in rabbits (n = 9) before and after challenge with cytokine GM-CSF or saline shows significant increase in ^{18}F-FDG uptake in atherosclerotic rabbits ($P < 0.001$). ^{18}F-FDG uptake is expressed as TBR compared with baseline imaging. (B) Representative image of ^{18}F-FDG signal enhancement demonstrating increased ^{18}F-FDG uptake in descending aorta before and after GM-CSF.

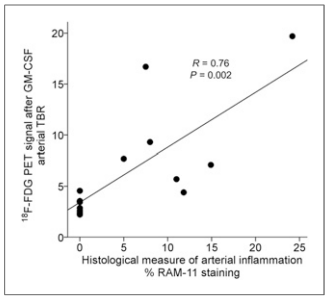

FIGURE 5. Relationship between arterial ^{18}F-FDG uptake (by PET/CT) and histologic macrophage accumulation. Rabbits that had received GM-CSF (4 atherosclerotic and 2 control) were imaged using ^{18}F-FDG PET/CT. Arterial ^{18}F-FDG uptake was recorded as TBR. Subsequently, the animals were sacrificed and macrophage concentration within aortic wall was determined histologically (%RAM11 staining). There was significant relationship between macrophage staining and TBR (R = 0.76, P = 0.002).

differentiate whether the ^{18}F-FDG signal originates within tumor or immune cells (especially after some chemotherapeutic regimens, which can activate immune cells while decreasing tumor activity). In these cases, the use of GM-CSF may improve diagnostic accuracy; an increase in lesional ^{18}F-FDG uptake on serial ^{18}F-FDG PET/CT imaging (repeated after GM-CSF) may suggest that the activity was localized to immune cells.

Furthermore, GM-CSF may prove useful as an adjunctive agent for other approaches targeting inflammation. GM-CSF might enhance macrophage activation sufficiently to increase uptake of other tracers targeting inflammation, such as gallium DOTATATE PET and superparamagnetic iron oxide nanoparticles. This is particularly facilitated by the fact that GM-CSF activates macrophages via mechanisms that promote both M2 (phagocytic) and mild M1 actions. With M2 activation comes an increase in uptake of nanoparticles such as superparamagnetic iron oxide (*39*). GM-CSF–enhanced imaging of superparamagnetic iron oxide and other nanoparticles should be further explored.

Limitations

This study is not without limitations. The optimal duration and dosing of GM-CSF was not examined in this study (only a 3-d GM-CSF regimen was examined). Thus, it is not clear from these data whether a single injection of GM-CSF would suffice to provide the desired boost in ^{18}F-FDG uptake. A multiday regimen would come at increased complexity, cost, and potential risks. Further, since only one imaging interval was studied, the optimal time point for ^{18}F-FDG PET/CT imaging after GM-CSF administration has not been determined. Future human studies are needed to assess the impact of a simplified GM-CSF regimen on ^{18}F-FDG PET/CT imaging.

CONCLUSION

GM-CSF augments macrophage glycolytic flux in vitro via a mechanism dependent on PFKFB3 and increases ^{18}F-FDG uptake in vivo in animal atherosclerotic models. GM-CSF is an approved and clinically used medication with an established safety profile. Future larger studies should explore the potential of using GM-CSF as an adjunctive imaging tool to improve detection of inflammation.

DISCLOSURE

The costs of publication of this article were defrayed in part by the payment of page charges. Therefore, and solely to indicate this fact, this article is hereby marked "advertisement" in accordance with 18 USC section 1734. James H.F. Rudd is in part supported by the NIHR Cambridge Biomedical Research Centre, the British Heart Foundation, and HEFCE. Zahi A. Fayad is supported by NIH/NHLBI R01 HL071021, R01 HL078667, NIH/NBIB R01 EB009638, and the NIH/NHLBI Program of Excellence in Nanotechnology (PEN) Award, contract HHSN268201000045C. Parmanand Singh was supported by a grant from the NHLBI (5T32 HL076136) and is funded by the Marfan Foundation. Lisardo Boscá was supported by SAF2014-52492R, RTC2015-3741 from MINECO, and RD12/0042/0019. Centro de Investigación Biomédica en Red de Enfermedades Hepáticas y Digestivas is funded by the Instituto de Salud Carlos III and S2010/BMD-2378 from Comunidad de Madrid. Ahmed Tawakol is supported by NIH/NHLBI R01 HL122177. No other potential conflict of interest relevant to this article was reported.

REFERENCES

1. Blankstein R, Osborne M, Naya M, et al. Cardiac positron emission tomography enhances prognostic assessments of patients with suspected cardiac sarcoidosis. *J Am Coll Cardiol.* 2014;63:329–336.
2. Osborne MT, Hulten EA, Singh A, et al. Reduction in ^{18}F-fluorodeoxyglucose uptake on serial cardiac positron emission tomography is associated with improved left ventricular ejection fraction in patients with cardiac sarcoidosis. *J Nucl Cardiol.* 2014;21:166–174.
3. Ricciardi A, Sordillo P, Ceccarelli L, et al. 18-fluoro-2-deoxyglucose positron emission tomography-computed tomography: an additional tool in the diagnosis of prosthetic valve endocarditis. *Int J Infect Dis.* 2014;28:219–224.
4. Sarrazin JF, Philippon F, Tessier M, et al. Usefulness of fluorine-18 positron emission tomography/computed tomography for identification of cardiovascular implantable electronic device infections. *J Am Coll Cardiol.* 2012;59:1616–1625.
5. Tahara N, Mukherjee J, de Haas HJ, et al. 2-deoxy-2-[^{18}F]fluoro-D-mannose positron emission tomography imaging in atherosclerosis. *Nat Med.* 2014;20:215–219.
6. Go AS, Mozaffarian D, Roger VL, et al. Heart disease and stroke statistics: 2014 update—a report from the American Heart Association. *Circulation.* 2014;129:e28–e292.
7. Libby P, Ridker PM, Maseri A. Inflammation and atherosclerosis. *Circulation.* 2002;105:1135–1143.
8. Libby P. Inflammation in atherosclerosis. *Nature.* 2002;420:868–874.
9. Tawakol A, Singh P, Mojena M, et al. HIF-1alpha and PFKFB3 mediate a tight relationship between proinflammatory activation and anaerobic metabolism in atherosclerotic macrophages. *Arterioscler Thromb Vasc Biol.* 2015;35:1463–1471.
10. Tawakol A, Migrino RQ, Hoffmann U, et al. Noninvasive in vivo measurement of vascular inflammation with F-18 fluorodeoxyglucose positron emission tomography. *J Nucl Cardiol.* 2005;12:294–301.
11. Rudd JH, Myers KS, Bansilal S, et al. Relationships among regional arterial inflammation, calcification, risk factors, and biomarkers: a prospective fluorodeoxyglucose positron-emission tomography/computed tomography imaging study. *Circ Cardiovasc Imaging.* 2009;2:107–115.
12. Pedersen SF, Graebe M, Fisker Hag AM, Hojgaard L, Sillesen H, Kjaer A. Gene expression and ^{18}FDG uptake in atherosclerotic carotid plaques. *Nucl Med Commun.* 2010;31:423–429.
13. Figueroa AL, Abdelbaky A, Truong QA, et al. Measurement of arterial activity on routine FDG PET/CT images improves prediction of risk of future CV events. *JACC Cardiovasc Imaging.* 2013;6:1250–1259.
14. Rominger A, Saam T, Wolpers S, et al. ^{18}F-FDG PET/CT identifies patients at risk for future vascular events in an otherwise asymptomatic cohort with neoplastic disease. *J Nucl Med.* 2009;50:1611–1620.
15. Fejer G, Wegner MD, Gyory I, et al. Nontransformed, GM-CSF-dependent macrophage lines are a unique model to study tissue macrophage functions. *Proc Natl Acad Sci USA.* 2013;110:E2191–E2198.
16. Fleetwood AJ, Lawrence T, Hamilton JA, Cook AD. Granulocyte-macrophage colony-stimulating factor (CSF) and macrophage CSF-dependent macrophage phenotypes display differences in cytokine profiles and transcription factor activities: implications for CSF blockade in inflammation. *J Immunol.* 2007;178:5245–5252.
17. Lacey DC, Achuthan A, Fleetwood AJ, et al. Defining GM-CSF- and macrophage-CSF-dependent macrophage responses by in vitro models. *J Immunol.* 2012;188:5752–5765.

18. Sugawara Y, Fisher SJ, Zasadny KR, Kison PV, Baker LH, Wahl RL. Preclinical and clinical studies of bone marrow uptake of fluorine-1-fluorodeoxyglucose with or without granulocyte colony-stimulating factor during chemotherapy. *J Clin Oncol.* 1998;16:173–180.
19. Miki T, Miura T, Nishino Y, et al. Granulocyte colony stimulating factor/macrophage colony stimulating factor improves postinfarct ventricular function by suppression of border zone remodelling in rats. *Clin Exp Pharmacol Physiol.* 2004;31:873–882.
20. Yano T, Miura T, Whittaker P, et al. Macrophage colony-stimulating factor treatment after myocardial infarction attenuates left ventricular dysfunction by accelerating infarct repair. *J Am Coll Cardiol.* 2006;47:626–634.
21. Bosca L, Rousseau GG, Hue L. Phorbol 12-myristate 13-acetate and insulin increase the concentration of fructose 2,6-bisphosphate and stimulate glycolysis in chicken embryo fibroblasts. *Proc Natl Acad Sci USA.* 1985;82:6440–6444.
22. Rodríguez-Prados JC, Traves PG, Cuenca J, et al. Substrate fate in activated macrophages: a comparison between innate, classic, and alternative activation. *J Immunol.* 2010;185:605–614.
23. Baumgartner HR. A new method for the induction of thrombi by controlled overdilatation of the vascular wall [in German]. *Z Gesamte Exp Med.* 1963;137:227–247.
24. Tawakol A, Migrino RQ, Bashian GG, et al. In vivo ^{18}F-fluorodeoxyglucose positron emission tomography imaging provides a noninvasive measure of carotid plaque inflammation in patients. *J Am Coll Cardiol.* 2006;48:1818–1824.
25. Arnberg H, Letocha H, Nou F, Westlin JF, Nilsson S. GM-CSF in chemotherapy-induced febrile neutropenia: a double-blind randomized study. *Anticancer Res.* 1998;18:1255–1260.
26. Campbell IK, van Nieuwenhuijze A, Segura E, et al. Differentiation of inflammatory dendritic cells is mediated by NF-kappaB1-dependent GM-CSF production in CD4 T cells. *J Immunol.* 2011;186:5468–5477.
27. Dhar-Mascareno M, Chen J, Zhang RH, Carcamo JM, Golde DW. Granulocyte-macrophage colony-stimulating factor signals for increased glucose transport via phosphatidylinositol 3-kinase- and hydrogen peroxide-dependent mechanisms. *J Biol Chem.* 2003;278:11107–11114.
28. Khameneh HJ, Isa SA, Min L, Nih FW, Ruedl C. GM-CSF signalling boosts dramatically IL-1 production. *PLoS One.* 2011;6:e23025.
29. Kim HJ, Oh JS, An SS, et al. Hypoxia-specific GM-CSF-overexpressing neural stem cells improve graft survival and functional recovery in spinal cord injury. *Gene Ther.* 2012;19:513–521.
30. Schneider UC, Schilling L, Schroeck H, Nebe CT, Vajkoczy P, Woitzik J. Granulocyte-macrophage colony-stimulating factor-induced vessel growth restores cerebral blood supply after bilateral carotid artery occlusion. *Stroke.* 2007;38:1320–1328.
31. Spielholz C, Heaney ML, Morrison ME, Houghton AN, Vera JC, Golde DW. Granulocyte-macrophage colony-stimulating factor signals for increased glucose uptake in human melanoma cells. *Blood.* 1995;85:973–980.
32. Kleemann R, Zadelaar S, Kooistra T. Cytokines and atherosclerosis: a comprehensive review of studies in mice. *Cardiovasc Res.* 2008;79:360–376.
33. Abdel-Latif A, Bolli R, Zuba-Surma EK, Tleyjeh IM, Hornung CA, Dawn B. Granulocyte colony-stimulating factor therapy for cardiac repair after acute myocardial infarction: a systematic review and meta-analysis of randomized controlled trials. *Am Heart J.* 2008;156:216-226 e219.
34. Domanchuk K, Ferrucci L, Guralnik JM, et al. Progenitor cell release plus exercise to improve functional performance in peripheral artery disease: the PROPEL Study. *Contemp Clin Trials.* 2013;36:502–509.
35. Subramaniyam V, Waller EK, Murrow JR, et al. Bone marrow mobilization with granulocyte macrophage colony-stimulating factor improves endothelial dysfunction and exercise capacity in patients with peripheral arterial disease. *Am Heart J.* 2009;158:53–60.e1.
36. Blockmans D, Knockaert D, Maes A, et al. Clinical value of [^{18}F]fluoro-deoxyglucose positron emission tomography for patients with fever of unknown origin. *Clin Infect Dis.* 2001;32:191–196.
37. Bleeker-Rovers CP, de Kleijn EM, Corstens FH, van der Meer JW, Oyen WJ. Clinical value of FDG PET in patients with fever of unknown origin and patients suspected of focal infection or inflammation. *Eur J Nucl Med Mol Imaging.* 2004;31:29–37.
38. Lardinois D, Weder W, Hany TF, et al. Staging of non-small-cell lung cancer with integrated positron-emission tomography and computed tomography. *N Engl J Med.* 2003;348:2500–2507.
39. Satomi T, Ogawa M, Mori I, et al. Comparison of contrast agents for atherosclerosis imaging using cultured macrophages: FDG versus ultrasmall superparamagnetic iron oxide. *J Nucl Med.* 2013;54:999–1004.

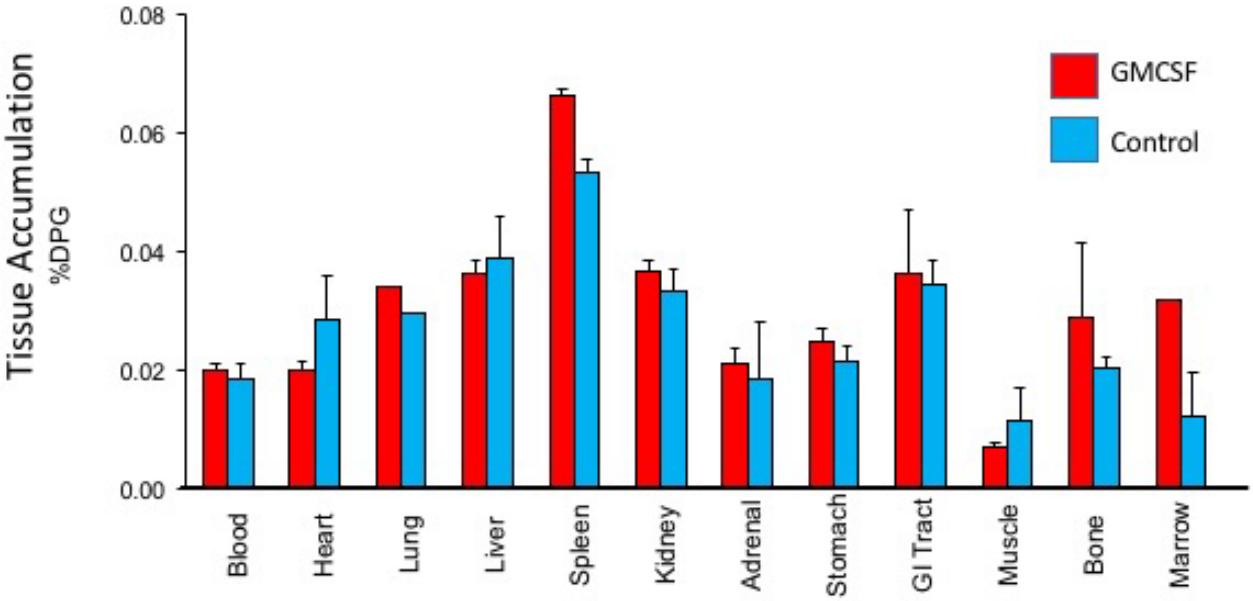

Supplemental Figure 1: Biodistribution Data. Biodistribution studies were done in a subset of 4 animals that had undergone PET/CT imaging (2 that had received GM-CSF and 2 after saline). Animals were killed with an overdose of pentobarbital sodium. To assess biodistribution, samples of blood, heart, lung, liver, spleen, kidney, adrenal gland, stomach, small intestine, skeletal muscle, and bone marrow were collected and weighed. A well-type gamma counter was used to measure radioactivity (LKB model 1282; LKB Instruments). Measurements were recorded as counts per minute less background and were corrected for radioactive decay. Results were expressed as percentage injected dose per gram (%ID/g).

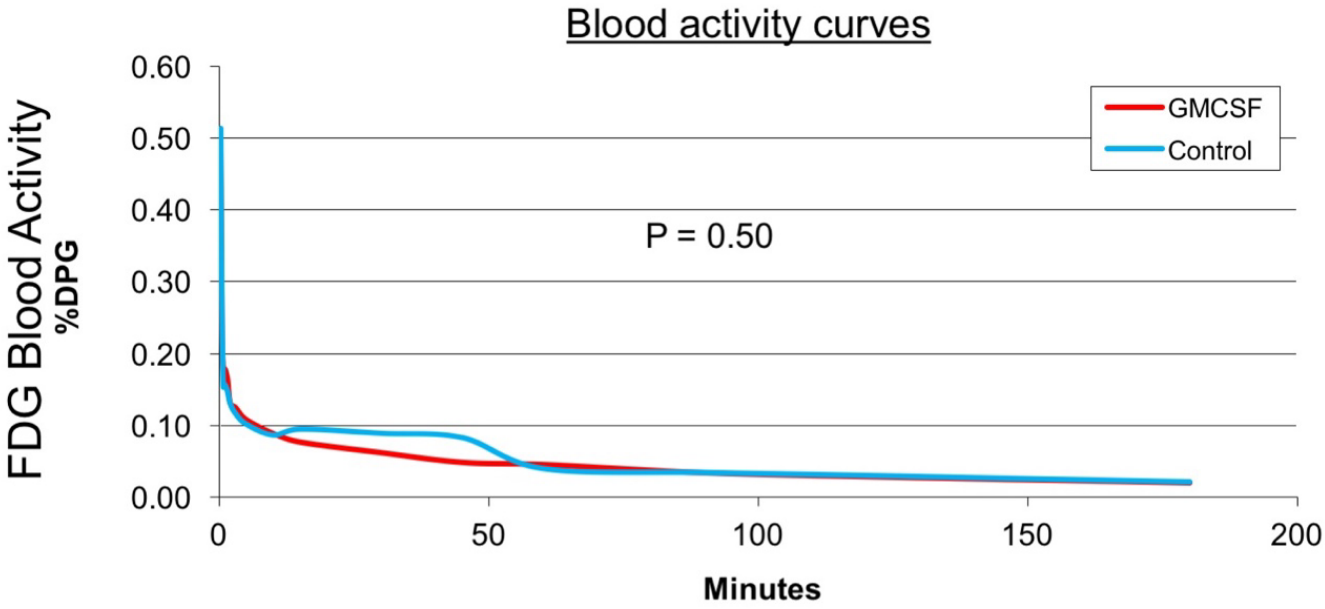

Supplemental Figure 2: Blood Time–Activity Curves. Blood time–activity studies were done in a subset of 4 animals (2 that had received GM-CSF and 2 after saline). After administration of ^{18}F-FDG (mCi), venous blood samples were taken at 16 time points. A well-type gamma counter was used to measure radioactivity (LKB model 1282; LKB Instruments). Measurements were recorded as counts per minute less background and were corrected for radioactive decay. Results were expressed as percentage injected dose per gram (%ID/g). There was no difference between the activity curves after GM-CSF vs. saline.

Metabolic signatures linked to macrophage polarization: from glucose metabolism to oxidative phosphorylation

Lisardo Boscá*†[1], Silvia González-Ramos*, Patricia Prieto*, María Fernández-Velasco*, Marina Mojena*, Paloma Martín-Sanz*† and Susana Alemany*

*Instituto de Investigaciones Biomédicas Alberto Sols, (Centro Mixto CSIC-UAM), Arturo Duperier 4, 28029 Madrid, Spain

†Centro de Investigación Biomédica en Red de Enfermedades Hepáticas y Digestivas (CIBERehd), Monforte de Lemos 3-5, Instituto de Salud Carlos III, 28029 Madrid, Spain

Abstract

Macrophages are present in a large variety of locations, playing distinct functions that are determined by its developmental origin and by the nature of the activators of the microenvironment. Macrophage activation can be classified as pro-inflammatory (M1 polarization) or anti-inflammatory-pro-resolution-deactivation (M2), these profiles coexisting in the course of the immune response and playing a relevant functional role in the onset of inflammation (Figure 1). Several groups have analysed the metabolic aspects associated with macrophage activation to answer the question about what changes in the regulation of energy metabolism and biosynthesis of anabolic precursors accompany the different types of polarization and to what extent they are necessary for the expression of the activation phenotypes. The interest of these studies is to regulate macrophage function by altering their metabolic activity in a 'therapeutic way'.

Macrophages: a heterogeneous population

Macrophages constitute a diverse population of cells that has been clarified in recent years; tissue macrophages have their own self-renewal mechanisms, starting from committed resident cells, whose origin appears to be related to early steps in the development from precursors of the yolk sac [1]. These highly specialized subsets receive distinct denominations as a function of their discovery and are present in adult organisms [2]. Examples of these are the microglia in the central nervous system, Kupffer cells in the liver and Langerhans cells in the skin [2]. These cells exhibit low rates of self-renewal, and express specific surface markers and anti-apoptotic genes of the B-cell lymphoma 2 (Bcl2)-Bcl-x_L family that ensure their long-lasting function [3]. In addition to this, circulating monocytes are recruited at the sites of inflammation and contribute to mount the innate immune response [2,4–6]. These infiltrating cells, upon activation, are maintained alive for 2–3 days, being removed by apoptosis [6].

Energy fuelling of macrophages

Macrophages are essentially glycolytic cells, regardless of the combination of phenotypic challenges; pro-inflammatory macrophages increased glucose metabolism in the absence of proliferation, whereas anti-inflammatory/pro-resolution macrophages retain the same dependence on glycolysis but exhibiting modest glucose consumption, like in resting or resident counterparts [7]. This high glycolytic capacity was recognized by Otto Warburg as a characteristic feature of cancer and immune cells, such as macrophages. It is the mimicry (or real) of hypoxic conditioning of macrophages the main driving force conveying to the expression of most of the genes associated to the glycolytic phenotype [7,8]. Therefore, targeting glycolysis has become an important objective in several anti-inflammatory therapeutic strategies in which macrophages are involved, from atherogenesis to cancer, fibrosis and different immune diseases. There are evidence-based reasons for such developments: high glycolytic flux contributes to biosynthetic pathways providing precursors for *de novo* ribonucleotide synthesis, amino acid replenishment for new protein synthesis and fatty acids biosynthesis. All these processes can be attenuated interfering glucose metabolism, as recently described for the development of atherogenesis [4,9].

The other main source of energy for most cells is the Krebs cycle/oxidative phosphorylation [tricarboxylic acid (TCA)/OXPHOS] pathway. One characteristics of pro-inflammatory polarization is the expression of nitric oxide (NO) synthase (NOS2) [10,11]. Under these conditions, NO acts as a potent inhibitor of cytochrome *c* oxidase in the OXPHOS pathway, avoiding mitochondrial respiration and ATP generation. However, in human macrophages, the inducibility of NOS2 is negligible and NO is not produced, preserving the activity of the OXPHOS [11]. Nevertheless, when O_2 consumption is analysed in M1

Key words: glycolysis, inflammation, inhibitors, isoenzyme, macrophage, metabolism.

Abbreviations: 3PO, dipyridinyl propenone 3-(3-pyridinyl)-1-(4-pyridinyl)-2-propen-1-one; ANT, adenine nt translocator; GLUT-1, glucose transporter 1; HIF, hypoxia-inducible factor; HK, hexokinase; HMGB1, high-mobility group box 1; IL, interleukin; LDH, lactate dehydrogenase; LPS, lipopolysaccharide; MCT4, monocarboxylate transporter 4; NO, nitric oxide; NOS, nitric oxide synthase; OXPHOS, oxidative phosphorylation; PEP, phosphor-enol-pyruvate; PFK, phosphofructokinase; PFKFB, 6-phosphofructo-2-kinase/fructose-2,6-bisphosphatase; PHM, muscle-type pyruvate kinase; PK, pyruvate kinase; TCA, tricarboxylic acid; TLR, toll-like receptor.

[1] **To whom correspondence should be addressed (email lbosca@iib.uam.es).**

Figure 1 | Schematic representation of macrophage stimulation and polarization

The different phenotypes are induced after challenges with the indicated stimuli, resulting in the expression of the indicated mediators (italic). Abbreviations: CC, chemokine; CK, cytokine; GR, glucocorticoid receptor; IFNγ, interferon γ; LTA, lipoteichoic acid; LXR, liver X receptor; MMP, matrix metalloproteinase; NLR, nt-binding domain and leucine-rich repeat; NOD, nt-binding oligomerization domain receptor; PG, prostaglandin; PGN, peptidoglycan; PPAR, peroxisome proliferator-activated receptor; RNI, reactive nitrogen intermediate; ROS, reactive oxygen species; TGF, transforming growth factor.

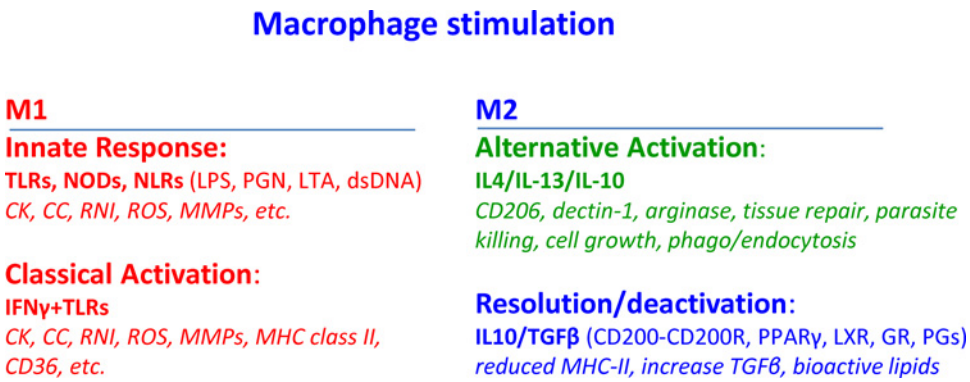

human macrophages the use of oxidative TCA/OXPHOS pathway is still impaired. The mechanisms interfering with this oxidative capacity remain elusive, but the inhibition of the pyruvate flux to the mitochondria and the accumulation of TCA and other intermediates altering the normal flux of electrons and substrates in the mitochondria may be under the mechanisms of this impaired metabolic issue. An ancillary consequence of this process is the loss of viability of M1 macrophages when glucose supply is reduced, as evidenced by the lack of recovery after mitochondrial depolarization [9].

Glucose fate regulation in macrophages

Regulation of glycolysis is very dependent on the cell type and on the energy demands in its environment. One way to accomplish this is through the expression of specific isoenzymes, adapting optimal kinetic and regulatory properties with the needs for cell function. This is in addition to covalent modifications in glycolytic enzymes and recent proteomic analysis shows a huge variety of post-translational stoichiometries that are explained on the basis of coexistence of spatially distributed, distinctly modified enzymes contributing to a fine tuning of its catalytic activity and opening an additional degree of complexity. This is true for macrophages confronted to specific stimuli, ranging from the presence of pathogens to death cells, all occurring under conditions of restricted availability of energetic substrates, such as glucose, amino acids and oxygen.

An additional emerging issue is the differential processing of the mRNA of glycolytic enzymes in macrophages, yielding isoforms with altered N-terminal domains due to alternative splicing. These differences involve the use of different promoters, which vary among mammalian species, the presence of non-coding RNA sequences, the occurrence of selective splicing etc. Perhaps the most paradigmatic situation is that of pyruvate kinase (PK) muscle-type 2 (PKM2) that, depending on its compartmentalization is involved in the metabolic activity, but also in transcriptional regulation, stabilization of hypoxia-inducible factor (HIF)-1α and secretion of high-mobility group box 1 (HMGB1) and interleukin (IL)-1β. Indeed, inhibition of PKM2 activity with shikonin protects mice form lethal septic shock through an impairment of the lower part of the glycolytic pathway [12,13]. These results stress the relevance of glycolysis to maintain the full pro-inflammatory phenotype in macrophages [14–17].

Glycolytic targeting of macrophages

Rewiring of glucose metabolism can be achieved by altering substrate availability, through directly targeting enzymes with selective inhibitors or by creating a metabolic imbalance among the different fluxes that use glucose (Figure 2). Altering substrate availability is a difficult issue, but diet-dependent conditioning of macrophage metabolism is an open issue; e.g., ketogenic diets or poly-unsaturated fatty acids that generate pro-resolution metabolites interfering with the basic programmes of macrophage polarization [18,19].

Several selective inhibitors of glycolytic enzymes have been developed in recent years. Since M1 macrophages have an enhanced glucose uptake due to overexpression of glucose transporter 1 (GLUT-1) the use of glucose analogues may serve to transiently attenuate glucose metabolism. This approach, because it affects to the upper part of glycolysis, not only prevents energy supply in the macrophage but also the use of glucose-6-phosphate by the oxidative pentose phosphate pathway arm that is critical to support NADPH replenishment and also for ribose synthesis [9,20]. Interestingly, the lower part of glycolysis, namely the balance between the lactate export/import is clearly imbalanced towards the export via the monocarboxylic acid transmem-

Figure 2 | Changes in glycolytic enzymes in macrophages in the course of activation

The main regulatory enzymes are shown in black (resting and anti-inflammatory phenotype) and red (pro-inflammatory phenotype. Post-traslational changes (phosphorylation) and alternative splicing isoenzymes are depicted as P and S respectively. The activators and inhibitors are described with the + or − signs. Abbreviations: ALD, aldolase; PPP, pentose phosphate pathway.

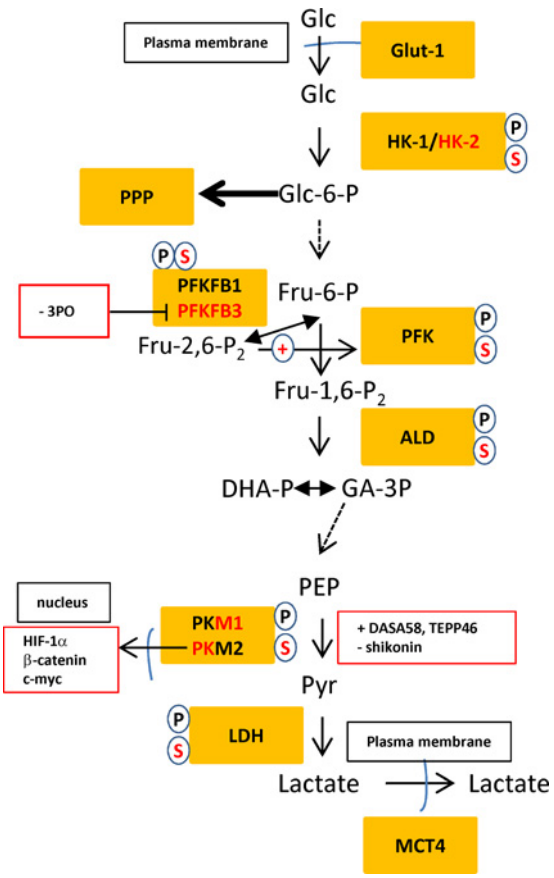

brane transporter MCT4 (monocarboxylate transporter 4; encoded by the *slc16a3* gene) that is highly expressed in M1 macrophages. The use of inhibitors for this transporter in oncology is under clinical trials. However, the protein encoding the import of lactate (MCT1) is minimally expressed in the macrophage membrane [21,22]. Indeed, it is to note that due to the high activity of lactate dehydrogenase (LDH) in the macrophage and because this enzyme maintains the intracellular balance between pyruvate and lactate, but also between NADH and NAD, all at concentrations in the range of the chemical equilibrium of the reaction, the export of lactate needs to be well-regulated to avoid NADH depletion.

Resting and M2-challenged macrophages express hexokinase (HK)-1 as the main activity phosphorylating glucose. However, in M1 macrophages HK-2 is highly expressed. This isoform is mainly present in the particulate fraction of macrophage extracts, associated to the mitochondrial adenine nt translocator (ANT)–permeability transition pore complex [23]. In cells exhibiting aerobic metabolism, this association of HK-2 to the ANT is thought to enhance the efficient use of the ATP generated by the mitochondria; however, this is not the case of macrophages that exhibit a modest OXPHOS activity and the biological significance of this accumulation of HK-2 in the mitochondrial fraction is unclear. In *ex vivo* experiments, the use of glucose isomers lacking the hydroxy group at the C-2 position retain the phosphorylation in the C-6 position but are unable to be converted into further glycolytic products at the time that accumulate and potently inhibit HK-1 and HK-2 activities. Indeed, 2-fluoro- or 2-deoxy-glucose or mannose derivatives have been used for the quantification of the rate of glucose uptake and phosphorylation of highly glycolytic cells and, upon accumulation, can deplete the intracellular ATP levels leading to cell death [9,24]. Although the Ki values of the different 2-deoxy-glucose isomers (including mannose) for HK has been a matter of debate, analysis of the kinetic properties using purified enzyme shows minimal differences among them [25]. However, the possibility of the use of these C-6 phosphoesters by phosphatases or other enzymes cleaving the phosphate group may lay on the basis of the different properties of these molecules as *in vivo* diagnosis tracers for the glycolytic capacity of the macrophages at different locations [24].

One relevant target to modulate glycolysis in macrophages are the 6-phosphofructo-2-kinase/fructose-2,6-bisphosphatase isoenzymes (PFKFB1-4) [26]. These isoenzymes maintain a tight control on the futile cycle involved in the synthesis and degradation of Fru-2,6-P_2, a potent activator of phosphofructokinase (PFK), the enzyme that catalyses the phosphorylation of Fru-6-P to Fru-1,6-P_2 and constitutes the second 'irreversible' step of glycolysis [27]. The main PFK activity present in macrophages is a combination of the liver (PFKL) and platelet (PFKP) isoenzymes, with a minimal representation of the skeletal muscle isoform (PFKM) and integrated into different hetero- or homo-tetrameric complexes. This enzyme is submitted to control by acidic pH that, in turn, enhances the sensitivity to the inhibition by several effectors, among them ATP as the main contributor to inhibit the flux through this step. However, Fru-2,6-P_2 provokes a conformational change that releases the inhibition caused by pH and ATP [27]. Therefore, tight control of Fru-2,6-P_2 levels appears to be a key regulator of the upper glycolytic flux. Regarding PFKFB isoenzymes, these are bifunctional enzymes consisting in the fusion of two separated domains, one containing the kinase activity and another independent domain carrying the bisphosphatase activity [26]. The balance between the kinase and bisphosphatase activities varies among the isoenzymes and can be regulated by covalent modification by several protein kinases [26,28,29]. Resting and tissue macrophages mainly express the liver type or PFKFB1 isoform, characterized by a dominant bisphosphatase compared with kinase activity, thus maintaining low levels of the effector Fru-2,6-P_2 [7]. However, M1 macrophages exhibit a rapid fall in the mRNA levels of PFKFB1 together with a progressive decline in its protein levels, accompanied by

a rise in the expression of the PFKFB3 isoform. This isoform has a dominant kinase compared with bisphosphatase activity resulting in a rise in the concentration of Fru-2,6-P_2 and full activation of upper glycolysis. In addition to this, PFKFB3 activity is also modulated in a positive way through phosphorylation by AMP-dependent protein kinase (AMPK), protein kinase A (PKA) and protein kinase C (PKC), all at Ser^{461} [26]. This shift in the PFKFB isoforms offers the advantage of the use of selective PFKFB3 inhibitors to interfere glycolysis. One of such inhibitors is the dipyridinyl propenone 3-(3-pyridinyl)-1-(4-pyridinyl)-2-propen-1-one (3PO), a molecule developed under a structure/activity computational analysis approach [9,30]. Indeed, recent advances on the knowledge of functions of PFKFB3 have revealed an important contribution for this isoenzyme in favouring angiogenesis by endothelial cells and proliferation of tumour cells [28,31–36]. In M1 macrophages silencing PFKFB3 with selective siRNAs or inhibition of its activity with 3PO has profound effects on cell viability and on the progress of atherogenesis in apolipoprotein E-deficient substitute (ApoE)-deficient mice fed a high-fat and cholesterol-rich diet [9].

In lower glycolysis, a key regulatory activity is PK. Recent data suggest a precedent unrecognized role for PK in macrophage glycolysis. PK catalyses the last major step in glycolysis transforming phosphor-enol-pyruvate (PEP) into pyruvate together with the generation of one ATP molecule from ADP. Macrophages express high levels of the PKM. From this locus two isoforms can be generated: PKM1 and PKM2. Both forms coexist in resting macrophages and are down-regulated in a time-dependent way upon activation with toll-like receptor (TLR) ligands (M1 cells). Under these conditions, the formation of different complexes PKM1–PKM2 is expected, but the PKM2 isoform is dominant in M1 macrophages. PKM2 retains the ability to be activated by Fru-1,6-P_2, integrating the co-ordination between the upper with the lower part of glycolysis [37–40]. In addition to this, PKM2 shows complex organization behaviour; the enzyme exists in equilibrium between dimeric and tetrameric forms [12,13,41,42]. PKM2 dimers exhibit a lesser affinity for PEP but can stabilize HIF-1α and activate HIF-1α-dependent transcription, among others, the expression of PFKFB3 and the HMGB1 proteins [13,35]. In addition to this, PKM2 dimers can bind directly to histone H3 and transfer the phosphate from PEP to histone H3 at Thr^{11} allowing the dissociation from cyclin D1 (CCND1) resulting in chromatin remodelling and epigenetic changes [37,39]. To modulate the balance between the metabolic and genomic actions of PKM2, several activators and inhibitors have been developed: N, N′-diarylsulfonamide NCGC00185916 (DASA-58) and thieno-[3,2-b]pyrrole [3,2-d]pyridazinone NCGC00186528 (TEPP-46) are activators that promote its metabolic activity, including an enhanced serine biosynthesis; whereas inhibition with shikonin reduces lactate release by macrophages and impairs the establishment of a full M1 polarization phenotype [12,13,37,38,41,43]. This modulation of PKM2 activity can be translated into functional responses; activation of PK inhibited lipopolysaccharide (LPS)- and *Salmonella typhimurium*-induced glycolytic reprogramming, succinate production and HIF-1α stabilization and inhibition with shikonin reduced serum lactate and HMGB1 levels and protected mice from lethal endotoxemia and sepsis [12,13]. Indeed, the presence of the two PKM isoforms establishes a competition for PEP as substrate and, in so doing, the fall in PEP levels results in an enhancement of the non-metabolic PKM2 functions, due to its lower affinity for the substrate.

Concluding remarks

Our data [7,9,44] and those from other groups support the view that regardless of the challenges used and the availability of alternative energy substrates, macrophage metabolism is by more than 90% glycolytic, with limited use of other fuels for energy purposes; however, the pathways to generate metabolites by the Krebs cycle and by glutaminolysis are fully functional and used in part for other purposes [7,45]. In this context, we have investigated the role of macrophages in the development of atherogenesis. These studies allowed us to develop new strategies to evaluate macrophage metabolism in atheromatous lesions and to stabilize them using specific metabolic-based signatures [9].

Funding

This work was supported by the Ministerio de Economía y Competitividad [grant numbers SAF2013-43713, SAF2014-52492 and IPT2012-1331-60000]; the Comunidad de Madrid [grant number S2010/BMD-2378]; and the Red Cardiovascular [grant numbers RD12/0042/0019].

References

1 Robbins, C.S., Hilgendorf, I., Weber, G.F., Theurl, I., Iwamoto, Y., Figueiredo, J.L., Gorbatov, R., Sukhova, G.K., Gerhardt, L.M., Smyth, D. et al. (2013) Local proliferation dominates lesional macrophage accumulation in atherosclerosis. Nat. Med. **19**, 1166–1172 CrossRef PubMed
2 Davies, L.C., Jenkins, S.J., Allen, J.E. and Taylor, P.R. (2013) Tissue-resident macrophages. Nat. Immunol. **14**, 986–995 CrossRef PubMed
3 Varol, C., Mildner, A. and Jung, S. (2015) Macrophages: development and tissue specialization. Annu. Rev. Immunol. **33**, 643–675 CrossRef PubMed
4 Fernandez-Velasco, M., Gonzalez-Ramos, S. and Bosca, L. (2014) Involvement of monocytes/macrophages as key factors in the development and progression of cardiovascular diseases. Biochem. J. **458**, 187–193 CrossRef PubMed
5 Gordon, S. and Martinez, F.O. (2010) Alternative activation of macrophages: mechanism and functions. Immunity **32**, 593–604 CrossRef PubMed
6 Mantovani, A. (2010) Molecular pathways linking inflammation and cancer. Curr. Mol. Med. **10**, 369–373 CrossRef PubMed
7 Rodriguez-Prados, J.C., Traves, P.G., Cuenca, J., Rico, D., Aragones, J., Martin-Sanz, P., Cascante, M. and Bosca, L. (2010) Substrate fate in activated macrophages: a comparison between innate, classic, and alternative activation. J. Immunol. **185**, 605–614 CrossRef PubMed
8 Peyssonnaux, C., Cejudo-Martin, P., Doedens, A., Zinkernagel, A.S., Johnson, R.S. and Nizet, V. (2007) Cutting edge: Essential role of hypoxia inducible factor-1α in development of lipopolysaccharide-induced sepsis. J. Immunol. **178**, 7516–7519 CrossRef PubMed
9 Tawakol, A., Singh, P., Mojena, M., Pimentel-Santillana, M., Emami, H., MacNabb, M., Rudd, J.H., Narula, J., Enriquez, J.A., Traves, P.G. et al. (2015) HIF-1α and PFKFB3 mediate a tight relationship between proinflammatory activation and anerobic metabolism in atherosclerotic macrophages. Arterioscler Thromb. Vasc. Biol., in the press

10 Bosca, L., Zeini, M., Traves, P.G. and Hortelano, S. (2005) Nitric oxide and cell viability in inflammatory cells: a role for NO in macrophage function and fate. Toxicology **208**, 249–258 CrossRef PubMed

11 Rico, D., Vaquerizas, J.M., Dopazo, H. and Bosca, L. (2007) Identification of conserved domains in the promoter regions of nitric oxide synthase 2: implications for the species-specific transcription and evolutionary differences. BMC Genomics **8**, 271 CrossRef PubMed

12 Palsson-McDermott, E.M., Curtis, A.M., Goel, G., Lauterbach, M.A., Sheedy, F.J., Gleeson, L.E., van den Bosch, M.W., Quinn, S.R., Domingo-Fernandez, R., Johnston, D.G. et al. (2015) Pyruvate kinase M2 regulates Hif-1α activity and IL-1β induction and is a critical determinant of the warburg effect in LPS-activated macrophages. Cell Metab. **21**, 65–80 CrossRef PubMed

13 Yang, L., Xie, M., Yang, M., Yu, Y., Zhu, S., Hou, W., Kang, R., Lotze, M.T., Billiar, T.R., Wang, H., Cao, L. and Tang, D. (2014) PKM2 regulates the Warburg effect and promotes HMGB1 release in sepsis. Nat. Commun. **5**, 4436 PubMed

14 Gordon, S., Pasare, C. and Medzhitov, R. (2007) The macrophage: past, present and future. Toll-like receptors: linking innate and adaptive immunity. Eur. J. Immunol. **37**, S9–S17 CrossRef PubMed

15 Martinez, F.O., Gordon, S., Locati, M. and Mantovani, A. (2006) Transcriptional profiling of the human monocyte-to-macrophage differentiation and polarization: new molecules and patterns of gene expression. J. Immunol. **177**, 7303–7311 CrossRef PubMed

16 Odegaard, J.I., Ricardo-Gonzalez, R.R., Red Eagle, A., Vats, D., Morel, C.R., Goforth, M.H., Subramanian, V., Mukundan, L., Ferrante, A.W. and Chawla, A. (2008) Alternative M2 activation of Kupffer cells by PPARδ ameliorates obesity-induced insulin resistance. Cell Metab. **7**, 496–507 CrossRef PubMed

17 Olefsky, J.M. and Glass, C.K. (2010) Macrophages, inflammation, and insulin resistance. Annu. Rev. Physiol. **72**, 219–246 CrossRef PubMed

18 Al-Lahham, S., Roelofsen, H., Rezaee, F., Weening, D., Hoek, A., Vonk, R. and Venema, K. (2012) Propionic acid affects immune status and metabolism in adipose tissue from overweight subjects. Eur. J. Clin. Invest. **42**, 357–364 CrossRef PubMed

19 Prieto, P., Cuenca, J., Traves, P.G., Fernandez-Velasco, M., Martin-Sanz, P. and Bosca, L. (2010) Lipoxin A4 impairment of apoptotic signaling in macrophages: implication of the PI3K/Akt and the ERK/Nrf-2 defense pathways. Cell Death Differ. **17**, 1179–1188 CrossRef PubMed

20 Folco, E.J., Sheikine, Y., Rocha, V.Z., Christen, T., Shvartz, E., Sukhova, G.K., Di Carli, M.F. and Libby, P. (2011) Hypoxia but not inflammation augments glucose uptake in human macrophages: Implications for imaging atherosclerosis with ^{18}F-labeled 2-deoxy-D-glucose positron emission tomography. J. Am. Coll. Cardiol. **58**, 603–614 CrossRef PubMed

21 Hahn, E.L., Halestrap, A.P. and Gamelli, R.L. (2000) Expression of the lactate transporter MCT1 in macrophages. Shock **13**, 253–260 CrossRef PubMed

22 Moreira, T.J., Pierre, K., Maekawa, F., Repond, C., Cebere, A., Liljequist, S. and Pellerin, L. (2009) Enhanced cerebral expression of MCT1 and MCT2 in a rat ischemia model occurs in activated microglial cells. J. Cereb. Blood Flow Metab. **29**, 1273–1283 CrossRef PubMed

23 Lazo, P.A. and Bosca, L. (1982) Mitochondrial membrane-bound hexokinase of ascites tumor cells. Functional implications of lysine residues studied by modification with imidoesters. Hoppe Seylers Z. Physiol. Chem. **363**, 635–641 CrossRef PubMed

24 Tahara, N., Mukherjee, J., de Haas, H.J., Petrov, A.D., Tawakol, A., Haider, N., Tahara, A., Constantinescu, C.C., Zhou, J., Boersma, H.H. et al. (2014) 2-deoxy-2-[^{18}F]fluoro-D-mannose positron emission tomography imaging in atherosclerosis. Nat. Med. **20**, 215–219 CrossRef PubMed

25 Sols, A. and Crane, R.K. (1954) Substrate specificity of brain hexokinase. J. Biol. Chem. **210**, 581–595 PubMed

26 Rider, M.H., Bertrand, L., Vertommen, D., Michels, P.A., Rousseau, G.G. and Hue, L. (2004) 6-phosphofructo-2-kinase/fructose-2, 6-bisphosphatase: head-to-head with a bifunctional enzyme that controls glycolysis. Biochem. J. **381**, 561–579 CrossRef PubMed

27 Bosca, L., Aragon, J.J. and Sols, A. (1985) Modulation of muscle phosphofructokinase at physiological concentration of enzyme. J. Biol. Chem. **260**, 2100–2107 PubMed

28 Bando, H., Atsumi, T., Nishio, T., Niwa, H., Mishima, S., Shimizu, C., Yoshioka, N., Bucala, R. and Koike, T. (2005) Phosphorylation of the 6-phosphofructo-2-kinase/fructose 2,6-bisphosphatase/PFKFB3 family of glycolytic regulators in human cancer. Clin. Cancer Res. **11**, 5784–5792 CrossRef PubMed

29 Fukasawa, M., Tsuchiya, T., Takayama, E., Shinomiya, N., Uyeda, K., Sakakibara, R. and Seki, S. (2004) Identification and characterization of the hypoxia-responsive element of the human placental 6-phosphofructo-2-kinase/fructose-2,6-bisphosphatase gene. J. Biochem. **136**, 273–277 CrossRef PubMed

30 Clem, B., Telang, S., Clem, A., Yalcin, A., Meier, J., Simmons, A., Rasku, M.A., Arumugam, S., Dean, W.L., Eaton, J. et al. (2008) Small-molecule inhibition of 6-phosphofructo-2-kinase activity suppresses glycolytic flux and tumor growth. Mol. Cancer Ther. **7**, 110–120 CrossRef PubMed

31 De Bock, K., Georgiadou, M., Schoors, S., Kuchnio, A., Wong, B.W., Cantelmo, A.R., Quaegebeur, A., Ghesquiere, B., Cauwenberghs, S., Eelen, G. et al. (2013) Role of PFKFB3-driven glycolysis in vessel sprouting. Cell **154**, 651–663 CrossRef PubMed

32 Eltzschig, H.K. and Carmeliet, P. (2011) Hypoxia and inflammation. N. Engl. J. Med. **364**, 656–665 CrossRef PubMed

33 Kawaguchi, T., Veech, R.L. and Uyeda, K. (2001) Regulation of energy metabolism in macrophages during hypoxia. Roles of fructose 2,6-bisphosphate and ribose 1,5-bisphosphate. J. Biol. Chem. **276**, 28554–28561 CrossRef PubMed

34 Minchenko, A., Leshchinsky, I., Opentanova, I., Sang, N., Srinivas, V., Armstead, V. and Caro, J. (2002) Hypoxia-inducible factor-1-mediated expression of the 6-phosphofructo-2-kinase/fructose-2, 6-bisphosphatase-3 (PFKFB3) gene. Its possible role in the Warburg effect. J. Biol. Chem. **277**, 6183–6187 CrossRef PubMed

35 Obach, M., Navarro-Sabate, A., Caro, J., Kong, X., Duran, J., Gomez, M., Perales, J.C., Ventura, F., Rosa, J.L. and Bartrons, R. (2004) 6-Phosphofructo-2-kinase (pfkfb3) gene promoter contains hypoxia-inducible factor-1 binding sites necessary for transactivation in response to hypoxia. J. Biol. Chem. **279**, 53562–53570 CrossRef PubMed

36 Telang, S., Yalcin, A., Clem, A.L., Bucala, R., Lane, A.N., Eaton, J.W. and Chesney, J. (2006) Ras transformation requires metabolic control by 6-phosphofructo-2-kinase. Oncogene **25**, 7225–7234 CrossRef PubMed

37 Anastasiou, D., Yu, Y., Israelsen, W.J., Jiang, J.K., Boxer, M.B., Hong, B.S., Tempel, W., Dimov, S., Shen, M., Jha, A. et al. (2012) Pyruvate kinase M2 activators promote tetramer formation and suppress tumorigenesis. Nat. Chem. Biol. **8**, 839–847 CrossRef PubMed

38 Chaneton, B. and Gottlieb, E. (2012) Rocking cell metabolism: revised functions of the key glycolytic regulator PKM2 in cancer. Trends Biochem. Sci. **37**, 309–316 CrossRef PubMed

39 Cortes-Cros, M., Hemmerlin, C., Ferretti, S., Zhang, J., Gounarides, J.S., Yin, H., Muller, A., Haberkorn, A., Chene, P., Sellers, W.R. and Hofmann, F. (2013) M2 isoform of pyruvate kinase is dispensable for tumor maintenance and growth. Proc. Natl. Acad. Sci. U.S.A. **110**, 489–494 CrossRef PubMed

40 Mulukutla, B.C., Khan, S., Lange, A. and Hu, W.S. (2010) Glucose metabolism in mammalian cell culture: new insights for tweaking vintage pathways. Trends Biotechnol. **28**, 476–484 CrossRef PubMed

41 Chaneton, B., Hillmann, P., Zheng, L., Martin, A.C., Maddocks, O.D., Chokkathukalam, A., Coyle, J.E., Jankevics, A., Holding, F.P., Vousden, K.H. et al. (2012) Serine is a natural ligand and allosteric activator of pyruvate kinase M2. Nature **491**, 458–462 CrossRef PubMed

42 Israelsen, W.J., Dayton, T.L., Davidson, S.M., Fiske, B.P., Hosios, A.M., Bellinger, G., Li, J., Yu, Y., Sasaki, M., Horner, J.W. et al. (2013) PKM2 isoform-specific deletion reveals a differential requirement for pyruvate kinase in tumor cells. Cell **155**, 397–409 CrossRef PubMed

43 Keller, K.E., Doctor, Z.M., Dwyer, Z.W. and Lee, Y.S. (2014) SAICAR induces protein kinase activity of PKM2 that is necessary for sustained proliferative signaling of cancer cells. Mol. Cell. **53**, 700–709 CrossRef PubMed

44 Traves, P.G., de Atauri, P., Marin, S., Pimentel-Santillana, M., Rodriguez-Prados, J.C., Marin de Mas, I., Selivanov, V.A., Martin-Sanz, P., Bosca, L. and Cascante, M. (2012) Relevance of the MEK/ERK signaling pathway in the metabolism of activated macrophages: a metabolomic approach. J. Immunol. **188**, 1402–1410 CrossRef PubMed

45 Newsholme, P. and Newsholme, E.A. (1989) Rates of utilization of glucose, glutamine and oleate and formation of end-products by mouse peritoneal macrophages in culture. Biochem. J. **261**, 211–218 PubMed

Received 07 May 2015
doi:10.1042/BST20150107

Cardiovascular Research Advance Access published April 22, 2015

Cardiovascular Research
doi:10.1093/cvr/cvv118

NOD1, a new player in cardiac function and calcium handling

Carmen Delgado[1,2†], Gema Ruiz-Hurtado[3†], Nieves Gómez-Hurtado[1†], Silvia González-Ramos[2†], Angelica Rueda[4], Gemma Benito[5], Patricia Prieto[2], Carlos Zaragoza[6], Esmerilda G. Delicado[7], Raquel Pérez-Sen[7], Maria Teresa Miras-Portugal[7], Gabriel Núñez[8], Lisardo Boscá[2*], and Maria Fernández-Velasco[5*]

[1]Departamento de Farmacología, Facultad de Medicina, Universidad Complutense de Madrid, Madrid, Spain; [2]Instituto de Investigaciones Biomédicas Alberto Sols, Consejo Superior de Investigaciones Científicas, Madrid, Spain; [3]Instituto de Investigación i + 12 Hospital Universitario 12 de Octubre and Instituto Pluridisciplinar, UCM, Madrid, Spain; [4]Departamento de Bioquímica, Cinvestav-IPN, México; [5]Instituto de Investigación Hospital Universitario La PAZ, IDIPAZ, Madrid, Spain; [6]Department of Cardiology, University Hospital Ramón y Cajal/University Francisco de Vitoria, Madrid, Spain; [7]Departamento de Bioquímica y Biología Molecular IV, Facultad de Veterinaria e Instituto Universitario de Investigación en Neuroquímica, Instituto de Investigación Sanitaria del Hospital Clínico San Carlos (IdISSC), Universidad Complutense, Madrid, Spain; and [8]Department of Pathology and Comprehensive Cancer Center, University of Michigan Medical School, Ann Arbor, MI, USA

Received 1 April 2014; revised 12 February 2015; accepted 5 March 2015

Time for primary review: 40 days

Aims Inflammation is a significant contributor to cardiovascular disease and its complications; however, whether the myocardial inflammatory response is harmonized after cardiac injury remains to be determined. Some receptors of the innate immune system, including the nucleotide-binding oligomerization domain-like receptors (NLRs), play key roles in the host response after cardiac damage. Nucleotide-binding oligomerization domain containing 1 (NOD1), a member of the NLR family, is expressed in the heart, but its functional role has not been elucidated. We determine whether selective NOD1 activation modulates cardiac function and Ca^{2+} signalling.

Methods and results Mice were treated for 3 days with the selective NOD1 agonist C12-iE-DAP (iE-DAP), and cardiac function and Ca^{2+} cycling were assessed. We found that iE-DAP treatment resulted in cardiac dysfunction, measured as a decrease in ejection fraction and fractional shortening. Cardiomyocytes isolated from iE-DAP-treated mice displayed a decrease in the L-type Ca^{2+} current, $[Ca^{2+}]_i$ transients and Ca^{2+} load, and decreased expression of phospho-phospholamban, sarcoplasmic reticulum-ATPase, and Na^{+}-Ca^{2+} exchanger. Furthermore, iE-DAP prompted 'diastolic Ca^{2+} leak' in cardiomyocytes, resulting from increased Ca^{2+} spark frequency and RyR_2 over-phosphorylation. Importantly, these iE-DAP-induced changes in Ca^{2+} cycling were lost in *NOD1*$^{-/-}$ mice, indicating that iE-DAP exerts its actions through NOD1. Co-treatment of mice with iE-DAP and a selective inhibitor of NF-κB (BAY11-7082) prevented cardiac dysfunction and Ca^{2+} handling impairment induced by iE-DAP.

Conclusion Our data provide the first evidence that NOD1 activation induces cardiac dysfunction associated with excitation–contraction coupling impairment through NF-κB activation and uncover a new pro-inflammatory player in the regulation of cardiovascular function.

Keywords NOD1 • Ca^{2+} handling • Ca^{2+} sparks • Cardiac dysfunction • NF-κB • Innate immune system

1. Introduction

Cardiovascular disease (CVD) is the leading cause of death worldwide. Cardiac dysfunction, cell death, and augmented fibrosis are common hallmarks of several CVDs, including heart failure and diabetic cardiomyopathy. Inflammation is now recognized as an important contributor to different manifestations of CVD.[1] Indeed, extensive literature supports the notion that pro-inflammatory cytokines released in response to

* Corresponding author: Instituto de Investigación Hospital la Paz, Idipaz, Paseo de la Castellana 261, 28046 Madrid, Spain. Fax: +34 914972747, Email: mvelasco@iib.uam.es; maria.fernandez@idipaz.es (M.F.-V.); IIB-Alberto Sols, Arturo Duperier 4, 28029 Madrid, Spain. Fax: +34 914972747, Email: lbosca@iib.uam.es (L.B.)

† These authors contributed equally.

heart damage contribute to pathological cardiac remodelling.[2–5] However, it is unclear whether myocardial inflammatory response is harmonized after cardiac injury.

A current view in the field suggests that receptors of the innate immune system are central players in host response after cardiac damage.[6–8] Toll-like receptors (TLRs) are the best characterized mediators of the innate immune response in the cardiovascular system. In heart, sustained activation of TLRs induces deleterious cardiac remodelling,[9] whereas TLR deletion reduces infarct size in murine models.[10,11] More recently, other receptors of the innate immune system, such as nucleotide-binding oligomerization domain-like receptors (NLRs), have been implicated in CVDs, including atherosclerosis, dilated cardiomyopathy, and ischaemia/reperfusion injury.[4,12,13]

Nucleotide-binding oligomerization domain containing 1 (NOD1) is an NLR family member involved in host defense that takes part in the response against certain pathogens by regulating the inflammatory response.[14,15] NOD1 is a cytosolic receptor that, upon activation, undergoes a conformational change that allows the recruitment and activation of receptor-interacting protein 2 (RIP-2). RIP-2 binds to nuclear factor κB (NF-κB) which then translocates to the nucleus to trigger the expression of pro-inflammatory mediators.[16,17] NF-κB is a key factor in inflammatory signalling and mediates the majority of the effects following NOD1 activation; indeed, the selectivity and potency of NOD1 agonists are frequently evaluated by their ability to activate NF-κB.[16,18] NOD1 is involved in many human pathologies including diabetes and cancer;[19–21] however, its role and relevance in the cardiovascular system are less understood. NOD1 can mediate the inflammatory response in vascular smooth muscle,[22,23] and recently we demonstrated NOD1 expression in murine heart, fibroblasts, and cardiomyocytes.[24] Although treatment of mice with the selective NOD1 agonist C12-iE-DAP induced an increase in pro-inflammatory and apoptotic responses,[24] its functional role has not been addressed.

Cardiac function and Ca^{2+} homeostasis are closely coupled in the heart. Cardiac contraction is tightly regulated by changes in intracellular calcium levels. Ca^{2+} is a key mediator of electrical activation, ion channel gating, and excitation-contraction coupling (EC coupling). EC coupling is initiated by an action potential that fires a small influx of Ca^{2+} via sarcolemmal L-type Ca channels (I_{CaL}) that trigger a large release of Ca^{2+} from the sarcoplasmic reticulum (SR) by ryanodine receptors (RyR_2),[25,26] increasing the intracellular Ca^{2+} concentration, $[Ca^{2+}]_i$. This rise in cytosolic Ca^{2+} results in the activation of the myofilaments to produce cell contraction. After contraction, Ca^{2+} is removed from the cytosol mainly by two mechanisms: (i) Ca^{2+} uptake by the SR-ATPase (SERCA) and (ii) Na^+/Ca^{2+} exchanger (NCX) activation that drives Ca^{2+} to the extracellular medium. SERCA activity is modulated by phospholamban (PLB). PLB inhibits the function of SERCA in the unphosphorylated state, but once PLB is phosphorylated, it unbinds from SERCA, which results in Ca^{2+} uptake to the SR.

As mentioned earlier, during cardiac EC coupling, Ca^{2+} entry through I_{CaL} serves as trigger of SR-Ca^{2+} release. The transient increase of $[Ca^{2+}]_i$ is due to the summation of elementary Ca^{2+} release events termed Ca^{2+}sparks. Ca^{2+}sparks were first defined at the beginning of the 1990s and reflect the *in situ* activity of RyR_2.[27] Enhanced Ca^{2+}sparks in quiescent cells may indicate an abnormal diastolic Ca^{2+} leak that is usually associated with certain acquired or inherited CVDs. Catecholaminergic polymorphic ventricular tachycardia (CPVT) is an example of an inherited disease associated with an augmented frequency of Ca^{2+}-sparks that is directly involved in the generation of arrhythmias.[28,29] Heart failure is an acquired CVD linked to abnormal diastolic Ca^{2+} leak.[30,31] Furthermore, certain pro-inflammatory cytokines such as cardiotrophin-1, which are involved in some CVDs, may induce pro-arrhythmogenic effects by increasing the occurrence of Ca^{2+}sparks.[32]

Using the selective NOD1 agonist, C12-iE-DAP (iE-DAP), we studied the role of NOD1 activation on cardiac function and Ca^{2+} homeostasis.[18,33,34] Our findings provide the first evidence that NOD1 activation induces a decrease in cardiac contraction in mice, associated with EC coupling impairment, mediated by NF-κB activation. Our data reveal a new pro-inflammatory player in the cardiac system since NOD1 might play an important role in the regulation of cardiac function through modulation of Ca^{2+} handling.

2. Methods

2.1 Animal care and cell isolation

The study was conducted following recommendations of the Spanish Animal Care and Use Committee, according to the guidelines for ethical care of experimental animals of the European Union (2010/63/EU). NOD1-deficient mice ($NOD1^{-/-}$) on a B6 (C57BL6/J) background have been described.[35] B6 mice were purchased from The Jackson Laboratory (Bar Harbor, ME, USA). Wild-type littermates were employed as a control. RT–PCR analysis of NOD1 expression in wild-type and $NOD1^{-/-}$ mice confirmed the absence of signal in NOD1-deficent mice (see Supplementary material online, *Figure S1*). Ventricular cardiomyocytes from male mice were isolated using standard enzymatic digestion.[36] Briefly, mice were heparinized (4 U/g IP) and injected with 'buprenorphine' (0.01 mg/kg), and were anaesthetized 30 min later with sodium pentobarbital (50 mg/kg). The hearts were excised and suspended on a Langendorff perfusion apparatus, the ascending aorta was cannulated, and a retrograde perfusion was initiated. The hearts were perfused for 2–3 min at 36–37°C with a standard calcium-free Tyrode's solution containing 0.2 mM EGTA, and then for ~3–4 min with the same Tyrode's solution containing collagenase type II (Worthington) and 0.1 mM $CaCl_2$. The hearts were removed from the Langendorff apparatus, and the ventricles were finely chopped into small pieces and gently stirred for 3 min in standard Tyrode's solution containing 0.1 mM $CaCl_2$. Cell suspensions were filtered through a 250 μm nylon mesh, pelleted by centrifugation for 3 min at 20 *g*, and suspended in Tyrode's solution containing 0.5 mM $CaCl_2$. Cells were centrifuged as before and suspended in a storage solution containing 1 mM $CaCl_2$. Tyrode's solution contained (in mM): 140 NaCl, 4 KCl, 1.1 $MgCl_2$, 10 HEPES, 10 glucose; pH = 7.4 with NaOH.

2.2 Treatments

Mice were treated for 3 days with 3.3 mg/kg of C12-iE-DAP: Lauroyl-γ-D-glutamyl-meso-diaminopimelic acid (iE-DAP), vehicle (Veh.), 3.3 mg/kg of iE-Lys or 3.3 mg/kg of iE-DAP plus 2.5 μg/g of BAY 11–7082 (BAY) by daily IP injection. The vehicle-injected group was the same for iE-DAP, iE-Lys, and iE-DAP + BAY11-7082 (<0.01% DMSO), and the volume injected was 0.1 mL in all cases. iE-DAP (Invivogen) is a selective NOD1 agonist with significant cell membrane permeability and high potency.[18,33,34] iE-Lys (Invivogen) is an inactive analogue of NOD1. BAY11-7082 (Calbiochem) was employed to selectively block the NF-κB pathway.[37–39]

2.3 Echocardiography recording

M-mode echocardiography was employed to analyse cardiac function. Mice were anaesthetized with 1.5% isoflurane gas, and animals were placed on the Integrated Rail System and Mouse Handling Table (VisualSonics, Toronto, Canada) allowing simultaneous acquisition of temperature data (37°C was maintained with the integrated heating pad). The chest of the mouse was carefully shaved, and warm ultrasound transmission gel was employed to permit optimal image quality. Mouse hearts were studied by echocardiography over time, using a high-frequency micro-ultrasound system

(Vevo 770, VisualSonics). Parasternal short-axis view images of the heart were recorded using a 30-MHz RMV scan head in a B-mode to allow M-mode recordings by positioning the cursor in the parasternal short-axis view perpendicular to the interventricular septum and posterior wall of the left ventricle. Heart rate, left-ventricle ejection fraction, fractional shortening, left-ventricle end-systolic diameter, left-ventricle end-diastolic diameter, systolic volume, and diastolic volume were determined using the on-site software cardiac package (VisualSonics).

2.4 Intracellular calcium imaging

$[Ca^{2+}]_i$ transients and Ca^{2+} sparks were recorded in intact myocytes previously loaded with the fluorescent Ca^{2+} dye (Fluo-3AM, 5 μmol/L) and under control Tyrode's solution perfusion. Experiments were performed at room temperature (20–23°C). To obtain $[Ca^{2+}]_i$ transients, cells were electrically excited at 2 Hz by field stimulation using two parallel Pt electrodes. Spontaneous Ca^{2+} sparks were obtained in quiescent cells after $[Ca^{2+}]_i$ transient recordings. SR Ca^{2+} load was estimated by rapid caffeine application (10 mM). Cells were excited for 1 min before caffeine addition.

Images were obtained with confocal microscopy (Meta Zeiss LSM 710, ×40 oil immersion objective with a 1.2 NA) by scanning the cell with an argon laser every 1.54 ms. Fluo-3AM was excited at 488 nm, and emitted fluorescence was collected at >505 nm. Data analysis was performed with homemade routines using IDL software (Research System Inc.). Images were corrected for background fluorescence. The fluorescence values (F) were normalized by the basal fluorescence (F_0) to obtain the fluorescence ratio (F/F_0). Ca^{2+} sparks were detected using an automated detection system and using a criterion that discriminated the detection of false events while detecting most Ca^{2+} sparks.[40]

2.5 I_{CaL} recording

Recording of L-type Ca^{2+} current (I_{CaL}) was performed at room temperature (22 ± 2°C) using the whole-cell configuration of the patch clamp technique. The patch pipette resistance was 1.0–1.2 MΩ. I_{CaL} was recorded using an Axopatch 200B (Axon Instruments). Current traces were digitized using Digidata 1322A and analysed using pClamp8 software (Axon Instruments). From a holding potential of −50 mV, voltage pulses (duration 300 ms) between −40 to +60 mV (with 10 mV steps) were applied at a frequency of 0.2 Hz. Ca^{2+} currents were normalized with cell capacitance to obtain current density. Membrane capacitance (C_m) was elicited by applying ± 10 mV voltage steps from −60 mV, and C_m was calculated according to the equation:

$$C_m = \frac{\tau_c I_0}{\Delta E_m [1 - (I_\infty / I_0)]}$$

where τ_c is the time constant of the membrane capacitance, I_0 the maximum capacitance current value, E_m the amplitude of the voltage step, and I the amplitude of the steady-state current. The extracellular solution for I_{CaL} recordings contained (in mM): 140 NaCl, 1.1 $MgCl_2$, 5.4 CsCl, 10 glucose, 5 HEPES, 1.8 $CaCl_2$; pH adjusted to 7.4 with NaOH. The intracellular recording pipette solution contained (in mM): 100 CsCl, 20 TEACl, 5 EGTA, 10 HEPES, 5 Na_2ATP, 0.4 Na_2GTP, 5 Na_2 creatine phosphate, 0.06 $CaCl_2$; pH adjusted to 7.4 with CsOH.

2.6 Western blot analysis

Cardiomyocytes were homogenized in a buffer containing (in mM): 50 Tris, 320 sucrose, 1 DTT, and protease/phosphatase inhibition cocktail (Sigma-Aldrich). Homogenates were centrifuged at 13 000 *g* for 15 min at 4°C, and cleared supernatants were used for immunoblotting. Proteins were separated on SDS–PAGE gels and then transferred to PVDF membranes. Membranes were blocked with 5% BSA and incubated overnight with the following primary antibodies: SERCA2a, phospho-PLB (Ser16), phospho-PLB (Thr17) and PLB, phospho-RyR_2 (Ser2815), phospho-RyR_2 (Ser2808) (Badrilla Ltd.), RyR_2 (Affinity Bioreagents), NCX (Swant antibodies), and GAPDH (Ambion). Membranes were then incubated with peroxidase-linked secondary antibodies (1:5.000) in 2% BSA for 60 min at room temperature. Immunoreactive bands were detected using the Amersham™ ECL™ Protein Detection System.

2.7 Statistics

Data are presented as mean ± SEM. Statistical analysis on the number of isolated cells/samples was carried out using a nested ANOVA, and *post hoc* comparisons were performed by Bonferroni's test. All statistical analyses were made using the SPSS 15.0 software (SPSS Inc., Chicago, IL, USA). Significance was assumed when $P < 0.05$.

3. Results

3.1 NOD1 activation induces cardiac dysfunction and impairment in EC coupling

C12-iE-DAP (iE-DAP) is a widely used selective agonist of NOD1.[18,33,34] We evaluated whether iE-DAP administration in mice was detrimental to cardiac function. Compared with vehicle-treated mice, ejection fraction, fractional shortening, and systolic volume were all decreased in mice treated for 3 days with iE-DAP (*Table 1*). However, heart rate, left-ventricle end-diastolic and end-systolic diameter, and also heart weight: body weight ratio, were unaffected by iE-DAP treatment (*Table 1*).

Since cardiac function and Ca^{2+} homeostasis are closely coupled in the heart, we investigated whether the reduced cardiac function induced by iE-DAP was associated with an impairment of EC coupling. I_{CaL} is a key player in cardiac EC coupling, chiefly through its ability to trigger $[Ca^{2+}]_i$ transients.[26] Using the patch clamp technique in the whole-cell configuration, we recorded I_{CaL} in myocytes isolated from vehicle or iE-DAP-treated mice. Average I_{CaL} density from 0 to +40 mV was significantly reduced ($P < 0.05$) in iE-DAP-treated mice

Table 1 Cardiac parameters collected after M-mode ultrasound evaluation of mice

	HW (mg)	BW (g)	HR (bpm)	EF (%)	FS (%)	LVESD (mm)	LVEDD (mm)	SV (μL)	DV (μL)	*n*
Vehicle	231.3 ± 7.1	25.9 ± 0.7	368.3 ± 14.3	72.6 ± 5.5	39.9 ± 5.4	1.9 ± 0.3	3.1 ± 0.2	11.4 ± 4.5	47.6 ± 4.9	6
iE	226.6 ± 13.3	25.5 ± 0.9	396.0 ± 22.0	47.9 ± 4.0***	28.5 ± 3.9**	2.5 ± 0.3	3.6 ± 0.2	21.9 ± 3.3**	56.4 ± 6.2	4
iE + BAY	218.7 ± 33.8	26.4 ± 0.9	389.5 ± 42.3	67.1 ± 8.5##	36.1 ± 6.6##	2.1 ± 0.3	3.4 ± 0.1	12.9 ± 2.2##	46.1 ± 4.2	4

Data are mean ± SEM.
HW, heart weight; BW, body weight; HR, heart rate; EF, left-ventricle ejection fraction; FS, fractional shortening; LVESD, left-ventricle end-systolic diameter; LVEDD, left-ventricle end-diastolic diameter; SV, systolic volume; DV, diastolic volume.
**$P < 0.01$, ***$P < 0.001$ vs. vehicle (Veh.); ##$P < 0.01$ vs. iE (iE = 3.3 mg/kg iEDAP-treated mice for 3 days, iE + BAY = 3.3 mg/kg iEDAP plus 2.5 g/kg BAY11-7082 treated mice for 3 days).

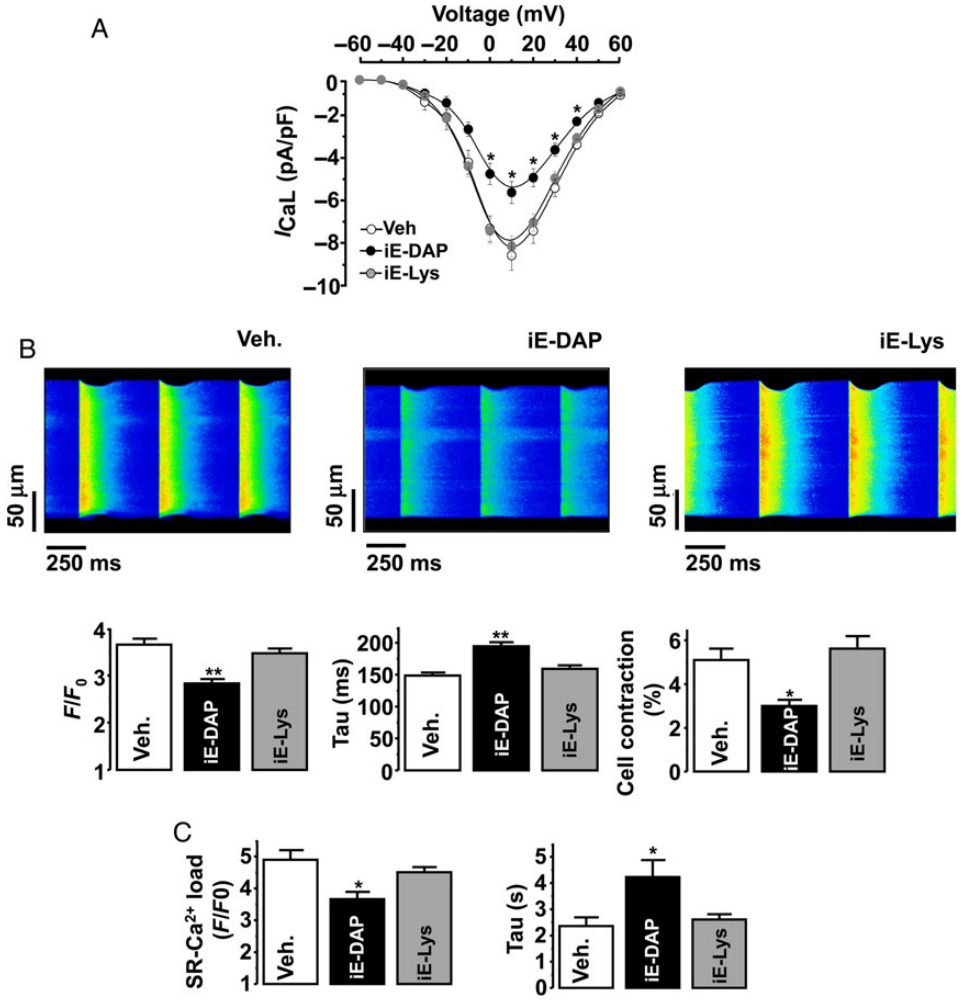

Figure 1 Short-term treatment of mice with iE-DAP induces a selective impairment in EC coupling. Mice were injected IP for 3 days with 3.3 mg/kg of C12-iE-DAP (iE-DAP), with 3.3 mg/kg of iE-Lys (inactive analogue of iE-DAP), or with vehicle (Veh.). (*A*) I-V relationships I_{CaL} in cardiomyocytes isolated from vehicle ($n = 12$ cells/4 mice), iE-DAP-treated mice ($n = 9$ cells/4 mice), and iE-Lys ($n = 19$ cells/3 mice). (*B*) Upper panels illustrate a representative example of line-scan confocal images obtained in cells from vehicle (left), iE-DAP-treated mice (middle), and iE-Lys-treated mice (right). Lower panels show the mean values of peak fluorescence $[Ca^{2+}]_i$ transients (F/F_0, left), decay time constant (Tau, middle), and cell contraction (%, right) obtained in vehicle ($n = 19$ cells/5 mice), iE-DAP ($n = 27$ cells/4 mice), and iE-Lys group ($n = 22$ cells/3 mice). (*C*) Histograms represent the mean values of caffeine-evoked $[Ca^{2+}]_i$ transients amplitude represented as F/F_0 (left) and its decay time constant (right) obtained in vehicle ($n = 15$ cells/3 mice), iE-DAP ($n = 16$ cells/3 mice), and iE-Lys conditions ($n = 27$ cells/3 mice). Results show mean ± SEM. $^*P < 0.05$, $^{**}P < 0.01$ vs. vehicle.

compared with vehicle-treated counterparts (*Figure 1A*). Moreover, iE-DAP significantly reduced the maximal I_{CaL} peak density obtained at +10 mV vs. vehicle (−5.3 ± 0.5 pA/pF, $n = 9$ in iE-DAP vs. −8.2 ± 0.7 pA/pF, $n = 14$ in vehicle $P < 0.05$). Notably, cardiomyocytes isolated from mice treated with the inactive analogue of iE-DAP, iE-Lys, exhibited similar values of I_{CaL} density to the vehicle group (*Figure 1A*).

The diminution on I_{CaL} induced by iE-DAP treatment can be related to changes in the I_{CaL} inactivation curve. Indeed, cardiomyocytes obtained from iE-DAP-treated mice exhibited a shift in the voltage dependence of I_{CaL} inactivation towards more negative values; the voltage of half-maximal inactivation was (V_{50}) −19.8 ± 1.8 mV in vehicle and −26.5 ± 1.9 mV in iE-DAP group ($P < 0.05$; see Supplementary material online, *Figure S2A*). Importantly, no changes in the mRNA expression of the molecular correlate of I_{CaL}, Cav 1.2, were detected between groups (see Supplementary material online, *Figure S2B*).

Subsequently, $[Ca^{2+}]_i$ transients electrically evoked by field stimulation at 2 Hz were recorded by confocal microscopy. An example of a line-scan image taken from a cardiomyocyte isolated from vehicle-, iE-DAP-, or iE-Lys-treated mice is shown in *Figure 1B* (upper panels). Cardiomyocytes obtained from iE-DAP-treated mice exhibited a decrease in the $[Ca^{2+}]_i$ transient amplitude together with a slower time constant of $[Ca^{2+}]_i$ transient decay (Tau), as well as a significant decrease in cell contraction, compared with the vehicle group (*Figure 1B* lower panels). In contrast, $[Ca^{2+}]_i$ transient properties and cell contraction were not affected by iE-Lys administration (*Figure 1B*, lower panels).

To examine whether the reduced $[Ca^{2+}]_i$ transients detected in the iE-DAP group were related to changes in the SR Ca^{2+} load, we measured caffeine-evoked $[Ca^{2+}]_i$ transients in cardiomyocytes isolated from both groups. Compared with vehicle-treated mice, caffeine-evoked $[Ca^{2+}]_i$ transients were reduced in the iE-DAP-treated group (*Figure 1C*, left panel) together with significantly slower rates of decay (*Figure 1C*, right

panel). As expected, Ca^{2+} load and time of decay of caffeine-evoked $[Ca^{2+}]_i$ transients were unaffected by iE-Lys administration (*Figure 1C*).

The observed iE-DAP-induced deceleration in the decay time of $[Ca^{2+}]_i$ transients may be linked to an impairment in SERCA and/or PLB expression. Thus, we analysed the phosphorylation status of PLB (P-PLB) at serine 16 (mediated by PKA activation) and threonine 17 (specific site for CaMKII activation), and also SERCA protein expression, in homogenates obtained from cardiomyocytes isolated from vehicle- and iE-DAP-treated mice. Results showed that both phosphorylation of PLB at ser16 (*Figure 2A*) and SERCA expression (*Figure 2C*) were decreased in the iE-DAP group compared with vehicle-treated mice. In contrast, phosphorylation of PLB at threonine 17 was unchanged between groups (*Figure 2B*).

Since SERCA function (*k* SERCA) can be assessed systematically from the decay rates of the systolic and caffeine-evoked Ca transients,[41] we calculated *k* SERCA by subtracting the rate constant of decay of the caffeine-evoked transient from that of the systolic Ca^{2+} transients. We found that *k* SERCA was $100 \pm 0.1\%$ ($n = 5$) in vehicle and $77.7 \pm 0.1\%$ ($n = 6$) in iE-DAP group ($P < 0.001$), supporting the idea that iE-DAP administration induces a decrease in the SERCA function.

On other hand, the decay time of caffeine-evoked $[Ca^{2+}]_i$ transients were increased in the iE-DAP-treated group (*Figure 1C*, right panel), suggesting an impairment of the Na^+/Ca^{2+} exchange (NCX) function. Thus, we investigated whether the expression of NCX was affected by the NOD1 agonist. As shown in *Figure 2D*, NCX protein levels were significantly decreased in the iE-DAP group vs. vehicle ($P < 0.05$).

Collectively, these data indicate that short-term iE-DAP treatment induces cardiac dysfunction by compromising the efficiency of EC coupling by decreasing I_{CaL}, $[Ca^{2+}]_i$ transients, and Ca^{2+} load, and also by impairing PLB function and down-regulating SERCA and NCX. Additionally, NOD1 expression was unchanged in cardiomyocytes after iE-DAP administration (data not shown). To evaluate whether NOD1 activation impairs the Ca^{2+} handling in isolated cardiomyocytes, we incubated cells obtained from hearts of wild-type mice with 40 μg/mL iE-DAP for 1–2 h and $[Ca^{2+}]_i$ transient properties and cell contraction were determined. Results showed that cells incubated with iE-DAP exhibited a decrease in the $[Ca^{2+}]_i$ transient amplitude (*Figure 3A*) together with a slower time constant of $[Ca^{2+}]_i$ transient decay (Tau; *Figure 3B*), as well as a significant reduction in cell contraction (*Figure 3C*), compared with vehicle-treated cells.

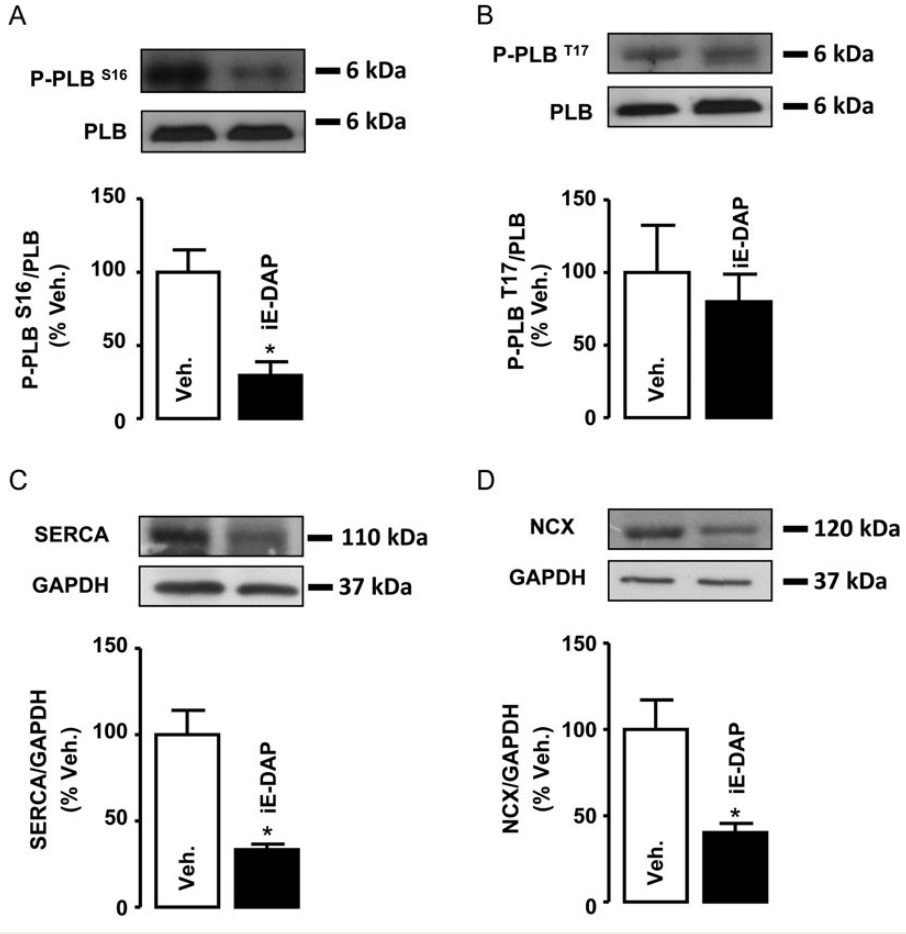

Figure 2 iE-DAP treatment promotes a decrease in SERCA and NCX levels and PLB phosphorylation at serine 16. (*A*) and (*B*) Immunoblots of phosphorylated phospholamban (P-PLB) at ser16 or thr17 and total PLB, and the corresponding mean values displayed in histograms obtained in vehicle and iE-DAP-treated mice. Representative blots of SERCA/GAPDH (*C*) and NCX/GAPDH (*D*) obtained from animals treated with iE-DAP or vehicle. Below, histograms summarize the mean data. Vehicle ($n = 3$ samples/3 mice) and iE-DAP group ($n = 3$ samples/3 mice). Results show mean ± SEM (band ratio) expressed as percentage vs. vehicle. *$P < 0.05$ vs. vehicle.

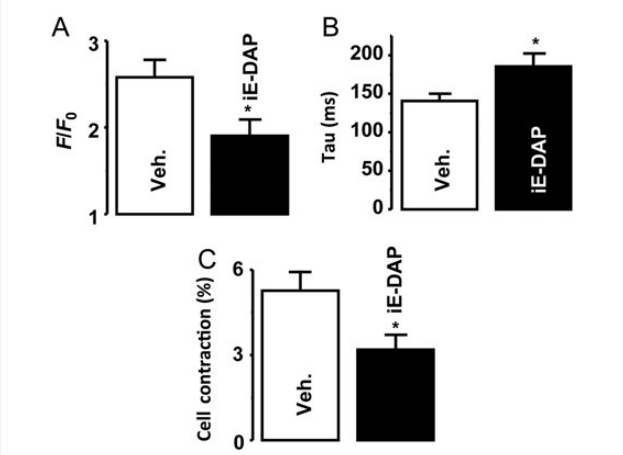

Figure 3 Cardiomyocytes treated with iE-DAP for 1–2 h showed altered $[Ca^{2+}]_i$ transients and cell contraction parameters. Histograms represent the mean values of peak fluorescence $[Ca^{2+}]_i$ transients (F/F_0, *A*), decay time constant (Tau, *B*), and cell contraction (%, *C*) obtained in vehicle-treated cells ($n = 13$ cells/3 mice) and cells treated for 1–2 h with 40 μg/mL iE-DAP ($n = 12$ cells/3 mice). *$P < 0.05$ vs. vehicle.

3.2 NOD1 activation induces SR-Ca^{2+} leak

Since diastolic Ca^{2+} leak is closely associated with SR-Ca^{2+} load decline, we analysed Ca^{2+} spark frequency and properties to measure spark-mediated Ca^{2+} leak.[28,42] An example of a line-scan confocal image of a cardiomyocyte taken from vehicle- or iE-DAP-treated mice is shown in *Figure 4A*. A significantly higher frequency of Ca^{2+} sparks was observed in cardiomyocytes taken from iE-DAP-treated mice compared with cardiomyocytes obtained from vehicle controls (*Figure 4B*). A comparison of the properties of the Ca^{2+} sparks showed that the amplitude was significantly lower in cardiomyocytes taken from iE-DAP-treated mice compared with those obtained from vehicle-treated mice (*Figure 4C*). This reduction in amplitude in cells isolated from iE-DAP-treated mice was due largely to a significant increase (39%, see Supplementary material online, *Table S1*) in the population of events with peaks around 1.3 (F/F_0), with a concomitant reduction of Ca^{2+} sparks with higher (above 1.5 F/F_0) amplitudes, as shown by histogram distribution (see Supplementary material online, *Figure S3A*). In contrast, the average duration and width of Ca^{2+} sparks were unchanged between groups (*Figure 4C*). Similarly, histogram distributions of Ca^{2+} spark durations and widths were comparable in cells isolated from iE-DAP- and vehicle-treated mice (see Supplementary material online, *Figure S3B* and *C*). Calculation of the overall spark-mediated Ca^{2+} leak gave an increase of 4.7-fold after iE-DAP treatment (see Supplementary material online, *Figure S4*). Thus, cardiomyocytes isolated from iE-DAP-treated mice have increased Ca^{2+} leak that is derived mainly from Ca^{2+} spark release. Furthermore, Ca^{2+} spark frequency was unchanged by iE-Lys administration (1.6 ± 0.4 sparks s^{-1} 100 μm^{-1} $n = 9/N = 3$ in vehicle, 6.4 ± 1.4 sparks s^{-1} 100 μm^{-1} $n = 16/N = 3$ in iE-DAP, and 1.4 ± 0.5 sparks s^{-1} 100 μm^{-1} $n = 12/N = 3$ in iE-Lys group). Ca^{2+} spark properties were also unchanged by iE-Lys treatment (see Supplementary material online, *Figure S5*).

Next, we analysed whether the increased Ca^{2+} sparks detected in the iE-DAP group impaired the resting cytoplasmic $[Ca^{2+}]_i$. Results showed that the intracellular $[Ca^{2+}]_i$ measured using Fura-2 (R340/R380) was significantly higher in cardiomyocytes isolated from iE-DAP-treated mice compared with equivalent vehicle-treated mice (see Supplementary material online, *Figure S6*).

As described above, Ca^{2+} spark recordings reflect the *in situ* activity of RyR_2.[27] Since Ca^{2+} spark frequency data pointed to augmented RyR_2 activity following iE-DAP treatment, we measured phosphorylation of RyR_2 at ser2808 (site for mainly PKA activation) and ser2815 (site for CaMKII activation). Results from immunoblotting showed that ser2808 phosphorylation of RyR_2 was significantly increased after iE-DAP treatment (*Figure 4D*), whereas ser2815 phosphorylation of RyR_2 was unchanged (*Figure 4E*).

Taken together, these results confirm that iE-DAP induces diastolic Ca^{2+} leak in isolated cardiomyocytes, resulting from increased Ca^{2+} spark frequency that can contribute to rise the resting cytoplasmic $[Ca^{2+}]_i$.

3.3 iE-DAP exerts a selective effect on EC coupling

To corroborate the selectivity of iE-DAP for Ca^{2+} handling modulation, we used cardiomyocytes isolated from NOD1-deficient mice ($NOD1^{-/-}$). We found that iE-DAP administration resulted in similar mean values of I_{CaL} density at all voltages tested (*Figure 5A*), $[Ca^{2+}]_i$ transient properties (*Figure 5B*, left and central panels), cell contraction (*Figure 5B*, right panel), and Ca^{2+} load (*Figure 5C*), as well as comparable values rates of decay of Ca^{2+} load (*Figure 5D*) to those obtained in $NOD1^{-/-}$ mice treated with vehicle. Moreover, Ca^{2+} spark frequency and the characteristics of Ca^{2+} sparks were also comparable between the two groups (*Figure 5E*, see Supplementary material online, *Figure S7*).

Thus, the lack of an effect of iE-DAP in $NOD1^{-/-}$ mice to induce changes in EC coupling supports the selectivity of iE-DAP on Ca^{2+} signalling.

3.4 NF-κB mediates iE-DAP-induced changes in EC coupling and cardiac function

Since we previously showed that iE-DAP treatment induces specific NF-κB activation in cardiac tissue and isolated cardiomyocytes,[24] we assessed whether NF-κB activation could mediate the effect of iE-DAP on Ca^{2+} dynamics. To do this, we employed the selective NF-κB inhibitor, BAY11-7082 (BAY).[37–39] In comparison with mice treated with iE-DAP alone, isolated cardiomyocytes from mice treated for 3 days with iE-DAP plus BAY had similar I_{CaL} values to vehicle-treated mice (*Figure 6A*). Moreover, co-treatment with BAY abrogated the iE-DAP-induced effects on amplitude and decay time of $[Ca^{2+}]_i$ transients, as well as cell contraction parameters (*Figure 6B*). Additionally, immunoblotting of cardiomyocytes demonstrated that co-treatment with BAY prevented both the iE-DAP-induced decrease in SERCA protein expression and PLB phosphorylation at ser16 (*Figure 6C*).

In accord with these changes, caffeine-evoked $[Ca^{2+}]_i$ transients in cardiomyocytes obtained after co-treatment of mice with iE-DAP plus BAY were comparable to those obtained from vehicle-treated mice, recovering the loss induced by iE-DAP treatment alone (*Figure 7A*, left panel). Also, both the increase in the rate of decay of caffeine-evoked $[Ca^{2+}]_i$ transients induced by iE-DAP (*Figure 7A*, right panel) and the occurrence of Ca^{2+} sparks (*Figure 7B*, left panel) were normalized in the presence of BAY. Additionally, the iE-DAP-induced increase in the phosphorylation of RyR_2 on ser2808 was abolished in mice co-treated with BAY (*Figure 7B*, right panel) and is consistent with the Ca^{2+} sparks recordings.

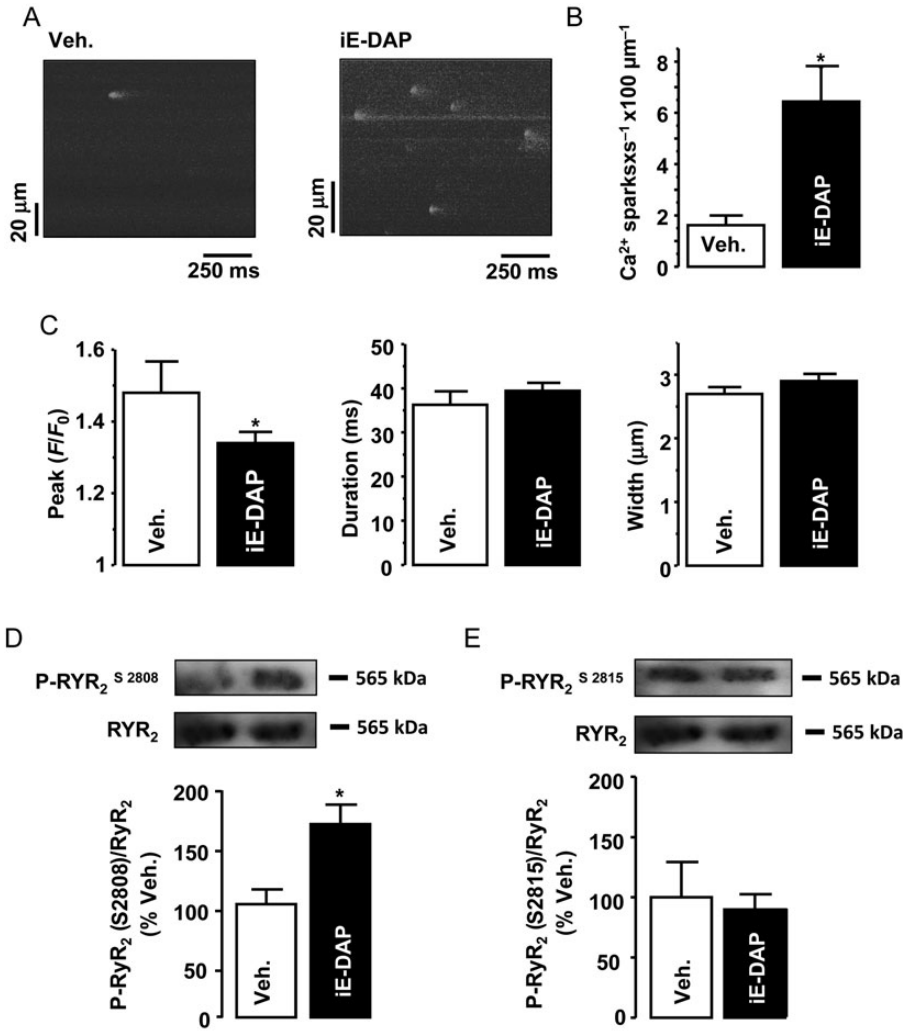

Figure 4 Frequency of Ca^{2+} sparks and phosphorylation of RyR_2 are enhanced in cardiomyocytes isolated from iE-DAP-treated mice. (*A*) Example of line-scan images of Ca^{2+} spark recordings obtained in a myocyte isolated from vehicle and iE-DAP-treated mice. (*B*) Average data of Ca^{2+} sparks occurrence obtained in both groups. (*C*) Mean values of Ca^{2+} sparks properties; peak (left panel), duration (middle panel), and width (right panel) obtained in cells isolated from vehicle ($n = 9$ cells/3 mice) and iE-DAP-treated mice ($n = 16$ cells/3 mice). Representative immunoblots of phosphorylated RyR_2 in ser2808 (panel *D*) or ser2815 (panel *E*) vs. total RyR_2, and the corresponding mean values obtained in vehicle and iE-DAP group ($n = 3$ samples/3 mice of each group). Histograms show the mean ± SEM (band ratio) expressed as percentage vs. vehicle. *$P < 0.05$ vs. vehicle.

Finally, co-treatment of BAY plus iE-DAP prevented the depressed cardiac function induced by iE-DAP administration alone (*Figure 7C* and *Table 1*). Taken together, these studies support the concept that the NF-κB pathway underlies the iE-DAP-induced effect on both cardiac dysfunction and impairment in cardiomyocyte Ca^{2+} handling.

4. Discussion

Our study provides the first direct evidence that selective activation of the innate immune receptor NOD1 results in cardiac dysfunction related to EC coupling impairment mediated through NF-κB signalling.

The innate immune system acts as a 'first warning response' to pathogens, infection, or organ injury. The best described mediators of the innate immune system are TLRs and NLRs. Both receptor families contain pattern recognition motifs that distinguish between self and non-self, by recognizing pathogen molecular motifs or endogenous host material derived from cellular injury/death. Cardiac damage activates some of these receptors to induce a protective response for tissue repair.[43–45] However, sustained activation of the innate immune system frequently results in maladaptive responses and leads to an increase in pro-inflammatory cytokines levels, which promote pathological cardiac remodelling.[45] Accordingly, up-regulation of TLR activity induces cardiac damage while mutations or targeted disruption of TLRs reduce infarct size, preventing cardiac dysfunction induced by ischaemia/reperfusion or myocardial infarction, and boost the stability atherosclerotic lesions.[11,46–49]

In addition to TLRs, NLRs are also cytosolic receptors of the innate immune system that play an important role in regulating the inflammatory response.[22] Recently, several studies have attributed roles for these mediators in CVDs; in particular, the NLR NLRP3 has been

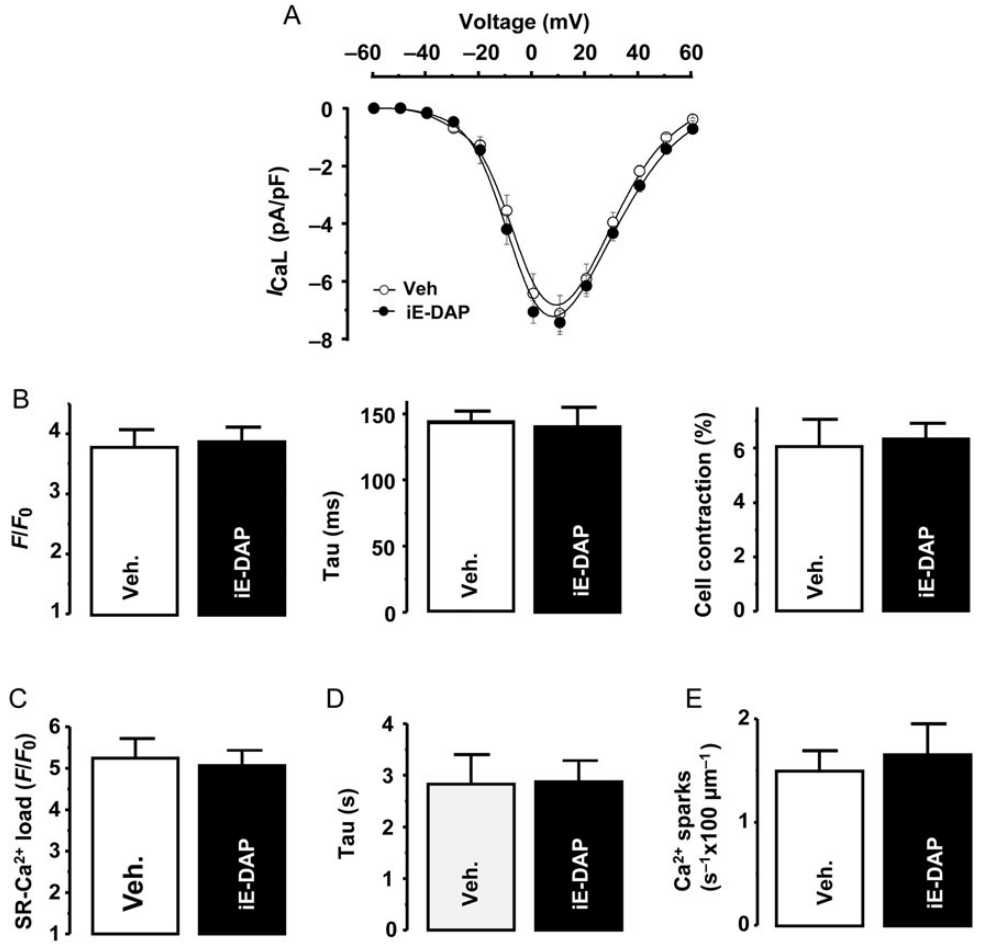

Figure 5 iE-DAP treatment does not modify EC coupling parameters in *NOD1*$^{-/-}$ mice. (*A*) I-V relationships I_{CaL} density in cardiomyocytes obtained in *NOD1*$^{-/-}$ mice ($n = 15$ cells/3 mice) and *NOD1*$^{-/-}$ mice treated with iE-DAP ($n = 15$ cells/3 mice). (*B*) Histograms show the mean values of peak fluorescence $[Ca^{2+}]_i$ transients (left panel), decay time constant (middle panel), and cell contraction (right panel) obtained in myocytes isolated in *NOD1*$^{-/-}$ mice ($n = 17$ cells/3 mice) and *NOD1*$^{-/-}$ mice treated with iE-DAP ($n = 22$ cells/3 mice). (*C*) Average data of caffeine-evoked $[Ca^{2+}]_i$ transients amplitude and its decay time (*D*) obtained in all experimental groups. (*E*) Average data of Ca^{2+} sparks occurrence obtained in cardiomyocytes isolated from *NOD1*$^{-/-}$ mice ($n = 17$ cells/3 mice) and *NOD1*$^{-/-}$ mice treated with iE-DAP ($n = 22$ cells/3 mice). Histograms represent the mean ± SEM expressed as percentage vs. vehicle. Results show mean ± SEM.

demonstrated to mediate pathological processes including atherosclerosis and dilated cardiomyopathy.[4,12,13] NOD1 is a member of the NLR family that is expressed ubiquitously. NOD1 regulates the inflammatory response in vascular smooth muscle,[22] and long-term treatment of mice with selective NOD1 agonists promotes vascular complications including coronary arteritis and valvulitis.[50] While NOD1 is expressed in murine cardiomyocytes,[24] its functional role in the heart has not yet been established.

In the present study, we found that NOD1 activation promotes a significant decrease in cardiac function, a feature shared by the majority of CVDs including heart failure, diabetic cardiomyopathy, and ischaemia–reperfusion injury. Moreover, cardiac dysfunction induced by administration of the NOD1 agonist iE-DAP was associated with an impairment in EC coupling in isolated murine cardiomyocytes; specifically, cardiomyocytes isolated from iE-DAP-treated mice displayed lower $[Ca^{2+}]_i$ transients amplitude compared with vehicle-treated counterparts. This effect could be due to modulation of (i) Ca^{2+} current, (ii) RyR_2 activity, (iii) and/or SR- Ca^{2+} load.

First, I_{CaL} density was significantly diminished after iE-DAP administration. Since I_{CaL} is the main trigger of SR-Ca^{2+} release via Ca^{2+}-induced Ca^{2+} release (CICR), I_{CaL} decline can be responsible, at least in part, for the decrease of $[Ca^{2+}]_i$ transients induced by iE-DAP administration (*Figure 1*). iE-DAP treatment also induces a slower decay time of $[Ca^{2+}]_i$ transients, and this effect can be correlated with changes in the Ca^{2+} SR-uptake. Accordingly, iE-DAP provoked a decrease of SERCA expression together with a decrease of PLB phosphorylation at serine 16, but not at threonine 17. Importantly, in some CVD, e.g. heart failure, depletion of $[Ca^{2+}]_i$ transients is accompanied by decreased SR-Ca^{2+} uptake due to changes in SERCA activity[51,52] and similar trends were observed in iE-DAP-treated mice.

In support of our data, Lee *et al.* have shown that the pro-inflammatory mediator TNF-α induces alterations in Ca^{2+} handling by decreasing SERCA expression in pulmonary vein cardiomyocytes.[53] This decrease in SERCA levels impacts on the Ca^{2+} SR reuptake and results in a longer decay time constant of $[Ca^{2+}]_i$ transients.[53] Similar EC coupling alterations have been described in experimental murine

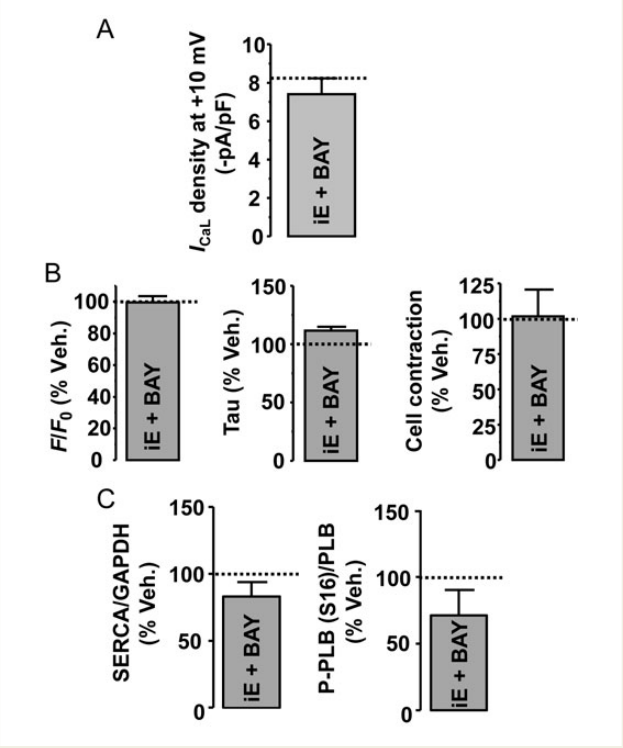

Figure 6 NF-κB activation mediates the effects induced by iE-DAP on I_{CaL} and $[Ca^{2+}]_i$ transients. (*A*) Bar graph representing the average I_{CaL} density (pA/pF) recorded at +10 mV in cardiomyocytes obtained in iE-DAP (3.3 mg/kg IP/3 days) plus BAY (BAY, 2.5 μg/g) treated mice ($n = 10$ cells/3 mice). (*B*) Histograms illustrate the average of $[Ca^{2+}]_i$ transients amplitude, its decay time, and the cell contraction data obtained in cells isolated from iE-DAP plus BAY-treated mice ($n = 15$ cells/3 mice). (*C*) Average data for SERCA (left panel) or P-PLB at ser16 (right panel) vs. GAPDH or PLB expression, respectively, from iE-DAP+BAY samples ($n = 3$ samples/3 mice). Data representing the mean ± SEM expressed as percentage of vehicle (dotted line).

models of sepsis.[54,55] Indeed, some bacterial cell membrane components, including bacterial peptidoglycan-associated lipoprotein, which participate in septic shock, induce altered $[Ca^{2+}]_i$ transients and cell shortening in murine cardiomyocytes.[56] Moreover, additional pro-inflammatory mediators such as IL-2 or cardiotrophin-1 may induce arrhythmogenic activity through impairment of Ca^{2+} handling in isolated myocytes.[32,53,57]

Secondly, Ca^{2+} sparks are a good indicator of the *in situ* activity of RyR_2. We show that iE-DAP induces an increase in the frequency of elementary Ca^{2+} release, supporting the idea that iE-DAP provokes an abnormal diastolic Ca^{2+} leak. The increased frequency of Ca^{2+} sparks also may contribute to reduce SR-Ca^{2+} load and systolic Ca^{2+} transients, increasing the resting cytosolic $[Ca^{2+}]_i$. Importantly, in heart failure, the Ca^{2+} leak measured as Ca^{2+} sparks induces cardiac arrhythmias since the increased Ca^{2+} release diffuses to neighbouring RyR_2 clusters leading to an induction of spontaneous Ca^{2+} waves, triggering cardiac arrhythmias. Notably, our results demonstrate that NOD1 activation promotes an abnormal diastolic Ca^{2+} leak in cardiomyocytes that might induce arrhythmias under pathological conditions such as heart failure or sepsis, where an enhanced pro-inflammatory milieu prevails. Consistent with this notion, treatment of isolated cardiomyocytes with the pro-inflammatory cytokine cardiotrophin-1 resulted in increased Ca^{2+} spark events, closely related to the pro-arrhythmogenic effect of this mediator.[58]

Regarding our observations on Ca^{2+} spark properties, their amplitude was significantly reduced after iE-DAP administration, without alterations in their duration or width. These results can be explained by the fact that driving force can be equivalently diminished with the SR-Ca^{2+} load decreased.[59,60]

Finally, Our results demonstrate that iE-DAP induces a decrease of SR-Ca^{2+} load measured as caffeine-evoked $[Ca^{2+}]_i$ transients. Thus, our data show that SERCA reduction, together with increased open probability of RyR_2 reflected by the enhanced frequency of Ca^{2+} sparks induced by iE-DAP, may contribute to decrease the SR Ca^{2+} load, compromising systolic Ca^{2+} transients and decreasing cell contraction, and therefore cardiac function. It would be interesting to confirm the changes in SR Ca^{2+} load by quantitative approaches involving measurement of NCX current integrals.

SR Ca^{2+} content reflects the balance between Ca^{2+} uptake, influx, and efflux mechanisms via at least four main Ca^{2+} handling proteins: SERCA, RyR, ICaL, and NCX. Indeed, under physiological steady-state conditions, one effect of a higher diastolic Ca^{2+} leak (proved by an increased Ca^{2+} spark frequency in iE-DAP cells) would be a partial depletion of SR Ca^{2+} content, which could be worsened by a reduced SERCA function. Thus, the outcome would be the reduction of the RyR-mediated Ca^{2+} leak, to reach a new steady-state condition. However, a possible mechanism involved in the preservation of SR Ca^{2+} load that maintains the sustained elevation of Ca^{2+} spark frequency under iE-DAP treatment might be related to the down-regulation of NCX (*Figure 2D*) induced by iE-DAP. The reduction in NCX expression contributes to increase resting cytosolic Ca^{2+} concentration (see Supplementary material online, *Figure S6*), extruding less Ca^{2+} outside the cell and favouring the reloading of the SR via SERCA at least partially, although this ATPase works slower. In this line, conditional SERCA-KO mice and pharmacological tools employed to reduce SERCA activity (thapsigargin) have shown that the down-regulation/inhibition of SERCA activity has minimal effects on overall SR Ca^{2+} content. This can be explained by two factors: the direct relationship between SR Ca^{2+} content and SERCA activity, and the linear dependence of the amplitude of the systolic Ca^{2+} transient on SR Ca^{2+} content, which in some cases low SR Ca^{2+}content promotes a decrease in the systolic SR Ca^{2+} efflux, thus maintaining the SR Ca^{2+} load. Indeed, our results show that the amplitude of Ca^{2+} transients are significantly lower in the iE-DAP group (*Figure 1B*); and also that iE-DAP administration induces a decrease in the SERCA function of around 20% (*K* SERCA) compared with veh. group. So, iE-DAP treatment gets SERCA working at least at ~80% to maintain SR Ca^{2+} content at a level sufficient that is enough to sustain spark-mediated Ca^{2+} leak (not below of ~400 μM, which could stop the release of Ca^{2+} in the form of sparks). Another key aspect is that although iE-DAP induces an increase in Ca^{2+} spark number, the mean amplitude of Ca^{2+} sparks was significantly lower in the iE-DAP group compared with the vehicle ones (*Figure 4C*), reducing the amount of Ca^{2+} released as Ca^{2+} sparks.

It was important to validate the NOD1 agonist iE-DAP. Although the selectivity of iE-DAP has been addressed by several studies in different organs and cells, we verified that iE-DAP exerts a selective effect on Ca^{2+} cycling in isolated myocytes. Accordingly, mice treated with the inactive analogue of iE-DAP, iE-Lys, and NOD1-deficient mice treated with iE-DAP, failed to modify the cardiac EC coupling parameters.

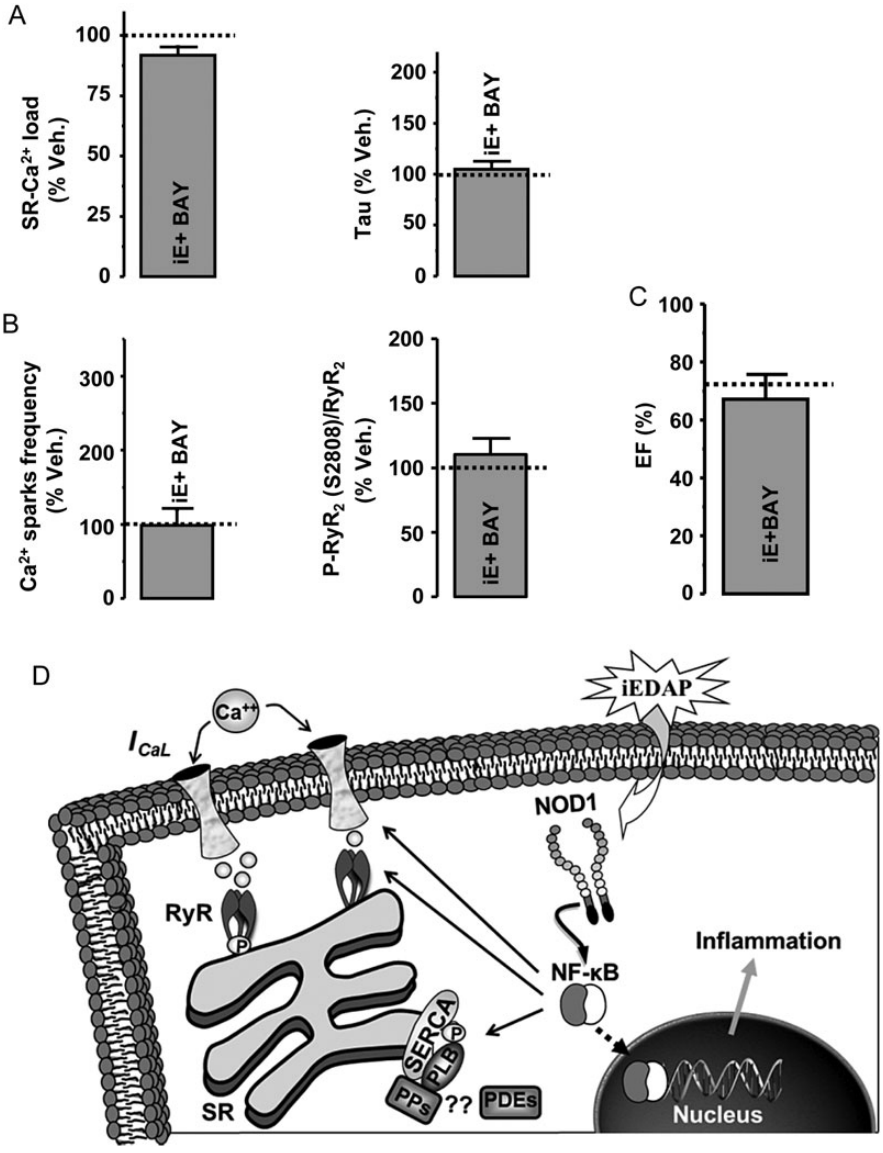

Figure 7 iE-DAP alters Ca^{2+} load, Ca^{2+} sparks occurrence, and cardiac contraction though NF-κB activation. Diagram represents the effects of NOD1 agonist in EC coupling. (*A*) Bar graphs representing the average of caffeine-evoked $[Ca^{2+}]_i$ transients (F/F_0) (left panel) and its decay time constant (right panel) obtained in iE-DAP plus BAY-treated mice ($n = 26$ cells/3 mice). (*B*) Left panel shows histogram summarizing the average data of Ca^{2+} sparks occurrence obtained in iE-DAP + BAY group. Right panel illustrates the average of P-RyR_2 in ser2808 vs. total expression of RyR_2 obtained in iE-DAP + BAY mice ($n = 3$ samples/3 mice). (*C*) Histogram reflects the average of cardiac ejection fraction values detected in iE-DAP + BAY-treated mice ($n = 4$ mice). Results show the mean ± SEM expressed as percentage of vehicle (dotted lines). (*D*) Diagram representing the possible mechanisms involved in the effects of iE-DAP in Ca^{2+} handling. iE-DAP induces selective NOD1 activation, involving NF-κB activation, and modulates I_{CaL} and RyR function as well as PLB and SERCA impairment, resulting in cardiac dysfunction. On one hand, the increased Ca^{2+} leak contributes to reduce the SR Ca^{2+} load, increasing the resting cytosolic $[Ca^{2+}]_i$ and compromising the systolic Ca^{2+} release. On the other hand, phosphatases and phosphodiesterases (PP, PDE) may act by decreasing the phosphorylation of PLB, contributing to decrease SR-Ca^{2+} load under iE-DAP administration.

This selectivity strengthens the findings that NOD1 participates in the regulation of Ca^{2+} handling.

Mechanistically, we show that the detrimental effect on Ca^{2+} handling and cardiac function induced by iE-DAP is mediated by the NF-κB pathway. NF-κB is a central player in the inflammatory response and mediates many of the effects derived from NOD1 activation. The precise role of NF-κB in heart remains controversial since both adaptive and maladaptive actions have been described. Thus, early NF-κB activation following acute cardiac damage may support adaptive mechanisms to prevent pathological remodelling. In contrast, sustained NF-κB activation would be maladaptive by preserving the inflammatory response.[61,62] In this context, the selective blockade of NF-κB may provide protection against ischaemia reperfusion damage, attenuating infarct size, reducing inflammation and cell death events, and improving cardiac function.[63–65]

NF-κB is involved in multiple signalling pathways related to Ca^{2+} homeostasis, e.g. calcineurin-NF-AT and IP_3.[66,67] Our results show that selective inhibition of NF-κB signalling with BAY completely

prevented the Ca^{2+} handling effects induced by administration of iE-DAP (*Figures 6* and *7*). Supporting these data, a recent report by Zhang *et al.*[65] has shown that NF-κB loss of function protects against cardiac damage by maintaining Ca^{2+} cycling. In this study, deletion of the NF-κB subunit p65 was associated with augmented SR-Ca^{2+} release and elevated PLB phosphorylation at ser16. These results suggest that NF-κB can modulate the Ca^{2+} SR uptake through PKA activation. Consistent with this, our results also show that NF-κB mediates the iE-DAP-induced effects on Ca^{2+} homeostasis, and blockade of the NF-κB pathway prevents also the PKA phosphorylation effects induced by the NOD1 agonist on PLB and RyR_2.

In conclusion, our results describe a new role for NOD1 outside of the immune setting, highlighting the importance of the pro-inflammatory response and its consequences on cardiac function (*Figure 7D*). Importantly, the effects of NOD1 activation in the heart share many of the features detected in relevant CVDs, such as heart failure. In this context, in addition to apoptotic and fibrotic events, the NOD1 agonist induces cardiac dysfunction by Ca^{2+} cycling impairment; all of which are detected in human and experimental models of heart failure. Notably, CVDs linked to RyR_2 gain of function show excessive channel activity that is associated with cardiac arrhythmias and contractile dysfunction, in addition to pathological cardiac remodelling. Our findings point to NOD1 as an important regulator of both systolic and diastolic Ca^{2+} release, and may provide a basis for the development of novel strategies for therapeutic intervention of Ca^{2+} handling impairment in specific CVD, such as dilated cardiomyopathy or ischaemia/reperfusion injury, where NLR activation has been described.

Supplementary material

Supplementary material is available at *Cardiovascular Research* online.

Acknowledgements

We thank the technical assistance of V. Terrón, M.J. Guillén, D. Navarro, and L. Sánchez. We thank A.M. Gómez and L. Pereira for careful reading of the manuscript and fruitful discussions and L. Saldaña for her assistance in the statistics analysis.

Conflict of interest: none declared.

Funding

M.F.-V. is Miguel Servet researcher of ISCIII. This work was supported by grants CP11/00080 and PI14/01078 from ISCIII, BFU2011-024760 and SAF2010-16377 from MICINN and RIC RD12/0042/0019. RIC is a network funded by the Carlos III Health Institute.

References

1. Hotamisligil GS. Inflammation and metabolic disorders. *Nature* 2006;**444**:860–867.
2. Lee Y, Schulte DJ, Shimada K, Chen S, Crother TR, Chiba N, Fishbein MC, Lehman TJ, Arditi M. Interleukin-1b is crucial for the induction of coronary artery inflammation in a mouse model of Kawasaki disease. *Circulation* 2012;**125**:1542–1550.
3. Wang JG, Williams JC, Davis BK, Jacobson K, Doerschuk CM, Ting JP, Mackman N. Monocytic microparticles activate endothelial cells in an IL-1b-dependent manner. *Blood* 2011; **118**:2366–2374.
4. Shimabukuro M, Hirata Y, Tabata M, Dagvasumberel M, Sato H, Kurobe H, Fukuda D, Soeki T, Kitagawa T, Takanashi S, Sata M. Epicardial adipose tissue volume and adipocytokine imbalance are strongly linked to human coronary atherosclerosis. *Arterioscler Thromb Vasc Biol* 2013;**33**:1077–1084.
5. Van Tassell BW, Toldo S, Mezzaroma E, Abbate A. Targeting interleukin-1 in heart disease. *Circulation* 2013;**128**:1910–1923.
6. Mann DL. The emerging role of innate immunity in the heart and vascular system: for whom the cell tolls. *Circ Res* 2011;**108**:1133–1145.
7. Frantz S, Kobzik L, Kim YD, Fukazawa R, Medzhitov R, Lee RT, Kelly RA. Toll4 (TLR4) expression in cardiac myocytes in normal and failing myocardium. *J Clin Invest* 1999; **104**:271–280.
8. Birks EJ, Felkin LE, Banner NR, Khaghani A, Barton PJ, Yacoub MH. Increased toll-like receptor 4 in the myocardium of patients requiring left ventricular assist devices. *J Heart Lung Transplant* 2004;**23**:228–235.
9. Sakata Y, Dong JW, Vallejo JG, Huang CH, Baker JS, Tracey KJ, Tacheuchi O, Akira S, Mann DL. Toll-like receptor 2 modulates left ventricular function following ischemia-reperfusion injury. *Am J Physiol* 2007;**292**:H503–H509.
10. Chong AJ, Shimamoto A, Hampton CR, Takayama H, Spring DJ, Rothnie CL, Yada M, Pohlman TH, Verrier ED. Toll-like receptor 4 mediates ischemia/reperfusion injury of the heart. *J Thorac Cardiovasc Surg* 2004;**128**:170–179.
11. Arslan F, Smeets MB, O'Neill LA, Keogh B, McGuirk P, Timmers L, Tersteeg C, Hoefer IE, Doevendans PA, Pasterkamp G, de Kleijn DP. Myocardial ischemia/reperfusion injury is mediated by leukocytic toll-like receptor-2 and reduced by systemic administration of a novel anti-toll-like receptor-2 antibody. *Circulation* 2010;**121**:80–90.
12. Sandanger O, Ranheim T, Vinge LE, Bliksoen M, Alfsnes K, Finsen AV, Dahl CP, Askevold ET, Florholmen G, Christensen G, Fitzgerald KA, Lien E, Valen G, Espevik T, Aukrust P, Yndestad A. The NLRP3 inflammasome is up-regulated in cardiac fibroblasts and mediates myocardial ischaemia-reperfusion injury. *Cardiovasc Res* 2013;**99**:164–174.
13. Luo B, Wang F, Li B, Dong Z, Liu X, Zhang C, An F. Association of nucleotide-binding oligomerization domain-like receptor 3 inflammasome and adverse clinical outcomes in patients with idiopathic dilated cardiomyopathy. *Clin Chem Lab Med* 2013;**51**: 1521–1528.
14. Franchi L, Warner N, Viani K, Nunez G. Function of Nod-like receptors in microbial recognition and host defense. *Immunol Rev* 2009;**227**:106–128.
15. Moreno L, Gatheral T. Therapeutic targeting of NOD1 receptors. *Br J Pharmacol* 2013; **170**:475–485.
16. Chamaillard M, Hashimoto M, Horie Y, Masumoto J, Qiu S, Saab L, Ogura Y, Kawasaki A, Fukase K, Kusumoto S, Valvano MA, Foster SJ, Mak TW, Nunez G, Inohara N. An essential role for NOD1 in host recognition of bacterial peptidoglycan containing diaminopimelic acid. *Nat Immunol* 2003;**4**:702–707.
17. Buchholz KR, Stephens RS. The cytosolic pattern recognition receptor NOD1 induces inflammatory interleukin-8 during Chlamydia trachomatis infection. *Infect Immun* 2008; **76**:3150–3155.
18. Jakopin Z, Gobec M, Kodela J, Hazdovac T, Mlinaric-Rascan I, Sollner Dolenc M. Synthesis of conformationally constrained g-D-glutamyl-meso-diaminopimelic acid derivatives as ligands of nucleotide-binding oligomerization domain protein 1 (Nod1). *Eur J Med Chem* 2013;**69**:232–243.
19. Schertzer JD, Tamrakar AK, Magalhaes JG, Pereira S, Bilan PJ, Fullerton MD, Liu Z, Steinberg GR, Giacca A, Philpott DJ, Klip A. NOD1 activators link innate immunity to insulin resistance. *Diabetes* 2011;**60**:2206–2215.
20. Inohara N, Nunez G. The NOD: a signaling module that regulates apoptosis and host defense against pathogens. *Oncogene* 2001;**20**:6473–6481.
21. Allison CC, Ferrand J, McLeod L, Hassan M, Kaparakis-Liaskos M, Grubman A, Bhathal PS, Dev A, Sievert W, Jenkins BJ, Ferrero RL. Nucleotide oligomerization domain 1 enhances IFN-g signaling in gastric epithelial cells during Helicobacter pylori infection and exacerbates disease severity. *J Immunol* 2013;**190**:3706–3715.
22. Moreno L, McMaster SK, Gatheral T, Bailey LK, Harrington LS, Cartwright N, Armstrong PC, Warner TD, Paul-Clark M, Mitchell JA. Nucleotide oligomerization domain 1 is a dominant pathway for NOS2 induction in vascular smooth muscle cells: comparison with Toll-like receptor 4 responses in macrophages. *Br J Pharmacol* 2010; **160**:1997–2007.
23. Gatheral T, Reed DM, Moreno L, Gough PJ, Votta BJ, Sehon CA, Rickard DJ, Bertin J, Lim E, Nicholson AG, Mitchell JA. A key role for the endothelium in NOD1 mediated vascular inflammation: comparison to TLR4 responses. *PLoS ONE* 2012;**7**:e42386.
24. Fernandez-Velasco M, Prieto P, Terron V, Benito G, Flores JM, Delgado C, Zaragoza C, Lavin B, Gomez-Parrizas M, Lopez-Collazo E, Martin-Sanz P, Bosca L. NOD1 activation induces cardiac dysfunction and modulates cardiac fibrosis and cardiomyocyte apoptosis. *PLoS ONE* 2012;**7**:e45260.
25. Fabiato A, Fabiato F. Calcium-induced release of calcium from the sarcoplasmic reticulum of skinned cells from adult human, dog, cat, rabbit, rat, and frog hearts and from fetal and new-born rat ventricles. *Ann NY Acad Sci* 1978;**307**:491–522.
26. Bers DM. Calcium and cardiac rhythms: physiological and pathophysiological. *Circ Res* 2002;**90**:14–17.
27. Cheng H, Lederer WJ, Cannell MB. Calcium sparks: elementary events underlying excitation-contraction coupling in heart muscle. *Science* 1993;**262**:740–744.
28. Fernandez-Velasco M, Rueda A, Rizzi N, Benitah JP, Colombi B, Napolitano C, Priori SG, Richard S, Gomez AM. Increased Ca^{2+} sensitivity of the ryanodine receptor mutant RyR2R4496C underlies catecholaminergic polymorphic ventricular tachycardia. *Circ Res* 2009;**104**:201–209, 212p following 209.
29. Terentyev D, Nori A, Santoro M, Viatchenko-Karpinski S, Kubalova Z, Gyorke I, Terentyeva R, Vedamoorthyrao S, Blom NA, Valle G, Napolitano C, Williams SC, Volpe P, Priori SG, Gyorke S. Abnormal interactions of calsequestrin with the ryanodine receptor calcium release channel complex linked to exercise-induced sudden cardiac death. *Circ Res* 2006;**98**:1151–1158.

30. Belevych A, Kubalova Z, Terentyev D, Hamlin RL, Carnes CA, Gyorke S. Enhanced ryanodine receptor-mediated calcium leak determines reduced sarcoplasmic reticulum calcium content in chronic canine heart failure. *Biophys J* 2007;**93**:4083–4092.
31. Kubalova Z, Terentyev D, Viatchenko-Karpinski S, Nishijima Y, Gyorke I, Terentyeva R, da Cunha DN, Sridhar A, Feldman DS, Hamlin RL, Carnes CA, Gyorke S. Abnormal intrastore calcium signaling in chronic heart failure. *Proc Natl Acad Sci USA* 2005;**102**:14104–14109.
32. Ruiz-Hurtado G, Gomez-Hurtado N, Fernandez-Velasco M, Calderon E, Smani T, Ordonez A, Cachofeiro V, Bosca L, Diez J, Gomez AM, Delgado C. Cardiotrophin-1 induces sarcoplasmic reticulum Ca^{2+} leak and arrhythmogenesis in adult rat ventricular myocytes. *Cardiovasc Res* 2012;**96**:81–89.
33. Masumoto J, Yang K, Varambally S, Hasegawa M, Tomlins SA, Qiu S, Fujimoto Y, Kawasaki A, Foster SJ, Horie Y, Mak TW, Nunez G, Chinnaiyan AM, Fukase K, Inohara N. Nod1 acts as an intracellular receptor to stimulate chemokine production and neutrophil recruitment in vivo. *J Exp Med* 2006;**203**:203–213.
34. Travassos LH, Carneiro LA, Girardin S, Philpott DJ. Nod proteins link bacterial sensing and autophagy. *Autophagy* 2010;**6**:409–411.
35. Park JH, Kim YG, Shaw M, Kanneganti TD, Fujimoto Y, Fukase K, Inohara N, Nunez G. Nod1/RICK and TLR signaling regulate chemokine and antimicrobial innate immune responses in mesothelial cells. *J Immunol* 2007;**179**:514–521.
36. Shioya T. A simple technique for isolating healthy heart cells from mouse models. *J Physiological Sci* 2007;**57**:327–335.
37. Keller SA, Hernandez-Hopkins D, Vider J, Ponomarev V, Hyjek E, Schattner EJ, Cesarman E. NF-kB is essential for the progression of KSHV- and EBV-infected lymphomas in vivo. *Blood* 2006;**107**:3295–3302.
38. Kamthong PJ, Wu M. Inhibitor of nuclear factor-kB induction by cAMP antagonizes interleukin-1-induced human macrophage-colony-stimulating-factor expression. *Biochem J* 2001;**356**:525–530.
39. Tsolmongyn B, Koide N, Odkhuu E, Haque A, Naiki Y, Komatsu T, Yoshida T, Yokochi T. Lipopolysaccharide prevents valproic acid-induced apoptosis via activation of nuclear factor-kB and inhibition of p53 activation. *Cell Immunol* 2013;**282**:100–105.
40. Gomez AM, Valdivia HH, Cheng H, Lederer MR, Santana LF, Cannell MB, McCune SA, Altschuld RA, Lederer WJ. Defective excitation-contraction coupling in experimental cardiac hypertrophy and heart failure. *Science* 1997;**276**:800–806.
41. Bode EF, Briston SJ, Overend CL, O'Neill SC, Trafford AW, Eisner DA. Changes of SERCA activity have only modest effects on sarcoplasmic reticulum $Ca2^{+}$ content in rat ventricular myocytes. *J Physiol* 2011;**589**:4723–4729.
42. Ai X, Curran JW, Shannon TR, Bers DM, Pogwizd SM. Ca^{2+}/calmodulin-dependent protein kinase modulates cardiac ryanodine receptor phosphorylation and sarcoplasmic reticulum Ca^{2+} leak in heart failure. *Circ Res* 2005;**97**:1314–1322.
43. Zwaka TP, Manolov D, Ozdemir C, Marx N, Kaya Z, Kochs M, Hoher M, Hombach V, Torzewski J. Complement and dilated cardiomyopathy: a role of sublytic terminal complement complex-induced tumor necrosis factor-a synthesis in cardiac myocytes. *Am J Pathol* 2002;**161**:449–457.
44. Dong JW, Vallejo JG, Tzeng HP, Thomas JA, Mann DL. Innate immunity mediates myocardial preconditioning through Toll-like receptor 2 and TIRAP-dependent signaling pathways. *Am J Physiol* 2010;**298**:H1079–H1087.
45. Holloway JW, Yang IA, Ye S. Variation in the toll-like receptor 4 gene and susceptibility to myocardial infarction. *Pharmacogenetic Genomic* 2005;**15**:15–21.
46. Oyama J, Blais C Jr, Liu X, Pu M, Kobzik L, Kelly RA, Bourcier T. Reduced myocardial ischemia-reperfusion injury in toll-like receptor 4-deficient mice. *Circulation* 2004;**109**:784–789.
47. Shishido T, Nozaki N, Yamaguchi S, Shibata Y, Nitobe J, Miyamoto T, Takahashi H, Arimoto T, Maeda K, Yamakawa M, Takeuchi O, Akira S, Takeishi Y, Kubota I. Toll-like receptor-2 modulates ventricular remodeling after myocardial infarction. *Circulation* 2003;**108**:2905–2910.
48. Kim SC, Ghanem A, Stapel H, Tiemann K, Knuefermann P, Hoeft A, Meyer R, Grohe C, Knowlton AA, Baumgarten G. Toll-like receptor 4 deficiency: smaller infarcts, but no gain in function. *BMC Physiol* 2007;**7**:5.
49. Michelsen KS, Wong MH, Shah PK, Zhang W, Yano J, Doherty TM, Akira S, Rajavashisth TB, Arditi M. Lack of Toll-like receptor 4 or myeloid differentiation factor 88 reduces atherosclerosis and alters plaque phenotype in mice deficient in apolipoprotein E. *Proc Natl Acad Sci USA* 2004;**101**:10679–10684.
50. Nishio H, Kanno S, Onoyama S, Ikeda K, Tanaka T, Kusuhara K, Fujimoto Y, Fukase K, Sueishi K, Hara T. Nod1 ligands induce site-specific vascular inflammation. *Arterioscler Thromb Vasc Biol* 2011;**31**:1093–1099.
51. Hasenfuss G, Pieske B. Calcium cycling in congestive heart failure. *J Mol Cell Cardiol* 2002;**34**:951–969.
52. Frank KF, Bolck B, Brixius K, Kranias EG, Schwinger RH. Modulation of SERCA: implications for the failing human heart. *Basic Res Cardiol* 2002;**97**(Suppl. 1):I72–I78.
53. Lee SH, Chen YC, Chen YJ, Chang SL, Tai CT, Wongcharoen W, Yeh HI, Lin CI, Chen SA. Tumor necrosis factor-a alters calcium handling and increases arrhythmogenesis of pulmonary vein cardiomyocytes. *Life Sci* 2007;**80**:1806–1815.
54. Patel D, Duke K, Light RB, Jacobs H, Mink SN, Bose D. Impaired sarcoplasmic calcium release inhibits myocardial contraction in experimental sepsis. *J Crit Care* 2000;**15**:64–72.
55. Yasuda S, Lew WY. Angiotensin II exacerbates lipopolysaccharide-induced contractile depression in rabbit cardiac myocytes. *Am J Physiol* 1999;**276**:H1442–H1449.
56. Zhu X, Bagchi A, Zhao H, Kirschning CJ, Hajjar RJ, Chao W, Hellman J, Schmidt U. Toll-like receptor 2 activation by bacterial peptidoglycan-associated lipoprotein activates cardiomyocyte inflammation and contractile dysfunction. *Crit Care Med* 2007;**35**:886–892.
57. Cao CM, Xia Q, Bruce IC, Shen YL, Ye ZG, Lin GH, Chen JZ, Li GR. Influence of interleukin-2 on Ca^{2+} handling in rat ventricular myocytes. *J Mol Cell Cardiol* 2003;**35**:1491–1503.
58. Ruiz-Hurtado G, Dominguez-Rodriguez A, Pereira L, Fernandez-Velasco M, Cassan C, Lezoualc'h F, Benitah JP, Gomez AM. Sustained Epac activation induces calmodulin dependent positive inotropic effect in adult cardiomyocytes. *J Mol Cell Cardiol* 2012;**53**:617–625.
59. Maier LS, Zhang T, Chen L, DeSantiago J, Brown JH, Bers DM. Transgenic CaMKIIdeltaC overexpression uniquely alters cardiac myocyte Ca^{2+} handling: reduced SR Ca^{2+} load and activated SR Ca^{2+} release. *Circ Res* 2003;**92**:904–911.
60. Pereira L, Metrich M, Fernandez-Velasco M, Lucas A, Leroy J, Perrier R, Morel E, Fischmeister R, Richard S, Benitah JP, Lezoualc'h F, Gomez AM. The cAMP binding protein Epac modulates Ca2+ sparks by a Ca^{2+}/calmodulin kinase signalling pathway in rat cardiac myocytes. *J Physiol* 2007;**583**:685–694.
61. Ling H, Gray CB, Zambon AC, Grimm M, Gu Y, Dalton N, Purcell NH, Peterson K, Brown JH. Ca^{2+}/Calmodulin-dependent protein kinase II delta mediates myocardial ischemia/reperfusion injury through nuclear factor-kB. *Circ Res* 2013;**112**:935–944.
62. Frantz S, Hu K, Bayer B, Gerondakis S, Strotmann J, Adamek A, Ertl G, Bauersachs J. Absence of NF-kB subunit p50 improves heart failure after myocardial infarction. *FASEB J* 2006;**20**:1918–1920.
63. Brown M, McGuinness M, Wright T, Ren X, Wang Y, Boivin GP, Hahn H, Feldman AM, Jones WK. Cardiac-specific blockade of NF-kB in cardiac pathophysiology: differences between acute and chronic stimuli in vivo. *Am J Physiol* 2005;**289**:H466–H476.
64. Onai Y, Suzuki J, Kakuta T, Maejima Y, Haraguchi G, Fukasawa H, Muto S, Itai A, Isobe M. Inhibition of IkB phosphorylation in cardiomyocytes attenuates myocardial ischemia/reperfusion injury. *Cardiovasc Res* 2004;**63**:51–59.
65. Zhang XQ, Tang R, Li L, Szucsik A, Javan H, Saegusa N, Spitzer KW, Selzman CH. Cardiomyocyte-specific p65 NF-kB deletion protects the injured heart by preservation of calcium handling. *Am J Physiol* 2013;**305**:H1089–H1097.
66. Heineke J, Molkentin JD. Regulation of cardiac hypertrophy by intracellular signalling pathways. *Nat Rev Mol Cell Biol* 2006;**7**:589–600.
67. Tiangco DA, Lattanzio FA Jr, Osgood CJ, Beebe SJ, Kerry JA, Hargrave BY. 3,4-Methylenedioxymethamphetamine activates nuclear factor-kB, increases intracellular calcium, and modulates gene transcription in rat heart cells. *Cardiovasc Toxicol* 2005;**5**:301–310.

Clinical Science (2014) **127**, 665–677 (Printed in Great Britain) doi: 10.1042/CS20140180

Original Paper

NOD1 receptor is up-regulated in diabetic human and murine myocardium

Patricia PRIETO*, María Teresa VALLEJO-CREMADES†[1], Gemma BENITO†[1], Pilar GONZÁLEZ-PERAMATO‡, Daniel FRANCÉS*, Noelia AGRA*, Verónica TERRÓN*, Silvia GÓNZALEZ-RAMOS*, Carmen DELGADO§, Mariano RUIZ-GAYO¶, Ivette PACHECO**, Juan P. VELASCO-MARTÍN††, Javier REGADERA††, Paloma MARTÍN-SANZ*, Eduardo LÓPEZ-COLLAZO†, Lisardo BOSCÁ* and María FERNÁNDEZ-VELASCO†

*Instituto de Investigaciones Biomédicas Alberto Sols, Centro Mixto CSIC-UAM, Madrid, Spain
†Instituto de Investigación Hospital Universitario La Paz (IDIPAZ), Madrid, Spain
‡Departamento de Anatomía Patológica, Hospital Universitario La Paz, Universidad Autonoma de Madrid, Madrid, Spain
§Centro de Investigaciones Biológicas. Facultad de Medicina, Universidad Complutense de Madrid, Madrid, Spain
¶Universidad CEU San Pablo, Madrid, Spain
**Hospital Militar de Managua, Managua, Nicaragua
††Departamento de Anatomía, Histología y Neurociencia, Facultad de Medicina, Universidad Autónoma de Madrid, Madrid, Spain

Abstract

Type 2 diabetes has a complex pathology that involves a chronic inflammatory state. Emerging evidence suggests a link between the innate immune system receptor NOD1 (nucleotide-binding and oligomerization domain 1) and the pathogenesis of diabetes, in monocytes and hepatic and adipose tissues. The aim of the present study was to assess the role of NOD1 in the progression of diabetic cardiomyopathy. We have measured NOD1 protein in cardiac tissue from Type 2 diabetic (*db*) mice. Heart and isolated cardiomyocytes from *db* mice revealed a significant increase in NOD1, together with an up-regulation of nuclear factor κB (NF-κB) and increased apoptosis. Heart tissue also exhibited an enhanced expression of pro-inflammatory cytokines. Selective NOD1 activation with C_{12}-γ-D-glutamyl-*m*-diaminopimelic acid (iEDAP) resulted in an increased NF-κB activation and apoptosis, demonstrating the involvement of NOD1 both in wild-type and *db* mice. Moreover, HL-1 cardiomyocytes exposed to elevated concentrations of glucose plus palmitate displayed an enhanced NF-κB activity and apoptotic profile, which was prevented by silencing of NOD1 expression. To address this issue in human pathology, NOD1 expression was evaluated in myocardium obtained from patients with Type 2 diabetes (T2DMH) and from normoglycaemic individuals without cardiovascular histories (NH). We have found that NOD1 was expressed in both NH and T2DMH; however, NOD1 expression was significantly pronounced in T2DMH. Furthermore, both the pro-inflammatory cytokine tumour necrosis factor α (TNF-α) and the apoptosis mediator caspase-3 were up-regulated in T2DMH samples. Taken together, our results define an active role for NOD1 in the heightened inflammatory environment associated with both experimental and human diabetic cardiac disease.

Key words: apoptosis, cardiomyocyte, human myocardium, inflammation, nucleotide-binding and oligomerization domain 1 (NOD1), Type 2 diabetes

INTRODUCTION

Diabetes mellitus is the world's fastest growing disease with high rates of morbidity and mortality. A significant number of diabetic patients develop cardiomyopathy, mainly by presenting left ventricular dysfunction independent of coronary artery disease or hypertension. Diabetes is characterized by deregulated lipid metabolism, insulin resistance, mitochondrial dysfunction and disturbances in adipokine secretion and signalling [1]. Myocyte loss and development of fibrosis contribute to the cardiac dysfunction observed in diabetic patients [1,2]. In addition, diabetes is associated with a chronic inflammatory state characterized by increased release of pro-inflammatory mediators [3–5]. In this context, activation of the innate immune system not only mediates the host response against pathogens, but can also contribute to insulin resistance and diabetes progression [6–9]. Accordingly,

Abbreviations: CARD, caspase recruitment domain; COX2, cyclo-oxygenase 2; *db* mouse, Type 2 diabetic mouse; H&E, haemotoxylin and eosin; HFD, high-fat diet; IκB, inhibitor of nuclear factor κB; IKK, inhibitor of nuclear factor κB kinase; iEDAP, γ-D-glutamyl-*m*-diaminopimelic acid; IL, interleukin; NF-κB, nuclear factor κB; NH, normoglycaemic individual(s) without a cardiovascular history; NLR, nucleotide-binding and oligomerization domain-like receptor; NOD1, nucleotide-binding and oligomerization domain 1; NOS2, NO synthase 2; RIP2, receptor-interacting protein 2; T2DMH, patient(s) with Type 2 diabetes; TLR, Toll-like receptor; TNF-α, tumour necrosis factor α; TUNEL, terminal deoxynucleotidyltransferase-mediated dUTP nick-end labelling; wt mouse, wild-type mouse; X-IAP, X-linked inhibitor of apoptosis.

[1]**These authors contributed equally to the study.**

Correspondence: Dr María Fernández-Velasco (email mvelasco@iib.uam.es or maria.fernandez@idipaz.es) or Professor Lisardo Boscá (email lbosca@iib.uam.es).

an increase of innate immune mediators such as Toll-like receptors (TLRs) has been detected in monocytes isolated from Type 2 diabetic patients [10].

In addition to TLRs, the innate response includes a family of cytoplasmic receptors that recognize components of microorganisms or abnormal/damaged host cells: the nucleotide-binding and oligomerization domain-like receptors (NLRs) [11]. Currently, 22 members of the NLR family have been identified in humans [12–14]. Nucleotide and oligomerization domain 1 (NOD1) is an NLR subfamily member that, upon activation, undergoes a conformational modification that allows the recruitment and activation of the protein serine-threonine kinase 2 [receptor-interacting protein 2 (RIP2)], resulting in nuclear factor κB (NF-κB) activation and initiation of inflammatory gene transcription. Dysregulation of NLR function has been described in various diseases, including chronic inflammation, autoimmunity and cancer pre-disposition [14,15]. Activation of NOD1 signalling has been related to the progression of vascular inflammation [16–19] and also to apoptosis [20,21]. Less information is available on the role of NLR signalling in cardiac tissue; however, we have reported previously that NOD1 is expressed in the mouse heart, and NOD1 activation with the selective agonist C_{12}-γ-D-glutamyl-*m*-diaminopimelic acid (referred to subsequently as iEDAP) induces cardiac fibrosis and apoptosis, and also impairs cardiac function [22].

Interestingly, NOD1 has been detected in tissues involved directly in glucose homoeostasis, such as liver, muscle and adipose tissue [23]. Indeed, NOD1 agonists induce insulin resistance both '*in vivo*' and '*in vitro*' through alterations in glucose production and clearance [7,24]. Recently, Shiny et al. [25] demonstrated that monocytes obtained from patients with Type 2 diabetes (T2DMH) have increased mRNA levels of NOD genes. To date, no data are available concerning the role of NOD1 in the inflammatory response in cardiac diseases, including those related to diabetes. Thus, the objective of the present work was to assess the participation of NOD1 in cardiac inflammation linked to diabetes. On this basis, we have determined NLR expression in hearts from *db/db* mice (subsequently referred to as *db*), a rodent model for Type 2 diabetes. Moreover, to gain insight into human pathophysiology of diabetes, we have assessed the presence of NOD1 in cardiac tissue from T2DMH and in myocardium of normoglycaemic individuals without cardiovascular histories (NHs). Our results indicate that the NOD1 pathway is up-regulated in myocardium in both experimental and human diabetes and is associated with an increased pro-inflammatory and apoptosis profile. Thus, NOD1 activation in the heart establishes a new paradigm for linking NLRs to cardiac inflammation related to Type 2 diabetes.

MATERIALS AND METHODS

Ethics

All experiments on humans and mice were performed with the approval of the Consejo Superior de Investigaciones Científicas (CSIC) and the La Paz Hospital human ethics and animal policy and welfare (Ref. DGG28079-37-A) following recommendations of the Spanish and European guidelines (2010/63/EU).

Animal model

The leptin-receptor-deficient *db* mice were used as a rodent model for obesity and Type 2 diabetes; *db*/+ (subsequently referred to as wt) mice were used as a wild-type group.

Chemicals

iEDAP was from InvivoGen and was used to selectively activate NOD1. Staurosporine was purchased from Calbiochem.

Cell isolation

Ventricular cardiomyocytes were isolated from control (wt) and diabetic (*db*) mice using a standard enzymatic digestion as described previously [26].

HL-1 culture

HL-1 cells were seeded in a fibronectin/gelatin (1 mg/ml and 0.02%) coating matrix. Cells were maintained with Claycomb medium (A.T.C.C.) supplemented with 10% FBS, 2 mmol/l L-glutamine, 0.1 mmol/l noradrenaline and 1% penicillin/streptomycin. Cells were grown at 37 °C in an atmosphere of 5% CO_2. Glucose plus palmitate supplementation was added to 1% of acid-free BSA fraction V in Claycomb medium.

NOD1 siRNA silencing

A specific siRNA (sense: 5′-CCGUCUCACGGUUAUCAGAtt-3′; antisense: 5′-UCUGAUAACCGUGAGACGGct-3′; Ambion) was used to silence the expression of the NOD1 gene; an equivalent scrambled sequence served as a control. HL-1 cells were transfected with 100 nM of siRNA using Lipofectamine™ 2000 (Invitrogen). The degree of NOD1 knockdown was determined by a fluorescein conjugate control of siRNA and by Western blot analysis at 24 h and 48 h after transfection. The transfection efficiency of the siRNAs was 70–80%. Transfection with a scrambled siRNA did not modify the NOD1 levels in vehicle and glucose plus palmitate-treated cells.

Glucose and palmitate supplementation and drug treatment

Palmitate stock solution was prepared in DMSO. Controls cells were treated with vehicle (BSA and DMSO). Glucose, palmitate and actinomycin D were from Sigma.

Preparation of total protein cell extracts

Tissues/cells were homogenized using a handheld blender in lysis buffer [50 mmol/l Tris/HCl (pH 7.0), 320 mmol/l sucrose and 1 mmol/l DTT plus a complete protease and phosphatase inhibitor solution (Sigma)]. The homogenate was centrifuged at 13 000 ***g*** for 10 min at 4 °C, and supernatants were frozen and stored at − 80 °C for Western blot analysis. Protein concentrations were determined by the Bradford assay (Bio-Rad).

Preparation of nuclear and cytosolic protein extracts for p65 analysis

Cardiac tissue was homogenized by 10 s sonication at 4 °C in homogenization cytosolic buffer [10 mmol/l Hepes (pH 8),

10 mmol/l KCl, 1 mmol/l EDTA, 1 mmol/l EGTA and 0.5% Nonidet P40]. Tissue pieces were vortex-mixed and centrifuged at 12 000 ***g*** for 30 min. Supernatant was taken as the cytosolic fraction. The pellet was re-suspended in 50 μl of ice-cold nuclear buffer [20 mmol/l Hepes (pH 8), 0.4 mmol/l NaCl, 1 mmol/l EDTA, 1 mmol/l EGTA and 20% glycerol] and vortex-mixed at 4 °C for 30 min. After centrifugation (12 000 ***g*** at 4 °C for 20 min), the supernatant (nuclear fraction) was collected. All buffers contained a protease and phosphatase inhibitor cocktail (Sigma).

Western blot analysis

Equal amounts of protein (20–80 μg) were separated by SDS/PAGE (10–12% gel). Proteins were size fractionated, transferred on to a Hybond-P membrane (GE Healthcare) and, after blocking with 5% non-fat dry milk, incubated with the corresponding antibodies. The blots were developed by the ECL protocol (GE Healthcare), and different exposure times were performed for each blot with a charge-coupled device camera in a luminescent image analyser (Molecular Imager, Bio-Rad) to ensure the linearity of the band intensities. Values of densitometry were determined using Quantity One software (Bio-Rad). Antibodies against NOD1, phospho-RIP2, RIP2, phospho-IKK (inhibitor of nuclear factor κB kinase), IKK, phospho-IκBα (inhibitor of nuclear factor κB α), IκBα, NOS2 (NO synthase 2), COX2 (cyclo-oxygenase 2), p65, caspase-3, BAX and X-IAP (X-linked inhibitor of apoptosis) were purchased from the Santa Cruz Biotechnology or the Cell Signaling Technology. An anti-[human NOD1 (hNOD1)] antibody was purchased from R&D Systems.

RNA isolation and reverse transcription–PCR

RNA was extracted from cells using TRI Reagent® solution (Ambion) and 1 μg was reverse-transcribed into cDNA using the Transcriptor first strand cDNA synthesis kit (Roche). Then, real-time PCR was performed with this template cDNA adding FastStart Universal SYBR Green Master (Roche) and the specific primers in a MyIQ thermocycler (Bio-Rad). Each sample was run in duplicate and was normalized to 18S RNA. The replicates were then averaged and fold induction was determined by $\Delta\Delta C_t$-based fold-change calculations. Primers sequence were the following tumour necrosis factor α (TNF-α) forward: 5′-CATCTTCTCAAAATTCGAGTGACAA-3′; reverse: 5′-TGGGAGTAGACAAGGTACAACCC-3′; IL (interleukin)-1β forward: 5′-GAAGCTGTGGCAGCTACCTG-3′; reverse: 5′-GAAAAGAAGGTGCTCATGTCC-3′; IL-6 forward: 5′-CTGCAAGAGACTTCCATCCAGTT-3′; reverse: 5′-GAAGTAGGGAAGGCCGTGG-3′; 18S forward: 5′-GCAATTATTCCCCATGAACGA-3′; reverse: 5′-AAAGGGAGGGACTTAATCAA-3′.

Cell death and viability detection

For detection and quantification of apoptosis, the terminal deoxynucleotidyltransferase-mediated dUTP nick-end labelling (TUNEL) commercial kit for cell death detection (Roche) was used. The cell survival assay relies on the capacity of cells to reduce MTT (Calbiochem) to a coloured formazan in metabolically active cells. Cardiomyocytes from both wt and *db* mice suspended in storage solution were incubated for 2 h with 0.5 mg/ml MTT in the dark at 37 °C, and then 100 μl of 50% dimethylformamide in 20% SDS (pH 4.7) was added. Absorbance was measured at 595 nm. All assays were performed in triplicate.

Table 1 Comparison of the biochemical data from human subjects

HbA_{1c}, glycated haemoglobin; HDL, high-density lipoprotein; LDL, low-density lipoprotein; ns, not significant.

Parameter	NH ($n=5$)	T2DMH ($n=6$)	*P* value
Age (years)	41.4 ± 7.8	72 ± 2.3	$P<0.01$
Weight (kg)	71.2 ± 3.3	81.9 ± 16.9	ns
Glucose (mg/dl)	84.5 ± 3.2	164.6 ± 20.5	$P<0.01$
HDL-cholesterol (mg/dl)	54.5 ± 2.0	30.2 ± 3.8	$P<0.01$
LDL-cholesterol (mg/dl)	111.7 ± 1.2	163.2 ± 45.5	ns
LDL/HDL-cholesterol ratio	2.7 ± 0.4	4.1 ± 0.6	$P<0.05$
HbA_{1c} (%)	4.4 ± 0.1	6.9 ± 0.7	$P<0.05$

Human specimens

Myocardial samples from six T2DMH and five NH were obtained during autopsy procedure at the La Paz Hospital. Human cardiac samples were taken during the forensic autopsy (post-mortem time <48 h). Post-mortem time was defined as the estimated time from death to autopsy. Cardiac tissues were processed rapidly to avoid possible deleterious changes at the cellular level. Full informed written consent was obtained from the family of all donors. Biochemical data of all subjects are included in Table 1. Gross and histopathological study of hearts from NH and T2DMH did not show any acute myocardial lesions. For histopathological procedures, tissues were processed by fixing in 4% buffered formalin and embedded in paraffin wax. The diabetic complications registered in the autopsy history included a patient who suffered an ictus and other individual who had acute kidney failure.

Immunohistochemistry

Serial 5-μm-thick transverse sections of left ventricular cardiac tissue were mounted on glass slides and allowed to dry. Sections were stained with haemotoxylin and eosin (H&E) or deparaffinized, unmasked and peroxidase-blocked by incubating in 0.1% H_2O_2 diluted in methanol, blocked in 1% BSA and 5% NGS (normal goat serum) in TBS for 2 h and then exposed to anti-NOD1 (1:100 dilution; R&D Systems), -TNF-α (1:400 dilution; Abcam) or -caspase-3 (1:100 dilution; Cell Signaling) antibody overnight at 4 °C. Antibodies were labelled with a biotinylated streptavidin-biotin method and visualized with diaminobenzidine. Slides were then counter-stained with haematoxylin before being dehydrated, cleared and mounted. Photographs were taken with a microscope (Olympus CX40).

Statistics

Data are presented as means ± S.E.M. Statistical significance was assessed using a Student's *t* test or ANOVA, followed by the

Bonferroni's test when appropriate. Differences with values of $P < 0.05$ were considered statistically significant.

RESULTS

Expression of NOD1 in the myocardium of diabetic mice

As previous evidence suggests that NOD1 can participate in diabetes [7,27–29], we have evaluated the expression of NOD1 in the myocardium of a transgenic *db* mouse model. *db* mice manifest several indicators common to patients with Type 2 diabetes, including obesity, hyperglycaemia, hyperinsulinaemia and depressed cardiac function [30–33]. Accordingly, *db* mice were significantly heavier than their wt counterparts and had increased blood concentrations of glucose and insulin (Supplementary Figure S1 at http://www.clinsci.org/cs/127/cs1270665add.htm). NOD1 protein expression, detected by Western blot analysis, was found in cardiac tissue from both *db* mice and corresponding wt mice; however, expression was significantly greater in *db* mice (Figure 1A, $P < 0.01$ compared with wt mice). Together with elevated NOD1 levels, cardiac tissue from *db* mice also exhibited an increase in the phosphorylation of the NOD1 adapter RIP2 that leads to NF-κB activation [34], demonstrated by increased levels of phospho-IKK/IKK and phospho-IκBα/IκBα (Figure 1A) and nuclear enrichment of p65 (Figure 1A, right panel). Interestingly, hearts from *db* mice also contained elevated levels of NOS2 and COX2, consistent with NF-κB activation (Figure 1B). These changes were also accompanied by significant increases in the levels of the pro-inflammatory cytokines TNF-α, IL-6 and IL-1β in hearts from *db* mice relative to wt mice (Figure 1B).

To validate these results in a second diabetes model, we have determined NOD1 expression in cardiac tissue from mice subjected to a high-fat diet (HFD) to provoke obesity. Predictably, mice fed on the HFD for 12 weeks were significantly heavier than chow-fed littermates and had significantly greater levels of serum glucose and insulin (Supplementary Figure S2 at http://www.clinsci.org/cs/127/cs1270665add.htm). Notably, HFD-fed mice also demonstrated increased expression of NOD1 in heart tissue compared with chow-fed littermates (Supplementary Figure S2). Thus, in two independent models of hyperglycaemia, NOD1 protein is elevated in cardiac tissue.

Given that cardiac apoptosis participates in the pathogenesis of diabetes [2], and a direct relationship between NOD1 activation and apoptosis induction has been previously established [20,21], we next questioned whether NOD1 activation was responsible for cardiomyocyte apoptosis. Thus, TUNEL assays were performed on cardiac tissue, and we have measured activated caspase-3, X-IAP and BAX protein in *db* and wt mice. In contrast with tissue from wt mice, ventricular tissue from *db* mice contained higher levels of the pro-apoptotic proteins caspase-3 and BAX and lower levels of the anti-apoptotic mediator X-IAP (Figure 1C). A similar result was obtained by TUNEL staining (Figure 1D), showing a greater degree of DNA fragmentation in cardiac tissue from *db* mice (7.7 ± 4.1 % of TUNEL-positive cells in *db* mice compared with 0.9 ± 1.0 % in wt mice).

Cardiomyocytes isolated from hearts of *db* mice exhibit NOD1 activation and increased apoptosis

To assess whether the pathological changes observed in the hearts of *db* mice were related to changes at the level of the cardiomyocyte, we have isolated cardiomyocytes from hearts of *db* and wt mice and analysed the expression of NOD1. Immunostaining of cardiomyocytes from wt and *db* mice revealed intense NOD1 reactivity in cardiomyocytes from *db* mice and reduced staining in cells from wt mice (Figure 2A). Similarly, Western blot analysis demonstrated a 3-fold increase in NOD1 expression in cardiomyocytes from *db* mice relative to controls (Figure 2B). In addition, NF-κB activation and expression of the COX2 target gene was also significantly greater in cardiomyocytes isolated from hearts of *db* mice (Figure 2B). Furthermore, cardiomyocytes isolated from hearts of *db* mice were more apoptotic, measured as the number of TUNEL-positive cells (Figure 2C), and their viability was reduced, as determined by an MTT assay (Figure 2D). Consequently, cardiomyocytes from *db* mice had greater levels of the pro-apoptotic proteins caspase-3 and BAX, together with reduced levels of the anti-apoptotic protein X-IAP (Figure 2E). Finally, to assess whether cardiomyocytes from *db* mice were more sensitive to cell death/apoptosis, we have treated cardiomyocytes from both *db* and wt mice with the alkaloid staurosporine to induce apoptosis. Interestingly, staurosporine-induced apoptosis was maximal in cells isolated from hearts of *db* mice, and they also exhibited the greatest loss in cell viability (Supplementary Figure S3 at http://www.clinsci.org/cs/127/cs1270665add.htm).

Selective stimulation of NOD1 induces activation of NF-κB and apoptosis

Given the results described above, we next investigated whether specific activation of NOD1 would lead to a similar inflammatory profile and activation of apoptosis in mice. To do this, we have taken advantage of the selective NOD1 agonist iEDAP [35,36]. wt and *db* mice were treated daily with an intraperitoneal injection of iEDAP (5 μg/g of body weight), or vehicle, over a 2-week period, and hearts were examined for activation of NOD1. Western blot analysis of heart tissue demonstrated that, compared with control mice, wt mice injected with iEDAP exhibited a statistically significant increase in both phospho-IKK/IKK and phospho-IκBα/IκBα expression and the NF-κB target genes NOS2 and COX2 (Supplementary Figure S4A at http://www.clinsci.org/cs/127/cs1270665add.htm) to levels comparable with those found in *db* mice. In addition, iEDAP treatment of *db* mice further increased the expression of these inflammatory markers (Supplementary Figure S4A). As anticipated, analysis of TUNEL-positive nuclei in treated and non-treated mice revealed that NOD1 activation by iEDAP increased the number of apoptotic cells in heart tissue compared with vehicle-treated animals (Supplementary Figure S4B). This was accentuated in iEDAP-treated *db* mice. Finally, analysis of pro-apoptotic protein expression mirrored the TUNEL analysis (Supplementary Figure S4C) and showed that iEDAP treatment up-regulates caspase-3 and BAX, while reducing X-IAP. Collectively, these results reinforce our findings in *db* mice and indicate that NOD1 stimulation is associated with increased apoptosis and inflammatory gene activation.

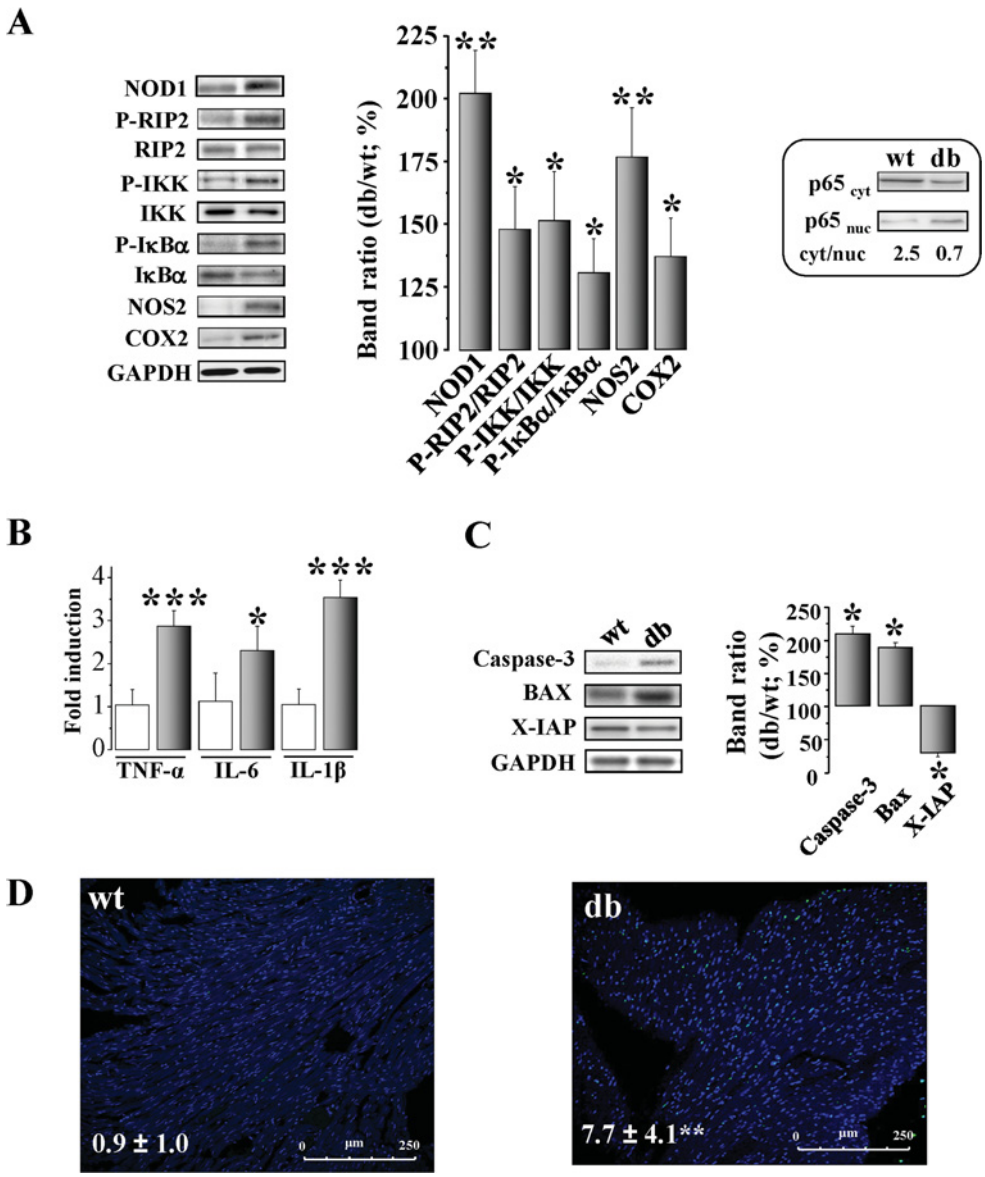

Figure 1 **Cardiac expression of NOD1, NF-κB and apoptotic pathways are enhanced in *db* mice**

(**A**) Left panel shows representative immunoblots of NOD1, phospho-RIP2, RIP2, phospho-IKK, IKK, phospho-IκBα, NOS2 and COX2 in hearts from wt and *db* mice. Glyceraldehyde-3-phosphate dehydrogenase (GAPDH) was used for normalization. Central panel shows histograms representing the mean ± S.E.M. values, expressed as a percentage compared with wt mice (100 %); $n = 4$–6 animals. Right panel shows a representative example of p65 distribution in cytosolic and nuclear fractions in the wt and *db* groups. (**B**) Fold induction of cardiac expression of TNF-α, IL-6 and IL-1β in hearts from *db* mice (shaded) relative to wt mice (white). (**C**) Left panel shows representative immunoblots of activated caspase-3, BAX and X-IAP obtained from heart tissue of wt and *db* mice and the corresponding densitometry (right panel, $n = 4$). GAPDH was used for normalization of loading. (**D**) Representative images of TUNEL (green) and DAPI (blue) staining in cardiac tissue sections of *db* and wt mice (×40, 5 μm/slide). Mean ± S.E.M. values of TUNEL-positive cells have been added to the images. Light transmission of TUNEL preparations point to cardiomyocytes as the main apoptotic phenotype involved. Data are expressed as means ± S.E.M. compared with wt mice (100 %). $^{*}P < 0.05$, $^{**}P < 0.01$ and $^{***}P < 0.001$ compared with wt mice.

High concentrations of palmitate and glucose induce the up-regulation of NOD1 and apoptotic signalling in HL-1 cells

In an attempt to mimic the diabetes-like pathological micro-environment found *in vivo*, we have used the HL-1 cardiomyocyte cell line, exposed these cells to high concentrations of glucose plus palmitate (lipid-induced insulin resistance model) for 48 h and assessed changes to the NOD1 signalling pathway. As expected, exposure of HL-1 cells to glucose plus palmitate resulted in lipid accumulation together with

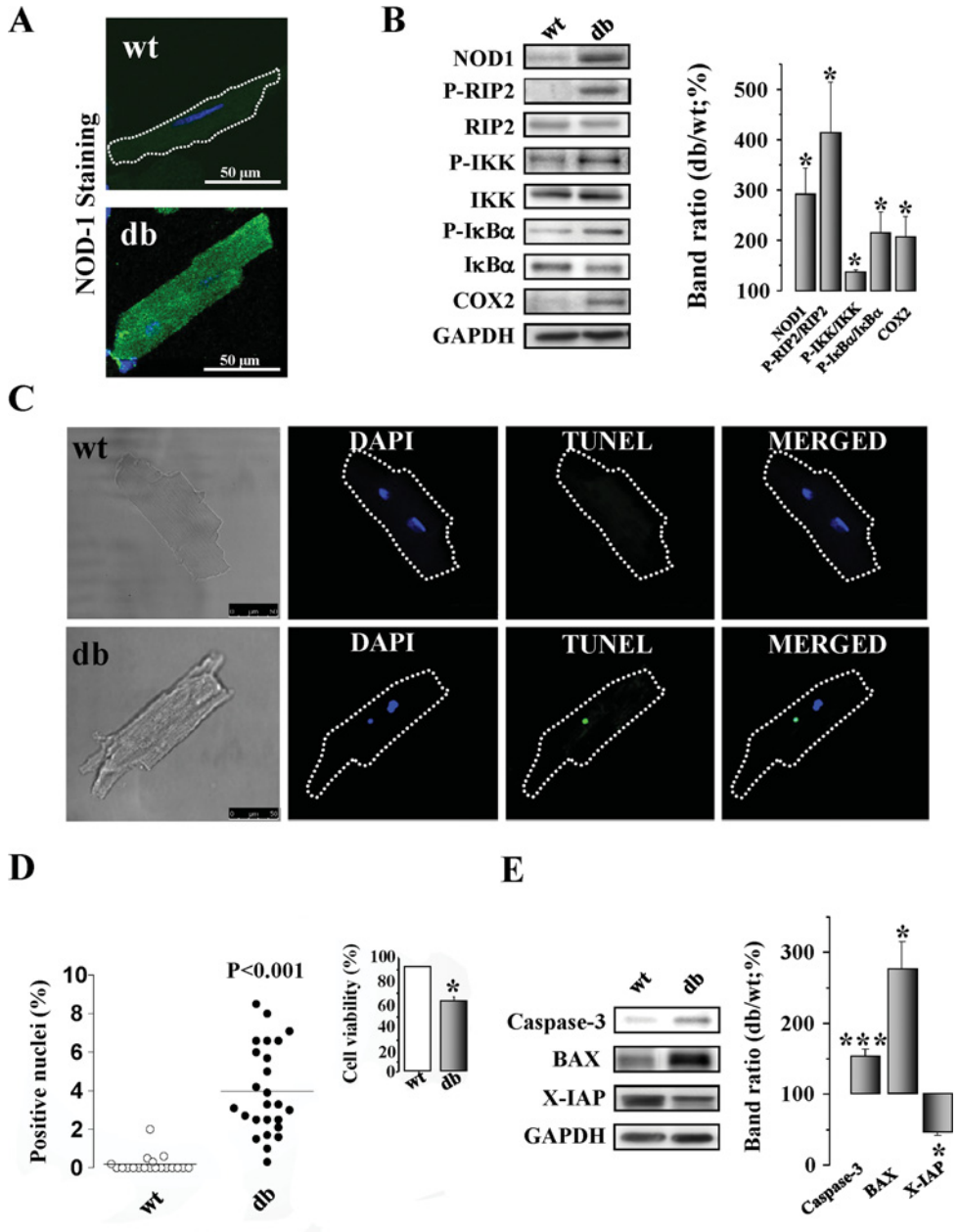

Figure 2 Cardiomyocytes isolated from *db* mice overexpress NOD1 and exhibit sustained activation of NF-κB and apoptosis pathways

(**A**) Confocal microscopy images of a representative cardiomyocyte isolated from the heart of a wt and *db* mouse stained for NOD1. (**B**) Immunoblot analysis of NOD1 signalling. Left panel shows representative blots of NOD1, phospho-RIP2/RIP2, phospho-IKK/IKK, phospho-IκBα/IκBα and COX2 from isolated cardiomyocytes of wt and *db* mice. Right panel shows the means ± S.E.M. ($n = 4$ cell preparations) expressed as a percentage compared with wt mice (100 %). (**C**) Representative TUNEL assay of cardiomyocytes from wt and *db* mice (green staining is TUNEL positive nuclei; blue corresponds to DAPI nuclei staining). Means ± S.E.M. are represented in (**D**); right panel shows cell viability measured by MTT ($n = 4$–6 assays per condition). (**E**) Representative immunoblots of activated caspase-3, BAX and X-IAP in isolated cardiomyocytes from hearts of wt and *db* mice. Means ± S.E.M. are expressed as a percentage of wt mice (100 %).$^{*}P < 0.05$ and $^{***}P < 0.001$ compared with wt mice ($n = 4$ cell preparations).

impairment of insulin signalling (Supplementary Figure S5 at http://www.clinsci.org/cs/127/cs1270665add.htm). In addition, HL-1 cells treated with glucose and palmitate showed increased expression of NOD1, as measured by immunofluorescence (Figure 3A) and Western blot analysis (Figure 3B). Moreover, RIP2 phosphorylation and NOS2 induction were increased similarly upon treatment (Figure 3B). Notably, siRNA silencing of NOD1 decreased the activation of downstream targets, including RIP2 and NOS2, in HL-1 cells exposed to glucose and palmitate (Figure 3B). Importantly, exposure of HL-1 cardiomyocytes

separately to glucose or palmitate failed to induce changes in NOD1 expression (results not shown). The addition of glucose plus palmitate to HL-1 cells also promoted the activation of pro-apoptotic pathways, increasing activated caspase-3 and decreasing the anti-apoptotic protein X-IAP (Figure 3C). Significantly, activation of apoptosis was prevented in cardiomyocytes silenced for NOD1 expression (Figure 3C). Importantly, NOD1 silencing did not affect pro-inflammatory and pro-apoptotic pathways under basal conditions (results not shown). To determine whether high glucose/fatty acid treatment up-regulated NOD1 at the transcriptional level, we have treated HL-1 cells as before together with a selective inhibitor of transcription (actinomycin D). Results revealed that the addition of actinomycin D prevented NOD1 up-regulation induced by the high glucose/fatty acids administration (Figure 3D), demonstrating that the increase in NOD1 expression occurs at the level of transcription.

NOD1 is overexpressed in the myocardium of diabetic patients

Having demonstrated the activation of NOD1 in diabetic murine myocardium, we next sought to identify whether a similar situation occurred in human pathology. To this end, we have measured NOD1 protein expression in myocardium samples of left ventricle from T2DMH and NH. Table 1 gives the human biochemical data from the patients. Representative immunohistochemistry images of NOD1 expression in a sample from an NH and T2DMH are shown in Figure 4. Transversal sections were stained with H&E to distinguish the underlying histology (Figures 4a and 4b). NOD1 expression was marked significantly in both transversal (Figures 4c and 4d) and longitudinal (Figures 4e and 4f) sections of T2DMH compared with NH. Importantly, no background staining was observed when using only the secondary antibody (Supplementary Figure S6 at http://www.clinsci.org/cs/127/cs1270665add.htm). In addition, immunofluorescence analysis showed that NOD1 protein expression in T2DMH was increased significantly (1.9 ± 0.1 arbitrary units in T2DMH compared with 1.1 ± 0.1 arbitrary units in NH; $P < 0.01$; Supplementary Figure S7 at http://www.clinsci.org/cs/127/cs1270665add.htm). Consistent with our *in vitro* experiments, immunohistochemical analysis suggested NOD1 overexpression in the cardiomyocyte population, defined as easily identifiable rod-shaped cells in longitudinal sections (Figures 4e and 4f, and Supplementary Figure S7). Furthermore, sections of hearts from T2DMH showed increased staining for the pro-inflammatory cytokine TNF-α (Figure 5A) together with a higher percentage of cells stained positively for caspase-3, compared with sections of hearts from NH ($1.7 \pm 0.2‰$ of caspase-3-positive cells in T2DMH compared with $0.0 \pm 0.0‰$ found in NH; $P < 0.01$, Figure 5B).

DISCUSSION

In the present report, we have demonstrated that the myocardium from mouse models of diabetes and human myocardium of patients with Type 2 diabetes overexpress the receptor of the innate immune system NOD1. This up-regulation occurred in cardiomyocytes and was associated with an increased apoptotic profile.

During their lifetime, humans are confronted frequently with pathogens. To resolve an infectious process, the innate immune system uses a complex signalling network to modulate the delicate balance between stimulation and inhibition of host immune responses. Imbalances in the innate immunity system promote chronic inflammatory and autoimmune processes that can potentially participate in the onset of several pathologies including diabetes [7,37]. In this context, it has been proposed that some mediators of the innate immune response might contribute to ongoing obesity-associated insulin resistance, indicating a connection between innate immunity and metabolic regulation. Both TLRs and NLRs, the most prominent mediators of the innate immune system, participate in coronary heart disease, myocardial infarction and diabetes [5,8,38–40]. NOD1, a member of the NLR family, has been associated with the induction of chronic inflammatory disorders, such as atopic eczema and asthma [41,42]. These examples underscore the importance of this receptor in the regulation of the immune response [43,44], including NF-κB activation, cytokine production and induction of apoptosis [45,46]. At the vascular level, NOD proteins can mediate several inflammatory responses [16,17]. However, despite the marked progress in understanding the role of NLR/NOD signalling in host defence, their contribution to inflammatory cardiac disorders remains poorly characterized [47].

Recent studies point to a direct relationship between NOD proteins and diabetes. In this respect, some studies have reported that NOD proteins participate in insulin resistance and inflammatory responses in hepatocytes from diabetic mice [7]. Cross-talk between diabetes-related inflammation and NOD1 activity appears to be a relevant physiopathological condition in some target tissues, such as the heart. In addition, other pro-inflammatory mediators have been considered as a bridge between metabolism and the immune system. This is the case with TLRs, which are additional pattern-recognition receptors implicated in insulin resistance. Accordingly, TLR4 has been proposed as an immune receptor that can alter metabolism [9] and can recognize not only exogenous but also endogenous ligands, for example modified low-density lipoprotein (LDL) [38], an established cardiovascular risk factor for Type 2 diabetes linked to obesity.

In the present report, we have demonstrated that cardiac tissue from mice with Type 2 diabetes expresses higher levels of NOD1, together with increased production of pro-inflammatory cytokines including TNF-α, IL-1β and IL-6. Supporting these findings, other studies have described that NOD1 activation promotes insulin resistance in adipocytes and hepatocytes [7,24,27,28]. Moreover, monocytes isolated from patients with Type 2 diabetes have higher expression of NOD1 compared with normoglycaemic individuals [25]. Furthermore, Schertzer et al. [7] have demonstrated in a model of Type 2 diabetes induced by an HFD that the absence of NOD protects against lipid accumulation and insulin resistance. Collectively, these observations support the involvement of NOD1 in metabolic disorders.

Regarding the mechanism responsible for activation of NOD1 in the heart of *db* mice, a plausible explanation might be that NOD1 is activated by fatty acids. This notion is supported by

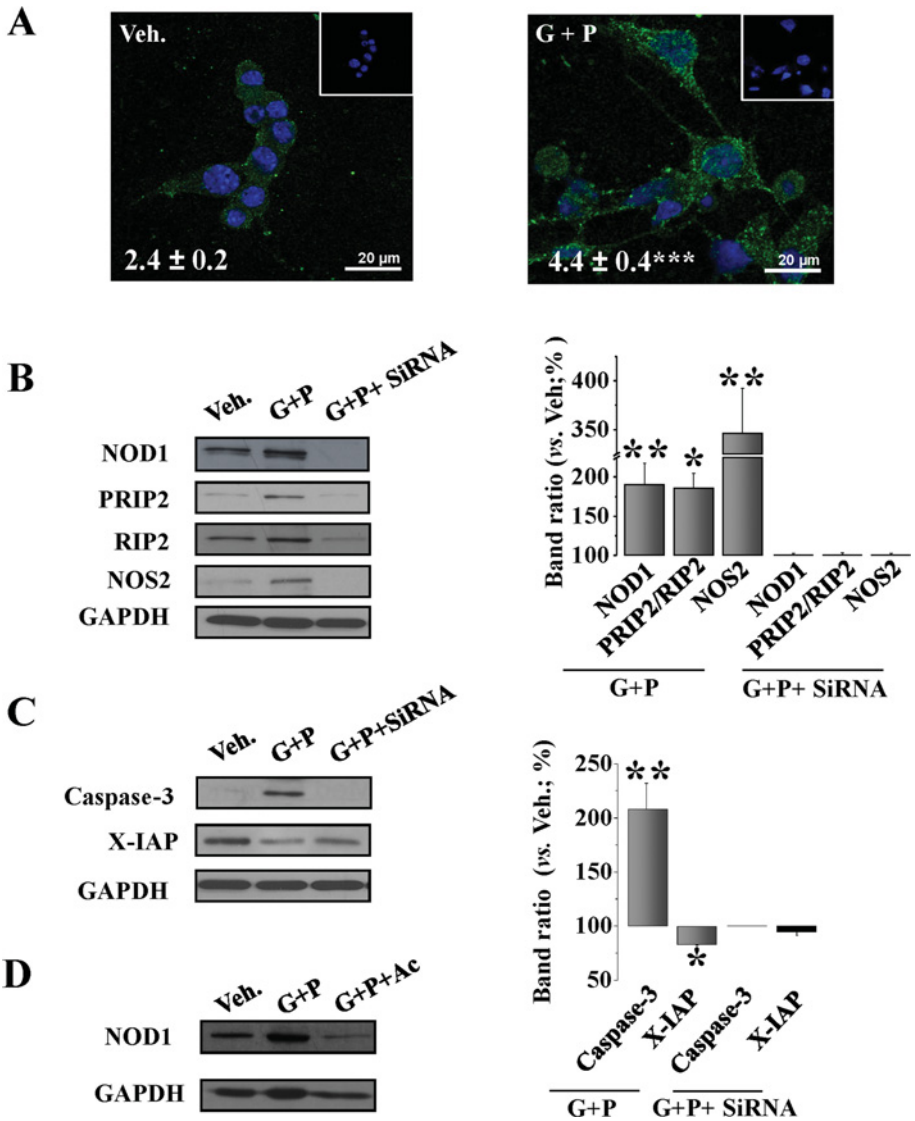

Figure 3 HL-1 cardiomyocytes incubated with high doses of glucose and palmitate promote NOD1 pathway activation and apoptosis induction

(**A**) Representative immunostaining of NOD1 obtained in HL-1 cardiomyocytes incubated 48 h with vehicle (Veh.) or with 50 mmol/l glucose plus 200 μmol/l palmitate (G + P); a negative control of each example is shown in the inset. Mean fluorescence values ± S.E.M. in arbitrary units are inserted in the images. (**B**) Representative blots of NOD1, phospho-RIP2/RIP2 and NOS2 obtained in HL-1 cells treated with Veh., G + P or G + P + siRNA of NOD1 (G + P + siRNA). (**C**) Left panel shows representative blot of activated caspase-3 and X-IAP obtained in Veh., G + P and G + P + siRNA-treated cells. (**D**) Representative blot of three different experiments representing NOD1 expression in HL-1 cells treated with Veh., G + P or G + P + 0.1 μg/ml actinomycin D (G + P + Ac). Means ± S.E.M. ($n = 3$–5) are expressed as a percentage compared with wt mice (100 %). $^{*}P < 0.05$, $^{**}P < 0.01$ and $^{***}P < 0.001$ compared with Veh.

our findings in cardiomyocytes treated with high concentrations of glucose and palmitate. This environment leads to transcriptional up-regulation of NOD1, together with activation of downstream signalling. Importantly, this activation was abrogated by siRNA silencing of NOD1 (Figure 3). Indeed, Zhao et al. [48] showed that increased lipid metabolites, associated with Type 2 diabetes, can be detected by NOD proteins, and, more recently, Cuda et al. [28] described that the Glu266Lys polymorphism in the *NOD1* gene affects the relationship between nutritional saturated fatty acid intake and insulin sensitivity.

Up-regulation of NOD1 oligomerization through its nucleotide-binding domain results in activation of different pathways, of which the best characterized is NF-κB [23]. Our data show that NF-κB is activated in cardiac tissue of *db* mice (Figure 1). The sustained up-regulation of the NOD1/NF-κB axis observed in the hearts of *db* mice correlates with NLR

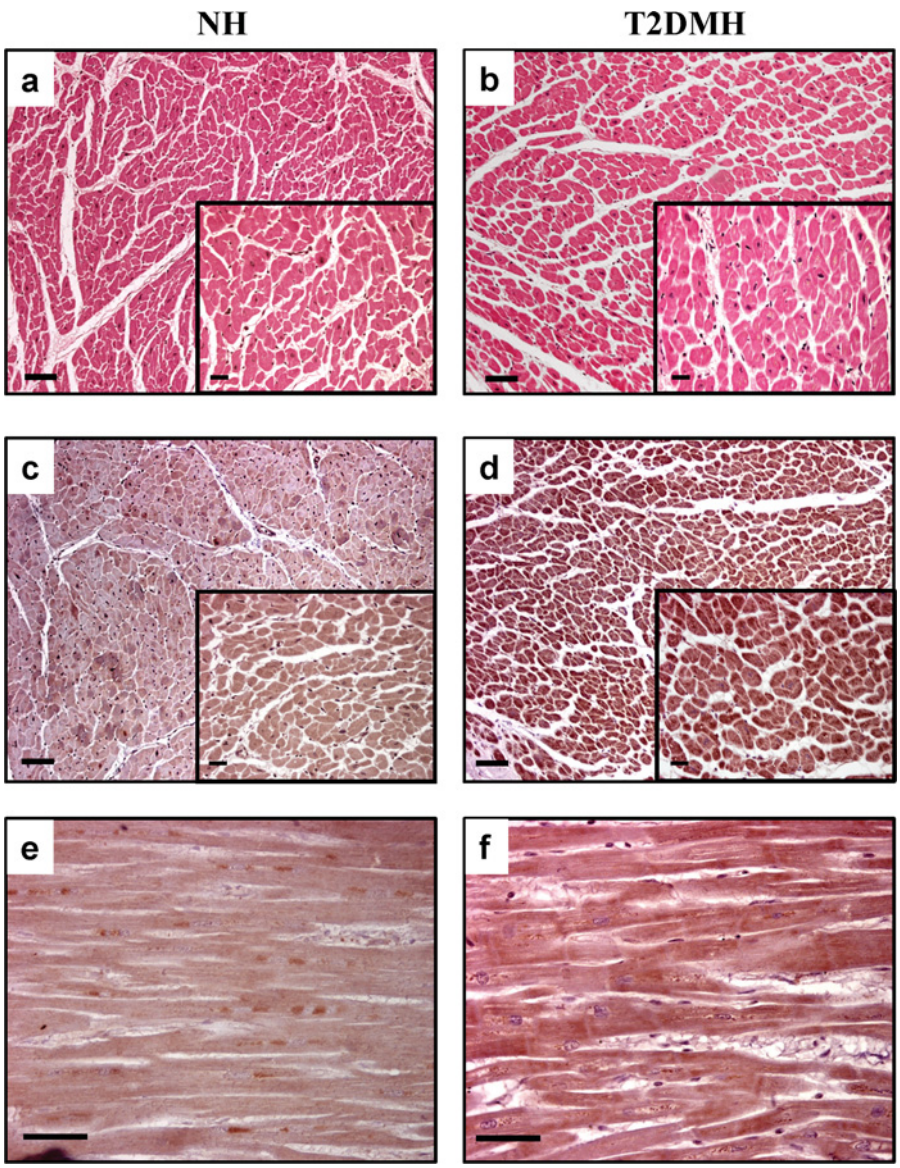

Figure 4 **NOD1 is up-regulated in cardiac tissue from Type 2 diabetic patients**
Representative H&E-stained slides of hearts from NH (**a**) and T2DMH (**b**) (×10). (**c**–**e**) Immunohistochemistry staining demonstrating that NOD1 is overexpressed in both transversal (**c**, **d**, ×10; insert ×40) as well as longitudinal (**e**, **f**, ×40) myocardial sections of hearts from T2DMH relative to NH. Bar = 100 μm.

activation in isolated cells. Thus, our results provide evidence of functional activation of the classical NF-κB pathway, including phosphorylation of IKK, and the expression of target genes such as COX2 and NOS2. NF-κB activation induced by NOD1 is the result of an interaction between the caspase recruitment domain (CARD) of NOD1 and the equivalent CARD of RIP2 [23], a kinase that specifically amplifies downstream signalling from NOD proteins but not from other TLRs [49–51]. The precise function of this kinase is not fully elucidated, but studies with genetic mouse models suggest that RIP2 activity is required for an appropriate innate immune response promoted via NOD receptors [52]. We have demonstrated that RIP2 is activated in both the hearts and cardiomyocytes of *db* mice, corroborating the pathway activation of this NLR in the cardiac milieu in our models.

Apoptotic events have been implicated in the diabetic process [53], although the precise mechanism(s) remain unknown. NLR proteins harbour functions beyond those engaged with the innate immune response, including the regulation of cell death [23,54]. Our previous work established that NOD1 activation induces apoptosis in the heart and in isolated cardiomyocytes [22]. In the present study, we have shown that both cardiac tissue and isolated cardiomyocytes from *db* mice display a prominent pro-apoptotic profile, exhibiting a greater degree of DNA fragmentation compared with wt mice. Furthermore, pro-apoptotic mediators, such as activated caspase-3 and BAX, were increased, whereas cell

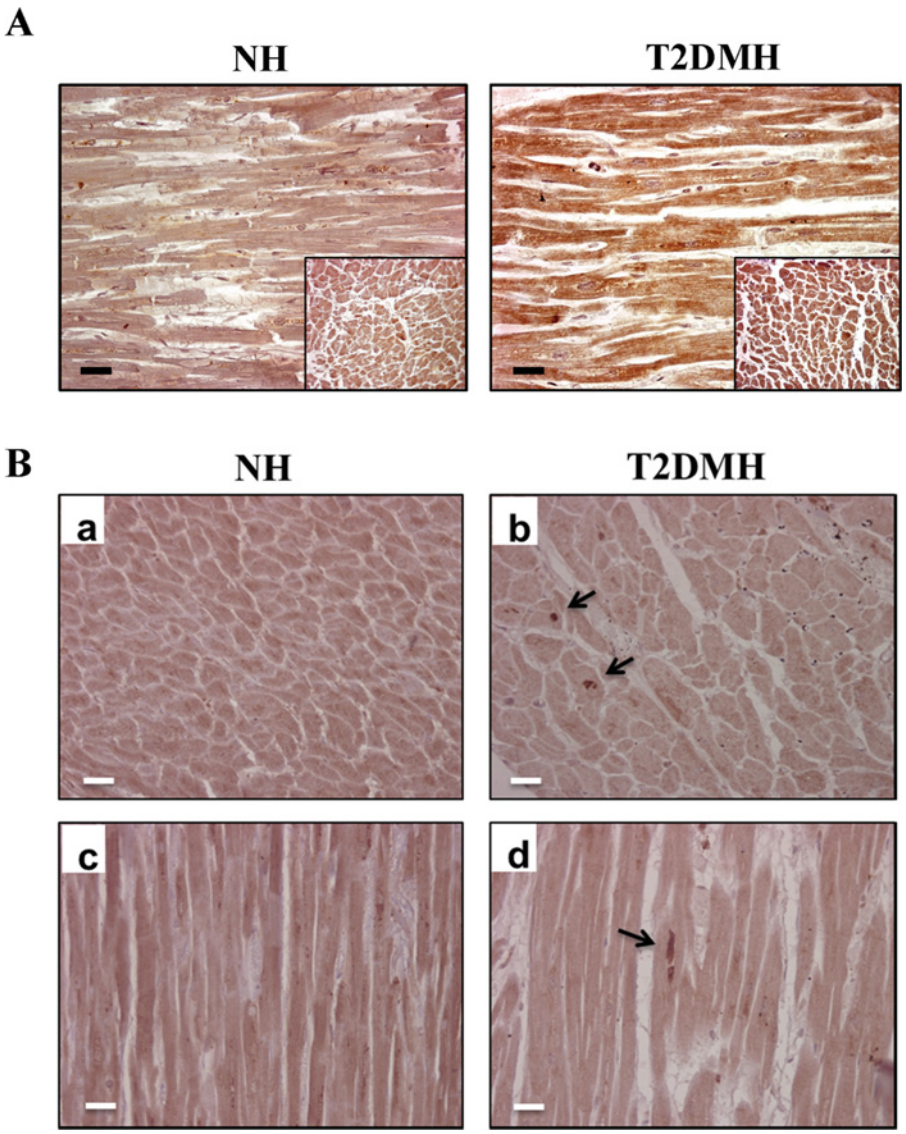

Figure 5 **TNF-α and caspase-3 are up-regulated in myocardium of Type 2 diabetic individuals**
(**A**) Myocardial longitudinal sections of hearts from NH and T2DMH were stained with an antibody to TNF-α ($\times$40); images from transversal sections are inserted in each photomicrograph. (**B**) Myocardial sections from NH and T2DMH were stained with an antibody to caspase-3 ($\times$40). Caspase-3 staining in both transversal (**b**) and longitudinal (**d**) sections of T2DMH shows a high expression of this mediator compared with NH (**a**, **c**).

viability and the anti-apoptotic protein X-IAP were reduced in cardiac tissue and cardiomyocytes from *db* mice. These results were validated in the HL-1 cardiomyocyte cell line. HL-1 cells treated with high concentrations of glucose plus palmitate displayed a pro-apoptotic profile, which was lost upon NOD1 silencing. This relationship between NOD1 activation and caspase-dependent apoptosis is well established by several groups, including ours [20,21,23]. Indeed, the CARD of NLR proteins can interact with the homologous CARD of caspases, triggering an induction of apoptosis. Reinforcing these results, treatment of *db* mice with a selective agonist of NOD1 induces both NF-κB and apoptosis pathways (Supplementary Figure S4), demonstrating the sensitivity of the *db* model to apoptosis induction by specific NOD1 stimulation.

In an attempt to connect our murine data to human pathology, we have analysed NOD1 protein in cardiac tissue from T2DMH and NH. Immunohistochemistry and immunofluorescence demonstrated that T2DMH samples exhibited greater NOD1 expression than NH; this increase was detected notably in cardiomyocytes. Furthermore, levels of the pro-inflammatory cytokine TNF-α were also enhanced in T2DMH compared with NH. Finally, consistent with our results, in the *db* mice model, the

T2DMH group also showed increased levels of the pro-apoptotic mediator caspase-3. To the best of our knowledge, this is the first demonstration of NLR activity in the human heart. In this context, other mediators of the innate immune system, such as TLR4, are increased in human failing myocardium [55], supporting the idea of cross-talk between innate immune mediators and cardiovascular disease.

During the last decade, the role of the inflammatory response during the onset of diabetes and potential inhibition of inflammatory mediators as alternative or complementary strategies for the management of this disease has received increased attention [56]. Moreover, some evidence supports the idea that chronic inflammation can be a consequence of an inability to shut down the inflammatory response. This is supported by studies demonstrating spontaneous inflammatory events in patients and animals with particular mutated or disrupted genes. Importantly, some of these genes encode proteins which are known to be highly pro-inflammatory, such as the transcription factor NF-κB, emphasizing the complexity of immune regulation. Although further studies will be required to address the specific role of NOD1 in diabetic cardiomyopathy, the present report uncovers a new immune player in the heightened inflammatory response in both human and murine diabetic diseases.

CLINICAL PERSPECTIVES

- NOD1 activity is associated with many pro-inflammatory conditions; however, little is known regarding its contribution to cardiovascular pathologies.
- Our data in animal models and in patients provide strong evidence for an association between Type 2 diabetes and overexpression of NOD1 in cardiac tissue. In addition, we have provided functional evidence, which links the up-regulation of NOD1 to its activation and contribution to chronic low-grade inflammation in the heart.
- Inhibitors of NOD1 are potential therapeutics for diseases with an inflammatory component. The present study identifies relevant targets to assess their potential efficacy in the management of cardiac dysfunction in Type 2 diabetes. Unravelling the therapeutic value of pharmacological inhibitors of NOD1 might provide additional tools for the assessment of cardiac dysfunction associated with up-regulation of NOD1.

AUTHOR CONTRIBUTION

María Vallejo Cremades and Gemma Benito contributed equally to the manuscript. María Fernández-Velasco and Lisardo Boscá conceived and designed the experiments. Patricia Prieto, María Vallejo-Cremades, Gemma Benito, Pilar González-Peramato, Daniel Francés, Javier Regadera, Verónica Terrón, Ivette Pacheco, Noelia Agra and Silvia Gónzalez-Ramos performed the experiments. Patricia Prieto, Javier Regadera, María Vallejo-Cremades and Gemma Benito analysed the data. Mariano Ruiz-Gayo, Carmen Delgado, Juan Velasco-Martín, Paloma Martín-Sanz and Eduardo López-Collazo contributed reagents, materials and analysis tools. María Fernández-Velasco and Lisardo Boscá wrote the paper.

ACKNOWLEDGEMENTS

We thank Dr AM Gómez and Dr L Pereira (INSERM U-637) for sharing samples in the preliminary analysis. We thank the technical assistance of Maria J. Guillén, Diego Navarro, Carmen Sanchez and Lucía Sánchez.

FUNDING

This work was supported by Instituto de Salud Carlos III (ISCIII), [grant numbers CP11/00080], Ministerio de Ciencia e Innovacion (MICINN) [grant numbers BFU2011-024760 and SAF2010-16377] and Fondo de Investigación Sanitaria (FIS)-Red Temática de Investigación Cooperativa en Enfermedades Cardiovasculares (RECAVA) [grant number RD12/0042/0019]. RECAVA and Ciberehd networks are funded by the Carlos III Health Institute.

REFERENCES

1 Haffner, S. M., Lehto, S., Ronnemaa, T., Pyorala, K. and Laakso, M. (1998) Mortality from coronary heart disease in subjects with type 2 diabetes and in nondiabetic subjects with and without prior myocardial infarction. N. Engl. J. Med. **339**, 229–234 CrossRef PubMed

2 Maya, L. and Villarreal, F. J. (2010) Diagnostic approaches for diabetic cardiomyopathy and myocardial fibrosis. J. Mol. Cell Cardiol. **48**, 524–529 CrossRef PubMed

3 Van Gaal, L. F., Mertens, I. L. and De Block, C. E. (2006) Mechanisms linking obesity with cardiovascular disease. Nature **444**, 875–880 CrossRef PubMed

4 Komers, R., Lindsley, J. N., Oyama, T. T., Schutzer, W. E., Reed, J. F., Mader, S. L. and Anderson, S. (2001) Immunohistochemical and functional correlations of renal cyclooxygenase-2 in experimental diabetes. J. Clin. Invest. **107**, 889–898 CrossRef PubMed

5 Vandanmagsar, B., Youm, Y. H., Ravussin, A., Galgani, J. E., Stadler, K., Mynatt, R. L., Ravussin, E., Stephens, J. M. and Dixit, V. D. (2011) The NLRP3 inflammasome instigates obesity-induced inflammation and insulin resistance. Nat. Med. **17**, 179–188 CrossRef PubMed

6 Pickup, J. C., Mattock, M. B., Chusney, G. D. and Burt, D. (1997) NIDDM as a disease of the innate immune system: association of acute-phase reactants and interleukin-6 with metabolic syndrome X. Diabetologia **40**, 1286–1292 CrossRef PubMed

7 Schertzer, J. D., Tamrakar, A. K., Magalhaes, J. G., Pereira, S., Bilan, P. J., Fullerton, M. D., Liu, Z., Steinberg, G. R., Giacca, A., Philpott, D. J. and Klip, A. (2011) NOD1 activators link innate immunity to insulin resistance. Diabetes **60**, 2206–2215 CrossRef PubMed

8 Wong, F. S., Hu, C., Zhang, L., Du, W., Alexopoulou, L., Flavell, R. A. and Wen, L. (2008) The role of Toll-like receptors 3 and 9 in the development of autoimmune diabetes in NOD mice. Ann. N.Y. Acad. Sci. **1150**, 146–148 CrossRef PubMed

9 Shi, H., Kokoeva, M. V., Inouye, K., Tzameli, I., Yin, H. and Flier, J. S. (2006) TLR4 links innate immunity and fatty acid-induced insulin resistance. J. Clin. Invest. **116**, 3015–3025 CrossRef PubMed

10 Dasu, M. R., Devaraj, S., Park, S. and Jialal, I. (2010) Increased Toll-like receptor (TLR) activation and TLR ligands in recently diagnosed type 2 diabetic subjects. Diabetes Care **33**, 861–868 CrossRef PubMed

11 Meylan, E., Tschopp, J. and Karin, M. (2006) Intracellular pattern recognition receptors in the host response. Nature **442**, 39–44 CrossRef PubMed

12 Correa, R. G., Khan, P. M., Askari, N., Zhai, D., Gerlic, M., Brown, B., Magnuson, G., Spreafico, R., Albani, S., Sergienko, E. et al. (2011) Discovery and characterization of 2-aminobenzimidazole derivatives as selective NOD1 inhibitors. Chem. Biol. **18**, 825–832 CrossRef PubMed

13 Harton, J. A., Linhoff, M. W., Zhang, J. and Ting, J. P. (2002) Cutting edge: CATERPILLER: a large family of mammalian genes containing CARD, pyrin, nucleotide-binding, and leucine-rich repeat domains. J. Immunol. **169**, 4088–4093 CrossRef PubMed

14 Carneiro, L. A., Magalhaes, J. G., Tattoli, I., Philpott, D. J. and Travassos, L. H. (2008) Nod-like proteins in inflammation and disease. J. Pathol. **214**, 136–148 CrossRef

15 Davis, B. K., Wen, H. and Ting, J. P. (2011) The inflammasome NLRs in immunity, inflammation, and associated diseases. Ann. Rev. Immunol. **29**, 707–735 CrossRef PubMed

16 Gatheral, T., Reed, D. M., Moreno, L., Gough, P. J., Votta, B. J., Sehon, C. A., Rickard, D. J., Bertin, J., Lim, E., Nicholson, A. G. and Mitchell, J. A. (2012) A key role for the endothelium in NOD1 mediated vascular inflammation: comparison to TLR4 responses. PLoS One **7**, e42386 CrossRef PubMed

17 Moreno, L., McMaster, S. K., Gatheral, T., Bailey, L. K., Harrington, L. S., Cartwright, N., Armstrong, P. C., Warner, T. D., Paul-Clark, M. and Mitchell, J. A. (2010) Nucleotide oligomerization domain 1 is a dominant pathway for NOS2 induction in vascular smooth muscle cells: comparison with Toll-like receptor 4 responses in macrophages. Br. J. Pharmacol. **160**, 1997–2007 CrossRef PubMed

18 Nishio, H., Kanno, S., Onoyama, S., Ikeda, K., Tanaka, T., Kusuhara, K., Fujimoto, Y., Fukase, K., Sueishi, K. and Hara, T. (2011) Nod1 ligands induce site-specific vascular inflammation. Arterioscler. Thromb. Vasc. Biol. **31**, 1093–1099 CrossRef PubMed

19 Moreno, L. and Gatheral, T. (2013) Therapeutic targeting of NOD1 receptors. Br. J. Pharmacol. **170**, 475–485 CrossRef PubMed

20 Ture-Ozdemir, F., Tulunay, A., Elbasi, M. O., Tatli, I., Maurer, A. M., Mumcu, G., Direskeneli, H. and Eksioglu-Demiralp, E. (2013) Pro-inflammatory cytokine and caspase-1 responses to pattern recognition receptor activation of neutrophils and dendritic cells in Behcet's disease. Rheumatology **52**, 800–805 CrossRef PubMed

21 Ver Heul, A. M., Fowler, A., Ramaswamy, S. and Piper, R. C. (2013) Ubiquitin regulates caspase recruitment domain mediated signaling by nucleotide binding oligomerization domain proteins NOD1 and NOD2. J. Biol. Chem. **288**, 6890–902 CrossRef PubMed

22 Fernandez-Velasco, M., Prieto, P., Terron, V., Benito, G., Flores, J. M., Delgado, C., Zaragoza, C., Lavin, B., Gomez-Parrizas, M., Lopez-Collazo, E. et al. (2012) NOD1 activation induces cardiac dysfunction and modulates cardiac fibrosis and cardiomyocyte apoptosis. PLoS One **7**, e45260 CrossRef PubMed

23 Inohara, N., Koseki, T., del Peso, L., Hu, Y., Yee, C., Chen, S., Carrio, R., Merino, J., Liu, D., Ni, J. and Nunez, G. (1999) Nod1, an Apaf-1-like activator of caspase-9 and nuclear factor-kappaB. J. Biol. Chem. **274**, 14560–14567 CrossRef PubMed

24 Zhao, L., Hu, P., Zhou, Y., Purohit, J. and Hwang, D. (2011) NOD1 activation induces proinflammatory gene expression and insulin resistance in 3T3-L1 adipocytes. Am. J. Physiol. Endocrinol. Metab. **301**, E587–E598 CrossRef PubMed

25 Shiny, A., Regin, B., Balachandar, V., Gokulakrishnan, K., Mohan, V., Babu, S. and Balasubramanyam, M. (2013) Convergence of innate immunity and insulin resistance as evidenced by increased nucleotide oligomerization domain (NOD) expression and signaling in monocytes from patients with type 2 diabetes. Cytokine **64**, 564–570 CrossRef PubMed

26 Fernandez-Velasco, M., Rueda, A., Rizzi, N., Benitah, J. P., Colombi, B., Napolitano, C., Priori, S. G., Richard, S. and Gomez, A. M. (2009) Increased Ca^{2+} sensitivity of the ryanodine receptor mutant RyR2R4496C underlies catecholaminergic polymorphic ventricular tachycardia. Circ. Res. **104**, 201–209 CrossRef PubMed

27 Zhou, Y. J., Zhou, H., Li, Y. and Song, Y. L. (2012) NOD1 activation induces innate immune responses and insulin resistance in human adipocytes. Diabetes Metab. **38**, 538–543 CrossRef PubMed

28 Cuda, C., Badawi, A., Karmali, M. and El-Sohemy, A. (2012) Effects of polymorphisms in nucleotide-binding oligomerization domains 1 and 2 on biomarkers of the metabolic syndrome and type II diabetes. Genes Nutr. **7**, 427–435 CrossRef PubMed

29 Amar, J., Chabo, C., Waget, A., Klopp, P., Vachoux, C., Bermudez-Humaran, L. G., Smirnova, N., Berge, M., Sulpice, T., Lahtinen, S. et al. (2011) Intestinal mucosal adherence and translocation of commensal bacteria at the early onset of type 2 diabetes: molecular mechanisms and probiotic treatment. EMBO Mol. Med. **3**, 559–572 CrossRef PubMed

30 Pereira, L., Matthes, J., Schuster, I., Valdivia, H. H., Herzig, S., Richard, S. and Gomez, A. M. (2006) Mechanisms of $[Ca^{2+}]i$ transient decrease in cardiomyopathy of db/db type 2 diabetic mice. Diabetes **55**, 608–615 CrossRef PubMed

31 Neubauer, N. and Kulkarni, R. N. (2006) Molecular approaches to study control of glucose homeostasis. ILAR J. **47**, 199–211 CrossRef PubMed

32 Leiter, E. H. and Reifsnyder, P. C. (2004) Differential levels of diabetogenic stress in two new mouse models of obesity and type 2 diabetes. Diabetes. **53** (Suppl. 1), S4–S11 CrossRef PubMed

33 Loskutoff, D. J., Fujisawa, K. and Samad, F. (2000) The fat mouse. A powerful genetic model to study hemostatic gene expression in obesity/NIDDM. Ann. N.Y. Acad. Sci. **902**, 272–281, discussion 281–272 CrossRef PubMed

34 Inohara, N., Ogura, Y., Chen, F. F., Muto, A. and Nunez, G. (2001) Human Nod1 confers responsiveness to bacterial lipopolysaccharides. J. Biol. Chem. **276**, 2551–2554 CrossRef PubMed

35 Jakopin, Z., Gobec, M., Kodela, J., Hazdovac, T., Mlinaric-Rascan, I. and Sollner Dolenc, M. (2013) Synthesis of conformationally constrained gamma-D-glutamyl-meso-diaminopimelic acid derivatives as ligands of nucleotide-binding oligomerization domain protein 1 (Nod1). Eur. J. Med. Chem. **69**, 232–243 CrossRef PubMed

36 Masumoto, J., Yang, K., Varambally, S., Hasegawa, M., Tomlins, S. A., Qiu, S., Fujimoto, Y., Kawasaki, A., Foster, S. J., Horie, Y. et al. (2006) Nod1 acts as an intracellular receptor to stimulate chemokine production and neutrophil recruitment *in vivo*. J. Exp. Med. **203**, 203–213 CrossRef PubMed

37 Pickup, J. C. and Crook, M. A. (1998) Is type II diabetes mellitus a disease of the innate immune system? Diabetologia **41**, 1241–1248 CrossRef PubMed

38 Xu, X. H., Shah, P. K., Faure, E., Equils, O., Thomas, L., Fishbein, M. C., Luthringer, D., Xu, X. P., Rajavashisth, T. B., Yano, J. et al. (2001) Toll-like receptor-4 is expressed by macrophages in murine and human lipid-rich atherosclerotic plaques and upregulated by oxidized LDL. Circulation **104**, 3103–3108 CrossRef PubMed

39 Edfeldt, K., Swedenborg, J., Hansson, G. K. and Yan, Z. Q. (2002) Expression of Toll-like receptors in human atherosclerotic lesions: a possible pathway for plaque activation. Circulation **105**, 1158–1161 PubMed

40 Duewell, P., Kono, H., Rayner, K. J., Sirois, C. M., Vladimer, G., Bauernfeind, F. G., Abela, G. S., Franchi, L., Nunez, G., Schnurr, M. et al. (2010) NLRP3 inflammasomes are required for atherogenesis and activated by cholesterol crystals. Nature **464**, 1357–1361 CrossRef PubMed

41 Fritz, J. H., Ferrero, R. L., Philpott, D. J. and Girardin, S. E. (2006) Nod-like proteins in immunity, inflammation and disease. Nat. Immunol. **7**, 1250–1257 CrossRef PubMed

42 Kanneganti, T. D., Lamkanfi, M. and Nunez, G. (2007) Intracellular NOD-like receptors in host defense and disease. Immunity **27**, 549–559 CrossRef PubMed

43 Hysi, P., Kabesch, M., Moffatt, M. F., Schedel, M., Carr, D., Zhang, Y., Boardman, B., von Mutius, E., Weiland, S. K., Leupold, W. et al. (2005) NOD1 variation, immunoglobulin E and asthma. Hum. Mol. Genet. **14**, 935–941 CrossRef PubMed

44 Weidinger, S., Klopp, N., Rummler, L., Wagenpfeil, S., Novak, N., Baurecht, H. J., Groer, W., Darsow, U., Heinrich, J., Gauger, A. et al. (2005) Association of NOD1 polymorphisms with atopic eczema and related phenotypes. J. Allergy Clin. Immunol. **116**, 177–184 CrossRef PubMed

45 Girardin, S. E., Tournebize, R., Mavris, M., Page, A. L., Li, X., Stark, G. R., Bertin, J., DiStefano, P. S., Yaniv, M., Sansonetti, P. J. and Philpott, D. J. (2001) CARD4/Nod1 mediates NF-kappaB and JNK activation by invasive *Shigella flexneri*. EMBO Rep. **2**, 736–742 CrossRef PubMed

46 da Silva Correia, J., Miranda, Y., Austin-Brown, N., Hsu, J., Mathison, J., Xiang, R., Zhou, H., Li, Q., Han, J. and Ulevitch, R. J. (2006) Nod1-dependent control of tumor growth. Proc. Natl. Acad. Sci. U.S.A. **103**, 1840–1845 CrossRef PubMed

47 Cartwright, N., Murch, O., McMaster, S. K., Paul-Clark, M. J., van Heel, D. A., Ryffel, B., Quesniaux, V. F., Evans, T. W., Thiemermann, C. and Mitchell, J. A. (2007) Selective NOD1 agonists cause shock and organ injury/dysfunction *in vivo*. Am. J. Respir. Crit. Care Med. **175**, 595–603 CrossRef PubMed

48 Zhao, L., Kwon, M. J., Huang, S., Lee, J. Y., Fukase, K., Inohara, N. and Hwang, D. H. (2007) Differential modulation of Nods signaling pathways by fatty acids in human colonic epithelial HCT116 cells. J. Biol. Chem. **282**, 11618–11628 CrossRef PubMed

49 Hasegawa, M., Fujimoto, Y., Lucas, P. C., Nakano, H., Fukase, K., Nunez, G. and Inohara, N. (2008) A critical role of RICK/RIP2 polyubiquitination in Nod-induced NF-kappaB activation. EMBO J. **27**, 373–383 CrossRef PubMed

50 Magalhaes, J. G., Lee, J., Geddes, K., Rubino, S., Philpott, D. J. and Girardin, S. E. (2011) Essential role of Rip2 in the modulation of innate and adaptive immunity triggered by Nod1 and Nod2 ligands. Eur. J. Immunol. **41**, 1445–1455 CrossRef PubMed

51 Park, J. H., Kim, Y. G., Shaw, M., Kanneganti, T. D., Fujimoto, Y., Fukase, K., Inohara, N. and Nunez, G. (2007) Nod1/RICK and TLR signaling regulate chemokine and antimicrobial innate immune responses in mesothelial cells. J. Immunol. **179**, 514–521 CrossRef PubMed

52 Nembrini, C., Kisielow, J., Shamshiev, A. T., Tortola, L., Coyle, A. J., Kopf, M. and Marsland, B. J. (2009) The kinase activity of Rip2 determines its stability and consequently Nod1- and Nod2-mediated immune responses. J. Biol. Chem. **284**, 19183–19188 CrossRef PubMed

53 Barouch, L. A., Gao, D., Chen, L., Miller, K. L., Xu, W., Phan, A. C., Kittleson, M. M., Minhas, K. M., Berkowitz, D. E., Wei, C. and Hare, J. M. (2006) Cardiac myocyte apoptosis is associated with increased DNA damage and decreased survival in murine models of obesity. Circ. Res. **98**, 119–124 CrossRef PubMed

54 da Silva Correia, J., Miranda, Y., Leonard, N., Hsu, J. and Ulevitch, R. J. (2007) Regulation of Nod1-mediated signaling pathways. Cell Death Differ. **14**, 830–839 CrossRef PubMed

55 Frantz, S., Kobzik, L., Kim, Y. D., Fukazawa, R., Medzhitov, R., Lee, R. T. and Kelly, R. A. (1999) Toll4 (TLR4) expression in cardiac myocytes in normal and failing myocardium. J. Clin. Invest. **104**, 271–280 CrossRef PubMed

56 Larsen, C. M., Faulenbach, M., Vaag, A., Volund, A., Ehses, J. A., Seifert, B., Mandrup-Poulsen, T. and Donath, M. Y. (2007) Interleukin-1-receptor antagonist in type 2 diabetes mellitus. N. Engl. J. Med. **356**, 1517–1526 CrossRef PubMed

Received 27 March 2014/21 May 2014; accepted 17 June 2014

Published as Immediate Publication 17 June 2014, doi: 10.1042/CS20140180

Clinical Science (2014) **127**, 665–677 (Printed in Great Britain) doi: 10.1042/CS20140180

online data

Original Paper

SUPPLEMENTARY ONLINE DATA

NOD1 receptor is up-regulated in diabetic human and murine myocardium

Patricia PRIETO*, María Teresa VALLEJO-CREMADES†[1], Gemma BENITO†[1], Pilar GONZÁLEZ-PERAMATO‡, Daniel FRANCÉS*, Noelia AGRA*, Verónica TERRÓN*, Silvia GÓNZALEZ-RAMOS*, Carmen DELGADO§, Mariano RUIZ-GAYO¶, Ivette PACHECO**, Juan P. VELASCO-MARTÍN††, Javier REGADERA††, Paloma MARTÍN-SANZ*, Eduardo LÓPEZ-COLLAZO†, Lisardo BOSCÁ* and María FERNÁNDEZ-VELASCO†

*Instituto de Investigaciones Biomédicas Alberto Sols, Centro Mixto CSIC-UAM, Madrid, Spain
†Instituto de Investigación Hospital Universitario La Paz (IDIPAZ), Madrid, Spain
‡Departamento de Anatomía Patológica, Hospital Universitario La Paz, Universidad Autonoma de Madrid, Madrid, Spain
§Centro de Investigaciones Biológicas. Facultad de Medicina, Universidad Complutense de Madrid, Madrid, Spain
¶Universidad CEU San Pablo, Madrid, Spain
**Hospital Militar de Managua, Managua, Nicaragua
††Departamento de Anatomía, Histología y Neurociencia, Facultad de Medicina, Universidad Autónoma de Madrid, Madrid Spain

MATERIALS AND METHODS

HFD feeding

For the high-fat diet (HFD) exeriments, 4-week-old C57BL/6J male mice (wt) weighing 16–18 g were housed under a 12/12-h light–dark cycle in a temperature-controlled room (22 °C), with standard food and water available *ad libitum*. Mice were divided into two groups of similar average body weight, housed four per cage and assigned to either a control regular chow diet or a 42% HFD (TD. 88137, Harlan Laboratories). Body weight and food intake were monitored once per week. After 12 weeks of treatment, mice were killed, and heart tissues were snap-frozen in liquid nitrogen and stored at − 80 °C.

Glucose and insulin determination

Plasma glucose was measured in a Reflotron plus (Roche). Insulin was quantified with the Rat/Mouse Insulin 96-Well Plate Assay Kit.

Immunofluorescence staining

HL-1 cells were seeded on to sterile eight-well Chamber Slides (Falcon) and fixed with 2% paraformaldehyde for 10 min. Cells were permeabilized in ice-cold methanol and incubated with 3% BSA for 30 min. After incubation with a rabbit antibody against glucose transporter 4 (GLUT-4) (1:500 dilution; Abcam) at 4 °C overnight, cells were washed with PBS followed by incubation with Alexa Fluor® 488-conjugated goat anti-rabbit secondary antibody (1:500 dilution; Molecular Probes) for 1 h at room temperature. Coverslips were mounted in Prolong Gold antifade reagent (Molecular Probes) and examined using a Leica TCS SP5 spectral confocal microscope. Alexa Fluor® fluorescence was excited using the 488 nm line of an argon laser and emission collected through a band-pass filter (505–530 nm). DAPI fluorescence was excited using a mercury lamp (band-pass 365/12) and emissions collected through a band-pass filter (480–520 nm). Fluorescence intensity measurements were performed using ImageJ software (NIH).

Immunohistochemistry of human samples

Samples were deparaffinized and then blocked by incubation for 60 min at room temperature with TBS, at pH 7.6, containing 10% goat serum and 1.5% BSA. Sections were then incubated overnight at 4 °C with an anti-NOD1 antibody followed by three 5-min washes with TBS. Bound primary antibody was detected by incubation for 45 min with biotinylated horse anti-goat secondary antibody (1:50 dilution; Vector Laboratories), followed by three 5-min washes with TBS and then incubation for 30 min with streptavidin conjugated to Alexa Fluor® 488 (1:1000 dilution; Molecular Probes). Slides were washed again three times in TBS, rinsed once briefly in water and mounted under a coverslip with VectaShield mounting medium with DAPI (Vector Laboratories). Samples were visualized by epifluorescence microscopy. Epifluorescence microscopy was performed on a Leica AF6000 by using a ×20 dry objective lens. Emission/excitation filters for DAPI and Alexa Fluor® 488 were used. A sample with no primary antibody was always included to control for background generated by the secondary antibody.

Quantification of lipid incorporation by HL-1 cells

Accumulation of lipid by HL-1 cells was determined using the lipophilic Nile Red fluorescent dye. Cells were incubated for 48 h with 50 mmol/l glucose and 200 μmol/l palmitic acid. HL-1 cells were trypsinized and centrifuged for 5 min at 200 ***g*** at 4 °C. Cell pellets were re-suspended and fixed with 2% paraformaldehyde at 4 °C. For flow cytometry, cells were sedimented as described above, re-suspended in PBS with a final Nile Red concentration of 0.4 μg/ml (30 min). Fluorescence emission was

[1]**These authors contributed equally to the study.**

Correspondence: Dr María Fernández-Velasco (email mvelasco@iib.uam.es or maria.fernandez@idipaz.es) or Professor Lisardo Boscá (email lbosca@iib.uam.es).

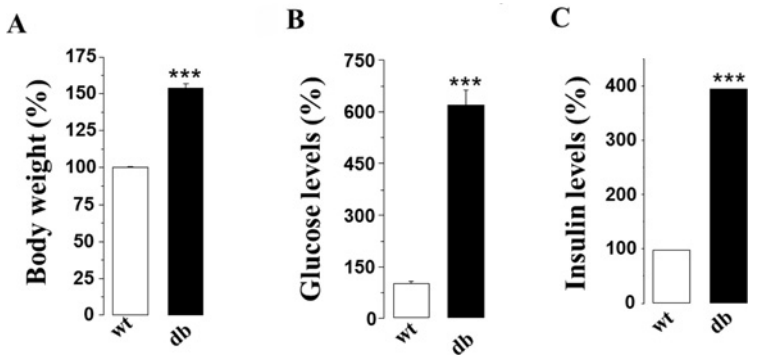

Figure S1 **Body weight and plasma levels of glucose and insulin in *db* mice**
Body weight (**A**), glucose (**B**) and insulin (**C**) plasma levels obtained in *db* mice. Data are expressed as means ± S.E.M. of the percentage of the corresponding wt mice (100%). ***$P < 0.001$ compared with their corresponding wt mice.

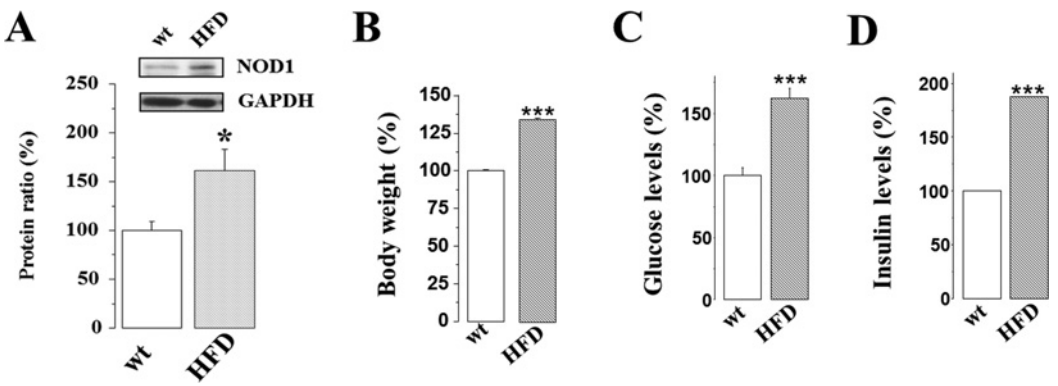

Figure S2 **NOD1 protein expression, body weight, and plasma levels of glucose and insulin obtained in HFD-treated mice**
Representative immunoblot and average data of NOD1/GAPDH expression obtained in cardiac tissue of wt mice and HFD-fed mice (**A**). Body weight (**B**), and glucose (**C**) and insulin (**D**) plasma levels obtained in HFD-fed mice for 12 weeks. Data are expressed as means ± S.E.M. of the percentage of the corresponding wt mice (100%). *$P < 0.05$ and ***$P < 0.001$ compared with the corresponding *wt*.

detected between 564 nm and 604 nm with band-pass filter using FACScan flow cytometer (FC-500 Becton Dickinson). Data analysis was presented using forward scatter (FSC) compared with fluorescence, where the percentage of lipid accumulation was calculated on the basis of the cells stained with high fluorescence values.

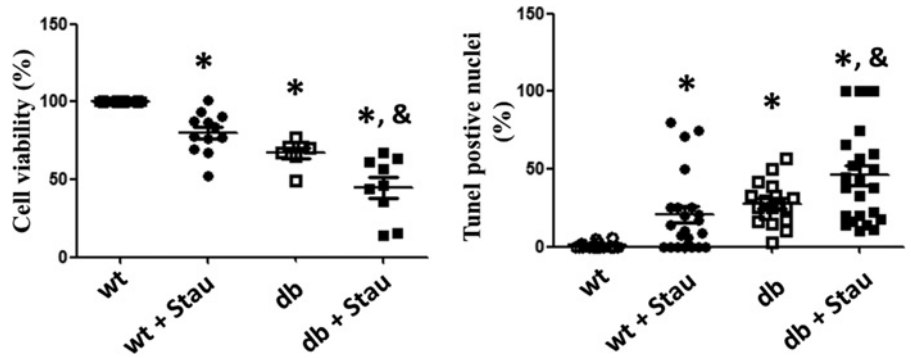

Figure S3 Staurosporine induces apoptosis in isolated native cardiomyocytes
Staurosporine (100 ng/ml) decreases cell viability (left panel) and increases the TUNEL-positive nuclei (right panel) in cardiomyocytes from wt and *db* mice. Data are expressed as means ± S.E.M. of the percentage of the corresponding wt mice (100 %); $n = 3$–5 animals per condition. $^{*}P < 0.05$ compared with wt mice; $^{\&}P < 0.05$ compared with *db* mice.

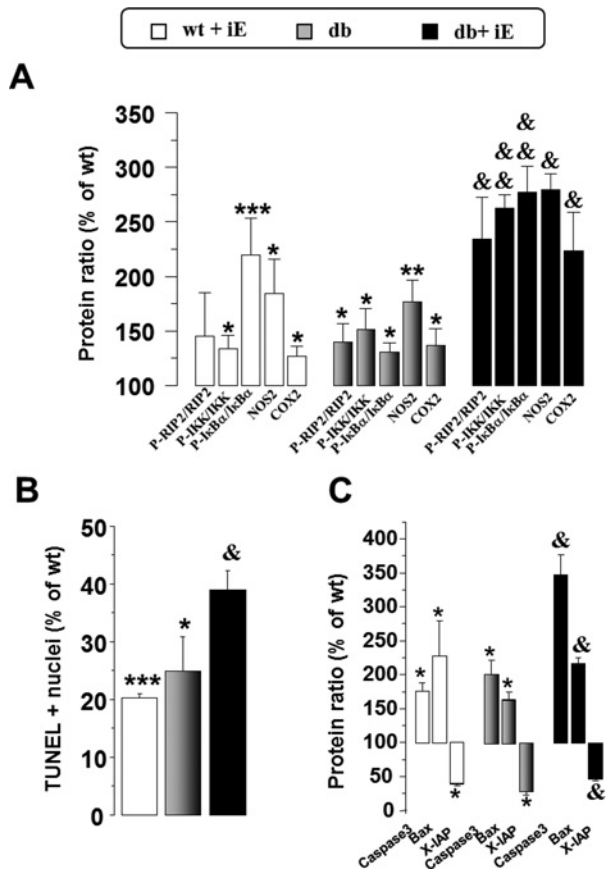

Figure S4 Selective stimulation of NOD1 induces NF-κB and apoptotic pathway activation
Animals received intraperitoneal iEDAP (5 μg/g of body weight; iE), a selective agonist of NOD1, or vehicle. After 2 weeks of treatment up-regulation of phospho-RIP2/RIP2, phospho-IKK/IKK, phospho-IκBα/IκBα, NOS2 and COX2 proteins were observed in hearts from wt and *db* mice (**A**). IE administration also promoted an increase in the number of TUNEL-positive nuclei (**B**), caspase-3 and BAX levels, and a decrease in X-IAP protein levels (**C**). Data are expressed as means ± S.E.M. compared with the corresponding wt mice (100 %). $^{*}P < 0.05$ compared with wt mice; $^{\&}P < 0.05$ compared with *db* mice; $n = 4$–6 animals.

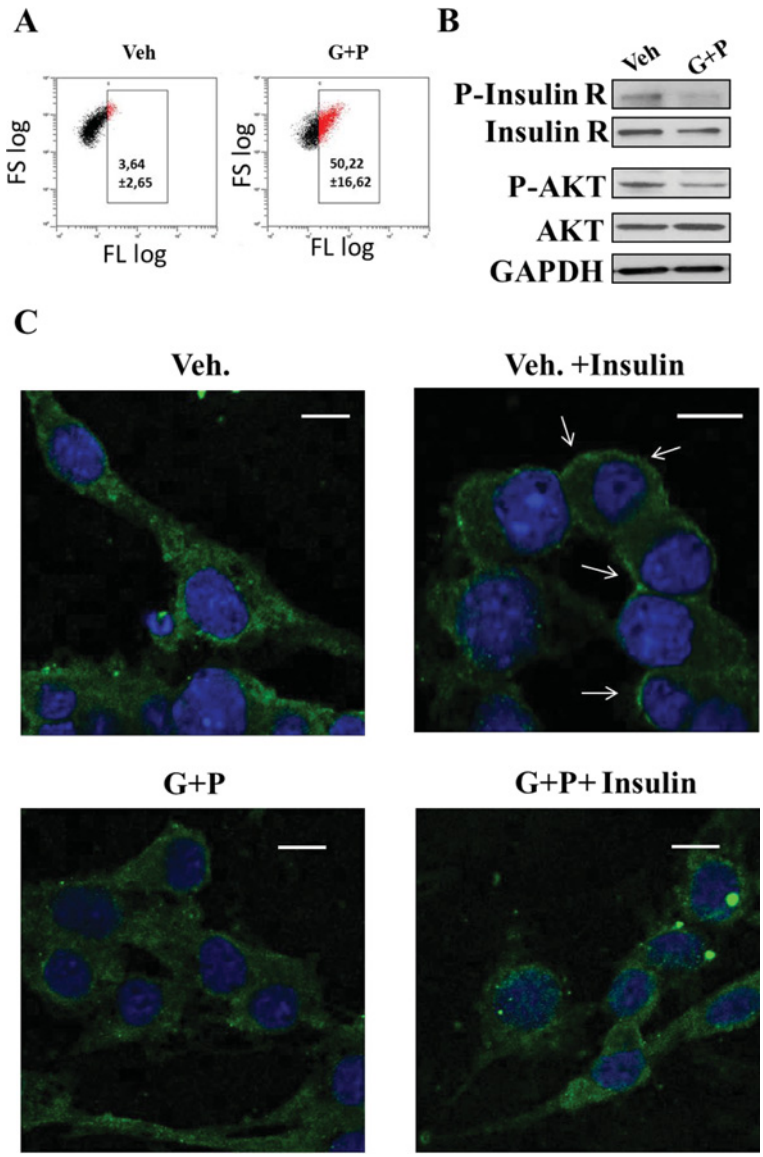

Figure S5 **HL-1 cells incubated with palmitate and glucose reveal changes in insulin signalling and lipid accumulation**
(**A**) Nile Red fluorescence staining demonstrates lipid incorporation in HL-1 cells incubated for 48 h with 50 mmol/l glucose and 200 μmol/l palmitate. Left panel shows an example obtained in vehicle-treated cells (Veh.) and the right panel illustrates an example obtained in cells incubated with glucose and palmitate (G + P). The mean values have been added to the Figure ($n = 3$). (**B**) Representative immunoblots of phospho-Akt/Akt, phospho-InsulinR/InsulinR (insulin receptor) and GAPDH from cells treated for 48 h with Veh. or with 50 mmol/l glucose and 200 μmol/l palmitate (G + P) and treated with insulin (100 nmol/l) for 5 min prior to collection. Insulin failed to phosphorylate both the Akt and InsulinR in G + P-treated cells. Representative immunoblots from three different experiments. (**C**) Immunofluorescence of GLUT-4 in HL-1 cells incubated with 50 mmol/l glucose and 200 μmol/l palmitate (G + P) for 48 h and treated with insulin (100 nmol/l) for 5 min. Vehicle-treated cells (Veh.) incubated with insulin for 5 min showed a prominent GLUT-4 transmembrane localization (arrows) compared with vehicle-treated cells under basal conditions (left panel). G + P-treated cells incubated with insulin did not show GLUT-4 transmembrane localization, suggesting that G + P-treatment induces an impairment in insulin-induced glucose transporter localization.

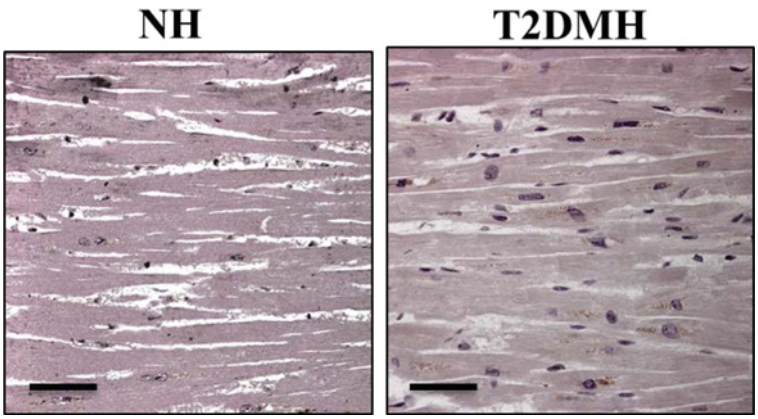

Figure S6 **Negative control for NOD1 immunohistochemistry staining**
Longitudinal heart section incubated with a mouse IgG instead of the primary antibody for NOD1. Scale = 100 μm.

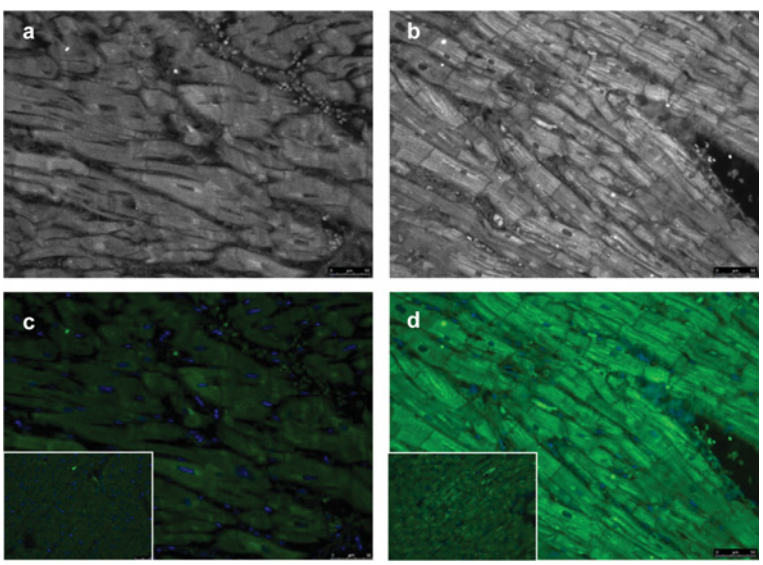

Figure S7 **NOD1 is up-regulated in the myocardium of T2DMH**
Myocardial sections of NH and T2DMH were stained with a NOD1 antibody (×40). Bright-field phase-contrast images are shown in panels (**a**) and (**b**). NOD1 staining revealed high expression of this NLR in T2DMH compared with NH (**c**, **d**). Negative controls obtained for each sample are shown in the insets.

Received 27 March 2014/21 May 2014; accepted 17 June 2014
Published as Immediate Publication 17 June 2014, doi: 10.1042/CS20140180

Biochem. J. (2014) **458**, 187–193 (Printed in Great Britain) doi:10.1042/BJ20131501

multimedia

REVIEW ARTICLE

Involvement of monocytes/macrophages as key factors in the development and progression of cardiovascular diseases

María FERNÁNDEZ-VELASCO*[1], Silvia GONZÁLEZ-RAMOS† and Lisardo BOSCÁ†[1]

*Instituto de Investigación Hospital Universitario La Paz, IdiPAZ, Paseo de la Castellana 261, 28046 Madrid, Spain
†Instituto de Investigaciones Biomédicas Alberto Sols, CSIC-UAM, Arturo Duperier 4, 28029 Madrid, Spain

Emerging evidence points to the involvement of specialized cells of the immune system as key drivers in the pathophysiology of cardiovascular diseases. Monocytes are an essential cell component of the innate immune system that rapidly mobilize from the bone marrow to wounded tissues where they differentiate into macrophages or dendritic cells and trigger an immune response. In the healthy heart a limited, but near-constant, number of resident macrophages have been detected; however, this number significantly increases during cardiac damage. Shortly after initial cardiac injury, e.g. myocardial infarction, a large number of macrophages harbouring a pro-inflammatory profile (M1) are rapidly recruited to the cardiac tissue, where they contribute to cardiac remodelling. After this initial period, resolution takes place in the wound, and the infiltrated macrophages display a predominant deactivation/pro-resolution profile (M2), promoting cardiac repair by mediating pro-fibrotic responses. In the present review we focus on the role of the immune cells, particularly in the monocyte/macrophage population, in the progression of the major cardiac pathologies myocardial infarction and atherosclerosis.

Key words: cardiovascular disease, fibrosis, inflammation, monocyte, macrophage.

INTRODUCTION

CVDs (cardiovascular diseases) are the leading cause of death in the developed world. Despite marked progress in the understanding of CVD, the underlying mechanisms involved in many of these pathologies have not been completely elucidated [1,2]. Most CVDs share a common low-grade chronic inflammatory state. Overwhelming evidence supports the view that specialized cells of the immune system, including Mo (monocytes)/Mφ (macrophages), contribute to CVD through cell–cell interactions by releasing pro-inflammatory and chemotactic factors and proteases that promote cell recruitment, cell apoptosis, angiogenesis and extracellular matrix remodelling [3–8]. Accordingly, clinical signs of inflammation in heart failure patients, such as elevated cytokine levels or enhanced C-reactive protein, are associated with detrimental ventricular remodelling [9].

Mo/Mφ constitute an important cell population of the innate immune system and are normally produced from haematopoietic stem cell precursors in the bone marrow. Specific changes in the number of blood Mo can be used as CVD markers. Indeed, a positive correlation between high blood levels of Mo has been reported in hypercholesterolaemic individuals with coronary heart disease [10]. In response to inflammatory signals, Mo can rapidly traffic from the blood to injured tissues and differentiate into Mφ or dendritic cells, triggering an immune response. More recently, studies in murine models of MI (myocardial infarction) have shown that Mo recruitment is not only derived from bone marrow precursors, but also by extramedullary monocytopoiesis in the spleen [11–14].

Resident Mφ in the healthy heart account for approximately 1–5 % of the cell population; however, their numbers rise significantly during cardiac damage [13,15–17]. Under physiological conditions, tissue Mφ express genes resembling an anti-inflammatory/deactivation profile (M2) [18]. After cardiac injury, e.g. MI, large numbers of Mφ harbouring a robust pro-inflammatory profile (M1) are rapidly recruited by the cardiac tissue early in the process. These inflammatory Mφ contribute to cardiac remodelling by accelerating cardiac apoptotic events. After injury, the resolution phase of the inflammatory response takes place in the heart wound, and the infiltrated Mφ predominantly display an M2 profile. Interestingly, cardiac fibrosis is a pathological process closely related to the inflammatory response during CVD [19] and Mo/Mφ participate in the initiation, progression and repair of cardiac fibrosis [20]. Accordingly, Mφ phagocytosis can act as pro- or anti-fibrotic, depending on the microenvironment, thereby modulating extracellular matrix deposition and promoting cardiac remodelling [21,22]. The present review focuses on the role of these specialized immune cells in some CVDs such as MI and atherosclerosis.

ONTOGENY AND FATE OF Mo/Mφ

Mo are innate immune cells derived from the myeloid lineage in the bone marrow [23]; however, under certain conditions, such as inflammation, extramedullary monocytopoiesis has been reported [12,24]. Consequently, some authors have suggested that resident Mo/Mφ can also be recruited at inflammatory sites, where they

Abbreviations: ACE, angiotensin-converting enzyme; CCR2, CC chemokine receptor 2; CVD, cardiovascular disease; CX3CR, CX3C chemokine receptor; ECM, extracellular matrix; FGF, fibroblast growth factor; IL, interleukin; LDL, low-density lipoprotein; Ly-6C, lymphocyte antigen 6C; M1, pro-inflammatory macrophage; M2, anti-inflammatory/deactivation macrophage; MCP-1, monocyte chemoattractant protein-1; Mφ, macrophage(s); MI, myocardial infarction; MMP, matrix metalloproteinase; Mo, monocyte(s); oxLDL, oxidized low-density lipoprotein; ROS, reactive oxygen species; TGF-β, transforming growth factor β; TLR, Toll-like receptor; TNF-α, tumour necrosis factor α; VEGFR2, vascular endothelial growth factor receptor 2.

[1] Correspondence may be addressed to either of these authors (email mvelasco@iib.uam.es/maria.fernandez@idipaz.es or lbosca@iib.uam.es).

Table 1 Major markers of monocyte subsets in both mice and humans

Mouse monocyte subsets	Distinctive markers	Human monocyte subsets	Distinctive markers
Ly-6C^{high}	CCR2^{high}, CX3CR1^{low}, CD62L^{+} and Gr1	CD14^{high}/CD16^{low}	CCR1, CCR2, CXCR1, CXCR2, CX3CR1, CD36, CD38, CD62L, CD64 and CD99
Ly-6C^{low}	CCR2^{low}, CX3CR1^{high}, CD62L^{-} and CD11c	CD14^{low}/CD16^{+}	CX3CR1, CD32, CD86 and MHC II
Ly-6C^{int}	CCR2^{high}, CCR7, CCR8 and Gr1	CD14^{high}/CD16^{+}	CCR2, CX3CR, CXR4, CD105, HLA-DR, ACE and VEGFR2

differentiate into activated Mφ and contribute to wound healing [25,26]. Mo from the bone marrow enter the blood via CCR2 (CC chemokine receptor 2) motifs [27], arriving at different tissues where they differentiate into Mφ. In mice, Mo are typically classified according to the expression of Ly-6C (lymphocyte antigen 6C). Ly-6C^{high} Mo are CCR2^{high}, CX3CR1^{low} (where CX3CR is CX3C chemokine receptor), CD62L^{+} and Gr1^{+}, whereas Ly-6C^{low} Mo are CCR2^{low}, CX3CR1^{high} and CD62L^{-} [26,28]. In addition, intermediate Ly-6C Mo (Ly-6C^{int}, CCR2^{high}, Gr1^{+}) have also been described to play an important role in the inflammatory response [29–31]. Ly-6C^{high} Mo were originally referred to as inflammatory or classical Mo/Mφ, accumulating in the inflammatory focus, where they rapidly give rise to polarized Mφ. Indeed, during inflammation, a significant increase in Ly-6C^{high} cells occurs, contributing to monocytic events [13]. Ly-6C^{low} Mo, named resident or non-classical Mo, have been reported to accumulate in tissues under homoeostatic conditions [32]. The percentages of Ly-6C^{high} and Ly-6C^{low} Mo are similar under healthy conditions, whereas upon cardiac injury the number of Ly-6C^{high} Mo are significantly augmented (see below) [7,13]. Although murine and human Mo share some common properties, many differences have been recently established related to function and phenotype in both species, therefore comparisons between them should be cautiously considered. Human Mo are classified according to their CD14/CD16 expression level [33]. Similar to murine Mo, at least two main subsets have been characterized to date. In healthy individuals, the majority of human Mo display a CD14^{high}/CD16^{low} (CD14^{++}/CD16^{-}) profile, rather than CD14^{low}/CD16^{+} (CD14^{+}/CD16^{+} or CD14^{dim}) which represents only 5–15 % of the Mo population. Recently, a third subset of Mo, CD14^{high}/CD16^{+} (CD14^{++}/CD16^{+}), has been identified in human blood [34]. This subtype is reminiscent of the Ly-6C^{high} Mo population in mice. With regards to the expression of adhesion molecules and chemokine receptors of each subtype, CD14^{high}/CD16^{low} Mo express CCR2, CX3CR1, CD62L and CD64, and are found to be significantly increased in an inflammatory context (sharing many features of murine Ly-6C^{high} cells). CD14^{dim} Mo lack CCR2 and express high levels of CX3CR1, CD32 and histocompatibility complex II. CD14^{dim} are closely associated with Ly-6C^{low} Mo [35,36]. The intermediate CD14^{high}/CD16^{+} Mo express higher levels of CX3CR, CXR4 and CCR2. This subset also expresses ACE (angiotensin-converting enzyme) and VEGFR2 (vascular endothelial growth factor receptor 2), which are intimately involved in angiogenesis and cardiac remodelling [37]. CD14^{high}/CD16^{+} Mo are also the main producers of ROS (reactive oxygen species). Functionally, CD14^{dim} are considered as sentinels of the vasculature, whereas CD14^{high}/CD16^{+} and CD14^{high}/CD16^{low} Mo contribute to inflammatory processes. Both CD14^{high}/CD16^{+} and CD14^{high}/CD16^{low} Mo respond to TLR2/4 (Toll-like receptor 2/4) ligands, whereas CD14^{dim} cells respond to TLR7/8 stimuli [35]. A summary of the comparison between the markers of human and murine Mφ is shown in Table 1.

Following the ontogeny lineage, Mφ acquire their main biological functions upon tissue accumulation. Nevertheless, a recent sophisticated view, based on complementary experimental evidence, points to the possibility of a non-haemopoietic origin of some tissue Mφ subsets (i.e. Langerhans cells in the skin or proliferation of recruited Mφ in the atheroma lesion [29,38]). Therefore this field remains open to new questions concerning the possible origin of these cells from local precursors that were seeded from the yolk sac before haemopoiesis was completed [39–41]. Indeed, Mo/Mφ constitute a heterogeneous cell population. Acknowledging the origin of Mφ, two lineages of Mφ have been recently defined in mice [42]: F4/80^{low} CD11b^{high} Mφ derived from bone marrow, and F4/80^{high} Mφ derived from the yolk sac. The specific functions of both populations are not yet completely understood. With regard to the classification of Mφ, many possibilities have been established, but the most common refers to the M1/M2 classification. Bone marrow precursors can be differentiated into Mφ *in vitro* in a variety of ways; those generated in the presence of GM-CSF (granulocyte/Mφ colony-stimulating factor), lipopolysaccharide or IFN-γ (interferon γ) are called M1 or classically activated Mφ. M1 Mφ produce high levels of pro-inflammatory mediators such as TNF-α (tumour necrosis factor α), IL (interleukin)-1β, IL-6, IL-12 and inducible nitric oxide synthase. Conversely, precursors maintained in the presence of IL-4, IL-10 or IL-13 generate M2 or alternatively activated Mφ, and produce anti-inflammatory products such as arginase-1, IL-10 and CD206, and display a pro-resolution profile [29,43,44].

Under homoeostatic conditions the majority of organs, including the heart, contain a small population of Mφ; however, when a pro-inflammatory injury occurs, increased numbers of blood Ly-6C^{high} Mo are extravasated into the tissue and differentiate into M1 Mφ. In the following resolution phase, M1 Mφ are replaced by M2 Mφ. Accordingly, a conversion of M1 into M2 has been proposed [45–47]. Nonetheless, in response to inflammatory damage Ly-6C^{low}, Mo can also extravasate into the heart where they differentiate into M2 Mφ, thus promoting cardiac repair and remodelling [48]. Alternatively, it has been suggested that M2 Mφ may also derive from Ly-6C^{high} Mo, that under a pro-resolution environment can differentiate into M2 subsets [49]; however, this hypothesis needs further confirmation.

ATHEROSCLEROSIS AND INFLAMMATORY MYELOID CELLS

Despite the exceptional advances in medicine arising during the last half century, CVD remains the most common cause of death in industrialized nations [2]. Atherosclerosis underlies the majority of CVD and its slow progression into a chronic disorder may cause thrombotic events [50]. Atherosclerosis affects the structure and function of arterial blood vessels, and results from the deposition of fatty material such as cholesterol and triacylglycerols into the lumen of arteries. Although atherosclerosis is a complex disease, important evidence suggests that inflammatory mediators may be key factors in disease progression [51–54]. In the initial stages of atherogenesis, activation of endothelium induces an increase in the expression of adhesion molecules, reducing barrier function and promoting leucocyte and Mo recruitment in the arterial wall [55,56]. In this scenario, Mo recruited to the endothelium of vessels quickly differentiate

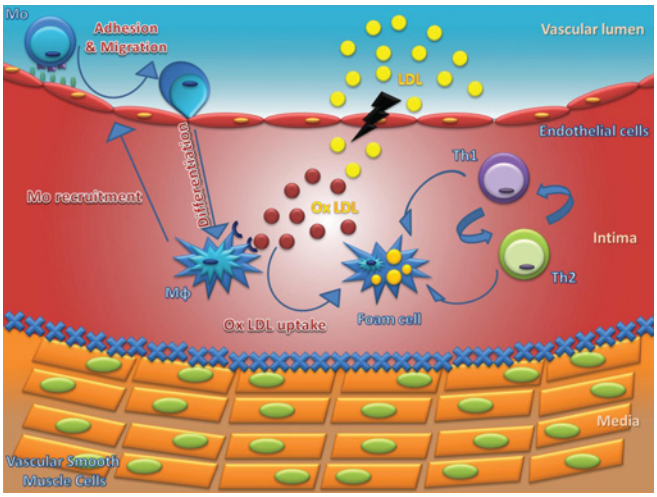

Figure 1 Initial phase of atherosclerosis

Plasma LDL is converted into oxLDL by various cellular and biochemical mediators in the subendothelial space. OxLDL promote, via endothelial cells, the differentiation of Mo into Mφ that take-up the oxLDL, converting them into foam cells. Activated Mφ express a variety of cytokines which stimulate endothelial cells to express adhesion proteins, supporting the binding of additional blood Mo to the endothelium and their recruitment into the intima. Interactions between Mφ and T-cells result in a broad range of cellular and humoral responses, establishing a chronic inflammatory process. Th1/2, T-helper cell type 1/2. An animation is available online at http://www.biochemj.org/bj/458/0187/bj4580187add.htm.

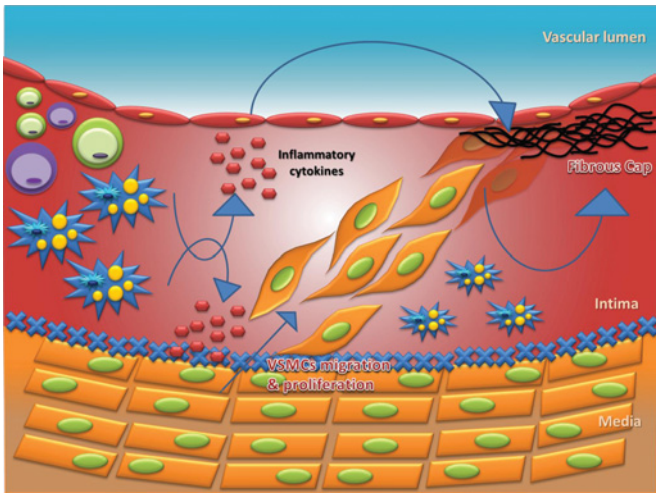

Figure 2 Atheroma progression phase

Cytokines released from Mφ and foam cells stimulate not only the VSMCs (vascular smooth muscle cells) to migrate into the intima, proliferate and secrete pro-fibrotic agents, but also the endothelial cells, to contribute to the resulting fibrous cap formation. An animation is available online at http://www.biochemj.org/bj/458/0187/bj4580187add.htm.

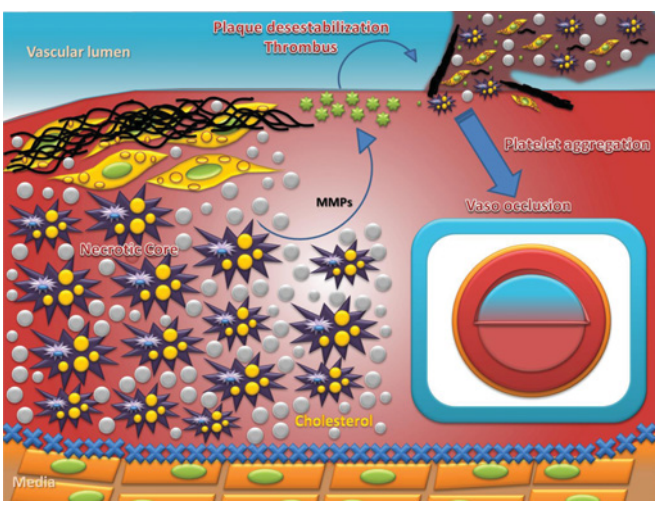

Figure 3 Plaque rupture and thrombosis

Necrosis of Mφ and smooth muscle cell-derived foam cells leads to the formation of a necrotic core and accumulation of extracellular cholesterol. Mφ secrete MMPs and promote neovascularization, contributing to weakening of the fibrous plaque. Plaque rupture exposes blood components to tissue factor, initiates coagulation, the recruitment of platelets and the formation of a thrombus, which narrows the arterial passage, restricting blood flow.

into Mφ that phagocytize modified lipids [oxLDL (oxidized low-density lipoprotein)] accumulated inside of arteries, leading to foam cell formation and contributing to the atheroma core development [6] (Figure 1). Furthermore, these Mφ amplify the inflammatory response through the release of pro-inflammatory cytokines and growth factors, promoting a local Mφ proliferation inside the atheroma lesion, hence offering new and previously unexpected therapeutic approaches [38,57]. This inflammatory amplification attracts additional immune cells into the vessel's intima, promoting the formation of advanced atherosclerotic plaques and increasing profibrotic and necrotic events (Figure 2 and see the animation online at http://www.biochemj.org/bj/458/0187/bj4580187add.htm). At the end of the process, the subendothelial prothrombotic material is exposed and the dissolution of the fibrous cap occurs. Thereafter, the coagulation cascade is activated, inducing thrombus formation and promoting vascular occlusion [58] (Figure 3). This process is aggravated when recurrent pro-inflammatory events occur, due to the capacity of Mφ to promote remodelling and destabilization of atheroma.

Many studies suggest that Mo are key factors in the initiation and progression of atherosclerotic lesions. Indeed, a rise in infiltration of Ly-6C^{high} cells in the atherosclerotic core mainly via CCR2 and CX3R1 has been reported by different groups [13,59,60]. When the inflammatory input persists, Ly-6C^{high} Mo differentiate into M1 Mφ by expressing inflammatory mediators and contribute to oxidative stress [24]. In contrast, Ly-6C^{low} cell infiltration is less frequent in atherosclerotic lesions [61]. Interestingly, Mo recruited to the atherosclerotic lesion not only derive from the bone marrow, but also from the splenic reservoir, and as previously mentioned, from local proliferation [24,38]. Experimental data obtained in Apo-E-deficient mice (hypercholesterolaemic mice) demonstrated that these mice fed with a high-fat diet display an increase in the number of blood Ly-6C^{high} Mo and their adhesion to the damaged endothelium was augmented, thus increasing their differentiation to detrimental Mφ [13,59,62]. The treatment of these mice with statins reduces the cholesterol blood levels, and decreases the number of Ly-6C^{high} Mo that diminish the lesion formation [13]. More recently, a study has reported that siRNA knockdown of CCR2 blocks Mo recruitment in atherosclerotic plaques, and reduces the infarct size after coronary occlusion [11].

In humans, a positive correlation between high blood levels of CD14^{dim} Mo and an increase in cholesterol and triacylglycerol levels have been reported in hypercholesterolaemic individuals with coronary heart disease [10]. Moreover, the percentage of CD16^{+} Mo is usually high in patients with coronary artery disease [63]. Mφ also play an important role in the progression of atherogenic lesions. On one hand, a rise of Mφ infiltration occurs in vascular lesions, increases the modified LDL (low-density lipoprotein) phagocytosis and raises the secretion of cytokines,

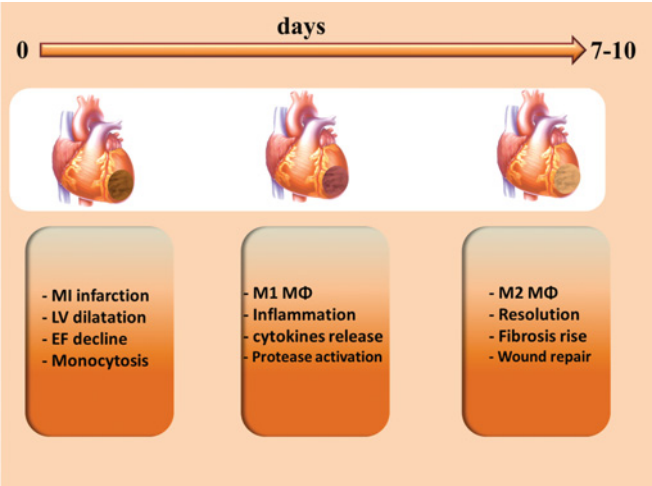

Figure 4 Diagram of the main features associated with MI disease

MI results from an injury. During the first minutes after MI, a significant accumulation of immune cells occurs in the healing infarct. Mo/Mφ are the main cell population that infiltrate into the MI area. First, pro-inflammatory Mφ (M1) dominate the infarcted region; in the second phase, M1 Mφ are replaced by a significant number of reduced pro-inflammatory myeloid cells (M2) that contribute to resolution. During the first phase of MI, important pro-inflammatory mediators and proteases are released in the cardiac wound. In the rebuilding phase, M2 cells release pro-angiogenic and profibrotic mediators that participate in wound repair, and new vessels and fibrotic tissue are formed. EF, ejection fraction; LV, left ventricle.

chemokines and ROS that promote tissue injury. Furthermore, Mφ induce plaque destabilization and rupture, reinforcing their harmful role [64]. Nevertheless, beneficial roles have been reported for Mφ in atherosclerotic disease and some authors suggest that Mφ can participate in the repair processes that rescue the physiological tissue homoeostasis [65].

ROLE OF Mo/Mφ IN MI DAMAGE

MI is one of the most common ischaemic cardiac diseases and constitutes a major proportion of the CVD rates. In most cases, MI results from an atherosclerotic injury, as rupture of the atheroma plaque promotes thrombus formation and impedes normal heart oxygenation. Consequently, cardiomyocyte necrosis occurs very quickly in the left ventricle (less than 1 h). MI takes place in a chronic inflammatory milieu with highly active haemopoietic and immune cells. During the first minutes after MI, a significant accumulation of leucocytes occurs in the healing infarct [66,67]. Initially, there is a high proportion of neutrophils and Mo in the infarcted region, whereas lymphocytes, dendritic cells and mast cells arrive at the wound in lower proportions. Mo/Mφ are the main cell population that infiltrate into the infarcted area. Two phases of infiltration are well defined after MI: first, Ly-6C^{high} Mo and corresponding pro-inflammatory Mφ (M1) dominate the infarcted region and are recruited in many cases via MCP-1 (Mo chemoattractant protein-1) activity [68]; in the second phase (approximately 4–7 days after MI), Ly-6C^{high} Mo are replaced by myeloid cells (Ly-6C$^{int/low}$ Mo/M2-Mφ) that are less pro-inflammatory and contribute to resolution (Figure 4). Significantly, a similar turnover of Mo/Mφ (M1 to M2) subsets are detected in blood from both murine models of MI and patients with acute MI [15,69].

Predictably, compared with murine models, less information is available on Mo and MI in humans. Although no data is available from cardiac tissue, some authors describe that CD14^{high}/CD16^{low} Mo are significantly increased in patients' blood on day 3 after MI, whereas at 5 days after infarct CD14^{high}/CD16^{+} cells appear to be the main Mo population found [69]. This pattern is similar to that observed in murine MI models [15]. Moreover, MI patients with high numbers of pro-inflammatory circulating Mo showed a significant cardiac contraction depression, and their prognosis worsened [69]. Possibly, these pro-inflammatory mediators aggravate the healing process after MI. More recently, Tapp et al. [70] have also differentiated intermediate and non-classical Mo in patients suffering MI. During the first phase of MI, important pro-inflammatory mediators such as TNF-α and proteases, derived from Ly-6C^{high}/M1 activation, are released in the cardiac wound. Thus activated Mφ contribute to the removal of debris in the infarcted region which is replaced by granulation tissue and scar formation. In the rebuilding phase, Ly-6C$^{int/low}$ M2 cells release pro-angiogenic and pro-fibrotic mediators (i.e. endothelial and transforming growth factors) that participate in wound repair [15]. Finally, in order to restore the cardiac damage, non-leucocyte populations such as endothelial cells and fibroblasts/myofibroblasts also participate in the reconstruction of the healing infarct; in many cases new vessels and fibrotic tissue are formed [71,72].

Recent studies suggest a role for Mφ in the regulation of red blood cell generation and also in the close relationship with pluripotent progenitor cells [73–75]. An interesting question has arisen with regard to how Mo/Mφ participate in tissue regeneration after MI. Indeed, Mo can differentiate into endothelial, epithelial or other types of cells under specific culture conditions. An attractive hypothesis suggests that Mφ can interact with cells that bear regenerative capacities, contributing to myocardium regeneration. Some studies report an enhancement of blood and spleen haemopoietic progenitors and an increased activity of bone marrow after MI [76–78]; however, their function is not yet fully understood.

CONTRIBUTION OF Mo/Mφ TO CARDIAC FIBROSIS DEVELOPMENT

Cardiac fibrosis is a common constituent of most cardiac pathologies and represents the outcome of nearly all types of cardiac injury [19]. It may appear in response to two distinct stimuli: cardiomyocyte death as in MI; or, after different insults (pressure overload, metabolic and toxic disturbances, brief ischaemic events, etc.) that do not lead to cardiomyocyte loss. Although in the first case the restorative response derives from the formation of a collagen-based scar, in the second case it arises as an adaptive response to maintain the pressure-generating ability of the heart that may finally evolve into a state of replacement fibrosis [79]. Fibrillar collagen that accumulates in the ECM (extracellular matrix) remodelling process is a common consequence of these pathophysiological conditions. This 'increase' in the collagen content relative to basal levels is the classical histopathological finding that the general term 'fibrosis' refers to.

Since Virchow's work in the 19th Century, it has been known that fibroblasts are the principal cell type responsible for the imbalance of ECM composition in cardiac fibrosis [80]. As will be explained below, changes in fibroblast phenotype, defined as changes in cell marker expression and function, occur in a dynamic fashion [81]. The healing response following MI encompasses inflammatory, proliferative (granulation) and maturation phases. During the initial phase, activated Mφ and inflammatory cells produce a wide range of cytokines and growth factors (fibrogenic mediators) including TGF-β (transforming growth factor β), PDGF (platelet-derived growth factor), FGF (fibroblast growth factor), TNF-α, CTGF (connective

tissue growth factor) and MCP-1, to stimulate proliferation and phenotypic differentiation of fibroblasts into myofibroblasts (α-smooth muscle actin-positive cells). In the granulation phase, myofibroblasts infiltrate the infarct area to contribute to injured ventricle repair via sequential matrix degradation by ECM-degrading MMPs (matrix metalloproteinases) and resynthesis of ECM proteins. Post-MI remodelling includes both infarcted and non-infarcted areas of the heart and causes enhanced interstitial fibrosis in the remaining non-infarcted area [82].

Paying particular attention to the role of the Mo/Mφ inflammatory cells in cardiac fibrosis, the effort to highlight the role that TGF-β plays through its effects on the inflammatory and restorative response in the infarcted heart is of paramount relevance. Experimental studies suggest that TGF-β may be the 'switcher' that mediates the transition from inflammation to scar formation following MI. Although TGF-β signalling can activate peripheral blood Mo (increasing cytokine synthesis and enhancing chemotaxis), it may deactivate Mφ (chemokine down-regulation and suppression of cytokine synthesis) and promote myofibroblast transdifferentiation and ECM preservation [83–85]. Thus strategies directed to impair Mo infiltration have been developed in an attempt to reduce fibrosis. In this respect, the use of anti-MCP-1 gene therapy prevents Mφ accumulation and attenuates perivascular and interstitial fibrosis in MI [86]. Therefore Mo/Mφ not only play important roles in initiation and progression of fibrotic responses, but may also mediate resolution of fibrosis [20]. Through their phagocytic properties, Mφ can exert pro-fibrotic and anti-fibrotic actions, removing dead cells (thus facilitating growth of restorative fibroblasts) and clearing apoptotic myofibroblasts and cellular and ECM debris (thus eliminating key pro-fibrotic stimuli) [87].

The exact role of the Mφ in scar healing has not been fully clarified. Mφ may regulate ECM dynamics through the synthesis of MMPs and their inhibitors [88]. In this sense, it has been reported that certain MMPs not only facilitate collagen degradation, but can also process pro-fibrotic signalling molecules. Thus MMPs, and hence Mφ, are likely to contribute to the degradation of relatively normal ECM structure as well as facilitate the deposition of a 'fibrotic' and dysfunctional myocardial ECM [21,22]. In fact, fibrotic tissues in general appear macroscopically pale, reflecting diminished perfusion. As a result of decreased microvasculature, fibrotic tissues are likely to contain reduced levels of VEGF and are often chronically hypoxic, which directly contributes to fibrogenesis through HIF (hypoxia-inducible factor)-1α-mediated signalling [89]. Accordingly, Mo/Mφ activate resident endothelial progenitor cells to form new vessels and this effect seems likely to be attributable to the paracrine secretion of growth factors and chemokines [90,91]. As previously stated, although large numbers of Mφ accumulate in injured hearts, and are located in close proximity to matrix-producing myofibroblasts [92], their role in regulation of the fibrotic response remains unknown. Following cardiac injury, the complexity of environmental conditions may result in generation of multiple Mφ subpopulations with distinct properties that mediate pro-inflammatory, anti-inflammatory or fibrogenic actions.

CONCLUSIONS

Although the knowledge of inflammatory pathways has significantly advanced, many questions involving the role of Mo/Mφ in CVD remain unanswered. Indeed, the identification of the mediators involved in M1/M2 polarization under physiopathological conditions, and the specific localization of these cell populations in defined cardiovascular injuries (i.e. atherosclerosis or MI), requires further characterization. A central question is whether the deletion of selective Mo populations will be beneficial or detrimental in certain stages of CVD. New *in vitro* and *in vivo* experimental models may provide a fine tool to elucidate the biological roles of Mo/Mφ under physiological and pathological conditions. Advances in the cardiovascular field are directed towards elucidating whether pharmacotherapy treatments may impair the function of these inflammatory myeloid cells or whether the manipulation of Mo/Mφ subsets affects the outcome of these patients. Further progress in this field may help to develop new pharmacological targets directed to circumvent the deleterious effects observed in the most common CVD, including atherosclerosis or MI.

FUNDING

M.F.-V. was supported by the Instituto de Salud Carlos III (Miguel Servet Program) [grant number CP11/00080]. S.G.-R. was funded by the Ministerio de Ciencia e Innovación (MICINN). This work was supported by the MICINN [grant numbers BFU2008-02161, BFU2011-024760 and SAF2010-16377] and by FIS-RIC [grant number RD12/0042/0019].

REFERENCES

1 Dahlof, B. (2010) Cardiovascular disease risk factors: epidemiology and risk assessment. Am. J. Cardiol. **105**, 3A–9A
2 Lloyd-Jones, D. M. (2010) Cardiovascular risk prediction: basic concepts, current status, and future directions. Circulation **121**, 1768–1777
3 Martinet, W., Schrijvers, D. M. and De Meyer, G. R. (2012) Molecular and cellular mechanisms of macrophage survival in atherosclerosis. Basic Res. Cardiol. **107**, 297
4 Nahrendorf, M. and Swirski, F. K. (2013) Monocyte and macrophage heterogeneity in the heart. Circ. Res. **112**, 1624–1633
5 Pardali, E. and Waltenberger, J. (2012) Monocyte function and trafficking in cardiovascular disease. Thromb. Haemost. **108**, 804–811
6 Woollard, K. J. (2013) Immunological aspects of atherosclerosis. Clin. Sci. **125**, 221–235
7 Woollard, K. J. and Geissmann, F. (2010) Monocytes in atherosclerosis: subsets and functions. Nat. Rev. Cardiol. **7**, 77–86
8 Zawada, A. M., Rogacev, K. S., Schirmer, S. H., Sester, M., Bohm, M., Fliser, D. and Heine, G. H. (2012) Monocyte heterogeneity in human cardiovascular disease. Immunobiology **217**, 1273–1284
9 Dixon, D. L., Griggs, K. M., Bersten, A. D. and De Pasquale, C. G. (2011) Systemic inflammation and cell activation reflects morbidity in chronic heart failure. Cytokine **56**, 593–599
10 Rothe, G., Herr, A. S., Stohr, J., Abletshauser, C., Weidinger, G. and Schmitz, G. (1999) A more mature phenotype of blood mononuclear phagocytes is induced by fluvastatin treatment in hypercholesterolemic patients with coronary heart disease. Atherosclerosis **144**, 251–261
11 Leuschner, F., Dutta, P., Gorbatov, R., Novobrantseva, T. I., Donahoe, J. S., Courties, G., Lee, K. M., Kim, J. I., Markmann, J. F., Marinelli, B. et al. (2011) Therapeutic siRNA silencing in inflammatory monocytes in mice. Nat. Biotechnol. **29**, 1005–1010
12 Leuschner, F., Rauch, P. J., Ueno, T., Gorbatov, R., Marinelli, B., Lee, W. W., Dutta, P., Wei, Y., Robbins, C., Iwamoto, Y. et al. (2012) Rapid monocyte kinetics in acute myocardial infarction are sustained by extramedullary monocytopoiesis. J. Exp. Med. **209**, 123–137
13 Swirski, F. K., Libby, P., Aikawa, E., Alcaide, P., Luscinskas, F. W., Weissleder, R. and Pittet, M. J. (2007) Ly-6Chi monocytes dominate hypercholesterolemia-associated monocytosis and give rise to macrophages in atheromata. J. Clin. Invest. **117**, 195–205
14 Swirski, F. K., Nahrendorf, M., Etzrodt, M., Wildgruber, M., Cortez-Retamozo, V., Panizzi, P., Figueiredo, J. L., Kohler, R. H., Chudnovskiy, A., Waterman, P. et al. (2009) Identification of splenic reservoir monocytes and their deployment to inflammatory sites. Science **325**, 612–616
15 Nahrendorf, M., Swirski, F. K., Aikawa, E., Stangenberg, L., Wurdinger, T., Figueiredo, J. L., Libby, P., Weissleder, R. and Pittet, M. J. (2007) The healing myocardium sequentially mobilizes two monocyte subsets with divergent and complementary functions. J. Exp. Med. **204**, 3037–3047
16 Swirski, F. K. and Nahrendorf, M. (2013) Leukocyte behavior in atherosclerosis, myocardial infarction, and heart failure. Science **339**, 161–166
17 Swirski, F. K. and Nahrendorf, M. (2013) Macrophage–stem cell crosstalk after myocardial infarction. J. Am. Coll. Cardiol. **62**, 1902–1904

18 Pinto, A. R., Paolicelli, R., Salimova, E., Gospocic, J., Slonimsky, E., Bilbao-Cortes, D., Godwin, J. W. and Rosenthal, N. A. (2012) An abundant tissue macrophage population in the adult murine heart with a distinct alternatively-activated macrophage profile. PLoS ONE **7**, e36814
19 Dobaczewski, M. and Frangogiannis, N. G. (2009) Chemokines and cardiac fibrosis. Front. Biosci. **1**, 391–405
20 Wynn, T. A. and Barron, L. (2010) Macrophages: master regulators of inflammation and fibrosis. Semin. Liver Dis. **30**, 245–257
21 Spinale, F. G., Mukherjee, R., Zavadzkas, J. A., Koval, C. N., Bouges, S., Stroud, R. E., Dobrucki, L. W. and Sinusas, A. J. (2010) Cardiac restricted overexpression of membrane type-1 matrix metalloproteinase causes adverse myocardial remodeling following myocardial infarction. J. Biol. Chem. **285**, 30316–30327
22 Tatti, O., Vehvilainen, P., Lehti, K. and Keski-Oja, J. (2008) MT1-MMP releases latent TGF-β1 from endothelial cell extracellular matrix via proteolytic processing of LTBP-1. Exp. Cell Res. **314**, 2501–2514
23 van Furth, R. and Cohn, Z. A. (1968) The origin and kinetics of mononuclear phagocytes. J. Exp. Med. **128**, 415–435
24 Robbins, C. S., Chudnovskiy, A., Rauch, P. J., Figueiredo, J. L., Iwamoto, Y., Gorbatov, R., Etzrodt, M., Weber, G. F., Ueno, T., van Rooijen, N. et al. (2012) Extramedullary hematopoiesis generates Ly-6C(high) monocytes that infiltrate atherosclerotic lesions. Circulation **125**, 364–374
25 Geissmann, F., Jung, S. and Littman, D. R. (2003) Blood monocytes consist of two principal subsets with distinct migratory properties. Immunity **19**, 71–82
26 Geissmann, F., Manz, M. G., Jung, S., Sieweke, M. H., Merad, M. and Ley, K. (2010) Development of monocytes, macrophages, and dendritic cells. Science **327**, 656–661
27 Serbina, N. V. and Pamer, E. G. (2006) Monocyte emigration from bone marrow during bacterial infection requires signals mediated by chemokine receptor CCR2. Nat. Immunol. **7**, 311–317
28 Geissmann, F., Gordon, S., Hume, D. A., Mowat, A. M. and Randolph, G. J. (2010) Unravelling mononuclear phagocyte heterogeneity. Nat. Rev. Immunol. **10**, 453–460
29 Gordon, S. and Taylor, P. R. (2005) Monocyte and macrophage heterogeneity. Nat. Rev. Immunol. **5**, 953–964
30 Qu, C., Edwards, E. W., Tacke, F., Angeli, V., Llodra, J., Sanchez-Schmitz, G., Garin, A., Haque, N. S., Peters, W., van Rooijen, N. et al. (2004) Role of CCR8 and other chemokine pathways in the migration of monocyte-derived dendritic cells to lymph nodes. J. Exp. Med. **200**, 1231–1241
31 Ziegler-Heitbrock, L., Ancuta, P., Crowe, S., Dalod, M., Grau, V., Hart, D. N., Leenen, P. J., Liu, Y. J., MacPherson, G., Randolph, G. J. et al. (2010) Nomenclature of monocytes and dendritic cells in blood. Blood **116**, e74–e80
32 Carlin, L. M., Stamatiades, E. G., Auffray, C., Hanna, R. N., Glover, L., Vizcay-Barrena, G., Hedrick, C. C., Cook, H. T., Diebold, S. and Geissmann, F. (2013) Nr4a1-dependent Ly6C(low) monocytes monitor endothelial cells and orchestrate their disposal. Cell **153**, 362–375
33 Passlick, B., Flieger, D. and Ziegler-Heitbrock, H. W. (1989) Identification and characterization of a novel monocyte subpopulation in human peripheral blood. Blood **74**, 2527–2534
34 Ancuta, P., Liu, K. Y., Misra, V., Wacleche, V. S., Gosselin, A., Zhou, X. and Gabuzda, D. (2009) Transcriptional profiling reveals developmental relationship and distinct biological functions of $CD16^+$ and $CD16^-$ monocyte subsets. BMC Genomics **10**, 403
35 Cros, J., Cagnard, N., Woollard, K., Patey, N., Zhang, S. Y., Senechal, B., Puel, A., Biswas, S. K., Moshous, D., Picard, C. et al. (2010) Human CD14dim monocytes patrol and sense nucleic acids and viruses via TLR7 and TLR8 receptors. Immunity **33**, 375 – 386
36 Heine, G. H., Ortiz, A., Massy, Z. A., Lindholm, B., Wiecek, A., Martinez-Castelao, A., Covic, A., Goldsmith, D., Suleymanlar, G., London, G. M. et al. (2012) Monocyte subpopulations and cardiovascular risk in chronic kidney disease. Nat. Rev. Nephrol. **8**, 362–369
37 Zawada, A. M., Rogacev, K. S., Rotter, B., Winter, P., Marell, R. R., Fliser, D. and Heine, G. H. (2011) SuperSAGE evidence for $CD14^{++}CD16^+$ monocytes as a third monocyte subset. Blood **118**, e50–e61
38 Robbins, C. S., Hilgendorf, I., Weber, G. F., Theurl, I., Iwamoto, Y., Figueiredo, J. L., Gorbatov, R., Sukhova, G. K., Gerhardt, L. M., Smyth, D. et al. (2013) Local proliferation dominates lesional macrophage accumulation in atherosclerosis. Nat. Med. **19**, 1166–1172
39 Ginhoux, F., Greter, M., Leboeuf, M., Nandi, S., See, P., Gokhan, S., Mehler, M. F., Conway, S. J., Ng, L. G., Stanley, E. R. et al. (2010) Fate mapping analysis reveals that adult microglia derive from primitive macrophages. Science **330**, 841–845
40 Hashimoto, D., Chow, A., Noizat, C., Teo, P., Beasley, M. B., Leboeuf, M., Becker, C. D., See, P., Price, J., Lucas, D. et al. (2013) Tissue-resident macrophages self-maintain locally throughout adult life with minimal contribution from circulating monocytes. Immunity **38**, 792–804
41 Wynn, T. A., Chawla, A. and Pollard, J. W. (2013) Macrophage biology in development, homeostasis and disease. Nature **496**, 445–455
42 Schulz, C., Gomez Perdiguero, E., Chorro, L., Szabo-Rogers, H., Cagnard, N., Kierdorf, K., Prinz, M., Wu, B., Jacobsen, S. E., Pollard, J. W. et al. (2012) A lineage of myeloid cells independent of Myb and hematopoietic stem cells. Science **336**, 86–90
43 Mosser, D. M. and Edwards, J. P. (2008) Exploring the full spectrum of macrophage activation. Nat. Rev. Immunol. **8**, 958–969
44 Sica, A. and Mantovani, A. (2012) Macrophage plasticity and polarization: *in vivo* veritas. J. Clin. Invest. **122**, 787–795
45 Arnold, L., Henry, A., Poron, F., Baba-Amer, Y., van Rooijen, N., Plonquet, A., Gherardi, R. K. and Chazaud, B. (2007) Inflammatory monocytes recruited after skeletal muscle injury switch into antiinflammatory macrophages to support myogenesis. J. Exp. Med. **204**, 1057–1069
46 Egawa, M., Mukai, K., Yoshikawa, S., Iki, M., Mukaida, N., Kawano, Y., Minegishi, Y. and Karasuyama, H. (2013) Inflammatory monocytes recruited to allergic skin acquire an anti-inflammatory M2 phenotype via basophil-derived interleukin-4. Immunity **38**, 570–580
47 Ramachandran, P., Pellicoro, A., Vernon, M. A., Boulter, L., Aucott, R. L., Ali, A., Hartland, S. N., Snowdon, V. K., Cappon, A., Gordon-Walker, T. T. et al. (2012) Differential Ly-6C expression identifies the recruited macrophage phenotype, which orchestrates the regression of murine liver fibrosis. Proc. Natl. Acad. Sci. U.S.A. **109**, E3186–E3195
48 Auffray, C., Sieweke, M. H. and Geissmann, F. (2009) Blood monocytes: development, heterogeneity, and relationship with dendritic cells. Annu. Rev. Immunol. **27**, 669–692
49 Yona, S., Kim, K. W., Wolf, Y., Mildner, A., Varol, D., Breker, M., Strauss-Ayali, D., Viukov, S., Guilliams, M., Misharin, A. et al. (2013) Fate mapping reveals origins and dynamics of monocytes and tissue macrophages under homeostasis. Immunity **38**, 79–91
50 Hansson, G. K. (2005) Inflammation, atherosclerosis, and coronary artery disease. N. Engl. J. Med. **352**, 1685–1695
51 Andersson, J., Libby, P. and Hansson, G. K. (2010) Adaptive immunity and atherosclerosis. Clin. Immunol. **134**, 33–46
52 Kzhyshkowska, J., Neyen, C. and Gordon, S. (2012) Role of macrophage scavenger receptors in atherosclerosis. Immunobiology **217**, 492–502
53 Ross, R. (1999) Atherosclerosis – an inflammatory disease. N. Engl. J. Med. **340**, 115–126
54 Weber, C., Zernecke, A. and Libby, P. (2008) The multifaceted contributions of leukocyte subsets to atherosclerosis: lessons from mouse models. Nat. Rev. Immunol. **8**, 802–815
55 Hansson, G. K. and Hermansson, A. (2011) The immune system in atherosclerosis. Nat. Immunol. **12**, 204–212
56 Zernecke, A., Shagdarsuren, E. and Weber, C. (2008) Chemokines in atherosclerosis: an update. Arterioscler. Thromb. Vasc. Biol. **28**, 1897–1908
57 Libby, P. (2002) Inflammation in atherosclerosis. Nature **420**, 868–874
58 Fuster, V., Moreno, P. R., Fayad, Z. A., Corti, R. and Badimon, J. J. (2005) Atherothrombosis and high-risk plaque: part I: evolving concepts. J. Am. Coll. Cardiol. **46**, 937–954
59 Combadiere, C., Potteaux, S., Rodero, M., Simon, T., Pezard, A., Esposito, B., Merval, R., Proudfoot, A., Tedgui, A. and Mallat, Z. (2008) Combined inhibition of CCL2, CX3CR1, and CCR5 abrogates Ly6C(hi) and Ly6C(lo) monocytosis and almost abolishes atherosclerosis in hypercholesterolemic mice. Circulation **117**, 1649–1657
60 Varol, C., Landsman, L., Fogg, D. K., Greenshtein, L., Gildor, B., Margalit, R., Kalchenko, V., Geissmann, F. and Jung, S. (2007) Monocytes give rise to mucosal, but not splenic, conventional dendritic cells. J. Exp. Med. **204**, 171–180
61 Wu, H., Gower, R. M., Wang, H., Perrard, X. Y., Ma, R., Bullard, D. C., Burns, A. R., Paul, A., Smith, C. W., Simon, S. I. and Ballantyne, C. M. (2009) Functional role of CD11c+ monocytes in atherogenesis associated with hypercholesterolemia. Circulation **119**, 2708–2717
62 Saederup, N., Chan, L., Lira, S. A. and Charo, I. F. (2008) Fractalkine deficiency markedly reduces macrophage accumulation and atherosclerotic lesion formation in $CCR2^{-/-}$ mice: evidence for independent chemokine functions in atherogenesis. Circulation **117**, 1642–1648
63 Schlitt, A., Heine, G. H., Blankenberg, S., Espinola-Klein, C., Dopheide, J. F., Bickel, C., Lackner, K. J., Iz, M., Meyer, J., Darius, H. and Rupprecht, H. J. (2004) $CD14^+CD16^+$ monocytes in coronary artery disease and their relationship to serum TNF-α levels. Thromb. Haemost. **92**, 419–424
64 Choudhury, R. P., Lee, J. M. and Greaves, D. R. (2005) Mechanisms of disease: macrophage-derived foam cells emerging as therapeutic targets in atherosclerosis. Nat. Clin. Pract. Cardiovasc. Med. **2**, 309–315
65 Gordon, S. (2003) Alternative activation of macrophages. Nat. Rev. Immunol. **3**, 23–35
66 Lee, S., Vinegoni, C., Feruglio, P. F., Fexon, L., Gorbatov, R., Pivoravov, M., Sbarbati, A., Nahrendorf, M. and Weissleder, R. (2012) Real-time *in vivo* imaging of the beating mouse heart at microscopic resolution. Nat. Commun. **3**, 1054
67 Jung, K., Kim, P., Leuschner, F., Gorbatov, R., Kim, J. K., Ueno, T., Nahrendorf, M. and Yun, S. H. (2013) Endoscopic time-lapse imaging of immune cells in infarcted mouse hearts. Circ. Res. **112**, 891–899

68 Dewald, O., Zymek, P., Winkelmann, K., Koerting, A., Ren, G., Abou-Khamis, T., Michael, L. H., Rollins, B. J., Entman, M. L. and Frangogiannis, N. G. (2005) CCL2/monocyte chemoattractant protein-1 regulates inflammatory responses critical to healing myocardial infarcts. Circ. Res. **96**, 881–889

69 Tsujioka, H., Imanishi, T., Ikejima, H., Kuroi, A., Takarada, S., Tanimoto, T., Kitabata, H., Okochi, K., Arita, Y., Ishibashi, K. et al. (2009) Impact of heterogeneity of human peripheral blood monocyte subsets on myocardial salvage in patients with primary acute myocardial infarction. J. Am. Coll. Cardiol. **54**, 130–138

70 Tapp, L. D., Shantsila, E., Wrigley, B. J., Pamukcu, B. and Lip, G. Y. (2012) The $CD14^{++}CD16^{+}$ monocyte subset and monocyte-platelet interactions in patients with ST-elevation myocardial infarction. J. Thromb. Haemost. **10**, 1231–1241

71 Iyer, R. P., Patterson, N. L., Fields, G. B. and Lindsey, M. L. (2012) The history of matrix metalloproteinases: milestones, myths, and misperceptions. Am. J. Physiol. Heart Circ. Physiol. **303**, H919–H930

72 Ren, G., Michael, L. H., Entman, M. L. and Frangogiannis, N. G. (2002) Morphological characteristics of the microvasculature in healing myocardial infarcts. J. Histochem. Cytochem. **50**, 71–79

73 Chow, A., Huggins, M., Ahmed, J., Hashimoto, D., Lucas, D., Kunisaki, Y., Pinho, S., Leboeuf, M., Noizat, C., van Rooijen, N. et al. (2013) $CD169^{+}$ macrophages provide a niche promoting erythropoiesis under homeostasis and stress. Nat. Med. **19**, 429–436

74 Ehninger, A. and Trumpp, A. (2011) The bone marrow stem cell niche grows up: mesenchymal stem cells and macrophages move in. J. Exp. Med. **208**, 421–428

75 Lo Celso, C. and Scadden, D. T. (2011) The haematopoietic stem cell niche at a glance. J. Cell Sci. **124**, 3529–3535

76 Assmus, B., Iwasaki, M., Schachinger, V., Roexe, T., Koyanagi, M., Iekushi, K., Xu, Q., Tonn, T., Seifried, E., Liebner, S. et al. (2012) Acute myocardial infarction activates progenitor cells and increases Wnt signalling in the bone marrow. Eur. Heart J. **33**, 1911–1919

77 Dutta, P., Courties, G., Wei, Y., Leuschner, F., Gorbatov, R., Robbins, C. S., Iwamoto, Y., Thompson, B., Carlson, A. L., Heidt, T. et al. (2012) Myocardial infarction accelerates atherosclerosis. Nature **487**, 325–329

78 Massa, M., Rosti, V., Ferrario, M., Campanelli, R., Ramajoli, I., Rosso, R., De Ferrari, G. M., Ferlini, M., Goffredo, L., Bertoletti, A. et al. (2005) Increased circulating hematopoietic and endothelial progenitor cells in the early phase of acute myocardial infarction. Blood **105**, 199–206

79 Isoyama, S. and Nitta-Komatsubara, Y. (2002) Acute and chronic adaptation to hemodynamic overload and ischemia in the aged heart. Heart Fail. Rev. **7**, 63–69

80 Virchow, R. (1989) Cellular pathology. As based upon physiological and pathological histology. Lecture XVI: Atheromatous affection of arteries. 1858. Nutr. Rev. **47**, 23–25

81 von Gise, A. and Pu, W. T. (2012) Endocardial and epicardial epithelial to mesenchymal transitions in heart development and disease. Circ. Res. **110**, 1628–1645

82 Gurtner, G. C., Werner, S., Barrandon, Y. and Longaker, M. T. (2008) Wound repair and regeneration. Nature **453**, 314–321

83 Ikeuchi, M., Tsutsui, H., Shiomi, T., Matsusaka, H., Matsushima, S., Wen, J., Kubota, T. and Takeshita, A. (2004) Inhibition of TGF-β signaling exacerbates early cardiac dysfunction but prevents late remodeling after infarction. Cardiovasc. Res. **64**, 526–535

84 Okada, H., Takemura, G., Kosai, K., Li, Y., Takahashi, T., Esaki, M., Yuge, K., Miyata, S., Maruyama, R., Mikami, A. et al. (2005) Postinfarction gene therapy against transforming growth factor-β signal modulates infarct tissue dynamics and attenuates left ventricular remodeling and heart failure. Circulation **111**, 2430–2437

85 Wahl, S. M., Hunt, D. A., Wakefield, L. M., McCartney-Francis, N., Wahl, L. M., Roberts, A. B. and Sporn, M. B. (1987) Transforming growth factor type β induces monocyte chemotaxis and growth factor production. Proc. Natl. Acad. Sci. U.S.A. **84**, 5788–5792

86 Hayashidani, S., Tsutsui, H., Shiomi, T., Ikeuchi, M., Matsusaka, H., Suematsu, N., Wen, J., Egashira, K. and Takeshita, A. (2003) Anti-monocyte chemoattractant protein-1 gene therapy attenuates left ventricular remodeling and failure after experimental myocardial infarction. Circulation **108**, 2134–2140

87 Frangogiannis, N. G., Mendoza, L. H., Ren, G., Akrivakis, S., Jackson, P. L., Michael, L. H., Smith, C. W. and Entman, M. L. (2003) MCSF expression is induced in healing myocardial infarcts and may regulate monocyte and endothelial cell phenotype. Am. J. Physiol. Heart Circ. Physiol. **285**, H483–H492

88 Ganz, T. (1993) Macrophage function. New Horiz. **1**, 23–27

89 Zeisberg, M. and Kalluri, R. (2013) Cellular mechanisms of tissue fibrosis. 1. Common and organ-specific mechanisms associated with tissue fibrosis. Am. J. Physiol. Cell Physiol. **304**, C216–C225

90 Rajantie, I., Ilmonen, M., Alminaite, A., Ozerdem, U., Alitalo, K. and Salven, P. (2004) Adult bone marrow-derived cells recruited during angiogenesis comprise precursors for periendothelial vascular mural cells. Blood **104**, 2084–2086

91 Ziegelhoeffer, T., Fernandez, B., Kostin, S., Heil, M., Voswinckel, R., Helisch, A. and Schaper, W. (2004) Bone marrow-derived cells do not incorporate into the adult growing vasculature. Circ. Res. **94**, 230–238

92 Frangogiannis, N. G., Shimoni, S., Chang, S. M., Ren, G., Shan, K., Aggeli, C., Reardon, M. J., Letsou, G. V., Espada, R., Ramchandani, M. et al. (2002) Evidence for an active inflammatory process in the hibernating human myocardium. Am. J. Pathol. **160**, 1425–1433

Received 15 November 2013/9 December 2013; accepted 18 December 2013
Published on the Internet 14 February 2014, doi:10.1042/BJ20131501

Determination of the Intracellular Calcium Concentration in Peritoneal Macrophages Using Microfluorimetry

Silvia González-Ramos[1], Luz María G. Carrasquero[2], Esmerilda G. Delicado[2], María T. Miras-Portugal[2], María Fernández-Velasco[2*] and Lisardo Boscá[2*]

[1]Cell Communiation, Instituto de Investigaciones Biomédicas Alberto Sols, Madrid, Spain;
[2]Biochemistry and Molecular Biology IV, Complutense University, Madrid, Spain
[*]For correspondence: mfvlorenzo@gmail.com; lbosca@iib.uam.es

[Abstract] Calcium is one of the most important intracellular messengers in biological systems. Ca^{2+} microfluorimetry is a valuable tool to assess information about mechanisms involved in the regulation of intracellular Ca^{2+} levels in research on cells and in living tissues. In essence, the use of a dye that fluoresces in the presence of a target substance allows the detection of changes in the concentration of this molecule by determining the changes in the fluorescence of the probe (increases or decreases, depending on the nature of the dye used; for a review see Tsien *et al*., 1985). In this regard, there have been developed two different methodologies to assess intracellular Ca^{2+} measurements. On the one hand, ratiometric methods are based on the use of a ratio between two fluorescence intensities linked to the physicochemical properties of the probe. This allows correction of artifacts due to bleaching, changes in focus, variations in laser intensity, *etc*. but makes measurements and data processing more complicated since they require more expensive equipment with the possibility to change the wavelength emission/detection in a rapid way. Some ratiometric Ca^{2+} indicators are Fura-2 and Indo-1. On the other hand, on binding to Ca^{2+}, indicators used for non-ratiometric measurements show a shift in their fluorescence intensity (the free indicator has usually a very weak fluorescence). Therefore, although an increase in fluorescence signal can be related directly to an increase in Ca^{2+} concentration, the fluorescence intensity depends on many factors such as acquisition conditions, probe concentration, optical path length, balance between the affinity constants of proteins binding Ca^{2+}, among others. However, the fluxes of Ca^{2+} are of such a magnitude that these interferences are minor contributors to biases in the measurements. There are many non-ratiometric calcium indicators, some of which are Fluo-3, Fluo-4 and Calcium-Green-3. Consequently, the most suitable Ca^{2+}-probe for each experiment will depend on the range of Ca^{2+} concentration that has to be evaluated, instrumentation, loading requirements, *etc*. In the present report we describe the protocol employed to quantify intracellular Ca^{2+} changes in peritoneal macrophages using Fura-2 as a fluorimetric probe and a microfluorimetric protocol that allows quantification of responding cells to a given stimulus, localization of the main intracellular domains sensing Ca^{2+} changes and a time-resolved analysis of the Fura-2 fluorescence that reflects the intracellular dynamics of Ca^{2+}

in these cells (Través *et al*., 2013).

Materials and Reagents

1. Fura 2-AM (Life Technologies)
2. DMSO (Sigma-Aldrich)
3. EGTA
4. $CaCl_2$
5. HEPES
6. Trypan Blue
7. FCS
8. Vacuum grease
9. Peritoneal macrophages obtained from Balb/c male mice (8-12 weeks old) 4 days after i.p. administration of 2.5 ml of 3% thioglycollate solution
   Note: In our study (Traves et al., 2013), the effect of prostaglandin E_2 on the response to P2X/P2Y agonists ATP and BzATP was studied in depth. All these molecules were purchased from Sigma-Aldrich (St. Louis, MO).
10. 10x DPBS without Ca^{2+} Mg^{2+} (Lonza)
11. Locke's solution (see Recipes) (supplemented with 1 mg/ml BSA)

Equipment

1. Coverslips 0.13-0.16 mm thickness (15 mm of diameter) (SCHOTT AG)
2. Forceps
3. 35 mm culture dishes
4. Basic water-jacket CO_2 incubator
5. Perfusion chamber RC-25F (Warner Instruments)
6. Valves employed for cell perfusion (Warner Instruments)
7. Perfusion valves controller VC 8 (Warner Instruments)
8. Vacuum pump
9. Water bath
10. NIKON TE-200 microscope with a Plan Fluor x20/0.5 water objective(Nikon Corporation, model:TE-200)
11. Dichroic mirror (430 nm) and a 510 nm band-pass filter (Omega Optical)
12. ORCA-ER C4742-80 camera (Hamamatsu Photonics K. K., model: C4742-80)
13. Filter wheel Lambda 10-2 (Sutter Instrument Company)

Software

1. MetaFluor 6.2r & PC software (UNIVERSAL SOLUTIONS)

Procedure

1. Firstly, a sterile coverslip was placed in the bottom of the culture dish (forceps may be helpful) where cells stuck from the very beginning. Macrophages were then carefully seeded in 1 ml of supplemented Locke's solution at a density of 300,000- 500,000 cells per 35 mm culture dish. Since they are non-dividing cells they were used in the following two or three days after seeded (likely, after this lapse time, macrophages will be completely adhered to coverslips). Extensive washing with 500 µl PBS 1X (three-four replicates) was used to ensure that cells were very adherent and alive. The percentage of apoptotic/necrotic cells after 3 days in culture was below 5% (determined by using the common Trypan Blue staining, see Notes).
   Note: Cell attaching to the coverslip is a critical step in order to perform the microfluorimetric analysis. If your plastic or glass interferes with the adherence of the macrophages, allow the support to dry with FCS (fetal calf serum) under the cabin to improve adherence. Avoid a high density cell culture. A 50-75% subconfluent culture with some cells interacting is desirable.
2. Incubate macrophages in 1 ml supplemented Locke's solution loaded with 5-7 µM Fura-2-AM (dissolved in DMSO, following the datasheet instructions) for 45 min approximately at 37 °C. Incubation does NOT involve either shaking or agitation, just a short and slightly balancing.
3. Wash thoroughly the culture monolayer with fresh 500 µl Locke's solution (serum also contains esterases that may degrade Fura-2-AM) and place the coverslip in a small superfusion chamber (34 µl volume). Junctions between the coverslip and the chamber are sealed with vacuum grease. Figure 1 depicts the superfusion chamber apparatus.
   Note: Locke's media or products perfused to the chamber are regulated using a valve system that works by gravity. The perfusion solutions are maintained in a water bath at 37 °C and the flow rate is kept constant at 1.5 ml/min. The vacuum pump aspires continuously the perfusion media after arriving to the chamber to prevent the accumulation of the hydrolysis products.
   Figure 2 shows the experimental setup described here.

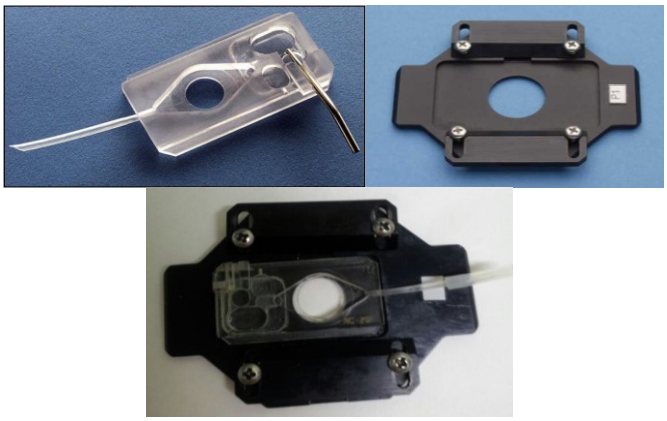

Figure 1. The superfusion chamber system. In the upper side of the figure, we can appreciate the superfusion chamber and the microscope stage. Immediately below these two pictures, both pieces are already assembled. The coverslip should be placed in the circular hollow remaining in the center.

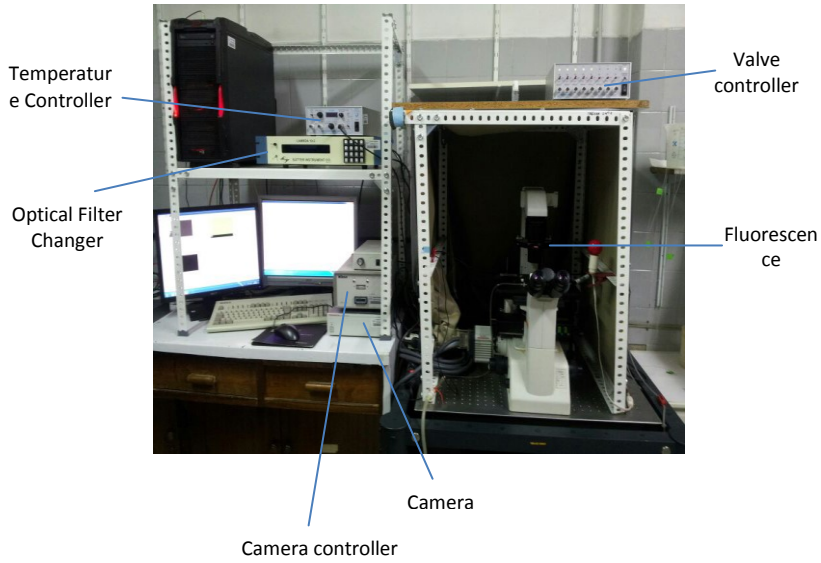

Figure 2. Experimental equipment for Fura-2-AM registers. The temperature and the valve controllers, the fluorescence microscope (including its optical filter changer) and the necessary equipment to record the fluorescence images (the camera and its controller) are depicted above.

4. Images of both control and treated cells are visualized using the Plan Fluor x20/0.5 objective of the microscope. In this regard, Fura-2-AM has entered the cell and intracellular esterases have hydrolyzed the compound providing free Fura-2 that senses Ca^{2+} with a high affinity. Fluorescence emission occurs in a broad range around 430 nm when the cells are excited at 340 nm.

Note: In our study (Traves et al., 2013), macrophages were preincubated with different prostanoids for at least 10 min and then stimulated for 30 s with a variety of purinergic receptor agonists at near-maximal effective concentrations: 100 μM ATP, 100 μM UTP, 10 μM UDP, 10 μM 2MeSADP, 1,000 μM α,β-meATP or 300 μM BzATP.

5. Excite cells for 300 ms at 340/380 nm (< 5 ms wavelength change) and select the emitted light using the dichroic mirror (430 nm) and a 510-nm band-pass filter.
   Note: The selection of these wavelengths matches with the maximum fluorescence registers for Fura-2 calcium-saturated solutions (340 nm) and calcium-free Fura-2 solutions (380 nm).
6. Fluorescence images are acquired with the camera every 1.5 seconds and controlled by the software. Sampling frequency is 2 Hz.

Data analysis

1. Images are processed by averaging signals from small elliptical regions within individual cells (Figure 3). The possibility exists to define specific areas of changes in the fluorescence emission (cell contact interactions, protrusions in the cytoplasm –cell polarization- or simply cells with different morphologies –round *vs.* shaped macrophages, depending on the treatments-).
   Note: Background signals are subtracted from each wavelength.

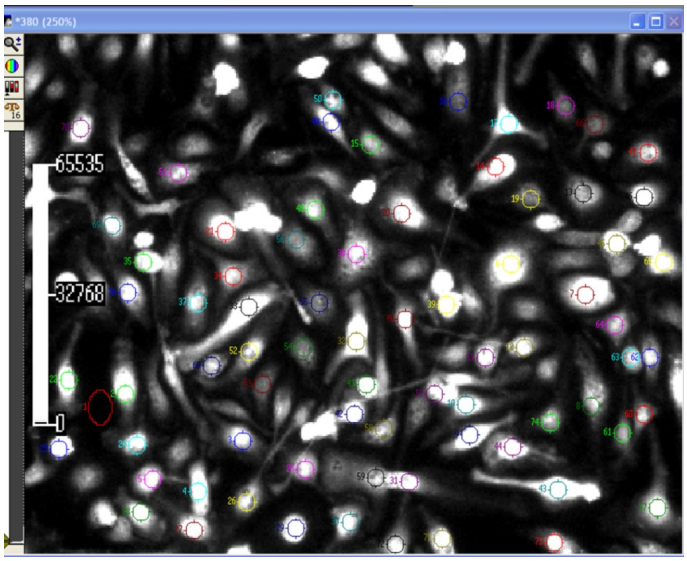

Figure 3. Metafluor screenshot of cells. ROIs (cells in which a shift in the fluorescence emission is recorded as a function of time) and background (normally areas without cells or non-responsive cells during the period of observation) are marked with a dot in the image. The scale bar on the left side refers to the time variable (in seconds).

2. The F340/F380 ratio is calculated on the basis of the initial peak magnitude that represents the initial transient components (Figure 4). The F340/F380 ratio is converted into a known calcium concentration using the Grynkiewicz equation:

   $[Ca^{2+}] = Kd * (R - R_{min}) / (R_{max} - R) * F_{380max}/F_{380min}$ (Grynkiewicz *et al*., 1985)

   Where:

   a. K_d is the dissociation constant (depends on the indicator, but also on pH, ionic strength, cell line, *etc*.).

   b. R is the observed fluorescence ratio at both wavelengths (F340/F380).

   c. R_{min} is the minimum ratio value (in absence of Ca^{2+}).

   d. R_{max} is the maximum ratio value (when Fura-2 is saturated by Ca^{2+}).

   e. F_{380max}/F_{380min} is a scaling factor (fluorescence intensity at 380 nm excitation in the absence of Ca^{2+} and at Ca^{2+} saturation).

   Note: A calibration curve is required to calculate the Kd value. The F_{380max} and F_{380min} values are obtained at the end of each analysis in the same experimental conditions (Fura-2-AM concentration, exposition time…). It is based in two calibration points, a maximum and a minimum corresponding, respectively, to a saturated calcium solution (2.5 mM $CaCl_2$) and a calcium-free solution (containing 10 µM EGTA). Alternatively, inhibition of the membrane reticulum Ca^{2+} pump with 200 nM thapsigargin or 500 nM ter-buthylbenzohydroquinone allow a saturation of the cytoplasmic Ca^{2+} concentration. Treatment of cells maintained in extracellular medium lacking or containing Ca^{2+} with a low dose of ionomycin (ca. 1 µM) to improve the entrance of the Ca^{2+} into the cell.

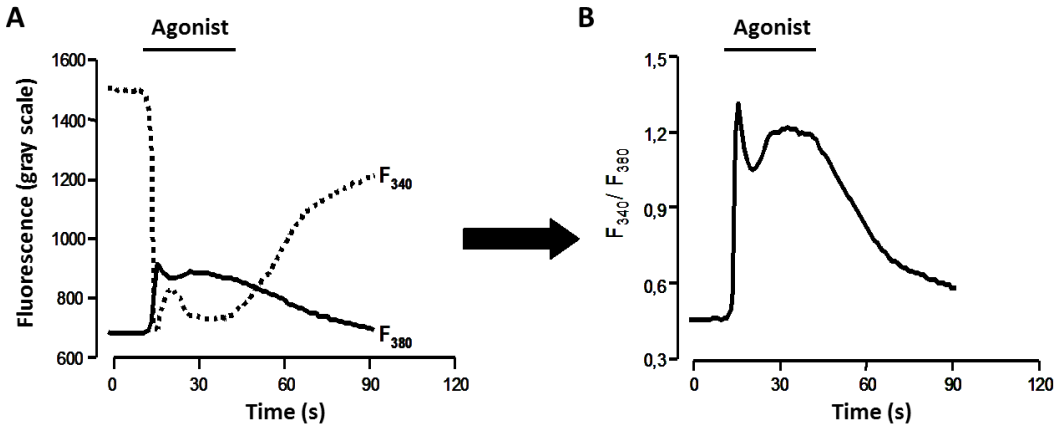

Figure 4. Fluorescence measured at 340/380 nm. A. Fluorescence intensity at both registered excitation wavelengths. B. Registers obtained over the time are divided to determine the F340/F380 ratio.

Notes

1. Trypan Blue staining can be used to discriminate between viable and non-viable cells. The protocol follows these typical steps:
   a. Dilute the cell sample (1:10) to a total volume of 20 µl in a 0.4% Trypan Blue dye solution (should be sterile filtered before using).
   b. While non-viable cells will be blue, viable cells will be unstained.
   c. Carefully and continuously fill the hemocytometer chamber with 10 µl of the solution each chamber (all hemocytometers consist of two chambers; each is divided into nine 1mm^2 squares).
   d. Count cells under the microscope in four 1 x 1 mm squares of one chamber and determine the average number of cells per square. If the cell density is higher than 200 cells/square, you should dilute your cell suspension.
   e. Total number of particles per ml in the cell sample can be calculated as follows: mean number of cells x 1/dilution factor x 10^4 cells/ml.

Recipes

1. Locke's Solution composition
   140 mM NaCl
   4.7 mM KCl
   2.5 mM $CaCl_2$
   1.2 mM KH_2PO_4
   1.2 mM $MgSO_4$
   5.5 mM glucose
   10 mM HEPES (pH 7.4)

Acknowledgments

This work was supported by grants CP11/00080 from ISCIII, BFU2011-024760 from MICINN and FIS-RECAVA RD12/0042/0019. RECAVA and Ciberehd networks are funded by the Carlos III Health Institute. A summary of the procedure was described in Traves *et al.* (2013).

References

1. Grynkiewicz, G., Poenie, M. and Tsien, R. Y. (1985). A new generation of Ca^{2+} indicators with greatly improved fluorescence properties. *J Biol Chem* 260(6): 3440-3450.

2. Traves, P. G., Pimentel-Santillana, M., Carrasquero, L. M., Perez-Sen, R., Delicado, E. G., Luque, A., Izquierdo, M., Martin-Sanz, P., Miras-Portugal, M. T. and Bosca, L. (2013). Selective impairment of P2Y signaling by prostaglandin E2 in macrophages: implications for Ca^{2+}-dependent responses. *J Immunol* 190(8): 4226-4235.
3. Tsien, R. Y., Rink, T. J. and Poenie, M. (1985). Measurement of cytosolic free Ca^{2+} in individual small cells using fluorescence microscopy with dual excitation wavelengths. *Cell Calcium* 6(1-2): 145-157.